IAEA-TECDOC-1179

Fuel chemistry and pellet–clad interaction related to high burnup fuel

Proceedings of the Technical Committee held in Nyköping, Sweden, 7–10 September 1998

INTERNATIONAL ATOMIC ENERGY AGENCY IAEA

October 2000

The originating Section of this publication in the IAEA was:

Nuclear Fuel Cycle and Materials Section
International Atomic Energy Agency
Wagramer Strasse 5
P.O. Box 100
A-1400 Vienna, Austria

FUEL CHEMISTRY AND PELLET–CLAD INTERACTION RELATED TO HIGH BURNUP FUEL
IAEA, VIENNA, 2000
IAEA-TECDOC-1179
ISSN 1011–4289

Printed by the IAEA in Austria
October 2000

FOREWORD

The Technical Committee Meeting on Fuel Chemistry and Pellet–Clad Interaction Related to High Burnup Fuel was organized by the International Atomic Energy Agency upon the recommendations of the 14th International Working Group on Fuel Performance and Technology in 1997. At the invitation of the Government of Sweden, the meeting was held in Nyköping in September 1998 and hosted by Studsvik Nuclear AB.

The purpose of the meeting was to review new developments in clad failures. Major findings regarding the causes of clad failures are presented in this publication, with the main topics being fuel chemistry and fission product behaviour, swelling and pellet–cladding mechanical interaction (PCMI), cladding failure mechanism at high burnup, thermal properties and fuel behaviour in off-normal conditions.

Clad failures represent a risk for the electricity producer and, at the same time, for the safety of the plant. Consequently, as the burnup of nuclear fuel elements is being increased in order to reduce the price of the fuel cycle, this meeting provided an excellent opportunity to assess the relative impact of this increase on potential clad failures.

The IAEA wishes to express its gratitude to the local organizing committee (the Swedish Nuclear Power Inspectorate, Vattenfall Fuel, OKG Aktiebolag and Studsvik Nuclear AB), and to all the participants who contributed to the success of this meeting. The IAEA officer responsible for the organization of the meeting and for the completion of this publication was P. Menut of the Division of Nuclear Fuel Cycle and Waste Technology.

EDITORIAL NOTE

This publication has been prepared from the original material as submitted by the authors. The views expressed do not necessarily reflect those of the IAEA, the governments of the nominating Member States or the nominating organizations.

The use of particular designations of countries or territories does not imply any judgement by the publisher, the IAEA, as to the legal status of such countries or territories, of their authorities and institutions or of the delimitation of their boundaries.

The mention of names of specific companies or products (whether or not indicated as registered) does not imply any intention to infringe proprietary rights, nor should it be construed as an endorsement or recommendation on the part of the IAEA.

The authors are responsible for having obtained the necessary permission for the IAEA to reproduce, translate or use material from sources already protected by copyrights.

CONTENTS

SUMMARY AND RECOMMENDATIONS

1. INTRODUCTION

Increasing the fuel burnup is a major challenge for nuclear activities worldwide. Thus, electricity producers hope to decrease the share of the electricity costs which is linked to the fuel, as by increasing the burnup, more electricity can be produced with the same amount of fuel, the waste will be reduced and the core management will be rendered easier. On the other hand, there are several disadvantages involved when fuel burnup is increased as the performance of the fuel element decreases with the burnup. These include thermal properties damage of the oxide, an increase in the number of failed fuel and of fission gas release, etc.

Through the International Working Group on Fuel Performance and Technology the IAEA has initiated an assessment of the consequences related to increasing the fuel burnup. In this context and in order to review existing information and to increase the knowledge on this topic, several technical committee meetings (TCMs) as well as IAEA co-operation in international seminars were proposed.

The first technical committee meeting on this subject, entitled "Advances in Fuel Pellet Technology for Improved Performance at High Burnup", was held in Tokyo, Japan from 28 October to 1 November 1996. As a result of this TCM, which showed that there was a considerable interest in a TCM on pellet–clad interaction (PCI) related to high burnup, the knowledge of the basic physical phenomena was improved.

These meetings have enabled the IAEA and Member States to obtain an overview of numerous issues linked to increasing the fuel burnup and to assess the advantages and disadvantages involved in this process.

2. SUMMARY OF THE TECHNICAL COMMITTEE MEETING

The Technical Committee Meeting on Fuel Chemistry and Pellet–clad Interaction Related to High Burnup Fuel, held in Nyköping, Sweden, 7–10 September 1998, was organized in 5 sessions in order to cover all topics related to the subject.

For high burnup fuel a limitation could be linked to the pellet to clad interaction which is responsible for the cladding failure. The gas swelling of the fuel and the resulting interaction of the pellet to the clad is one mechanism that may be involved in the rupture. This fuel swelling takes its origin in the fuel chemistry (most generally linked to It is established now that the fission gas release is increasingly important at high burnup. the fission gas behaviour) and in the fuel behaviour in off normal conditions. The thermal property of the high burnup fuel has to be considered as a part of the cause if it is degraded with the burnup.

Models should continue to be improved and it is therefore necessary to develop programmes to collect data. These may come from puncture measurements for high burnup and energy ramp injection, or from microsampling in order to obtain more accurate measurements of the gas distribution in the fuel. Post-irradiation examinations already performed are a good way for establishing the role of the fission gas related to fuel swelling and must be continued for higher burnup.

Many experiments using a re-fabricated rod with pre-irradiated fuel were reported in ramp test conditions. The role of fission gas behaviour in fuel swelling was demonstrated for hold times less than 30 minutes. However, data are missing for a ramp longer time swelling.

The role of the clad behaviour was reported regarding the cladding failure mechanisms at high burnup. The hydride effect is well understood, as well as the temperature effects. This resulted in the proposal for a modelling of failure criteria in different codes.

The fuel temperature in normal use is affected by the rim effect at high burnup and by the degradation of the thermal property. A new model to give the thermal property of UO_2 was presented showing the falling off at higher burnups compared to the previously used formula. The change in the pellet centre temperature according to the rim effect was reported. For 60 GW·d/t U and linear heat rate of 300 W/cm the influence of the rim effect on the pellet centre temperature was found to be small. It is expected to be significant at burnups over 75 GW·d/t U.

3. SUMMARIES OF THE SESSIONS

3.1. Fuel chemistry and fission product behaviour (Session 1)

3.1.1. Summary

Four papers on a range of topics were presented in this session.

In the Swedish paper on "Isotopic Composition of Fission Gases in LWR Fuel" some valuable insights have been gathered through a thoughtful re-evaluation of collected fission gas isotopic data. By careful selection and plotting of isotope ratios it is possible to obtain additional information about the origin of the released gases. For example, the ratios are quite different in MOX fuel and somewhat different in Gad fuel compared to standard UO_2. It is also shown that low power base irradiation gas is mostly released from the whole fuel pellet, while in ramp tests it is largely released from the fuel centre. The isotope ratios in simulated defective rods were radically different from sound rods. It was argued from half-life considerations that this was due to the enhanced diffusion of the selenium and tellurium precursors of Kr and Xe, respectively, under oxidizing conditions.

There was interest in using this approach to determine releases from rim structures and there is a need to understand the mechanism of enhanced Se and Te diffusion.

Programmes to collect data for fission gas modelling code validation were described in the paper by French experts on "Fission Gas Release from High Burnup Fuel During Power Transients: Experimental Data for Modelling". Special attention was paid to experimental techniques to non-destructively determine fission gas release (FGR) and to distinguish between grain boundary gas and intragranular gas. The non-destructive method (^{85}Kr in plenum) allowed separate measurements of base irradiation release and transient release. The ADAGIO experimental method involves a short time, low temperature re-irradiation of the fuel samples to create a uniform distribution of radioactive tracer gas atoms in the fuel matrix. A temperature anneal in an oxidizing atmosphere releases ^{85}Kr from the grain boundaries for measurements. This is followed by a high temperature anneal to measure the complete

inventory of gas in the sample. The radioactive tracer gas facilitates distinguishing between the two gas fractions.

From puncture measurements, a consistent set of data showed the effects of burnup and ramp hold time on FGR. From microsampling and ADAGIO measurements, data were collected to compare inter- and intra-granular gas distributions at the centre and the periphery of the fuel. This ingenious technique will be used to generate data in support of mechanistic FGR and swelling models.

Design, irradiation and post-irradiation examination of a small array of pathfinder PWR rods was described in the paper by the Chinese Institute of Atomic Energy on "Pie of Test Assembly of Qinshan Nuclear Power Plant". The post irradiation examination (PIE) was careful and comprehensive. At 25 GWd/tU cladding creepdown, ridging and dish filling were observed. Fission gas release was higher than expected, which was due to a network of cracks in the as-fabricated fuel. This microstructure has not been used in the Quinshan plant.

The effect of increased fuel oxygen potential on fuel behaviour has been studied by fabricating and by irradiating uranium fuel with an O/U ratio of 2.05, as shown in the paper on "Behaviour of High O/U Fuel", by participants from GE Nuclear Energy, USA. This fuel survived pellet clad interaction (PCI) ramp tests where standard nonbarrier fuel would have been expected to fail. PIE showed large cladding strains and fuel swelling but lower than expected fission gas release.

In the strained region of the cladding there were very many incipient PCI cracks, but none had propagated through the cladding. It was hypothesized that oxygen was effectively blocking the transport of iodine atoms to the crack tip. It was noted that the 2 phase fuel microstructure present in the as-fabricated material was not evident after irradiation. It was hypothesized that the concentration of foreign atoms in the matrix inhibited the phase transformation on cooldown. It was pointed out that some of the observations were probably due to enhanced diffusion of vacancies.

3.1.2. Recommendations

- At high burnup, fission gas release behaviour is increasingly important and should continue to receive special attention from fuel modellers and experimentalists.

- A lot of experimental data has been generated. Experimenters and modellers should be encouraged to revisit and re-evaluate these data in different ways to get the more out of them.

- Mechanistic models need more and different kinds of data to validate them Experimenters should continue to develop new techniques and collect data to support this need.

- Experimenters should design and perform experiments to elucidate the reported behaviours of hyperstoichiometric fuel and to ascertain if they have any practical applications.

- The importance of pathfinder irradiation tests and fuel surveillance programmes cannot be overemphasised.

- Experimentalists are encouraged to develop techniques to ascertain the fraction of gas released from the pellet rim at high burnup.

3.2. Swelling and PCMI (Session 2)

3.2.1. Summary

UO_2 and MOX fuel rods were preirradiated in power reactors to a burnup (BU) of 15, 24, and 26 to 50 MW·d/kg M. Short segmented rods were made, which were power ramped in research reactors to final ramp powers between 350 W/cm and 480 W/cm with hold times of zero seconds, few minutes, several hours, and up to 6 days. Diameter evolution was measured in-pile and after ramping and also fission gas release, and fuel restructuring with PIE. Measurements were compared with calculations with different codes.

15 MW·d/kg M (MOX-PHWR rod):

Measured ridging can be reproduced with a purely elastic finite element method (FEM) code. Fission gas swelling thus seems to be of low importance.

24 MW·d/kg U (PWR rods):

"Local code 2D — TOUTATIS" (no full fuel rod modelling) is a mainly mechanical FEM code, which predicts well the correlation of cladding deformation and local heat rating. However, since TOUTATIS does not have a fission gas swelling model, it significantly underpredicts clad deformation in the 12 hours hold time case, where fg-swelling clearly developed; good prediction is given for the short hold times (typical times in experiments to stress corrosion cracking [SCC] failure), where measurements show that fg-swelling is still small.

26–50 MW·d/kg M rods:

The full fuel rod analysis code METEOR/TRANSURANUS (no FEM code, but with fuel and clad mechanics) describes well fission gas release and clad deformation, when fg-swelling is modelled. fg-swelling occurs already after 30 minutes. When fission gas release is overestimated — like in the MOX case — clad deformation is underestimated. Elongation measurements are also well described by the code (with strong coupling modelled).

Halden elongation measurements show strong coupling of fuel pellets and cladding at high BU (55 MW·d/kg U). At lower BU ratchetting effects may occur after shutdowns, leading however only to elastic straining which quickly relaxes.

3.2.2. Recommendations

- Study importance of fission gas swelling with power ramps on segments with BU >50 MW·d/kg U.

- Study importance of fission gas swelling with power ramps with less than 30 minutes hold time.

- Improve modelling of fission gas swelling by doing quantitative microscopy (optical, SEM, TEM, EPMA) on non-ramped and ramped high BU fuel (radial porosity profiles).

- Extend Halden elongation measurements to BU > 55 MW·d/kg UO_2, and with different cladding types.

- Assess importance of fuel swelling (including gas swelling) and strong coupling of fuel pellets and cladding for PCIOMR (**P**re **C**onditioning **I**nterim **O**perating **M**anagement **R**ecommendation).

- The French paper on "The Effect of Fission Gas Swelling on Cladding Strain During Power Ramp Tests" shows that fission gas release and fission gas swelling models are becoming increasingly mechanistic. Consequently, there is a need for developing experimental techniques and generating data from existing techniques, which help qualify the models.

- There is a need for fuel swelling data for ramp hold times of less than 30 minutes.

3.3. Cladding failure mechanisms at high burnup (Session 3)

3.3.1. Summary

3.3.1.1. Effects of hydrides in cladding

Rods with high hydrogen contents were ramped to high power levels and still survived. Incipient cracks in existing hydrides and signs of delayed hydrogen cracking were seen. Out of pile mechanical testing of hydrided cladding were performed and showed agreement with observations after the in pile ramp tests. That is, one fast cracking mode where existing hydrides crack and another slow or delayed mode where stress assisted hydride precipitation allowed propagation of cracks to continue.

3.3.1.2. Cladding temperature effects

High temperatures in the cladding were observed to be beneficial against PCI failure and low temperatures increased failure propensity.

3.3.1.3. Modelling of failure criteria

Using empirical PCI failure data up to 35 MW·d/kg U the British Energy ENIGMA code was used to extend the calculated stress failure criterion to 60 MW·d/kg U. Although no failure levels for Gd rods were available it was deemed conservative to use the UO_2 criterion also for Gd rods.

The BACO code was described and results from statistical variation of the fuel rod parameters in the input data were shown.

3.3.1.4. PCI failure of MOX fuel

A rod with a very low addition of Pu to the fuel failed at a burnup of 15 MW·d/kg M with a typical SCC crack after ramping to 360 W/cm. Metallography revealed a missing fuel

chip at the position of failure and in the discussion this was pointed out as the main reason for the low failure level.

3.3.2. Recommendations

- Performing the same mechanical behaviour studies with other cladding alloys like Zr-Nb.
- Ramp testing of PWR rods in the range of temperatures used for operating reactors.
- Extend the failure level database up to and beyond 60 MW·d/kg U.

3.4. Thermal properties (Session 4)

3.4.1. Summary

Two important phenomena affect the fuel temperature at high burnup: degradation of the thermal conductivity of UO_2 and the rim effect. Both topics were covered in two papers.

A new model for the thermal conductivity of UO_2 and (U, Gd)O_2 fuel was presented in the Siemens paper on "A Fuel Thermal Conductivity Correlation Based on Latest Experimental Results", using an arctan formulation of the phonon-scattering term, which leads to a falling off of the degradation effect at higher burnups or dopant concentrations compared to the previously used formulation (which is equivalent at lower burnups). The new arctan model agrees well with the Halden fuel temperature database with very good agreement up to about 60 MW·d/kg U and to even higher burnup when including the "rim effect" as well. The new formulation also agrees very well with unirradiated gadolinia fuel, and suggests that the additive effect of Gd and burnup are less than previously believed. The effect modelled also agrees with laser flash thermal diffusivity measurements of irradiated fuel after partial annealing, but does not model the irradiation damage effect which is seen on unannealed irradiated fuel.

An analysis of the pellet centre temperature increase due to the rim effect porosity was presented in a paper prepared jointly by experts from Japan and the Netherlands on "Influence of RIM effect on Fuel Centre Temperature". The analysis was performed for a pellet burnup of 60 GWd/tU and linear heat rate of 300 W/cm using the decreased thermal conductivity calculated by finite element analysis of the effect of an experimentally determined porosity distribution at the rim of high burnup fuel. This showed that the porosity could be modelled as spheres. The rim effect on the fuel centre temperature was found to be small (about 20–30^{o}C) at 60 GWd/tU but is expected to be significant at pellet average burnups over 75 GWd/tU if the high burnup structure then extends significantly into the pellet. Data on the composition of released fission gas in high burnup 9 × 9 BWR fuel indicated that the release at high burnup did not predominantly come from the rim region. Previous 8 × 8 BWR FGR data with large scatter was attributed to the dominant effect of rod power, masking such information; it was commented that a similar observation had been made for Swedish 10 × 10 fuel compared to 8 × 8 fuel. It was suggested that the local porosity fraction should be determined and plotted as a function of local burnup in the rim region.

3.4.2. Recommendations

- More data are needed for thermal properties at pellet burnups well above 60 MW·d/Kg U to verify and improve the thermal conductivity correlation. (It should be remembered that changes in thermal conductivity models may require a revision of other parts of empirically tuned models).
- More data for rim growth in the ultra high burnup region should be collected to evaluate fuel performance more accurately.
- More experimental data is required to fully understand the mechanism of rim formation; for instance, whether the rim structure is formed due to recrystallisation or subdivision of original grains.
- The recommendations from the 1996 Tokyo TCM (TECDOC-1036) regarding data qualification should be re-emphasized.

3.5. Fuel behaviour in off-normal conditions (Session 5)

3.5.1. Summary

Two papers were presented in this session:

The features of a mechanistic fuel performance code FAIR were presented in the Indian paper on "Assessment of Clad Integrity of PHWR Fuel Pin Following a Postulated Severe Accident". The FAIR code can analyse fuel behaviour under normal, off-normal and accident conditions. The code is based on the application of finite element method for thermo–mechanical modelling and mechanistic modelling of various phenomena affecting the fuel behaviour. The code is also capable of analysing the effects of high burnup on fuel behaviour. The individual models have been tested and validated against standard benchmark cases published in the literature. The assessment of clad integrity of PHWR fuel pin following postulated severe accidents was performed using the FAIR code.

A paper from Studsvik AB, Sweden, on "Characteristics of Axial Splits in Failed BWR Fuel Rods" describes observations from the PIE of long cracks in failed BWR fuel cladding and discusses mechanisms and driving forces of the cracks. The axial propagation of long cracks in Zircaloy cladding is faster in the outer and colder part of the cladding. Propagation can occur in cladding with fairly low hydrogen content. The typical propagation can be disturbed by high hydrogen content in the cladding. The fracture is mainly brittle. The fracture propagates inwards and some plastic deformation around the fracture can be observed as wall thinning of the cladding. The driving force for the propagation of the cracks is hoop stress and the cracks can start from primary cracks of different kinds.

3.5.2. Recommendation

Experimentalists and modellers should be encouraged to develop an explanation for apparently brittle fracture of intrinsically ductile cladding.

FUEL CHEMISTRY AND FISSION PRODUCT BEHAVIOUR
(Session 1)

Chairpersons

J. DAVIES
United States of America

B. GRAPENGIESER
Sweden

ISOTOPIC COMPOSITION OF FISSION GASES IN LWR FUEL

T. JONSSON
Studsvik Nuclear AB,
Hot Cell Laboratory,
Nyköping, Sweden

Abstract

Many fuel rods from power reactors and test reactors have been punctured during past years for determination of fission gas release. In many cases the released gas was also analysed by mass spectrometry. The isotopic composition shows systematic variations between different rods, which are much larger than the uncertainties in the analysis. This paper discusses some possibilities and problems with use of the isotopic composition to decide from which part of the fuel the gas was released. In high burnup fuel from thermal reactors loaded with uranium fuel a significant part of the fissions occur in plutonium isotopes. The ratio Xe/Kr generated in the fuel is strongly dependent on the fissioning species. In addition, the isotopic composition of Kr and Xe shows a well detectable difference between fissions in different fissile nuclides.

1. INTRODUCTION

Most LWRs use low enriched uranium oxide as fuel. Thermal fissions in U-235 dominate during the earlier part of the irradiation. Due to the build-up of heavier actinides during the irradiation fissions in Pu-239 and Pu-241 increase in importance as the burnup of the fuel increases. The composition of the fission products varies with the composition of the fuel and the irradiation conditions. The isotopic composition of fission gases is often determined in connection with measurement of gases in the plenum of punctured fuel rods. It can be of interest to discuss how more information on the fuel behaviour can be obtained by use of information available from already performed determinations of gas compositions.

2. FISSION YIELDS

The fission gases are dominated by Xe and Kr. He is also produced in quite significant amounts but is not discussed in this paper.

2.1. Xenon

Xe-131, Xe-132, Xe-133, Xe-134, Xe-135 and Xe-136 are the six dominant xenon isotopes formed by the fission process in nuclear fuel. Xe-133 and Xe-135 are radioactive with half-lives of 5.2 days and 9.1 hours respectively.

Xe-135 has a very large capture cross-section and is transformed to Xe-136 to a large extent depending on the neutron flux. Xe-131 also has a large capture cross-section and is transformed to Xe-132 to a significant extent.

The total yield of the xenon isotopes is rather similar for different uranium and plutonium isotopes. However, the relative amounts of the xenon isotopes are somewhat dependent upon the kind of fission. The quotient (Xe-131 + Xe-132)/Xe-134 is tentatively used to describe this variation. This quotient was chosen, as it will change only slightly upon continued irradiation due to small neutron cross sections for isotopes influencing this quotient. The correctness of this assumption was also checked by ORIGEN calculations.

2.2. Krypton

Kr-83, Kr-84, Kr-85 and Kr-86 are the four dominant krypton isotopes formed by the fission process in nuclear fuel. Kr-85 is radioactive with a half-life of 10.7 years. Kr-83 has a large capture cross-section and is transformed to Kr-84 to a significant extent.

The yield of the krypton isotopes is very different between the different uranium and plutonium isotopes. The Kr yield is generally smaller for fission of the heavier isotopes. The relative amounts of the krypton isotopes are also somewhat dependent upon the kind of fission. The quotient (Kr-83 + Kr-84)/Kr-86 is tentatively used to describe this variation. This quotient was chosen, as it will change only slightly upon continued irradiation due to small neutron cross sections for isotopes influencing this quotient. The correctness of this assumption was also checked by ORIGEN calculations.

2.3. Comparison between yields

The yields of the chosen isotopes are illustrated in Figure 1. It can be observed that the yields of the krypton isotopes decline with increasing weight of the fissile isotopes. It should also be observed that the yield of Xe-134 is fairly independent of the origin. As a test of the usefulness 3 different quotients are plotted against each other in Figure 2. The quotient Kr-86/Xe-134 decreases with increasing weight of the fissioning isotope whereas the use of the quotients (Kr-83 + Kr84)/Kr-86 and (Xe-131 + Xe-132)/Xe-134can be disturbed by the small values of these quotients for Pu-241.

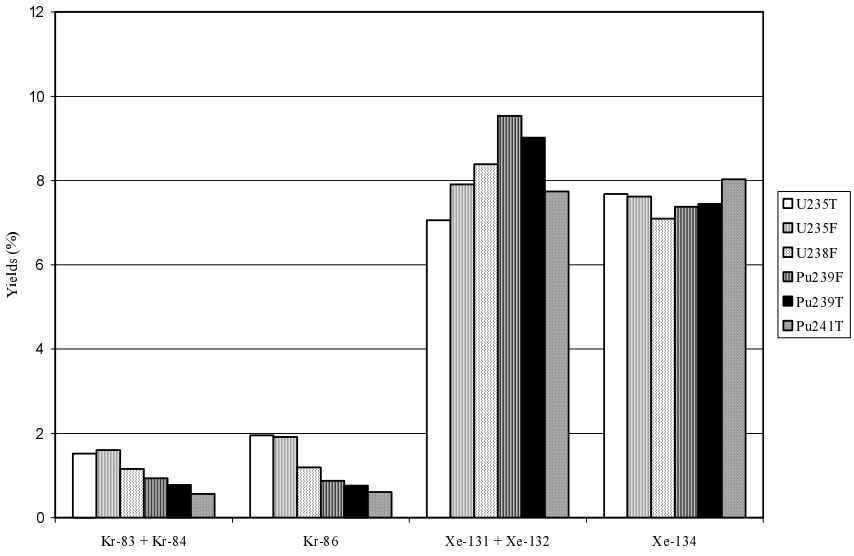

FIG. 1. Fission yields from some heavy nuclides.

3. EXPERIMENTAL DATA

Analysis of the composition of the gases in the plenum exists from many post-irradiation examinations of fuel rods. Results from the majority of the performed determinations in Studsvik of isotopic composition of fission gases with gas mass spectrometry are included in Figure 3[1]. The quotients (Kr-83 + Kr-84)/Kr-86 and (Xe-131 + Xe-132)/Xe-134 are plotted against the quotient Kr-86/Xe-134.

The experimental accuracy is better for the determination of the relative abundance between isotopes of the same element than for comparison between isotopes of different elements.

The two sets of data points in Figure 3 fall mainly along two fairly straight lines in the figure.

[1] Available results from fission gas analysis were only omitted due to apparent errors in the determination of the isotopic composition (insufficient pumping to remove reference gases) or due to uncertainties in the analysis due small amounts of fission gas. (Results are omitted if Kr-84 is less than 0,01 % of the gas content).

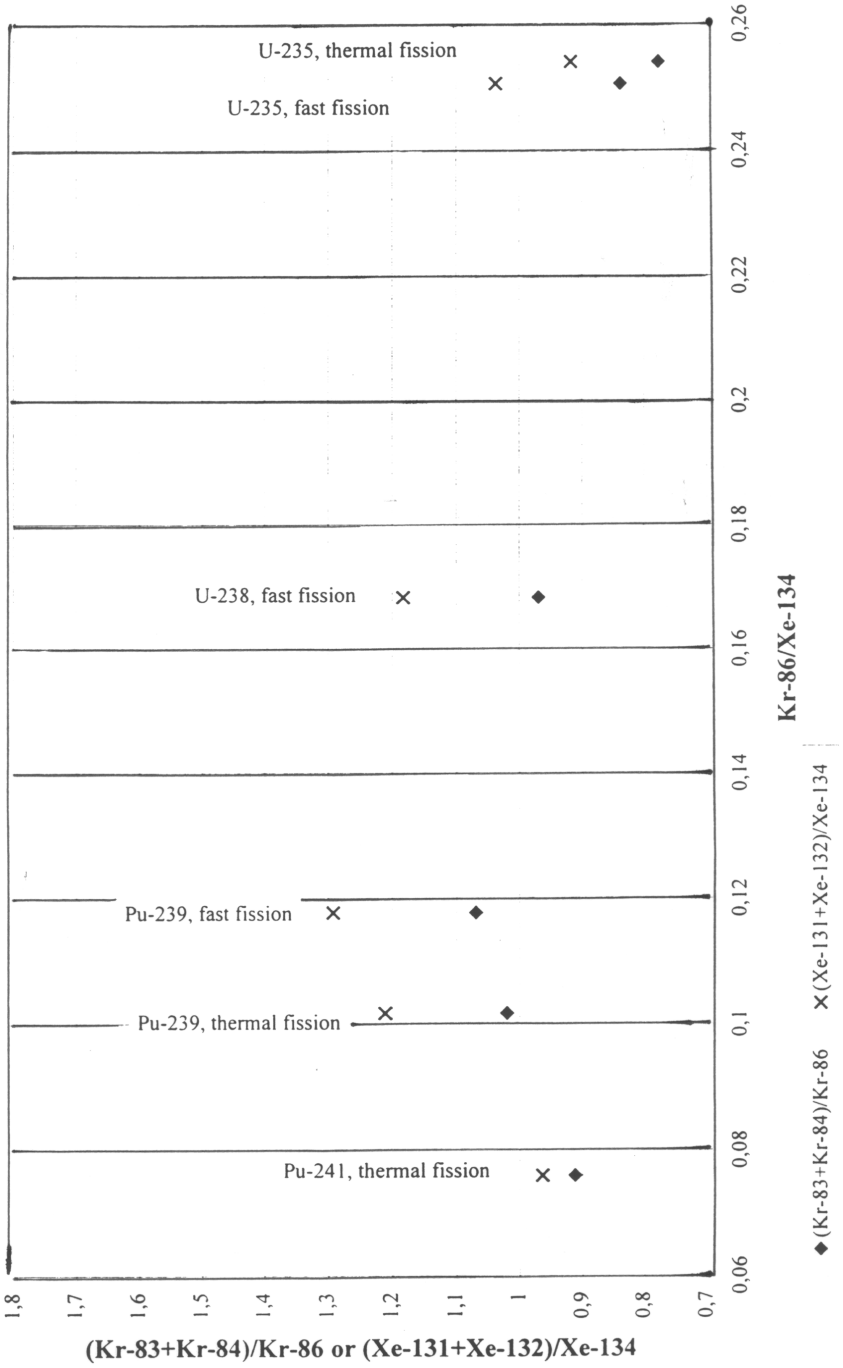

FIG. 2. Quotients between yields.

3.1. Defect fuel

Identification of data points, which deviate most from the general pattern, shows that these points originate from short time tests with fuel irradiated with a high water content in the rods. The explanation for the different composition of the released gas in these cases is presumably changed diffusion in hyperstoichiometric fuel (UO_{2+x}).

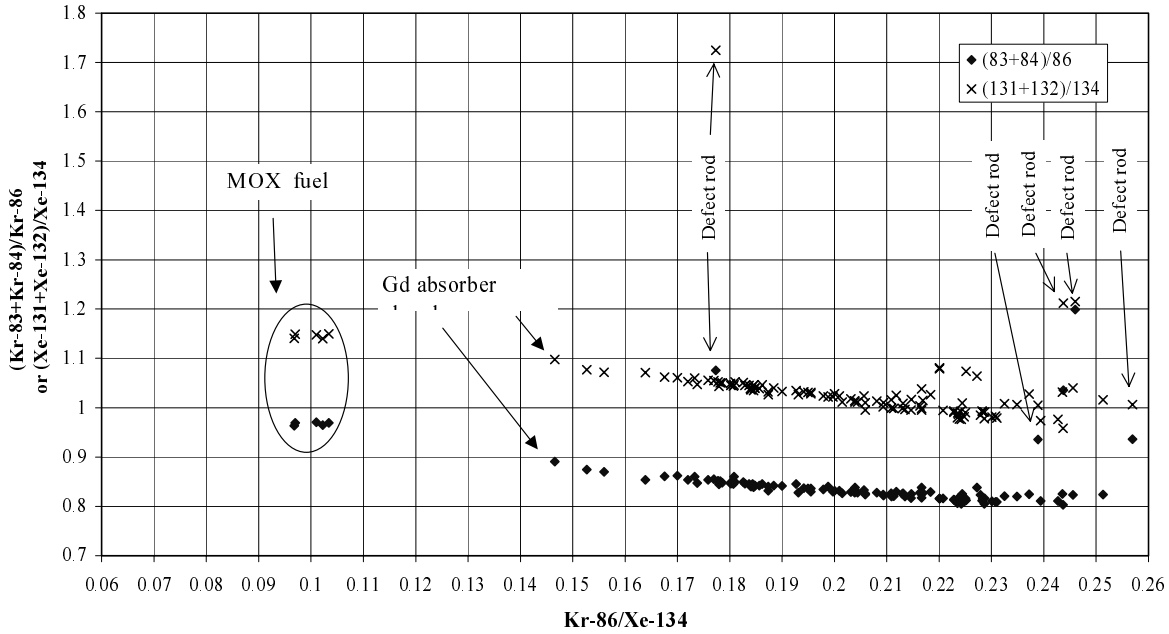

FIG. 3. Relation between quotients, defect and intact rods.

The changed composition of Kr can be explained by a faster diffusion of Br (or Se) in hyperstoichiometric fuel. The krypton isotopes are formed by decay of bromine isotopes. The half-lives of the bromine, selenium and arsenic isotopes are:

Isotope	Half-life	Isotope	Half-life	Isotope	Half-life
As-83	13 seconds	Se-83* Se-83m*	22 minutes 1.2 minutes	Br-83	2.4 hours
As-84	5 seconds	Se-84	3.2 minutes	Br-84	32 minutes
As-86	0,9 seconds	Se-86	15 seconds	Br-86	58 seconds
As decays to Se		Se decays to Br		Br decays to Kr	

* The decay chain for mass number 83 is such that about 1/3 passes the isotope Se-83 and 2/3 passes isotope Se-83m.

The relative amounts of the krypton isotopes are different in fuel rods containing water in such a way that Kr-83 has increased, Kr-84 is about unchanged and the relative content of Kr-86 has decreased.

The changed composition of the released krypton is almost certainly due to increased diffusion velocities of the parent isotopes of krypton, but it is not possible to decide only from these data if the increased diffusion occurs for one or several of the elements bromine, selenium and arsenic.

The changed composition of Xe in fuel with hyperstoichiometric fuel can also be supposed to be caused by faster diffusion of parent nuclides in the decay chain before the formation of Xe. The xenon isotopes are formed by decay of iodine isotopes. The half-lives of the iodine, tellurium and antimony isotopes are:

Isotope	Half-life	Isotope	Half-life	Isotope	Half-life
Sb-131	23 minutes	Te-131* Te-131m*	1.25 days 25 minutes	I-131	8 days
Sb-132	4.2 minutes 2.8 minutes	Te-132	3.3 days	I-132 I-132m	2.3 hours 1.4 hours
Sb-134	10.4 seconds	Te-134	42 minutes	I-134 I-134m	53 minutes 3.5 minutes
Sb decays to Te		Te decays to I		I decays to Xe	

* The decay chain for mass number 131 is such that about 1/8 passes the isotope Te-131 and 7/8 passes isotope Te-131m.

The largest (Xe-131 + Xe-132)/Xe-134 quotients are due to greatly increased content of Xe-132, which can be suspected to be caused by fast diffusion of Te-132 in hyperstoichiometric fuel. A fast diffusion of iodine would instead result in an increased release of Xe-131 due to the longer half-life of I-131. More specifically this indicates that the diffusion of tellurium must be faster than the diffusion of iodine or xenon to explain the experimental results by different diffusion velocities.

In analogy with this it can be suspected that the increase of the quotient (Kr-83 + Kr-84)/Kr-86 in hyperstoichiometric fuel is caused by faster diffusion of the selenium isotopes and not of the bromine isotopes. This analogy is based on the chemical similarity between the two halogens bromine and iodine and between the two group VI elements selenium and tellurium.

3.2. Intact fuel

The 5 points with the smallest Kr-86/Xe-134 quotients in Figure 3 originate from analysis of gas from MOX fuel. Most fissions in MOX fuel occur in plutonium and a smaller Kr-86/Xe-134 quotient can be expected.

The analysis of a fuel rod with Gd also shows a rather small Kr-86/Xe-134 quotient. It is reasonable that the fraction of plutonium fissions can be somewhat larger in a gadolinium rod with a depressed thermal neutron flux.

There is also some other data points in figure 3, which have a large quotient (Xe-131 + Xe-132)/Xe-134. The explanation of these deviations is unclear for the moment and will not be discussed here.

3.3. Ramping of refabricated rods

Figure 4 shows some examples of analysis of released gas in father rods irradiated in power reactors together with analysis of released gas in refabricated rods after test in the R2 reactor in Studsvik.

The measured compositions show that the released gas during ramp in most cases originate to larger extent from U-235 fission than gas released during base irradiation. It is evident that the release during the ramp is dominated by release from the central parts of the fuel with relatively small build-up of plutonium. The release during base irradiation should to a large extent originate from more peripheral parts of the fuel with larger build-up of plutonium.

The release during base irradiation is in all cases below 1 % except for the rod with the highest burnup (70 MWd/kgU). It is likely from the power history that most of the release occurred early during the irradiation of this rod. It is consequently logical that the released gases during the ramp originate to a larger extent from plutonium than the gases released during the base irradiation for this rod.

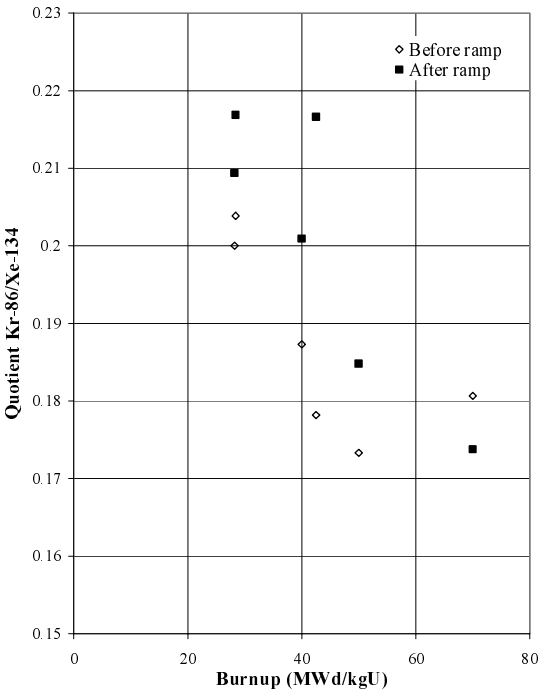

FIG. 4.Comparison between base irradiation and ramp.

4. SUMMARY

The quotient between released krypton and xenon or preferably between the isotopes Kr-86 and Xe-134 gives information about the origin of the released gases. A study of the isotopic compositions of krypton and xenon can in some cases give additional information.

Fuel rods have been irradiated in Studsvik with purposely added water. The isotopic composition of the released gases from the fuel in these rods does not correspond to the composition of the generated gases. It can be ruled out that this is due to separation of the isotopes of the inert gases. It is suggested that separation can occur due to different life times of parent nuclides in the decay chain before formation of krypton and xenon. The suggested explanation is that selenium and tellurium have faster diffusion velocities than inert gases in hyperstoichiometric uranium dioxide fuel.

Several short test rods have been refabricated from power reactor rods for tests in the Studsvik R2 reactor. In some cases gas analysis is available both from the base irradiation and from the R2 test. The fission gas compositions are in such cases different due to release at different times and from different parts of the fuel.

FISSION GAS RELEASE FROM HIGH BURNUP FUEL DURING POWER TRANSIENTS: EXPERIMENTAL DATA FOR MODELLING

R. SALOT, L. CAILLOT
Direction des Réacteurs Nucléaires, CEA, Grenoble

P. BLANPAIN, L.-C. BERNARD
FRAMATOME Nuclear Fuel, Lyon

M.-C. GRANDJEAN
EDF SEPTEN, Villeurbanne

France

Abstract

The present paper aims at presenting recent experimental programmes and results on fission gas release during power transients at high burnups obtained on French PWR fuel rods delivered by FRAMATOME Nuclear Fuel. This type of results are needed for modelling purposes, since the pressure increase due to fission gas release is one of the main limitations to burnup extension. The first experimental programme presented here consisted in power ramps performed in the Studsvik R2 reactor on four refabricated fuel rods pre-irradiated during 5 cycles in Gravelines (standard operation) and during 4 cycles in Cruas (grid regulation operation) Electricité de France (EDF) units. These ramps were undertaken with Pellet Cladding Mechanical Interaction (PCMI) analysis objectives. Given that no failure occurred on these rods, gas punctures and measures after ramps (1 to 12 hours holding time at maximum power) gave interesting global data on fission gas release for the calibration of models. The results are presented and discussed. Nevertheless, in order to develop accurate and mechanistic models, data on the fission gas release kinetics and on the gas localization in fuel are needed. With this aim, the French Atomic Energy Commission (CEA), FRAMATOME Nuclear Fuel and EDF undertook the REGATE experimental programme. This analytical programme performed in Grenoble, with SILOE reactor and LAMA hot laboratory facilities, consisted in calibrated power transients on four PWR fuel segments pre-irradiated in Gravelines unit up to 50 $GW{\cdot}d.t_M^{-1}$. The maximum power levels ranged from 290 to 390 $W.cm^{-1}$, while the holding time at power ranged from 20 minutes to 6 hours. The increment of fission gas release during transients were determined by differences between gas puncture results after re-irradiation and non destructive determination of the amount of ^{85}Kr released during PWR operation. The ^{85}Kr technique and results are presented and discussed. Elsewhere, complementary data were obtained from PIE: the precipitation in bubbles of fission gas was characterized by optical microscopy and the localization of gas in the fuel was determined using the ADAGIO technique recently developed in Grenoble. This technique allows to quantify separately the gas retention in grain and at grain boundaries.

1. INTRODUCTION

The prediction of fission gas release at high burnup in PWR fuel rods is one of the main concerns of modelling, knowing that the internal pressure increase is a limitation to burnup extension. Moreover, in the French context, this prediction must be efficient both in base irradiation and in transient conditions. This is due to the fact that EDF has to operate its nuclear power plants with grid regulation in order to adapt the production to the requirements of the electrical system. This operating mode, with subsequent power variations, has consequences on the fuel thermo-mechanical behaviour and then on the fission gas release especially at high burnup.

The EDF's calculation methodology has been developed with few fission gas release data for high burnup fuels irradiated in standard or load follow operations. Large safety margins have thus been taken, which is contradictory to EDF's operating manoeuvrability needs. In order to improve this methodology and to decrease margins an experimental programme is being conducted in the frame of a collaboration between EDF, FRAMATOME and CEA. This programme is intended to give

information about the fission gas release process during power transients for high burnup fuels. It will help to develop more accurate and mechanistic models.

The present paper aims at presenting recent results obtained in this programme on French PWR commercial fuel rods delivered by FRAGEMA. These results extend in the range of high-burnups the data base already available. The needs for code validation are achieved by:

— the use of Fission Gas Release (FGR) results from four Pellet Cladding Mechanical Interaction (PCMI) ramps performed in R2 reactor,
— five dedicated ramps in SILOE reactor: four segments (intermediate power and relatively short holding time) irradiated in the REGATE programme and one additional rod from the GONCOR programme (high power and long holding time).

Moreover, in order to go further in the development of a more mechanistic modelling of fission gas release in UO_2 fuel, a specific analytical technique was developed at the LAMA hot laboratory with the ADAGIO facility.

2. EXPERIMENTAL DATA

2.1. Studied fuels

The results reported in this paper were obtained from FRAMATOME 17 × 17 design fuel rods fabricated with standard Zircaloy-4 clad and dry route UO_2 pellets. These rods were previously irradiated 4 or 5 cycles in Cruas and Gravelines EDF 900 MWe power reactors. While the experimental rods used for the PCMI ramps were refabricated, the ones dedicated to analytical power transients (except the GONCOR rod) came from segmented rods.

During the power reactor irradiations, under typical EDF PWR normal operating conditions, the FGR was low: less than 2% for all of the rods.

Only the central intergrids of the PWR rods were used for the re-irradiation, in order to have fairly uniform axial power and burnup distributions.

2.2. Studsvik programmes and techniques

Four short rods, refabricated with the Fabrice technique from four full length fuel rods, were ramp tested in the Swedish R2 reactor at Studsvik in November 1993 and in February 1994. Three of the four full length fuel rods were irradiated to a burnup of 52 GW·d/t M and the fourth rod to 62 GW·d/t M. The objective of the programme was to establish the PCMI failure threshold.

2.2.1. Irradiation conditions

After a conditioning irradiation for about 16 hours at a linear heat rate of about 175 W/cm, the rods were ramped, at a ramp rate of about 100 W/cm/min, to a final power level in the range of 400 to 440 W/cm. For these tests the ramp rate depends on the combined influence of increase/decrease of the R2 power and decrease/increase of the He-3 pressure.

The rods were hold at their ramp terminal level from 1 hour to 12 hours with no indication of failure.

2.2.2. Post irradiation examinations

As none of the rods experienced failure during the holding, it was possible to realise FGR measurement after rod puncture. Metallography and ceramography were then performed on a cross section from each of the rods.

2.3. Analytical programmes and techniques

Five analytical power transients were conducted in the SILOE experimental reactor at CEA-Grenoble. Four of them were part of the REGATE experimental programme and the last one, named GONCOR, was more specifically dedicated to the study of fuel swelling due to fission gases [1]. The burnup the rods irradiated four cycles in PWR was close to 50 GW·d/t M. On each rod, standard Post Irradiation Examination were performed.

2.3.1. Irradiation conditions

The power transients were performed in nucleate boiling irradiation rigs which allow to obtain typical PWR conditions (coolant pressure and external temperature of the cladding). The irradiation power is adjusted by varying the distance of the rig from the SILOE core. Due to the height of the core (~0.6 m), the power profile depends on the length of the rod. As the GONCOR rod is relatively short (~0.2 m), the ratio average power/maximal power (P_{av}/P_{max}) is equal to 1. This is not the case in the REGATE programme, the total fuel length is ~0.44 m leading to values of P_{av}/P_{max} of 0.9 and P_{min}/P_{max} of 0.65.

For the different REGATE rods, the irradiation histories are similar and presented in Figure 1. Concerning GONCOR, the first plateau was performed at 250 W/cm and the power increase was faster (50 W/cm/mn). The irradiation was stopped at the end of the plateau at P_{max} (6 days at 400 W/cm).

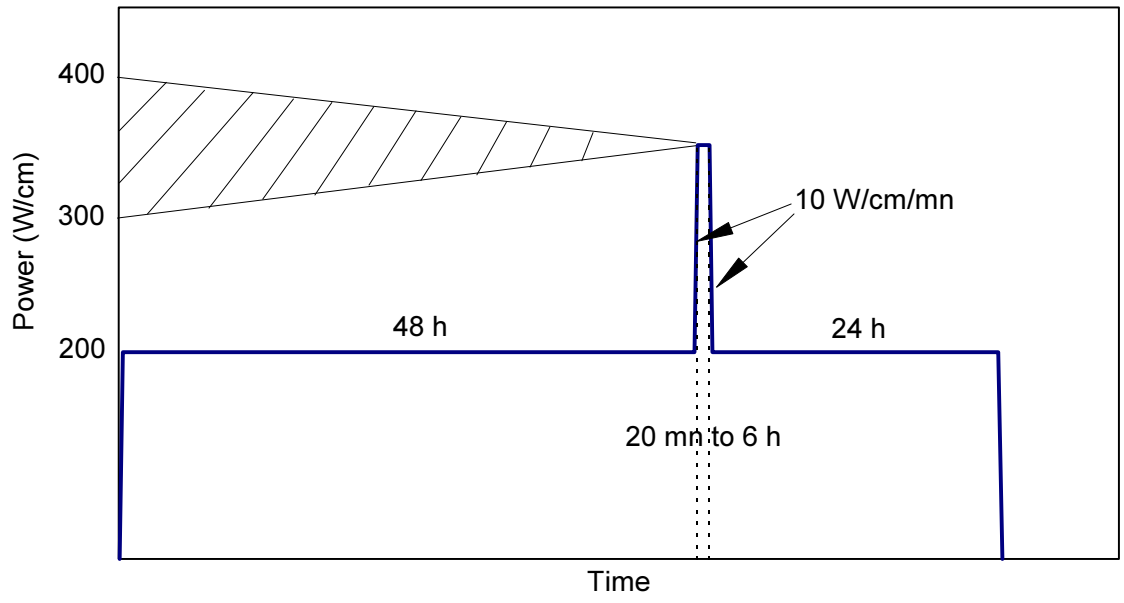

FIG. 1. Irradiation histories of the REGATE segments in SILOE reactor.

2.3.2. FGR measurements

One of the main interest of the REGATE rods is that they come from segmented rods. The absence of refabrication means that the atmosphere and the chemical conditions inside the rods are not modified for the re-irradiation. As a consequence, no puncture of fission gas is possible between steady state irradiation and power transients. In order to get round this difficulty, a non destructive FGR determination based on ^{85}Kr activity measurements was developed. ^{85}Kr is the only long life radioactive fission gas (10.71 year).

The points which make the measurement difficult are:

— the fission yield of ^{85}Kr is relatively low. Due to the burnup of REGATE rods, the ratio $^{85}Kr/(\Sigma$ stable gases) is about 0.5%.

— the decay of ^{85}Kr is only accompanied by the emission of 0.44 γ (514 keV) per 100 disintegrations.

Moreover, this ray interferes with:

1) the annihilation peak (511 keV) which results from the recombination of one e^+/e^- pair created by β^+ and β^- disintegration ($e^+ + e^- \rightarrow$ two 511 keV photons),

2) the 512 keV peak induced by the decay of ^{106}Rh

3) continuous distribution due to Compton scattering. In the plenum of a PWR rod, presence of Co in the spring gives rise to a strong activity through 1173 and 1332 keV gamma radiation. That is the reason why most of the published results on non destructive ^{85}Kr measurement are obtained on fuel rods designed with a special plenum (without spring) allowing to reduce the ratio ^{85}Kr signal/background signal. The REGATE rods were not designed with such a plenum which constituted an additional difficulty.

The measurements were performed with a high purity Ge detector. The characteristics of the γ spectrometry line and of the acquisitions were optimized in order to improve the 514 keV peak resolution and enhance its deconvolution:

- collimator width 0.5 x 1.7 mm
- long acquisition times (duration 50000s)
- time constant of the amplifier is 4 μs instead of 0.25 μs used for quantitative γ spectrometry on fuel pellets. This adjustment is possible because of the low count rate.
- increase of the energy resolution (0.25 keV/channel)

The absolute calibration of the spectrometry line is based on the measurement of a ^{152}Eu source and a γ attenuation calculation. The ratio (volume of the zone measured by γ spectrometry) / (free volume of the rod) is evaluated thanks to rod fabrication data coupled with non destructive examinations (metrology, X ray radiography). The quantity of ^{85}Kr produced during the irradiation results from a calculation of the PF evolution and a quantitative γ spectrometry of the fuel.

The technique was qualified by comparison with usual measurements (gamma spectrometry and gaseous chromatography after puncture of the rod) different segments of the REGATE programme (see below).

2.4. FGR measurement results

The FGR measurement results during PCMI ramps and analytical power transients are presented on Tables I and II and summarized in Figure 2.

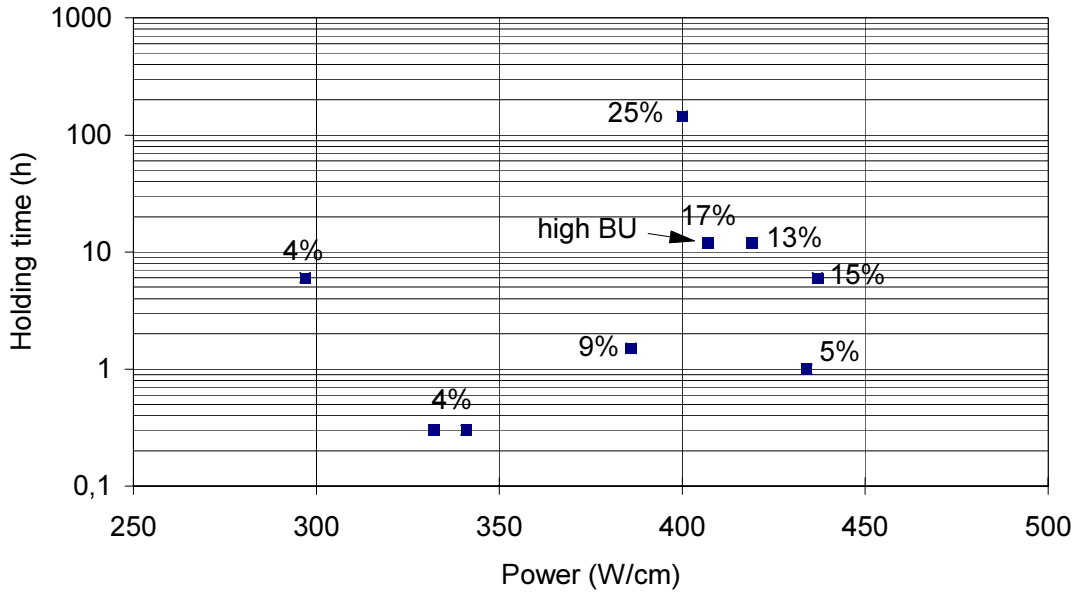

FIG. 2. FGR for different transient powers and holding times.

TABLE I. FGR AFTER PCMI RAMPS

Rod	Burnup (GW·d/t M)	$P_{max\ ramp}$ (W/cm)	Holding time (h)	FGR after power transient (%)
S1	52.5	419	12	12.9
S2	52.8	437	6	14.9
S3	52.4	434	1	5.2
S4	62.8	407	12	16.8

TABLE II. FGR AFTER PWR IRRADIATION AND POWER TRANSIENT FOR REGATE AND GONCOR RODS

Segment	Type of measurement	FGR after PWR irradiation (%)	$P_{transient}$ (W/cm)	Holding time	FGR after power transient (%)
R0	^{85}Kr in plenum	1,7	/	/	/
	After rod puncture	2,1			/
R1	^{85}Kr in plenum	1,2	297	6 h	4,5
	After rod puncture				5,0
R2	^{85}Kr in plenum	1,5	332	20 mn	5,5
	After rod puncture				5,7
R3	^{85}Kr in plenum	1,3	341	20 mn	3,9
	After rod puncture				5,1
R4	^{85}Kr in plenum	1,6	386	1h30	9,3
	After rod puncture	t65566611			10,2
G	After rod puncture		400	6 days	25

First, the REGATE results allow to validate the non destructive ^{85}Kr measurement technique. An acceptable agreement is observed between the non destructive ^{85}Kr measurement and the other techniques prior to and after power transient. The error (3σ) on the results with this technique is estimated to be ±15%. It is mainly due to the deconvolution of the 514 keV peak and to the fact that the measured volume is very small compared to the free volume (~2%).

Then, information on the influence of irradiation parameters can be obtained. In a qualitative way, the tendency of FGR values is consistent with the irradiation histories (transient power and holding time) even if a direct comparison is difficult because a few experimental parameters may differ: burnup, rod length, axial power distribution, neutron flux spectrum, initial atmosphere of the rod (segment or refabricated rod). The effect of several physical parameters can be focused through these data.

2.4.1. Effect of burnup

It is illustrated by the difference between S1 and S4 as shown on Table I. Both rods have the same holding time (12h) and very close peak powers but the burnup of S4 is greater by about 10 GW·d/t M. The higher gas release of S4 is quite understandable. There is a large consensus that transient fission gas release is an addition of a burst effect and a diffusional effect. At higher burnups, the amount of gas available at grain boundaries is increased and can then be released at the beginning of the transient. Moreover, it is largely acknowledged that there is a degradation of pellet thermal conductivity with burnup. Hence, at a given power level, the pellet central temperature and the fission gas release increase with burnup.

2.4.2. Effect of holding time

The effect of holding time is emphasized by direct comparisons between the results of different rods (S2-S3, R1-R3 and R4-G).

Rods S2 and S3 exhibit very different FGR (5 and 15%) while they were irradiated at the same power (about 435 W/cm) but with different holding times (1 and 6 hours). On the contrary, rods R1 and R3 released the same fraction of gas (5%) while their transient powers were significantly different (300 and 340 W/cm). The effect of the temperature on FGR appears to be compensated by the holding time (20 minutes and 6 hours).

The influence of holding time is more pronounced in the case of the G rod compared to R4. Indeed, 25% of gas was released for the G rod against only 8.5% for R4 (during the power transient). Nevertheless, the direct comparison between these values is difficult since the G rod was shorter and consequently had a constant power along all the rod during the re-irradiation.

3. FGR RESULTS ANALYSIS AND COMPLEMENTARY CHARACTERIZATIONS

3.1 Code validation

The parametric experiments yield a data base on FGR in a wide range of burnup, power increase and transient duration. As a consequence, these results are very useful for the global calibration of models. Figure 3 shows the comparison between measured FGR and the FGR predicted with the COPERNIC code developed at FRAMATOME [2].

If the global FGR results are of main interest for the global code validation, some intermediary data on the behaviour of fission gas are required to support development of mechanistic modelling on FGR. These models aim at describing FGR as an assembly of several phenomena involving elementary mechanisms with associated physical constants:

- gas migration in the fuel grains (atomic diffusion/bubble migration),
- intergranular retention which plays a major role since it leads to a threshold in FGR corresponding to stable escape paths formation (tunnels).

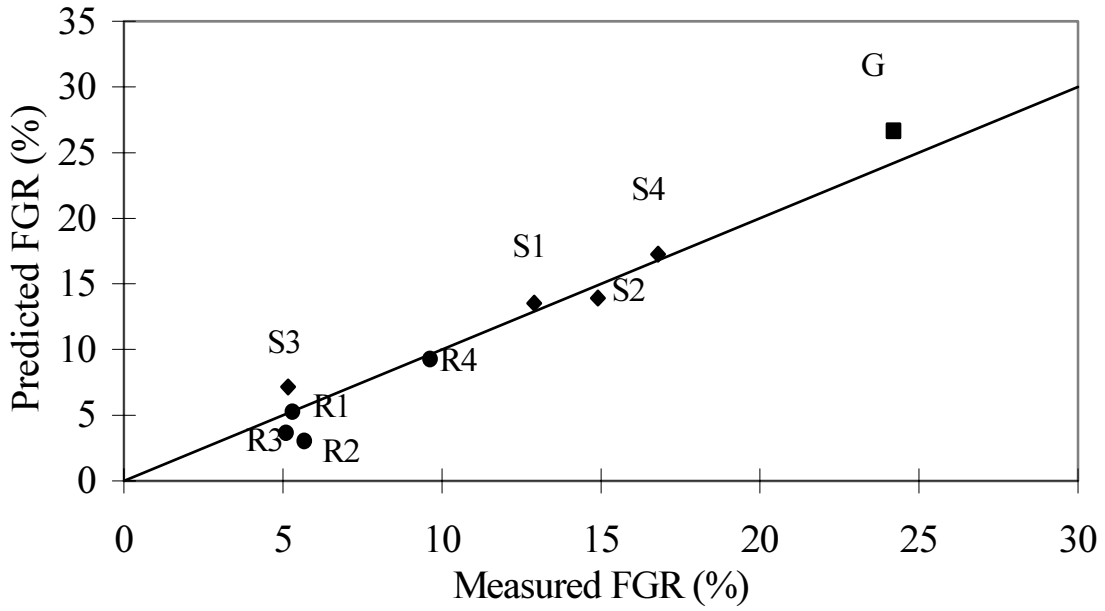

FIG. 3. Validation of the COPERNIC [2] FGR model with PCMI ramps and analytical power transients.

With the purpose of obtaining intermediary results for calibration of elementary phenomena, complementary characterizations were performed:

- microstructural evolutions were analysed through optical microscopy examinations in order to determine the zone affected by gas precipitation,
- a new technique was developed in order to obtain the grain boundary and intragranular gas fission inventories and their thermal dependency. These data are expected to allow separate adjustment of time constants for gas migration and grain retention capability.

3.2. Analysis of FGR results through microstructural evolution

Effects of burnup and holding time were presented in paragraph 2.4. through comparisons between FGR results. Their influence on microstructural evolution was also examined.

The first point that was analysed is the radius of the intragranular bubbles precipitation zone. The value of the $r_{nucleation}$ /r_{pellet} ratio increases with the irradiation power (Cf. Table III). It appears to be independent on the holding time (for a duration higher than 20 min) and directly linked to the temperature (at constant burnup). In the range of considered burnup, intergranular bubbles are observed for temperatures above 1000°C.

TABLE III. INFLUENCE OF THE TRANSIENT POWER ON THE INTRAGRANULAR PRECIPITATION ZONE

Rod	$P_{transient}$ (W/cm)	$r_{precipitation}/r_{pellet}$
R1	297	0.52
R3	341	0.58
R4	386	0.72
G	400	0.73

The phenomenon is different in the case of intergranular precipitation. Indeed, while in the case of G rod intergranular bubbles are observed for $r/r_0 < 0.73$, it is only the case for $r/r_0 = 0.52$ on R4. The size and interconnection of these bubbles are also greatly influenced by holding time (Cf. Figure 4). Escape paths are thus more developed in the G rod which leads to a higher FGR. It can also be noticed that intragranular bubbles seem to be reduced in the G rod. This phenomenon could provide an additional contribution to the FGR.

Concerning R1 and R3, intra and intergranular bubbles are observed in the central region for each rod (Cf. Figure 5). Strings of intergranular bubbles appear to be slightly more developed in the case of R1. As the FGR is directly linked with the evolution of bubble morphology and interlinkage, the 5% gas release is consistent with the microstructural observations.

3.3. Quantitative characterizations of microstructural evolution: the ADAGIO technique

Knowledge of the grain-boundary fission gas inventory, and its radial variations, has been identified as a data of major interest. A new technique called ADAGIO [3], and based on previous work of AECL on CANDU fuel [4–5], was developed at the LAMA hot laboratory of the CEA-Grenoble. Such a technique allows to obtain additional data to those resulting from Electron Probe Micro-Analysis (EPMA) or X Ray Fluorescence (XRF) examinations. Fuel can be studied either after steady state irradiation, power transient or off-normal conditions irradiation (RIA test for instance). An ADAGIO experiment requires:

- a re-irradiation in an experimental reactor, at low temperature and under inert atmosphere, in order to create short half-life fission products distributed throughout the fuel matrix. Since the temperature is low, the newly generated fission product tracers do not migrate and are located within the grains of the matrix,

- a core-sampling by ultra-sonic drilling in fuel rod slices. This operation is difficult due to the fragmentation of the pellet. But it must be as accurate as possible in order to obtain well located samples in zone irradiated with homogeneous conditions (burnup and temperature),

a heat treatment under air at low temperature in order to release the part of the gas located at the grain boundaries. Indeed, preferential oxidation occurs along grain boundaries. The UO_2 to U_3O_8 transformation leads to a swelling and then to the opening of the grain boundaries. After this step, temperature is increased (up to 1400°C) to release the complete inventory of fission gases, — monitoring of the gases by on-line gamma spectrometry. The short life radioactive gases (^{133}Xe), created within the grains during the re-irradiation, are the tracers of the intragranular gases. Comparisons between ^{85}Kr (long life, concentration and location non affected by the re-irradiation) and ^{133}Xe leads to the determination of the fraction of gas located at the grain boundaries.

This technique was used at CEA-Grenoble for the first time on the R4 segment. A length of 3 pellets was cut in the maximal flux zone (local FGR > 10%). Measurements on samples with different sizes (internal region with $\phi < 3$ mm and $\phi < 6.5$ mm, external region with $\phi > 6.5$ mm) were performed (Cf. Figure 6). The main results are presented in Table IV:

- in the central zone, about 50% of the gas was released during the irradiation (steady state + power transient). 80% of the remaining gas is present at the grain boundaries (Cf. Figure 7a),
- in the peripheral zone, only about 10% of the gas is at the grain boundaries (Cf. Figure 7b).

These results prove the efficiency of the technique to determine locally the inter/intragranular distribution of the fission gases and the FGR. They are consistent with the observed microstructure and with the global FGR of R4 (10%).

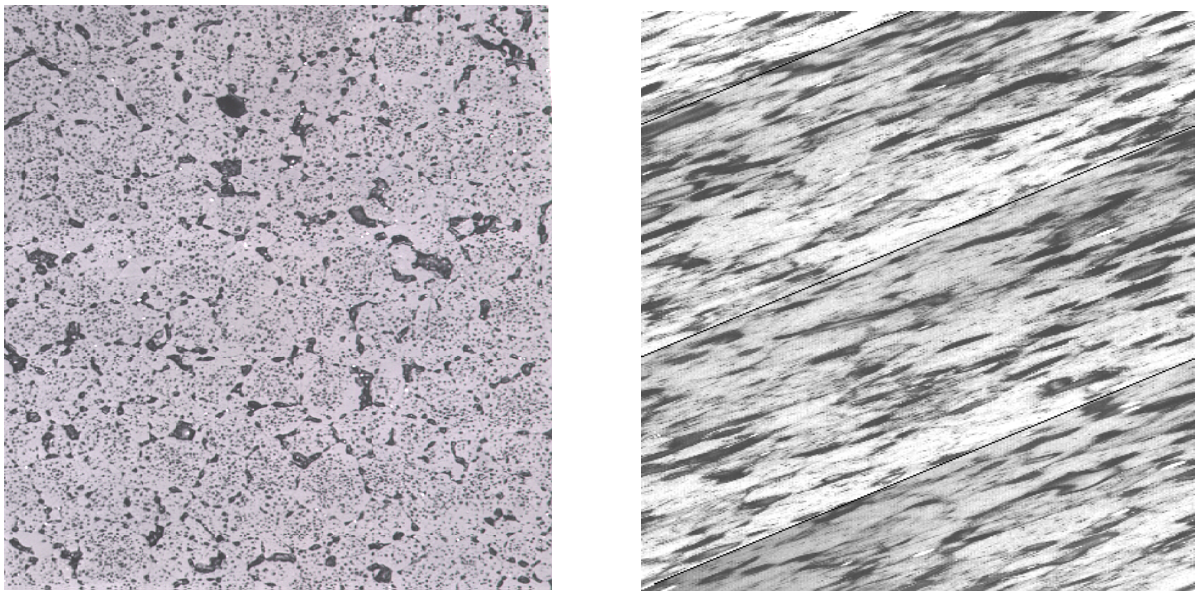

FIG. 4. Microstructure in the center region of (a) R4 irradiated 1h30 at 386 W/cm and (b) G irradiated 6 days at 400 W/cm.

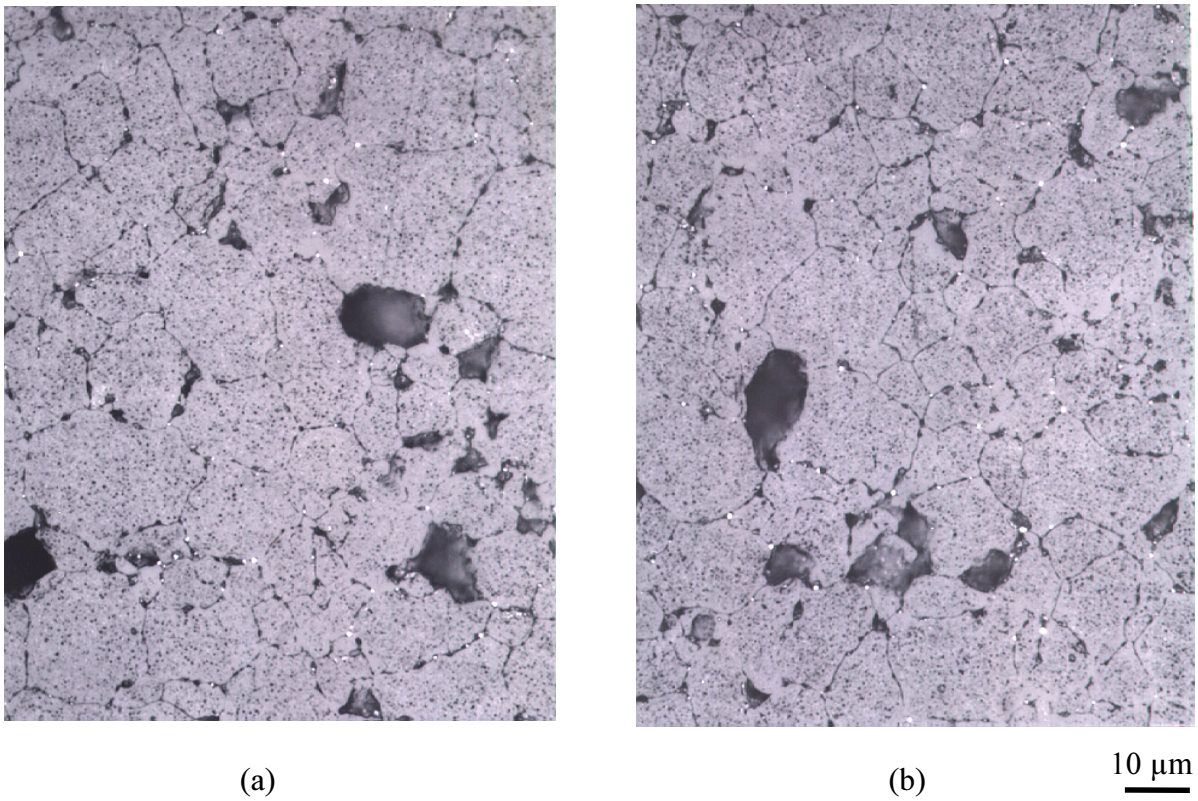

FIG. 5. Microstructure in the centre region of (a) R1 irradiated 6 hours at 297 W/cm *and (b) R3 irradiated 20 minutes at341* W/*cm.*

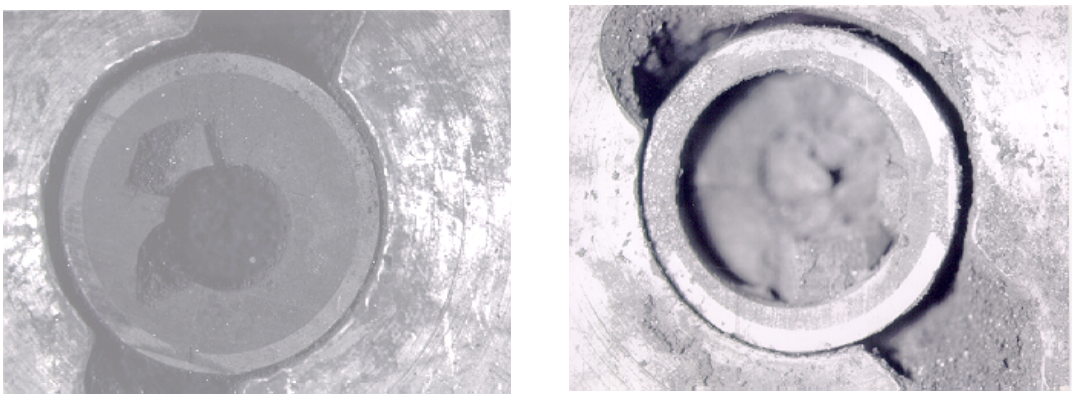

(a) (b)

FIG. 6. Aspect of the pellet after drilling (a) of the centre region (b) of the medium region.

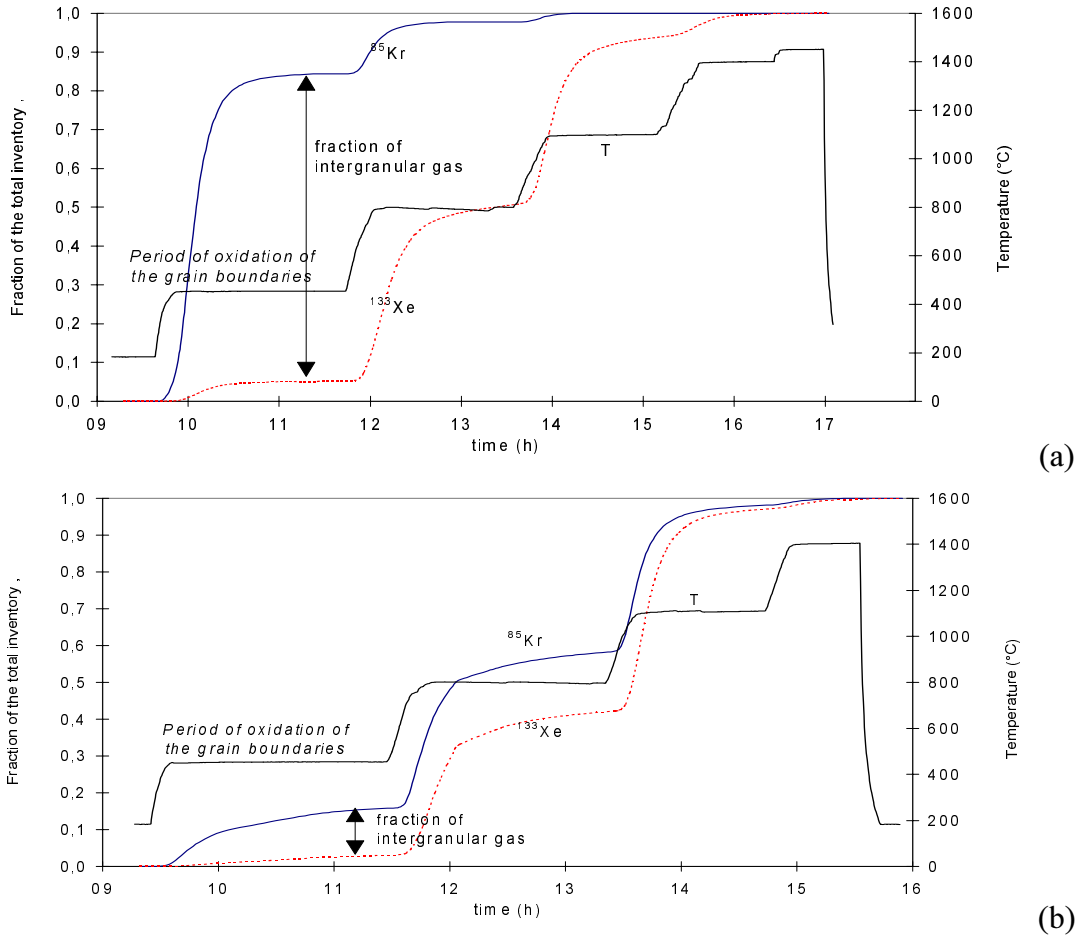

FIG. 7. ^{133}Xe and ^{85}Kr release in the centre (a) and peripheral (b) regions of R4 during the ADAGIO experiment.

4. CONCLUSION

The results of the different experimental programmes presented in this paper constitute a complete database for the validation of FGR codes for high burnup fuels. Indeed, a large range of data is covered: burnup (50–60 GW·d/t M), power (300–440 W/cm), holding time (20mn–6days). Nevertheless, further progress in modelling of the phenomena still implies more accurate data concerning the fission gases behaviour in the fuel and the release kinetics. The ADAGIO facility gives the opportunity to obtain local quantitative results on the repartition of the fission gases in the fuel.

ACKNOWLEDGEMENTS

The authors would like to acknowledge G. DELETTE, T. PETIT, S. RAVEL and J. P. PIRON for their fruitful discussions.

REFERENCES

[1] GARCIA, P., et al., "The effect of fission gas swelling on cladding strains during power ramp test", this conference.

[2] BONNAUD, E., et al., "COPERNIC: a state of the art fuel rod performance code", ANS Winter Meeting, Albuquerque, N.M., U.S.A., 1997.

[3] RAVEL, S., et al., "Partition of grain boundary and matrix gas inventories in nuclear fuel: The Adagio facility", To be presented at the European Hot Laboratory and Remote Handling Working Group Meeting, Windscale, September 1998.

[4] HUNT, C.E.L., et al., "Fission Product Grain Boundary Inventory", Canadian Nuclear Society, 10th Annual Conference, June 1989.

[5] HELDER, P.H., et al., "New post-irradiation examination techniques at Chalk River laboratories: gamma tomography and grain boundary inventory measurements on irradiated fuels", IAEA Technical Committee Meeting on "Recent developments on post-irradiation techniques for water reactor fuels", Cadarache, 17–21 October 1994.

PIE OF TEST ASSEMBLY OF QINSHAN NUCLEAR POWER PLANT

M. RAN, J. YAN, S. WANG
China Institute of Atomic Energy,
Beijing, China

Abstract

The small dimensional test fuel assembly (3x3-2) for the Qinshan Nuclear Power Plant was irradiated up to 25.7 Gwd/tU in the in-pile loop (15.5 Mpa,320 C) in Heavy Water Research Reactor (HWRR), CIAE, at simulative condition to Qinshan PWR normal and short time overpower operation for verifying the design, technology, and material properties of the fuel assembly. Comprehensive post-irradiation examination (PIE) including dimension measurement, gamma scanning, eddy current test, X ray, radiography, measurement of fission gas release, and quantitative metallography etc. were performed. PIE results show that the diameter of the fuel rods changed, ridges appeared on the cladding, pellets swelled, and the rate of fission gas release was higher than what we expected. The results would be an important basis for further improvement of design, technology and material properties for Qinshan PWR assembly.

1. INTRODUCTION

The Qinshan Nuclear Power Plant is the first PWR nuclear power plant designed and built in our country. In order to test and verify the design and manufacture techniques, 3x3-2 assembly was tested in high temperature and high pressure in-pile loop in HWRR in CIAE. When the assembly reached an average burnup of 25.7 Gwd/tU, it was transferred to the hot cells and PIE was carried out there.

This paper will introduce some results of examination.

2. TEST ASSEMBLY AND PARAMETERS

The test assembly composed of 7 fuel rods and 2 control rods (Fig. 1), three grids were point welded to the guide tubes of the control rod. Average burnup of the assembly is 25.7 Gwd/tU, Average burnup of each fuel rod is between 19 and 27 Gwd/tU (see Table I).

Fuel rod: length 1146 mm, ϕ 10 mm
$U0_2$ pellet: 10x ϕ 8.43 mm
Zr-4 cladding: wall thickness 0.7 mm, ϕ 10 mm
The maximum neutron flux for Zr-4 cladding is $9.4 \times 10^{20} n.cm^{-2}$ (E>1Mev).

TABLE I. BURNUP VALUE OF THE FUEL RODS (Unit: Mwd/tU)

Fuel rod	2”	3”	4”	5”	6”	7”	8”
Average burnup	24900	27323	25607	18813	25979	27407	24625
Maximum burnup	30876	33881	31753	23328	32214	33984	30622

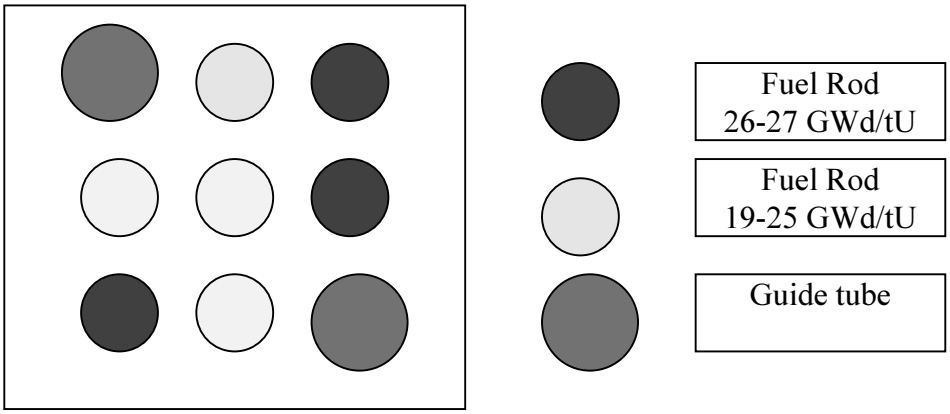

FIG. 1. 3x3-2 small test assembly.

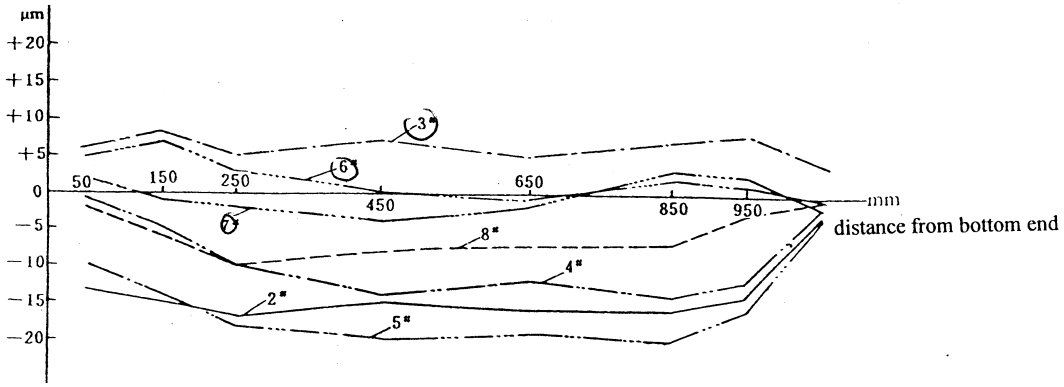

FIG. 2. Dimension measurement results.

3. RESULTS AND DISCUSSION

In this section, the test results are introduced in three parts.

3.1. Non-destructive examination

According to the test results of dimension measurements, the diameter of the fuel rod with higher burnup (26-27 Gwd/tU for rod $3^{\#}$,$6^{\#}$,$7^{\#}$) is similar to the original data, and those with lower burnup (19-25 Gwd/tU for rod $2^{\#}$,$4^{\#}$,$5^{\#}$, $8^{\#}$) is little lower than the original data (see Fig. 2). Both dimension measurement and eddy current test showed that ridges occurred on each fuel rod, the ridge height is 3~8 μm, the maximum one is 10 μm (see Fig. 3), which indicates that cladding creep down took place under the lower burnup and that pellet swelling, leading to cladding expansion PCMI and ridges appearance, took place under the higher burnup.

Relative burnup distribution measured by gamma scanning was basically corresponding to the calculated value.

No through-wall defect in the fuel rods was found by the eddy current test.

The gap between cladding and pellets became narrower and some pellets stuck to the cladding tube, especially in the middle part of the fuel rods. Dishes between pellets in the higher burnup fuel rods changed apparently (see Fig. 4). From Figure 4, photos of X ray photography, we can see that dish gap of higher burnup fuel rod ($7^{\#}$) changed more than that of the lower burnup one ($5^{\#}$) at the same axial position.

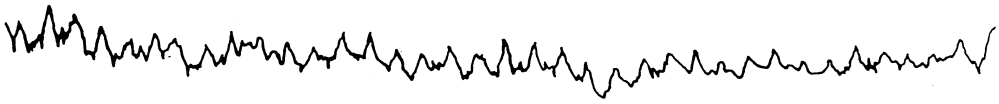

FIG.3. Ridge curve of rod 7# in the middle part.

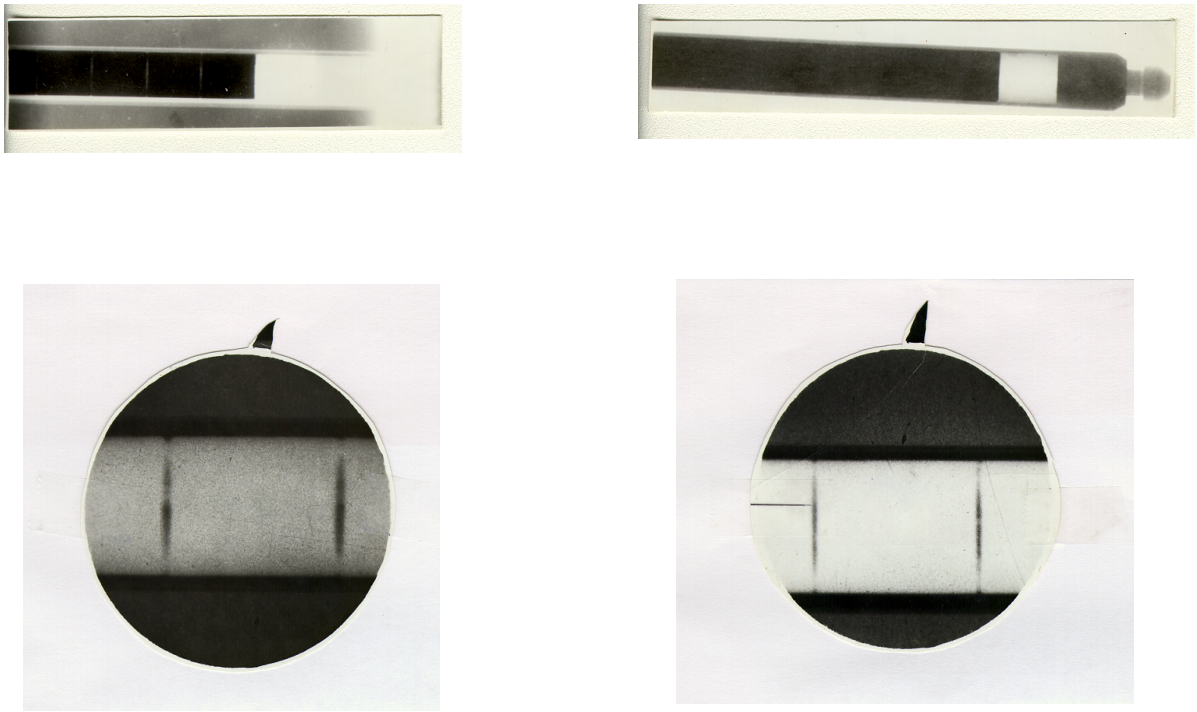

rod 5# *rod 7#*

FIG. 4. X ray radiography test results.

3.2. Fission gas measurement.

By the fission gas measurement, we get the following results: (1) The higher the burnup, the higher the release rate of fission gas. (2) The pressure inside the fuel rods increases with the release rate of fission gas. Nevertheless, the release rate of fission gas is 10%-23% which is much higher than expected. This result is due to the higher linear power of fuel rod (43.0~46.0 kw/m) and 104 power cycles, two times of the ramp test during irradiation.

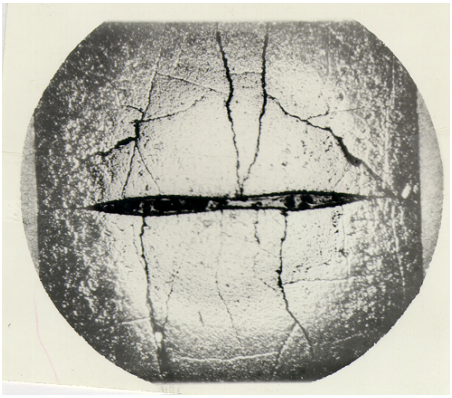

FIG. 5. Dish gap between pellets (rod 7#).

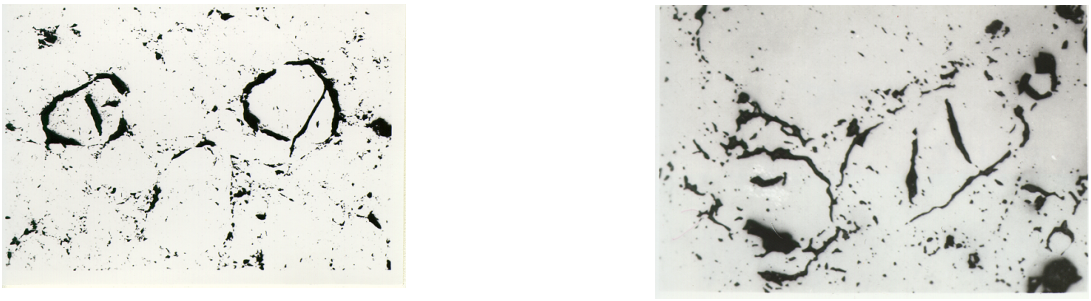

Pre-irradiation *Post-irradiation*

FIG.6. Cracks on the particle boundary of UO_2 pellet (rod $7^{\#}$).

3.3. Destructive examination

After irradiation, dish gap decreased to 0.27~0.47mm from the original 0.7 mm (see Fig. 5), which means that the central height of pellets increased by 2.5%~4.6% (height of pellet was 10 mm).

Metallographic examination [3] showed that there are cracks on the particle boundary of $U0_2$ pellet, which already existed before irradiation. These are the channels which are favourable for fission gas release and unfavourable for irradiation behaviour of the pellet (see Fig. 6). Thus, those cracks should be avoided during pellet manufacture.

Because the central temperature of the fuel rod is very high, it is easy for fission gases to coalesce and immigrate from crystal center to its boundary. It is apparent that when the central temperature of $U0_2$ is at that of equiaxial growth (above 1500°C), pellet swells and leads to dish gap decreasing, PCMI, and ridges appearance.

4. CONCLUSION

PIE results showed that the fuel rods maintained integrity up to 25 Gwd/tU. cladding creep down, PCMI, and pellet swelling took place during irradiation which depend on operation history and depth of burnup. The main causes of the higher release rate of fission gas are higher liner power, frequent power cycles, ramp tests during irradiation and existing particle boundaries of the pellet.

REFERENCES

[1] S.R.WANG, Symposium on the Irradiation and Corrosion Behaviour of Fuel and Pellet of Power Reactor, Beijing, 1989, p. 131.

[2] J.H.LUO, Symposium on the Irradiation and Corrosion Behaviour of Fuel and Pellet of Power Reactor, Beijing,1989, p.170.

[3] D.G.PAN, Symposium on the Irradiation and Corrosion Behaviour of Fuel and Pellet of Power Reactor, Beijing, 1989, p. 202.

BEHAVIOUR OF HIGH O/U FUEL[*]

J.H. DAVIES, E.V. HOSHI, D.L. ZIMMERMAN
GE Nuclear Energy,
Vallecitos Nuclear Center,
California, United States of America

Summary

The effect of increased fuel oxygen potential on fuel behaviour has been studied by fabricating and irradiating urania fuel with an average O/U ratio of 2.05.

The fuel was fabricated by re-sintering standard urania pellets in a controlled oxygen potential environment and irradiated in a segmented rod bundle in a U.S. BWR. Preirradiation ceramographic characterization of the pellets revealed the well-known Widmanstätten precipitation of U-409 platelets in the $U0_2$ matrix.

The high O/U fuel pellets were clad in Zircaloy-2 and irradiated to over 20 GWd/MT. Ramp tests were performed in a test reactor and detailed postirradiation examinations of both ramped and nonramped rods have been performed. The cladding inner surface condition, fission gas release and swelling behavior of high 0/U fuel have been characterized and compared with standard UO_2 pellets.

Although fuel microstructural features in ramp-tested high O/U fuel showed evidence of higher fuel temperatures and/or enhanced transport processes, fission gas release to the fuel rod free space was less than for similarly tested standard UO_2 fuel. However, fuel swelling and cladding strains were significantly greater. In spite of high cladding strains, PCI crack propagation was inhibited in the high O/U fuel l rods. Evidence is presented that the crystallographically oriented etch features often noted in peripheral regions of high burnup fuels are not an indication of higher oxides of uranium.

[*] The full paper of this presentation has been published in the Journal of Nuclear Materials, Vol. 270 (1999), 87-95.

SWELLING AND PCMI
(Session 2)

Chairpersons

F. SONTHEIMER
Germany

P. RUDLING
Sweden

THE EFFECT OF FISSION GAS SWELLING ON CLADDING STRAIN DURING POWER RAMP TESTS

Ph. GARCIA, C. STRUZIK, M. AGARD-MOYNE
Commissariat à l'énergie atomique,
Centre d'études de Cadarache,
Saint-Paul-lez-Durance, France

Abstract

The ultimate aim of most fuel performance codes is to determine the operating conditions under which a fuel rod runs no risk of failing. Off-normal operating conditions can lead to pellet cladding interaction (PCI), which may in turn lead to cladding failure, the immediate cause of which has been identified as stress corrosion cracking. However, it is reasonable to assume that predicting the risk of failure requires an accurate description of the amplitude and kinetics of PCI induced cladding strains. The purpose of this paper is to review and validate the modelling hypotheses implemented within the framework of the METEOR/TRANSURANUS fuel behaviour code by assessing calculation results against a set of relevant experimental data. Our purpose is also to show how the analysis of the calculations performed can help understand and quantify the contribution to overall cladding strains of elementary physical mechanisms such as fission gas swelling (FGS). How these elementary phenomena interact is also discussed. The experimental data upon which this analysis is based has been generated from power ramp tests performed in the OSIRIS test reactor at CEA/Saclay. These tests were carried out on segmented fuel rods initially base irradiated in an Electricité de France (EDF) commercial power reactor over a two cycle period (equivalent to approximately 22.0GWd/Mt). The maximum power and hold times at maximum power constitute the main differences from one power ramp to another. Pre and post ramp cladding diameter measurements along with extensive post irradiation examinations (PIE), such as optical micrographs, make up most of the experimental data generated. Ramp tests carried out in the SILOE test reactor in Grenoble, which provide in-pile cladding diameter measurements, also prove to be of invaluable use in assessing our fuel rod modelling and thus interpreting the experiment. A ramp test performed at Studsvik on a MOX fuel rod is also presented. Our interpretation of tests results are used to show how the modelling of transient fuel rod behaviour can be improved.

1. INTRODUCTION

Stress corrosion cracking as a result of pellet cladding interaction (PCI) in pressurized water reactors (PWRs) has, for many years now, been identified as a possible cause of cladding failure [1]. This has triggered the need for computational tools capable of assessing the operating conditions under which a fuel rod runs no risk of failing. One of the main objectives at CEA, is to design a tool which is both predictive and a help in circumscribing, understanding and quantifying the physical processes which are relevant to PCI. It is with these general objectives in mind that the METEOR/TRANSURANUS code is being developed.

As regards PCI, the aim is to qualify the code against data generated through extensive programmes carried out in CEA test reactors (Siloë [2] and Osiris [3,4]). A close comparison of computed and experimental cladding strains (generated over as wide a range of operating conditions as possible) is viewed as essential in assessing the code's overall performance under PCI conditions. An interpretation of a power ramp performed at Studsvik on a MOX type fuel is also included. Post irradiation examinations (PIE) are used when available, either to further qualify code models, or to interpret a given power ramp test. The adopted strategy is to develop and implant models which are as mechanistic as possible but that do not undermine other aspects pertaining to code performance such as numerical stability and run-time constraints, areas which are treated with the utmost care.

The subject matter of this paper concerns the modelling of power transients with the METEOR/ TRANSURANUS fuel behaviour code. Our aim is also, through model calculations, to quantify the elementary processes relevant to PCI conditions.

The paper comprises a description of the experimental data against which the assessment is performed. The models that affect calculations mostly, i.e. the fuel and cladding mechanical behaviour and transient fission gas behaviour models, are described in part 3. Part 4 addresses the teachings to be drawn from the assessment exercise (e.g. the amplitude and kinetics of FGS and its effect on cladding strains). Finally suggestions are made to improve our modelling and experimental knowledge of transient fuel rod behaviour which paves the way for a more mechanistic and predictive approach to PCI.

2. EXPERIMENTAL DATA

The test cases presented in this paper make up only part of the power ramps used to validate the code under PCI conditions. Ramp and base irradiation conditions are reported in Table I for all six cases presented here.

TABLE I

	Case 1	Case 2	Case 3	Case 4	Case 5	Case 1
Burnup GWd/Mt	26.2	26	26.9	27	30.5	49.7
Base irradiation power			<250 W/cm			

	Case 1	Case 2	Case 3	Case 4	Case 5	Case 6
Pre-ramp power level W/cm			200–250			254
Pre-ramp hold time hours			12–14			23
Ramp rate W/cm/mn			100			50
Maximum power level W/cm			410–480			400
Hold time	Short	Short	Long	Short	Long	6 days

short: less than 30 mins
long: around 12 Hours

As mentioned above, an extensive set of power ramp tests were performed in the OSIRIS test reactor on refabricated fuel rods (approximately 350 mm long) and initially irradiated over a two cycle period in a power reactor. Four of these cases are discussed here to cover a range of linear heat generation rates and hold times at maximum power. The steady state irradiation of fuel rods from cases 1 through 4 are all comparable, which makes it easier to draw conclusions from ramp test results.

The main experimental results consist of pre and post ramp cladding diameter measurements and optical micrographs.

The fifth case pertains to a power ramp performed at Studsvik, and base irradiated in an EDF power reactor to approximately 30GWd/Mt. This ramp was included for two reasons. Firstly because it extends the validation data base of the code to MOX fuels, and also because the experimental data include in pile cladding length measurements and extensive microprobe examinations, all of which can be used to assess how accurately the code models PCI and related phenomena.

The sixth case studied involves a fuel rod initially irradiated over a four cycle period which reached a local burnup of approximately 48GWd/Mt. A section of the fuel rod was subsequently re-fabricated and ramped in the Siloë test reactor. This experiment was designed to quantify the effect of high burnup fission gas induced fuel swelling and release. It is alluded to, both because it extends the burnup range over which the code is validated and because it was performed in a DECOR type experimental rig [5] which provides continuous in-pile cladding diameter measurements that span the whole length of the re-fabricated rod. As is shown below, this information is used to validate the modelling hypotheses and quantify the phenomena which occur during the ramp.

3. MODELLING ASSUMPTIONS

3.1. Introduction

The aim of this section is to review the models, (i.e. the fuel rod mechanical behaviour model and the transient fission gas behaviour model), which affect our computation of ramps mostly. They are essential to power ramp calculations because they describe phenomena that are of first order importance. Also, both models interact since the fuel rod mechanical model is used to generate a realistic stress distribution in the pellet. This is necessary when calculating other notoriously stress dependent phenomena such as fuel creep and FGS.

This section comprises a concise description of the fuel rod mechanical model, extensively presented in reference [6], and a concise description of the transient fission gas behaviour model.

3.2. Mechanical modelling

3.2.1. Introduction

The mechanical description used in all METEOR/TRANSURANUS calculations presented in this paper is based on the assumptions widely applied to mono-dimensional fuel performance applications [7]. The fuel rod is considered as a stack of axial slices for which an axi-symmetric, isotropic and ‘generalized’ plane strain analysis is performed, the immediate consequence of which is that at any given point in the structure the stress and strain components that remain are those in the r, q and z directions (i.e. the principal axes of stress).

3.2.2. Fuel cracking

The novelty of the mechanical model applied lies essentially in its treatment of fuel cracking. Fuel cracking is an efficient means of stress relaxation, which is thought to occur at linear heat generation rates as low as 60W/cm [8] when, because of the temperature gradient in the fuel pellet, the low temperature, brittle fuel periphery is loaded in tension. The model describes radial and axial cracks that appear as a result of the hoop or axial stresses exceeding the assumed fuel fracture stress. In a given slice, the fuel pellet is divided into meshes over which the mechanical properties are assumed to remain constant. Each mesh may take on four distinct crack related states, i.e. uncracked, radial crack open and axial crack closed, axial crack open and radial crack closed, radial and axial cracks open.

In reference [6], it is shown that each mesh state is governed by a single differential equation. The state of each mesh may change in the course of the computation according to the values of stresses and strains in that mesh.

3.2.3. Fuel and cladding creep

Fuel and cladding creep are both modelled and treated implicitly. However, an iterative scheme is applied so as to converge over a time step on a value of $\dot{\varepsilon}/s_e$, where $\dot{\varepsilon}$ is the creep rate and s_e the Von Mises stress. Furthermore, the user has the choice of describing the effects of high creep rates, by forcing a mesh into a hydrostatic state of stress. This condition defines a fifth possible state for a fuel mesh, governed by a corresponding differential equation.

3.3. Transient fission gas modelling

3.3.1. Introduction

Describing how fission gases behave is also essential to any detailed understanding of how a fuel rod is loaded in the course of its irradiation history. It is all the more important to model fission gas release and swelling when simulating fuel rod behaviour during a power ramp. Nano-metric intragranular fission gas bubbles or bigger inter-granular bubbles which have nucleated during the steady state irradiation are indeed liable to swell. Section 3.3 describes the main phenomena and assumptions that make up the model [9].

3.3.2. Basic assumptions

Three gas populations are modelled. These include intragranular and intergranular gas along with the coarse grain corner porosity. Intragranular gas is assumed to be either dissolved in the fuel matrix, or contained in initially small bubbles. The entire intergranular fission gas population is on the other hand contained in bubbles, the concentration of which is a model parameter. At a given radius of the fuel pellet, only a single bubble size is considered per population.

3.3.3. Gas release and transfer kinetics

Gas release from the fuel to the free volumes in the rod is described as a three stage process. Firstly, intragranular bubbles migrate to grain boundaries. The assumed mechanism is surface diffusion in a temperature gradient. The flow of grain boundary gas to the interconnected porosity then occurs if the estimated grain surface occupied by intergranular bubbles exceeds 30% of the total grain boundary surface area. The transfer kinetics from the grain boundary to the interconnected porosity is assumed to be proportional to the difference in pressure between the corresponding gas populations. Finally, the flow of gas through the interconnected porosity to the free volumes which ultimately leads to its release is modelled as following a percolation law.

Inter and intragranular swelling is considered. The interconnected porosity is thought to consist of relatively large pores which contain a low pressure gas. In other words, a change in the pressure in the cavity will not lead to a notable increase in its size. Hence its contribution to fuel swelling is neglected.

Intragranular bubbles coarsen as a result of both the influx of gas atoms from the matrix and of coalescence of moving bubbles. However, the coarsening kinetics is dictated at high temperature (above ~1200°C) by the diffusion and trapping of vacancies. The fuel swelling computation is therefore based on the rate at which vacancies are captured by bubbles. The thermodynamic force governing the rate at which vacancies are captured by bubbles is proportional to the difference in vacancy concentrations between the concentration at the bubble surface and the thermal equilibrium

vacancy concentration. This is at least true in the hottest part of the pellet, i.e. the central part, most affected by FGS. A differential equation expressing bubble growth can thus be set up :

$$\frac{dr_b}{dt} = -\frac{D_u}{kT}\Omega\frac{1}{r_b}\left(P_{ext} + \frac{2\gamma}{r_b} - P_{\text{int}}\right)$$

where r_b is the bubble radius, D_u the uranium self diffusion coefficient, T the local fuel temperature, P_{ext} and P_{int} are the surrounding hydrostatic stress (calculated by the fuel mechanical behaviour model) and bubble inner pressure respectively, g the fuel surface tension and W the volume occupied by a molecule of UO_2 in the lattice. A Van Der Waals equation is used as equation of state for the gas. A similar treatment is applied to intergranular swelling, only bubbles are described as taking on a lenticular shape.

The above equation is important as it shows how the fission gas and mechanical behaviour models are coupled. Small, highly pressurized bubbles will have a tendency to grow. However, bubble growth is hindered as compressive stresses are set up in the fuel during a PCI event. In our model, fission gas fuel swelling appears as a balance which results from the diffusive phenomena involved: fission gas, uranium vacancy diffusion and fuel creep.

4. MODEL APPLICATION AND DISCUSSION

4.1. Introduction

In order to compute power ramps designed to simulate incidental operating conditions, a computation is performed of the steady state irradiation using standard models and in particular the mechanical behaviour model. All the data generated by the steady state calculation is then stored and used as input data for the second calculation pertaining to the ramp test proper. The appropriate fuel rod geometry, which usually translates as a shortening of the fissile column as a result of re-fabrication, and irradiation conditions specific to the experimental reactor involved are applied.

Since the fission gas behaviour model is applied at the beginning of the actual power ramp, and has been specifically designed to treat short hold times at maximum power (~ a few days), it is important to define the parameters and hypotheses used for each set of calculations presented in this section. Calculation assumptions regarding cases 1 trough 5 are identical. In particular the initial intergranular bubble concentration ($5.5\ 10^6$ /mm^2) and radius (0.15mm) were estimated from micrographs performed on a representative fuel pellet section. The choice of strictly identical pre-transient data is justified by the fact that the five cases concern fuel rods irradiated to similar burnups and at comparable linear ratings (Table I). However, case 5 concerns a MOX fuel, the microstructure of which is quite different from standard UO_2 fuels. The impact of this on calculation results will be discussed in section 4.1.3 devoted to MOX fuel behaviour. Data taken from [10] were used to estimate the initial intragranular bubble concentration (10^{13}/mm^3).

For case 6 on the other hand, it is assumed (from lack of data) that intergranular bubbles are in equilibrium with the surrounding solid. The initial intragranular bubble concentration was chosen to be one order of magnitude below the value used for cases 1 to 5 because of the increased burnup.

4.2. Case 6 (GONCOR experiment)

We start with case number 6, which serves to illustrate explicitly the effects of fission gas related fuel swelling on cladding strains. The refabricated fuel rod was subjected to a linear power history comprising an initial rise to ~250W/cm and a subsequent power ramp to 400W/cm. The maximum power was held for approximately 6 days (see Fig. 1). A comparison of measured and calculated cladding strains is also shown in Fig. 1. The cladding diameter measurements reported here

are those performed at the axial location where the linear rating is maximum. The values indicated in Fig.1 were measured at three adjacent positions, at a pellet-pellet interface, at the mid pellet plane and in between these positions. It shows that, prior to the power increase to 400W/cm, only a primary ridge approximately 10mm high is apparent. As the power is increased, a 20 mm ridge appears at the mid pellet plane, which we hereafter refer to as the secondary ridge. As is seen below, this phenomenon is characteristic of ramped UO_2 fuel rods. The cause of primary ridging is widely regarded as being the radial temperature gradient which causes the internal part of the pellet to expand axially more than the peripheral part. However, the exact cause of secondary ridging is not fully elucidated. This phenomenon could be interpreted as resulting from fuel creep and FGS. On the scale of a fuel pellet, the mid-pellet plane is a plane of symmetry, and remains as such in the course of the irradiation. Therefore, the displacement field in that plane is uniform and plane strain conditions apply. Whatever the cause of irreversible strains (fuel creep and/or FGS), these plane strain conditions have a tendency to translate as an increase in fuel hence cladding diameter. On the other hand, since the fuel pellets are dished, plane strain conditions certainly do not apply in the vicinity of a primary ridge and fuel creep and FGS will preferentially combine to fill the pellet ends.

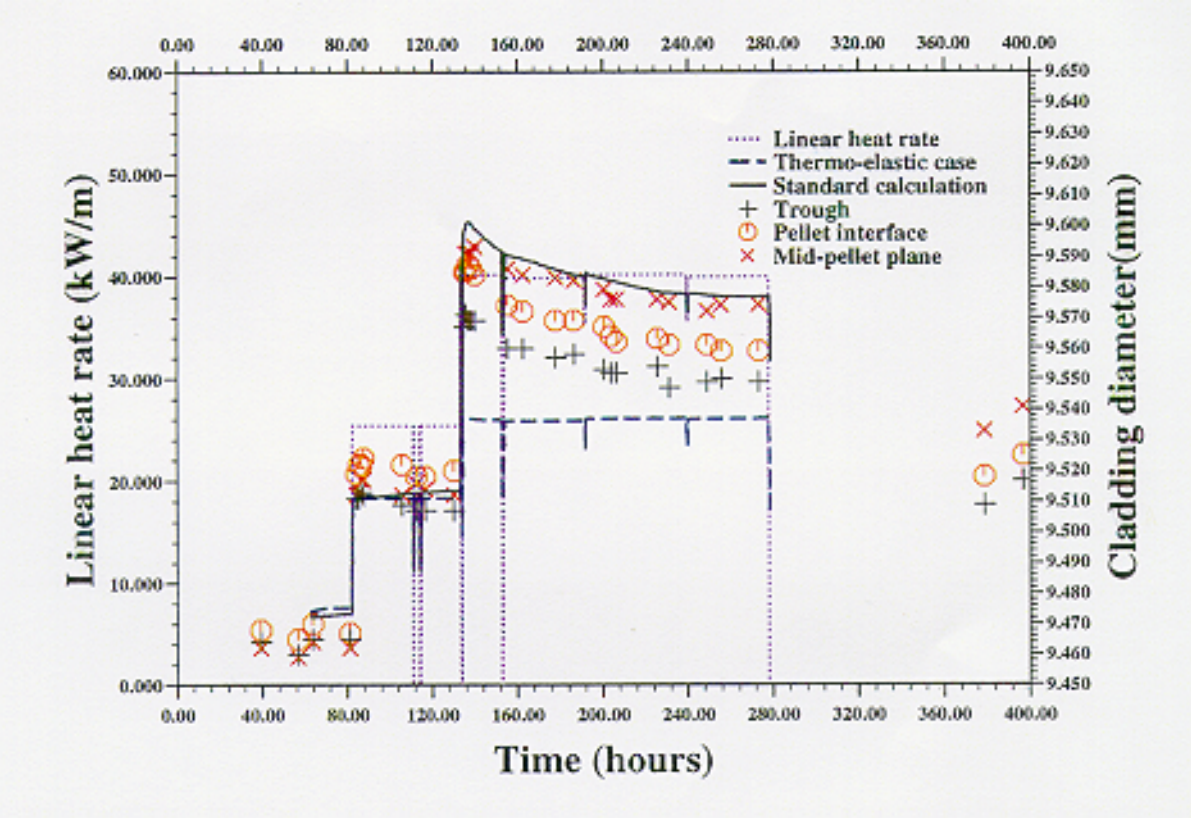

FIG. 1. Case 6, measured vs. calculated cladding diameters.

We base our interpretation of the characteristic cladding diameter changes (irrespective of the axial position) illustrated in Fig. 1, on the fact that there is a close agreement between the measured and calculated values, both as regards the general shape of the curves and, for the mid-pellet plane, the actual values themselves. As the power and temperature rise, diffusion processes are activated as a result of which the fuel pellets swell. This translates as a sharp increase in the cladding diameter. The cladding diameter then reaches a maximum as the intergranular gas begins to flow from the grain boundaries to the grain corner porosity. The fuel then gradually deflates as the interconnected porosity gas percolates out of the fuel.

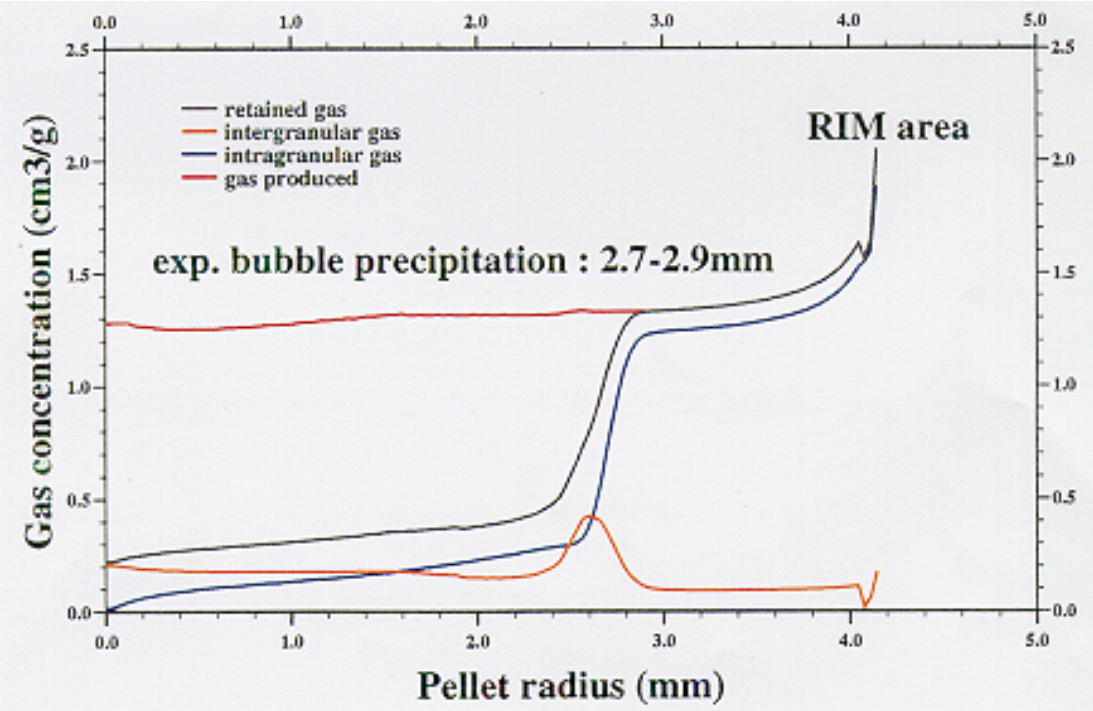

FIG. 2. Case 6, calculated fission gas distribution.

Quantifying both the overall effect of fuel swelling and the corresponding kinetics is made possible by comparison of experimental and model calculation results. The results of a thermo-elastic computation is also shown in Fig. 1. It indicates that the effect of swelling (at 400W/cm for a 48GWd/Mt fuel rod) is a diameter increase that ranges between 30mm and 50mm. Furthermore, our calculations also show that after 15min at 400W/cm, the cladding diameter increase, for a power increase from 250W/cm to 400W/cm, has reached 85% of its maximum value. This is indicative of the importance of fission gas behaviour on cladding loading in transient conditions and associated kinetics.

The calculated overall FGR tally with PIE results. Measured values are estimated at 25% and the calculated value is 26.8%. Optical microscopy examinations also corroborate to a certain point model calculations. These reveal a circular ring of intragranular bubbles located between 71% and 65% of the outer pellet radius. The fission gas model predicts a drop in the intragranular gas concentration, at the end of the experiment, that spreads over an area located between 73% and 70% of the pellet radius. Calculations predict that the temperature of the outer part of this zone varies between 1020°C and 1100°C, which is high enough for bubble nucleation to occur but too low to result in any appreciable bubble movement (Fig. 2).

4.3. Cases 1 through 4

4.3.1. Cladding diameter measurements in relation to FG behaviour

Figures 3 through 6 show a comparison of the measured and calculated cladding diameter increases during the four power ramp tests studied in this section. Also included in the above-mentioned figures are the results of calculations performed with no FGS. The figures reveal that all but case 1 show extensive signs of fuel swelling. Our calculations predict that fuel swelling contributes to an increase in diameter of between 20mm (case 2, i.e. maximum power ~430W/cm, short hold time) and 40 mm (case 3, approximately same maximum power, long hold time). Comparing cases 2 and 3 is interesting because it is indicative of swelling kinetics.

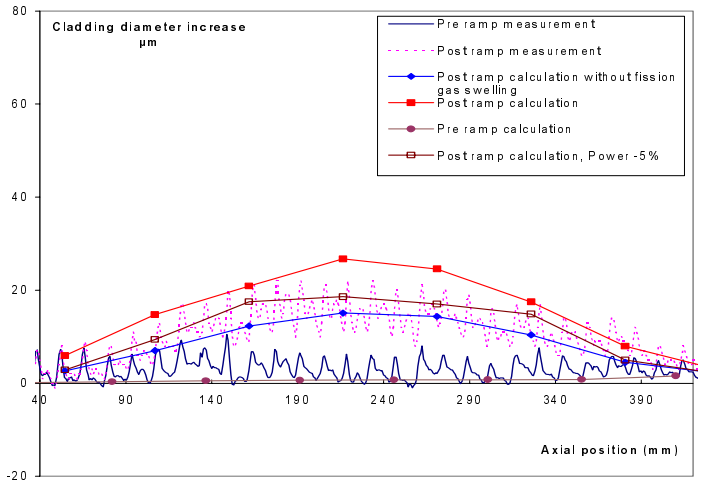

FIG. 3. Case 1, measured vs. calculated pre and post ramp cladding diameters.

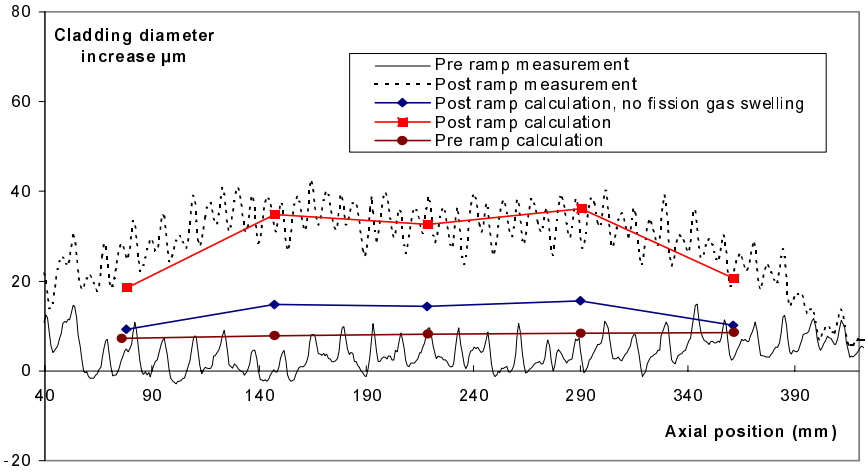

FIG. 4. Case 2, measured vs. calculated pre and post ramp cladding diameters.

FGS is also apparent in case 4 (maximum power ~460 W/cm, short hold time) and contributes to a diameter increase of approximately 20mm. Case 1 is interesting because it seems to lie in the power and hold time range for which FGS appears to be of negligible importance. However, one should bear in mind that the power uncertainty (taken to be +/- 5% for a 95% confidence interval) could also be the cause of the apparent discrepancy between model calculations and experimental results (see Fig. 3).

One could also argue, from an experimental point of view, that all of the four ramped rods (including case 1) show signs of secondary ridging. If creep is the cause of secondary ridging, then in principle, there is no reason why at least intragranular swelling is not possible. The reason for this is that creep and fuel swelling are, under PCI conditions, controlled by the flow of point defects in the pellet. Figure 7 shows how fast the stress field, which is highly compressive in the central part of the fuel pellet, changes. It gives an indication of the extent of fuel creep.

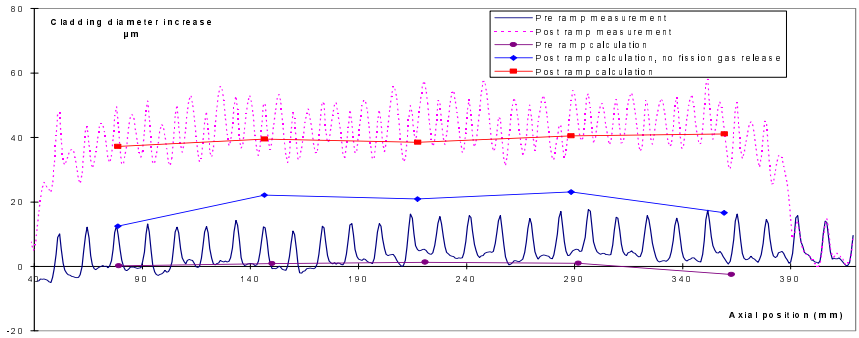

FIG. 5. Case 3, measured vs. calculated pre and post ramp cladding diameters.

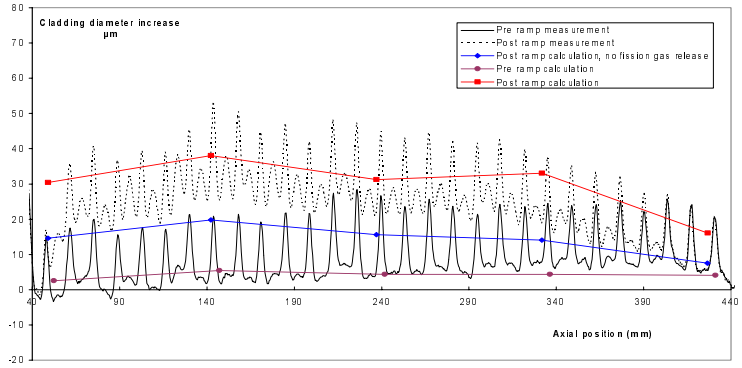

FIG. 6. Case 4, measured vs. calculated pre and post ramp cladding diameters.

4.3.2. Fission gas behaviour

There is a relatively good agreement between calculated and available FGR data. More importantly maybe, optical microscope observations confirm either the fission gas retention profile across the pellet for long hold times, or, the intragranular bubble precipitation radius for short hold times (Figs. 8 and 9). The study of case 3 shows that intragranular bubble precipitation occurs at approximately 1270°C.

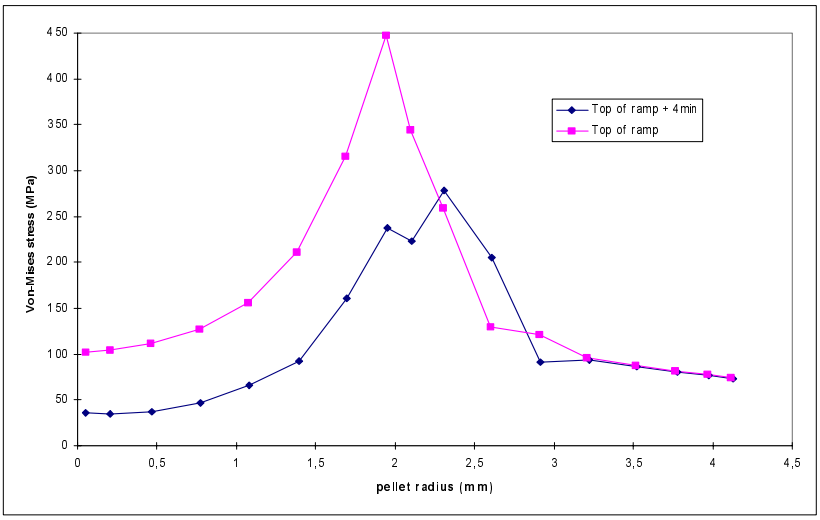

FIG. 7. Case 2, calculated Von-Mises stress in the pellet (T = 0 and T = 0+4 min).

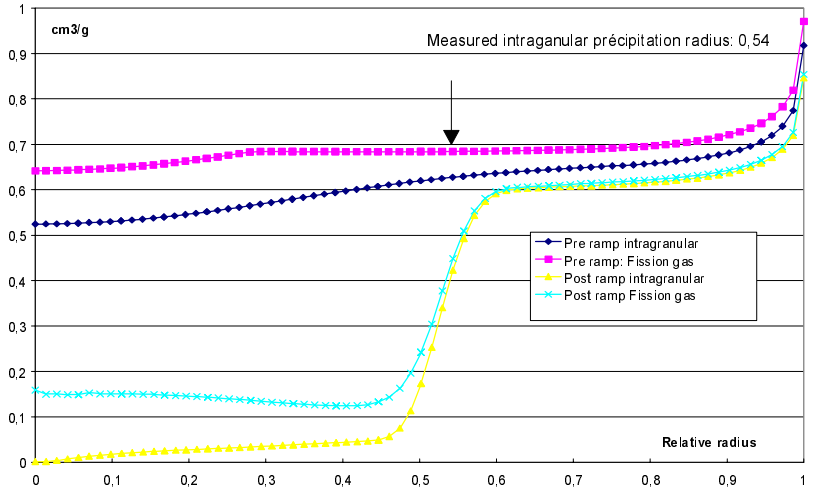

FIG. 8. Case 3, retained fission gas after 12 hours.

As proven from the analysis of cladding diameter measurements, microscope observations of fuels reveal extensive signs of fission gas swelling. Intragranular bubble precipitation is clearly apparent in case 2 (short hold time, Fig. 10) and the dished pellet ends were reported to be partially filled. In some cases also, micrographs can be used to confirm that the mechanisms modelled actually occur. Figure 11 (case 3) indicates extensive bubble migration in a temperature gradient. Case 4 (short hold time) is also extremely interesting because it shows that pellet ends are completely filled. There are also signs of extensive swelling in their immediate vicinity, which is a potent illustration of the stress dependency of FGS.

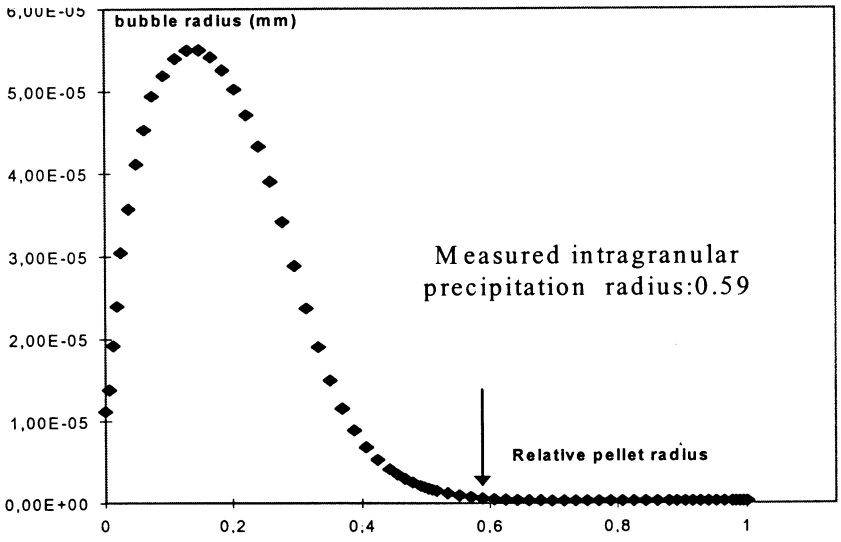

FIG. 9. Case 2, calculated intragranular bubble radius.

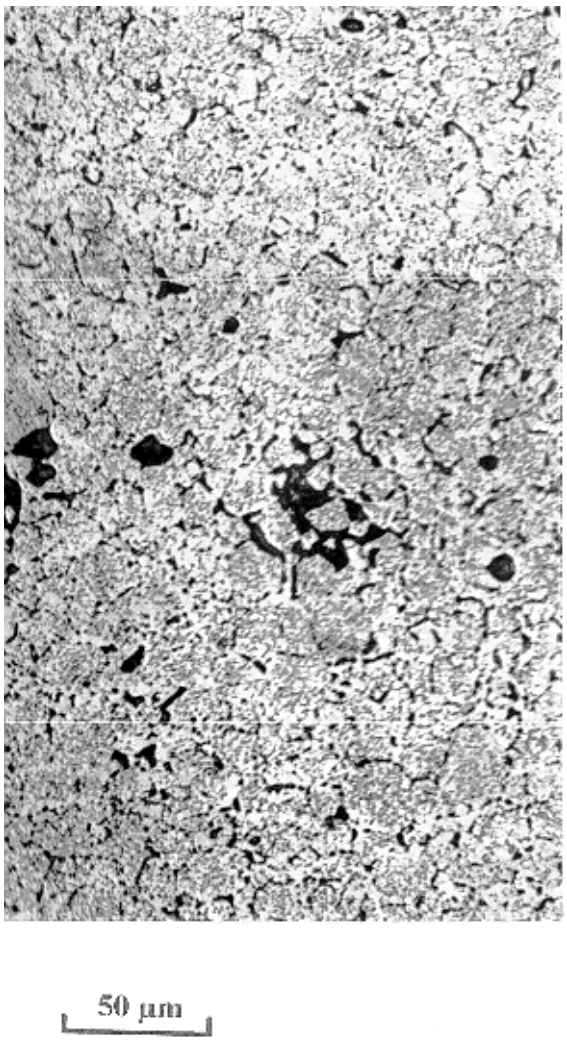

FIG. 10. optical examination of fuel from case 2.

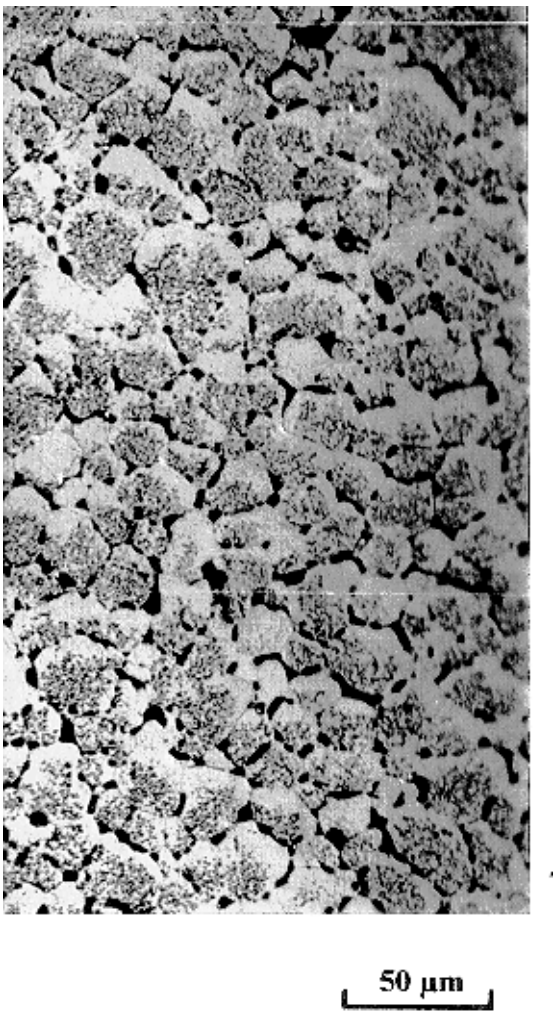

FIG. 11. Case 3, experimental evidence of bubble movement.

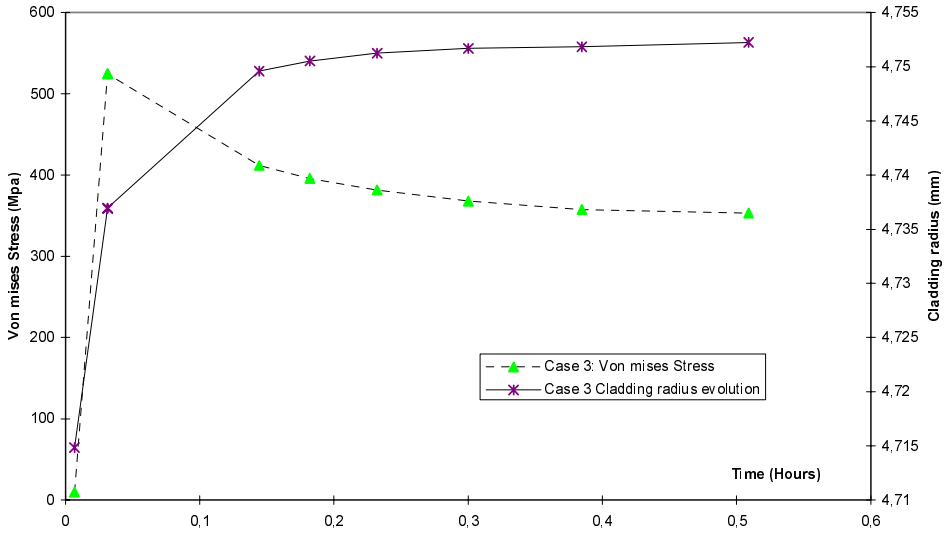

FIG. 12. Cases 3, Von-Mises stress evolution and cladding diameter changes.

4.3.3. Cladding behaviour

It is interesting to note cladding diameter and Von-Mises stress changes as a function of time for case 3 (Fig. 12). It is indeed a general feature that the cladding Von-Mises stress is at its maximum as the linear rating reaches its peak value. Therefore, if a cladding failure event occurs during the hold period at maximum power, the inner cladding stress will have already begun to decrease. However, because of fission gas swelling, model calculations predict that the cladding diameter continues to increase (Fig. 12) for approximately 50 min. This could be an indication that a physically based failure criterion should take strain into account.

The question obviously arises of the point a which FGS contributes significantly to cladding loading. Although the evidence from case 2 strongly suggests that at a reasonably high linear heat rate, and for a short hold time, there is substantial swelling, more experimental work is needed regarding shorter hold times (~5 min).

4.4. Case 5: MOX Fuel behaviour and modelling

As reported previously this ramp was performed in the Studsvik test reactor at a maximum linear rating of 480W/cm. The fuel is a MOX MIMAS type. The PIE indicate that the pellet ends were totally filled. There are also signs of fuel restructuring (columnar grain growth), characteristic of high temperatures and temperature gradients across the pellet [11], and fuel swelling (maximum diameter increase of 90 mm). The originally heterogeneous fuel microstructure showed extensive Pu homogenisation in the hot, central part of the pellet.

Calculated and measured cladding diameter increases are reported in Fig. 13. The figure shows a considerable underestimation (20-30 mm) of the computed cladding strains for linear heat rates above (430-440W/cm). We ascribe these discrepancies to both the fission gas behaviour model which was originally designed for UO_2 type fuels and to the fact that cladding plasticity is not treated in the current version of the code. The calculated peak inner cladding Von-Mises stress exceeds the yield stress by at least 100 MPa.

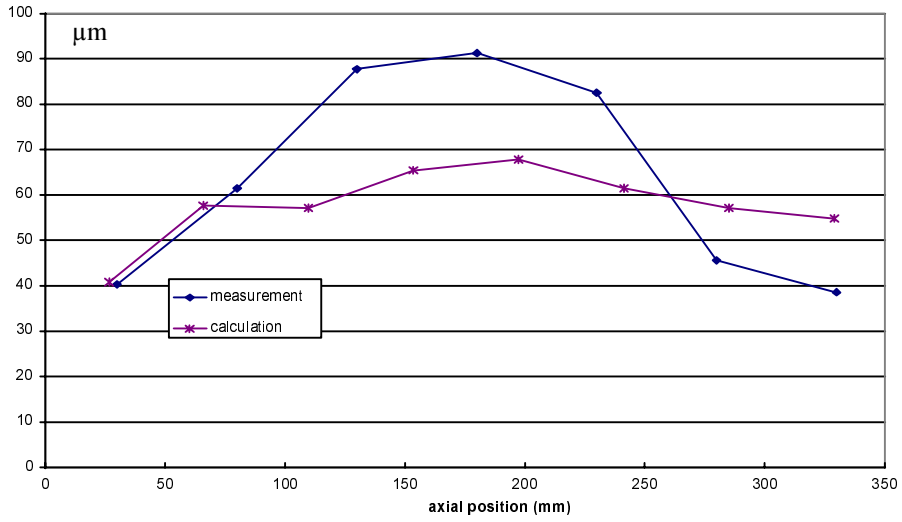

FIG. 13. Case 5, measured vs. calculated cladding diameter increases.

However, cladding elongation calculations are in satisfactory agreement with the measured in-pile values (Fig 14), despite lying above them by approximately 300 mm. It is interesting to note that the volume of the dished pellet ends, which are not modelled in our mono-dimensional computation, equates to about the same value (~385 mm). This no doubt constitutes an added cause of discrepancy. These results clearly validate however the hypothesis whereby there is no relative axial movement between the cladding and the fuel stack once the fuel-cladding gap is closed.

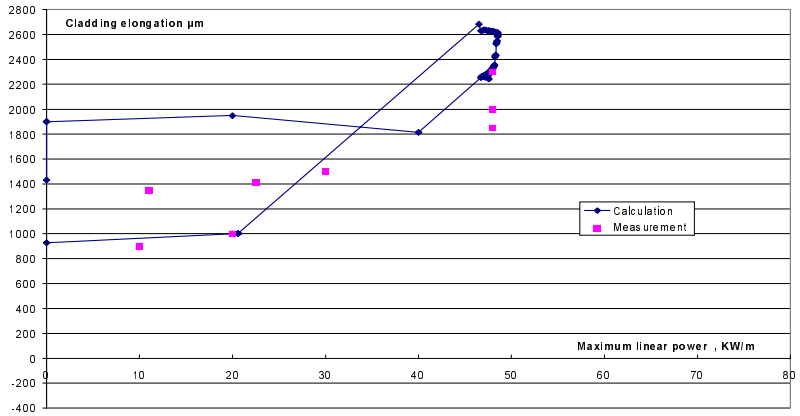

FIG. 14. Case 5, measured vs. calculated cladding elongation measurements.

Measured and calculated (17cm^3 - 22cm^3) overall fission gas release values are also in satisfactory agreement and xenon microprobe examinations seem to corroborate our retained fission gas calculations (see Fig. 15). However, the fission gas release values are slightly overestimated which is consistent with the fact that the radius below which virtually no fission gases are present is slightly greater than the micro probe results indicate.

These observations are consistent with the observed cladding diameter discrepancies. The retained fission gases in the 1350°C to 1550°C temperature range could be the cause of the underestimation of cladding strains.

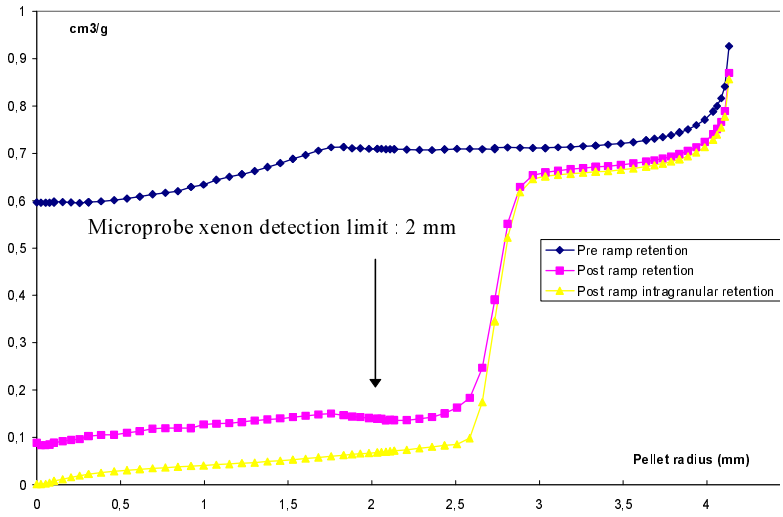

FIG. 15. Case 5, retained fission gas profile.

5. CONCLUSIONS

An important conclusion to be drawn from our study is that mechanical and physical processes are coupled. Therefore, a reasonably accurate description of stresses in the fuel pellet makes it possible to estimate FGS under PCI conditions.

For UO_2 type fuels, the models implemented in the METEOR/TRANSURANUS fuel behaviour code provide a satisfactory level of agreement, under PCI conditions, between calculated and measured cladding diameter values. Model calculations are also consistent with PIE results pertaining to fission gas behaviour. Our data base should be extended for MOX fuels to cover a wider range of linear rates, hold times and burnups.

It is also quite obvious from this study that any comprehensive modelling hence understanding of PCI (encompassing both UO_2 and MOX fuel behaviour and high burnups) must include a description of fission gases. For UO2 type fuels, there is evidence of FGS over short hold time periods (less than 30 minutes). More experimental work is needed if one is to ascertain swelling kinetics for shorter hold times.

The rod containing MOX fuel, presented in this paper also shows that FGS affects cladding strains considerably. From the point of view of modelling, it appears that cladding plasticity should be included along with an improved treatment of fission gases behaviour at high linear heat rate.

ACKNOWLEDGEMENTS

We gratefully acknowledge the excellent experimental work carried out in the hot cell laboratories in CEA-Saclay and CEA-Grenoble along with the quality of the irradiation programmes that generated the data we allude to in this paper. We are also happy to thank EDF and FRAMATOME for their contribution and support.

REFERENCES

[1] C. LEMAIGNAN, SMIRT Conference, Water reactor fuel damage mechanisms. SMIRT 14, August 17–22 1997, France.

[2] L. CAILLOT, C. LEMAIGNAN, J. JOSEPH, In-situ measurements of cladding strains during power transients using the decor device, Proc ANS International topical meeting on LWR fuel performance, West Palm Beach, 94.

[3] S. BOURREAU, S. LANSIART, P. COUFFIN, C. VERDEAU, G.C. DECROIX, M. H. GRANDJEAN, H HUGOT, F. MERMAZ, E. VAN SCHEL, Influence of hold period on the fuel rod behaviour during power ramp, this conference.

[4] A. ALBERMAN, M. ROCHE, P. COUFFIN, S BENDOTTI, D.J. MOULIN, J.L. BOUTFROY, Nuclear Engineering and Design, 168 (1997) 293–303, Technique for power ramp tests in the ISABELLE 1 loop of the OSIRIS reactor.

[5] R. SALOT , "Fission gas release from high burnup fuel during power transients. Experimental data for modelling", this conference.

[6] Ph. GARCIA, M. MOYNE, SMIRT Conference. Modelling the steady state and transient mechanical behaviour of fuel rods. SMIRT 14, August 17–22 1997, France.

[7] K LASSMANN, H BLANK, Nuclear Engineering and Design 106 (1988) 291–313, Modelling of fuel rod behaviour code and recent advances of the TRANSURANUS code.

[8] Y .R. RASHID, Nuclear Engineering and Design 29 (1974), Mathematical modelling and analysis of fuel rods.

[9] C. STRUZIK, M. MOYNE, JP. PIRON, “High burn up modelling of UO_2 and mox fuel with METEOR/TRANSURANUS version 1.5”, ANS Portland March, 97.

[10] KASHIBE, UNE, NOGITA, Journal of nuclear material 206 (1993) 22–24, Formation and growth of intragranular fission gas bubbles in UO_2 fuels with burnup of 6–83 GW·d/t.

[11] D. OLANDER, Fundamental aspects of nuclear reactor fuel elements.

STUDIES OF PCMI FROM CLADDING ELONGATION MEASUREMENTS PERFORMED IN THE HBWR

T. TVERBERG
Institutt for Energiteknikk,
OECD Halden Reactor Project,
Halden, Norway

Abstract

The fuels and materials testing programmes carried out at the OECD Halden Reactor Project have for more than 30 years provided data on fuel behaviour in different situations. The investigations are focused on long term property changes, and irradiation techniques and instrumentations have been developed over the years which enable to assess fuel behaviour and properties in-pile. This paper presents data on pellet-cladding mechanical interaction (PCMI) from experiments carried out in the Halden Boiling Water Reactor (HBWR) instrumented with cladding elongation sensors. The experiments considered here range from fresh fuel to mid- and high-burnup fuel (exceeding 50 MWd/kgUO_2). The paper addresses the development of the point of onset of PCMI with burnup, showing how the power of onset decreases as higher burnups are achieved. The effects of ratchetting associated with shutdowns, power reductions and repeated power cyclings are discussed, as well as the relaxation behaviour of cladding axial strain during irradiation.

1. INTRODUCTION

The Halden Reactor Project has during its more than 40 years of existence developed different techniques and instrumentation to study fuel behaviour in different situations in-pile. The instrumentation provides capabilities for investigating different subjects such as fuel thermal properties as function of burnup, fission gas release, gaseous and solid fuel swelling and pellet-cladding mechanical interaction (PCMI) [1]. PCMI is an important factor in plant operation and may set restrictions on plant operation. It is therefore of great importance to obtain reliable data to get a good understanding of this phenomenon. One instrument that has shown to be very reliable in providing useful data for PCMI studies is the cladding elongation detector. This paper presents cladding elongation measurements from three different experiments carried out in the Halden Boiling Water Reactor (HBWR) with burnups ranging from fresh to high burnup fuel exceeding 55 MWd/kgUO_2.

2. CASE 1: FRESH BWR FUEL

2.1. Initial startup and low burnup PCMI

Four BWR type fuel rods were irradiated in the HBWR reaching a burnup of approximately 35 MWd/kgUO_2. Active length was 768 mm, pellet diameter 12.59 mm and diametral gap 170 mm. The rods were equipped with cladding elongation sensors which functioned satisfactorily throughout the whole irradiation period.

Figure 1 shows a plot of elongation versus rod power for three early power cycles for one of the rods. The figure shows that pellet-cladding interaction occurs at a low power at the beginning of the irradiation. During the first ramp, shown as the bottom curve in the figure, PCMI occurs already at a linear heat rate of around 10 kW/m, when the slope of the curve is departing from the calculated thermal expansion due to temperature rise with power. It should be noted that the calculated hot gap is still open at powers exceeding 40 kW/m, thus thermal expansion alone cannot account for this behaviour. This behaviour can be attributed to random eccentric stacking of the pellets of which some are in contact with the cladding even at zero power. The simultaneous radial and axial expansion of the pellets during the power increase then generates friction forces which cause the observed cladding elongation.

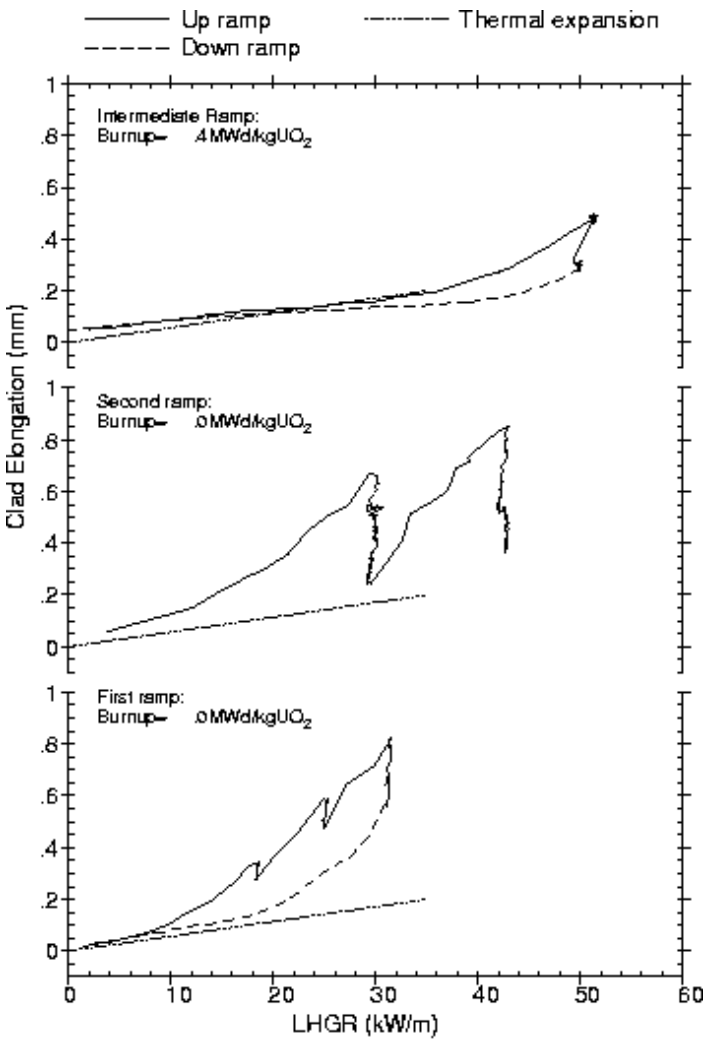

FIG. 1. Early power ramps for fresh BWR fuel rod. The dashed line shows free thermal expansion.

The first ramp was performed in three steps: from zero to 18 kW/m, next from 18 to 25 kW/m and finally from 25 to the maximum at 32 kW/m. At both intermediate power levels, the hold time was 2 hours, whereas peak power was kept for 8 hours. At each power step, relaxation can be seen: from 0.35 to 0.3 mm at the first level, 0.6 to 0.5 during the second, and finally the cladding reaches an elongation of 0.8 mm at peak power, before relaxing to 0.55 mm.

The second ramp shows the same features. This ramp has one intermediate level at 30 kW/m (hold time is 28 hours) where the cladding relaxes from a maximum of 0.65 mm down to 0.25 mm. Next, when the power is raised to 42 kW/m, the corresponding numbers are 0.85 and 0.4 mm. It should be noted that during the second ramp, the measured elongation is lower compared with the first ramp at each power level. Two effects can be considered for explaining this behaviour. During the first up-ramp, the pellets are pushed to more concentric positions which should result in reduced PCMI during the second and following ramps. However, some of this effect is counteracted by pellet cracking and relocation. The third ramp shows that the point of onset of interaction (defined as the point of deviation from free thermal expansion) is shifted further upwards with increased power levels. The maximum power is 51 kW/m with a corresponding elongation of 0.55 mm. Again we see that although power is increased above previous levels, the maximum elongation actually decreases.

2.2. Long term developments

Moving to the more long term characteristics, Fig. 2 shows the whole elongation history for the rod discussed in section 2.1. The plot also includes measurements at hot-stand-by (HSB), i.e. zero power and moderator temperature close to 240 ¼C. The top curve shows a condensed power history. For the elongation measurements, relaxation can be observed following power increases after reactor shut downs throughout the history. The hot-stand-by data show that after some time, a permanent elongation due to mechanical strain and irradiation induced growth builds up. The irradiation growth at end of irradiation was calculated to be 0.4 mm for the rods, using the MATPRO relation [2], which is in the same range as what the HSB data show. As the power decreases due to fuel depletion, the measured interaction decreases as well. At the end of irradiation, when the rod power is reduced to ~ 20 kW/m, there is, however, still pellet cladding contact as the point of onset shifts downwards with solid fission product fuel swelling. This is shown in Fig. 3, where elongation versus power for four rods are shown for altogether five down ramps at different burnup levels (the curves are shifted vertically for clarity). After the initial pellet cracking and relocation, the fuel stack settles, and interaction starts at a higher power level than at the very beginning. Later on the onset of interaction moves downwards with burnup. It seems that fuel and cladding accommodate to each other by maintaining a slight contact as the power gradually decreases with burnup and the fuel swells. This is indicated by a small interaction only around the highest power.

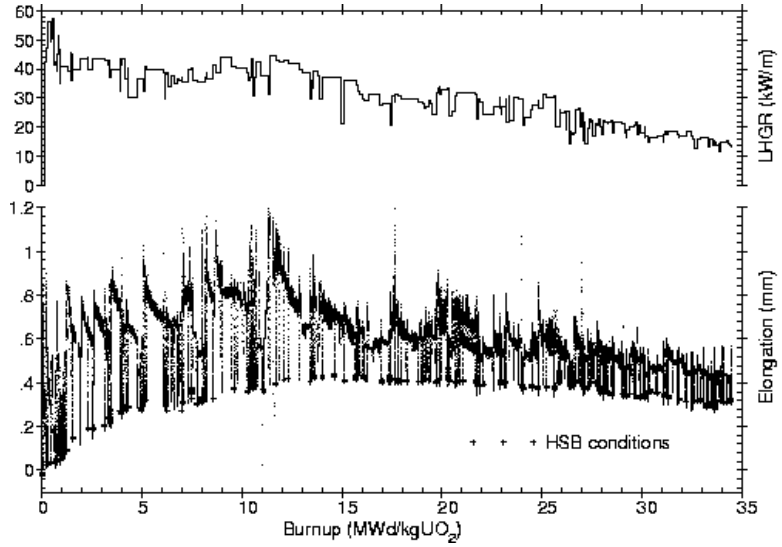

FIG. 2. Cladding elongation history and condensed power history for BWR type rod.

2.3. Power cycling

In Fig. 4 is shown a snapshot of the history of rod 1 from a period mid time in the irradiation (burnup range is ~20 to 22 MWd/kg$UO_{2)}$ during which a power cycling test was performed in a neighbouring rig. The power cycling caused power changes up to as much as 20% in this rig, ranging from ca. 27 to 33 kW/m. The elongation follows these power changes closely with corresponding elongation of ca. 0.55 and 0.8 mm, indicating that there is good contact between pellet and cladding throughout the power range. This is consistent with Fig. 3, where it is seen that the point of interaction in this burnup range is between 15 and 20 kW/m. During hold times at high power, relaxation can be seen. When the power is reduced to zero (shut downs), contact is lost completely. When returning to power again after a shut down, ratchetting can be observed when power is re-increased. The strong elongation variations during the cycling do not result in any permanent elongation change, showing that only elastic deformation occurs. See also Fig. 5, where elongation versus heat rate is shown for the last shut down in the period shown in Fig. 4.

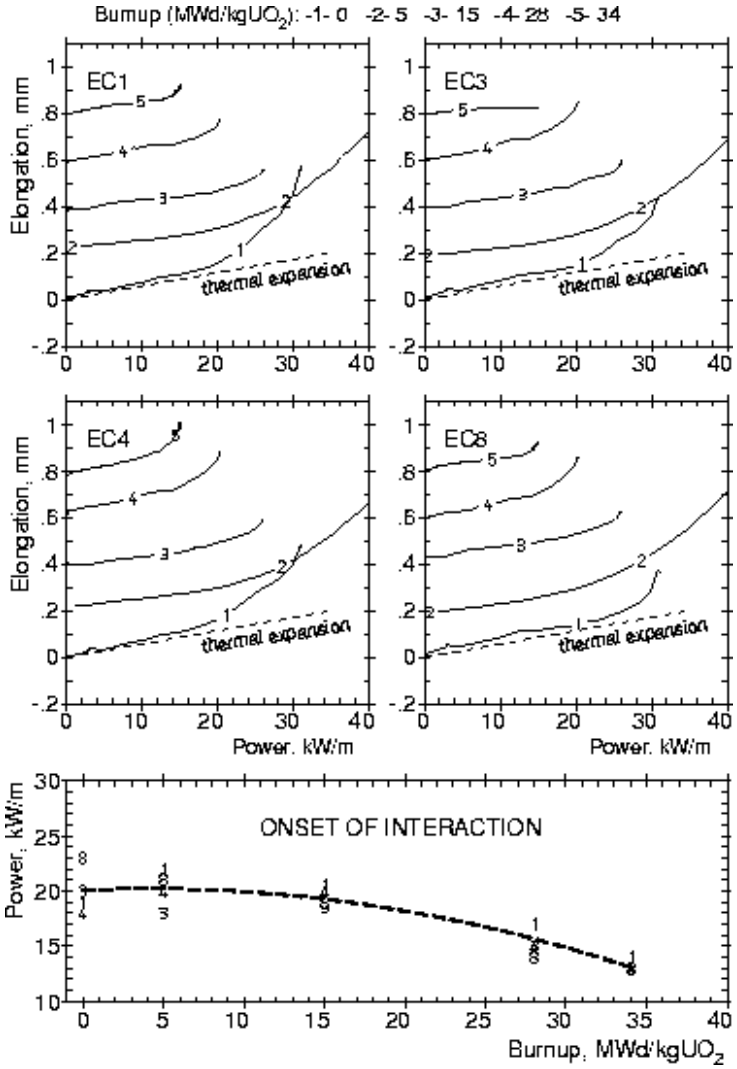

FIG. 3. Development of point of onset of interaction with increased burnup. (The curves are shifted vertically for clarity).

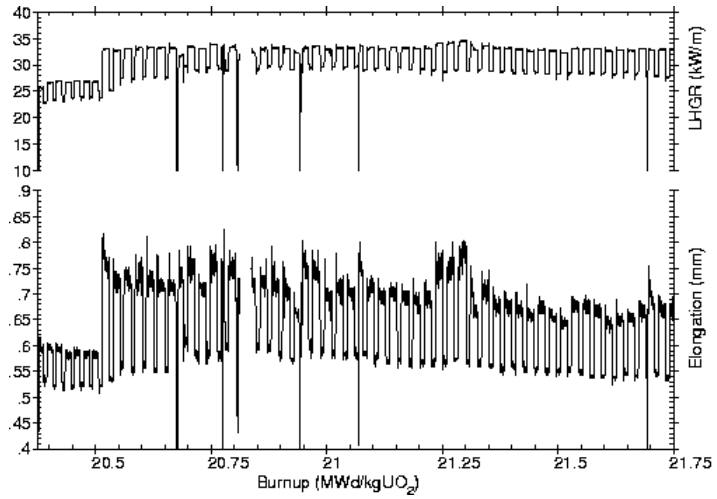

FIG. 4. Cladding elongation response to up to 20% power variations during a power cycle test in a neighbouring rig. Relaxation can be seen at holding levels at high powers as well as ratchetting after shut downs.

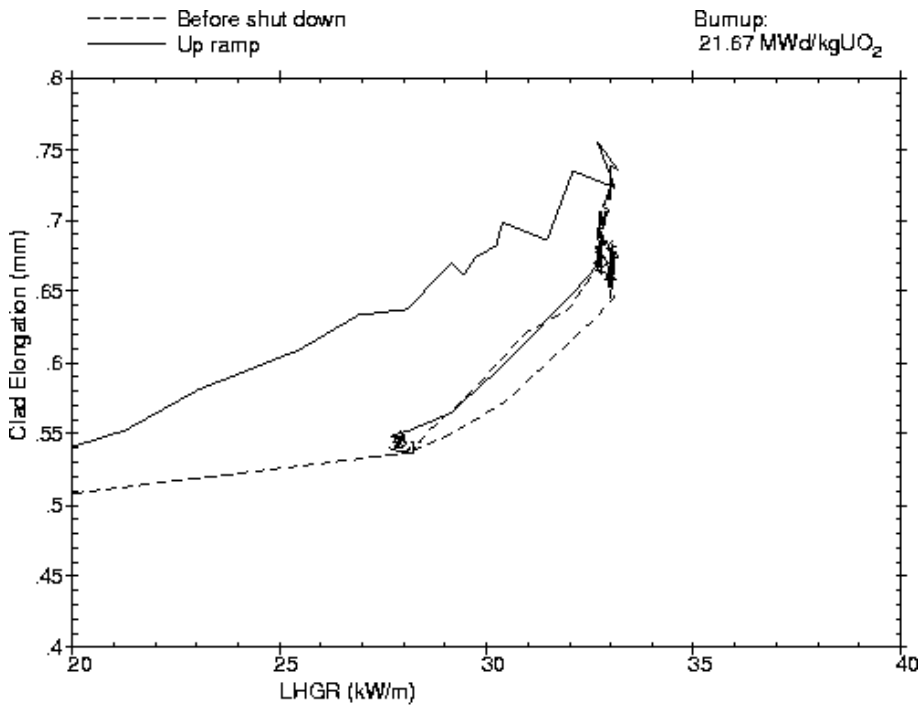

FIG. 5. Clad elongation versus heat rate before and after the last shut down seen in Fig. 4. Dashed lines show the last cycle before shut down and the shut down itself. Solid lines show the up-ramp and first power cycle after shut down.

3. CASE 2: MEDIUM BURNUP COMMERCIAL PWR FUEL INTERACTION BEHAVIOUR

Two fuel rods previously irradiated in a commercial PWR to a burnup of ca. 29 MWd/kgUO_2 were re-instrumented with cladding elongation sensors and irradiated in the HBWR reaching a burnup of 35 MWd/kgUO2. The rods have an active length of 433 mm, fuel diameter 9.12 mm and an as fabricated gap of 170 mm. Grain sizes are 8.5 (rod 1) and 22 mm (rod 2). During base irradiation, the rods experienced a linear heat rate of about 27 kW/m.

3.1. Early stages of irradiation

Figures 6 and 7 show the first three ramps for both rods. The two rods show very similar behaviour. During the first ramp slight interaction can be seen already at powers between 15 and 20 kW/m, when the curve deviates from the calculated thermal expansion curve. This is more pronounced for the large grain rod (Fig 7.). During the second ramp, a maximum power of 34 kW/m is reached, and interaction starts between 25 and 30 kW/m; i.e approximately the same power level as the rods were running at during base irradiation. According to code calculations, gap closure at a heat rate of 30 kW/m gives a cold gap of about 70 mm for this burnup. The third ramp peaks at an even higher level than the second: close to 40 kW/m, and the point of onset for interaction is further upshifted to a heat rate between 30 and 35 kW/m.

This behaviour of early interaction in the beginning and step wise upshifting of interaction point as higher powers are reached, is similar to what was found in chapter 1 for fresh fuel. Although in the case considered in this section, the rods are not fresh fuel rods, transport and handling will inevitably cause some repositioning of the pellets, thus giving rise to an early interaction. Later, as noted in chapter 1, contact between fuel and cladding will reorganise the pellets to more concentric positions, and the point of onset of PCMI shift upwards, as can be deduced from these figures.

There are no clear signs of relaxation during the cycles shown in these figures. It should be noted, however, that the hold times at peak power levels are only about 3 days and that the power overlap above the point of interaction is low for all ramps.

3.2. Long term development

Figure 8 shows the total irradiation history for both rods. It is seen that while the linear heat rate decreases with fuel depletion, the elongation data show a general increase for both rods, which reflects that there is some interaction. The fast flux in the 4-rods configuration of this experiment is estimated to be 2.0 10^{13}n/cm^{2}s. An irradiation growth of about 50mm is calculated for the rods. This agrees well with the measured data at hot stand by, which show an increase of about 60 and 80 mm for rod 1 and 2 respectively. The tendency of elongation with burnup becomes more clear if the elongation data are normalised to a constant heat rate. This is done in Fig. 9, where an attempt to normalise the elongation to a heat rate of 35 kW/m (above where PCMI occurs, ref. Fig. 6 and 7) is shown. At the beginning, some relaxation seems to occur, before the cladding elongation increases with increasing burnup. Ratchetting can also be seen after shut-downs, followed by relaxation to the previous level before the shut-down. The curve for a solid fission product fuel swelling rate of 0.75% per 10 MWd/kgUO2 (➀V/V) is included in the plot. It is clear that the inferred elongation growth rate does not reflect fuel swelling. The elongation increase seems rather to be a combination of irradiation growth and cladding creep due to PCMI.

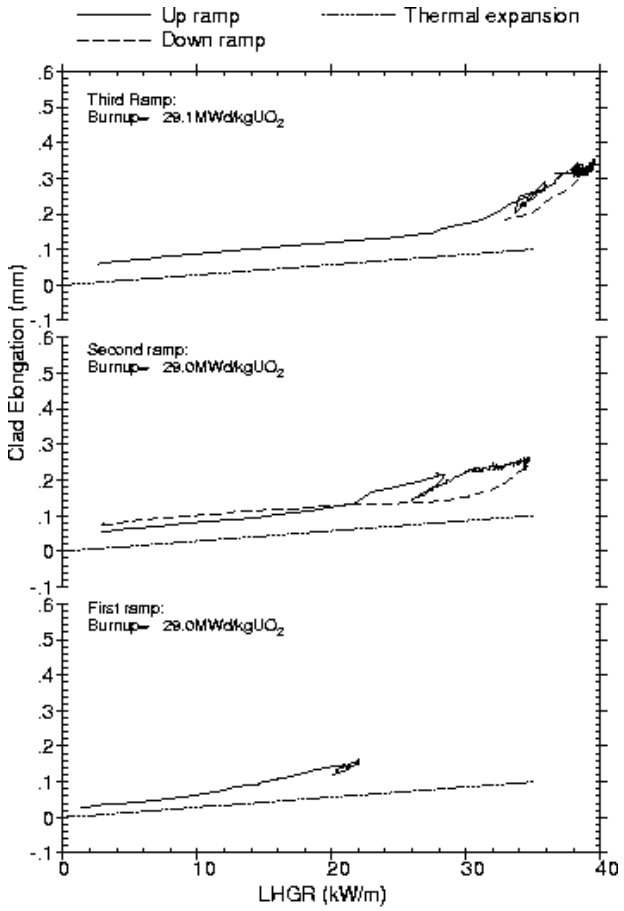

FIG. 6. Early power ramps for medium burnup PWR rod. Rod 1, normal grain size.

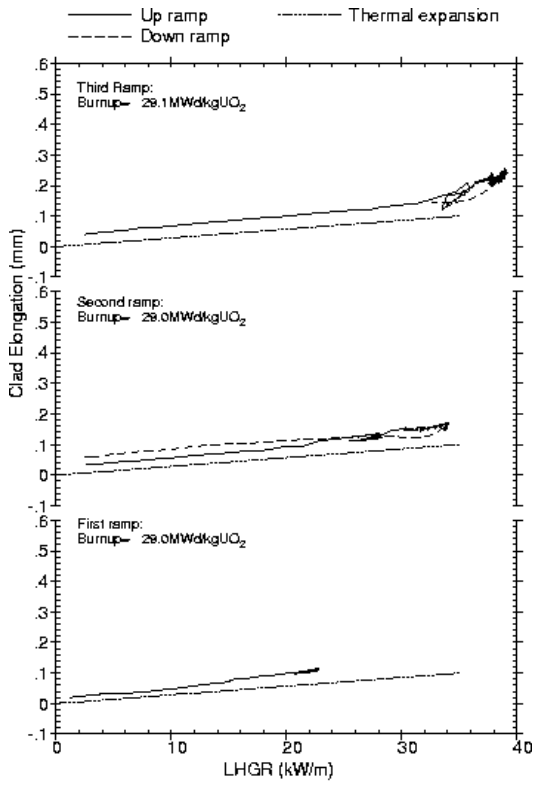

Figure 7. Early power ramps for medium burnup PWR rod. Rod 2, large grain size.

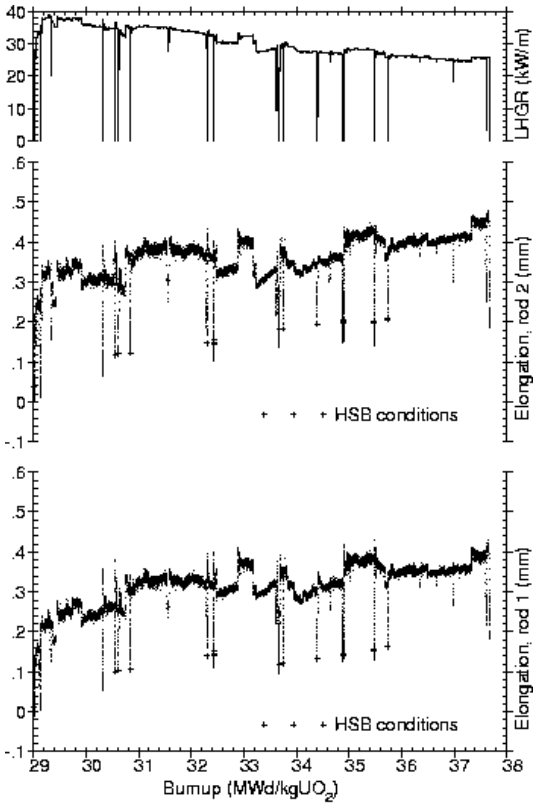

Figure 8. Cladding elongation history and condensed power history for medium burnup PWR fuel rods.

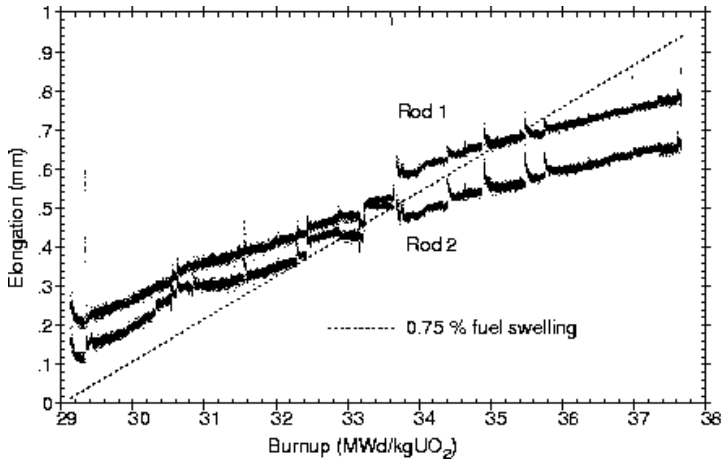

Figure 9. Cladding elongation normalised to a linear heat rate of 35 kW/m for medium burnup PWR fuel rods.

4. CASE 3: HIGH BURNUP COMMERIAL PWR FUEL INTERACTION BEHAVIOUR

Two fuel rods previously irradiated in a commercial PWR to a burnup of 52 MWd/kgUO_2 were re-instrumented with cladding elongation sensors and irradiated in the HBWR reaching a burnup of 55 MWd/kgUO2. The rods have the same dimensions as the ones considered in Case 2, with the exception of grain sizes, which in this case are 22 (rod 1) and 38 mm (rod 2). The operating power during the last cycle in the PWR was around 20 kW/m for both rods.

4.1. Early stages of irradiation

In Figures 10 and Fig. 11 the lower curve shows the first power ramp for rod 1 and rod 2 respectively. A slight deviation from the curve showing calculated thermal expansion can be seen. This is in accordance with what was seen for the medium burnup rods of the same type discussed in the previous chapter. After moving and handling of the rods, interaction at low heat rates is expected. The second curve in the figures shows the second ramp where it can be seen that the onset of interaction is at ~20 - 21 kW/m. As for the medium burnup case, PCMI starts at the power level the rods experienced during their base irradiation. A closed gap at power at this heat rate corresponds to a cold gap of 50 mm. For both rods, some relaxation, approaching 0.1 mm from the maximums of 0.7 mm for rod 1 and 0.4 mm for rod 2, can also be seen at peak powers (31.5 and 30.5 kW/m) for rod 1 and rod 2 respectively) during this ramp. Hold time for the maximum power is 19 hours in this case.

4.2. Long term development

The upper curves of Fig. 10 and 11 show the last power cycle (15 days) for the two rods. For rod 1, the point of onset of interaction has shifted downwards to somewhere between 15 and 20 kW/m. Code calculations predict a closed hot gap at 18 kW/m for a 40 mm gap for this burnup. When normalising the measured elongation to a constant power of 25 kW/m, a trend as shown in Fig. 12 appears. The initial relaxation noted in section 4.1 is seen. Shut downs reveal a tendency of ratchetting followed by relaxation as was the case for the rods discussed in chapter 3. Regarding the rate of increase during the irradiation, the rate coincides with, and possibly even exceeds the typical fuel swelling rate of 0.75% per 10 MWd/kgUO_2 which is also shown in the plot.

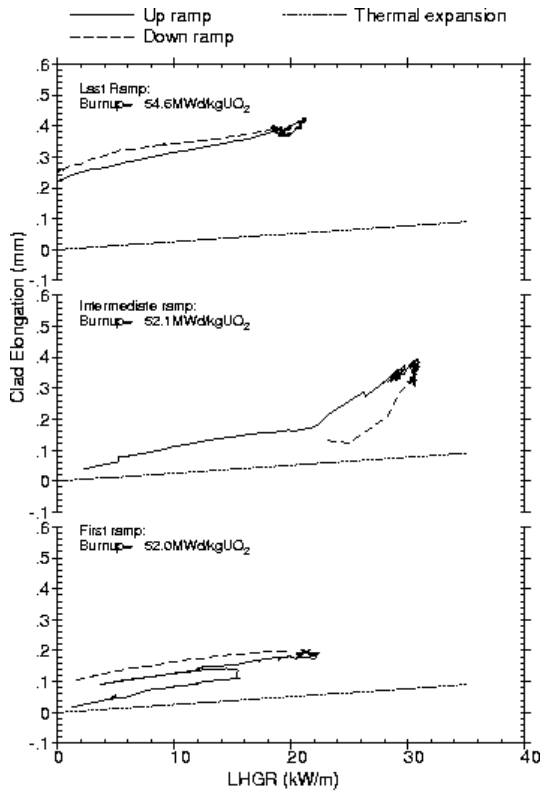

FIG. 10. Early power ramps for high burnup PWR rod. Rod 1, large grain size.

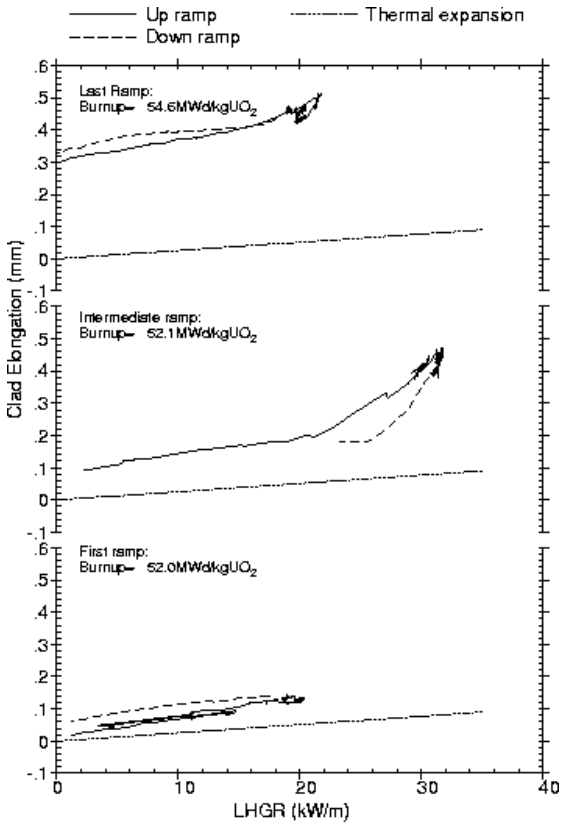

FIG. 11. Early power ramps for high burnup PWR rod. Rod 2, large grain size.

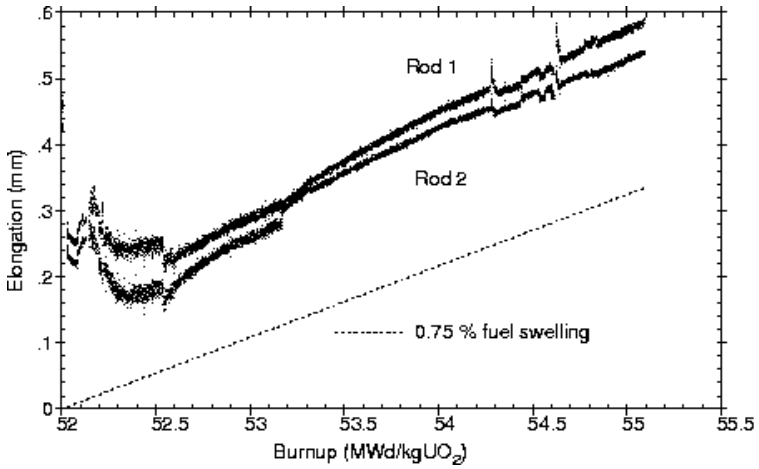

FIG. 12. Cladding elongation normalised to a linear heat rate of 25 kW/m for high burnup PWR fuel rods.

5. SUMMARY

Measurements of cladding elongation have been shown for three different experiments with fuel ranging from fresh to high burnup (55 MWd/kgUO_2).

The following points can be derived from the data:

- Strong PCMI during the first start-ups attributed to random pellet stacking, fuel cracking and relocation.
- Permanent elongation mainly due to irradiation induced growth.
- With increasing burnup, fuel and cladding accommodates to each other with little PCMI as long as previous power levels are not exceeded.
- A ratchetting effect is observed during shut-down/start-up cycles when contact is lost between fuel and cladding.
- Neither ratchetting nor power cycling led to additional permanent elongation.
- The fuel maintains the capability of relaxation also at high burnup.
- At high burnup and good contact between fuel and cladding, the cladding elongation indicates solid fission product fuel swelling.

REFERENCES

[1] AARRESTAD, O., Fuel rod instrumentation, IAEA meeting on ÔIn core Instrumentation and In-situ Measurements in Connection with Fuel behaviourÕ, Petten, NL (1992).

[2] MATPRO - VERSION 11 A Handbook of Materials Properties for use in the Analysis of Light Water Reactor Fuel Behaviour, NUREG/CR-0497 TREF-1280, EG&G Idaho Inc., Idaho Falls, Idaho (1979).

INFLUENCE OF THE HOLD PERIOD ON THE FUEL ROD BEHAVIOUR DURING A POWER RAMP

S. BOURREAU, S. LANSIART, P. COUFFIN, C. VERDEAU, G.M. DECROIX
CEA, Saclay

M.-C. GRANDJEAN, H. HUGOT
EDF, Villeurbanne

F. MERMAZ, E. VAN SCHEL
FRAMATOME Nuclear Fuel,
Lyon

France

Abstract

This paper presents three examples of power ramp tests performed in the OSIRIS experimental reactor, located at Saclay (France). The rods tested during these experiments stem from the same segmented « mother » rod, pre-irradiated for two cycles in a French PWR. They underwent very similar power transient conditions, except for the hold time at Ramp Terminal Level (RTL) - respectively 41.5 kW/m (J12/2), 40.7 kW/m (J12/4) and 39.5 kW/m (J12/5) for RTL, but zero (J12/2), 16 minutes (J12/4) and 12 hours (J12/5) for the hold time at RTL. No failure was detected for any of the three experiments despite the relatively high mechanical stress applied to the cladding in the case of J12/2. Moreover, although no hold time was maintained at RTL, a permanent deformation clearly appeared on the clad during the power transient. An analysis of the cladding deformation has also been undertaken concerning the J12/2, J12/4 and J12/5 experiments. This study was realized by carrying out post-calculations of the three experiments with a 2D fuel modelling code using the finite element method. The computations satisfactorily reproduce the influence of hold time on the cladding deformation during the power transients, especially for the J12/2 and J12/4 experiments with hold times enclosing the failure times experimentally observed for power ramp tests. For the hold time of 12 hours, the micrographic observations of the fuel, compared to the case of the 16 minutes hold time, support the hypothesis of weak but noticeable gaseous swelling.

1. INTRODUCTION

Pellet-Cladding Mechanical Interaction (PCMI) and related phenomena such as Stress Corrosion Cracking have been identified as a major cause of potential cladding damage in normal and incidental transient conditions. Thus, in co-operation with EDF and Framatome, an extensive programme of power ramp tests is being conducted by the CEA in order to study the effect of PCMI on the PWR fuel rod behaviour.

The three power ramp tests presented in this paper concern three segments of the same « mother » rod (J12). The experiments are described and the results of the examinations performed on the rods before and after the power transients are presented and discussed, more with respect to the cladding deformation.

A detailed analysis of cladding deformation has also been achieved by carrying out post-calculations of the three experiments with a 2D fuel modelling code using the finite element method. The comparison between those results and the measurements is discussed too.

2. EXPERIMENTS

2.1. Fuel rods characterization and refabrication

The PWR « mother » rod from which stem the J12/2, J12/4 and J12/5 fuel segments was designed by FRAMATOME. It contained UO_2 pellets, initially enriched up to 4.5% in ^{235}U, and was

irradiated during two cycles in an EDF French 900MW(e) PWR to finally reach a mean burnup of 23.8 GW·d/t U. The average rod linear density power experienced during its last PWR cycle was 22.3 kW/m.

Moreover this « mother » rod is segmented, which means that it is composed of a stacked assembly of sub-rods, independent from one another. The fuel rods presented here correspond to three segments extracted respectively in the second, fourth and fifth floors — from the lower end — of the UO_2 fuel « mother » rod described above. Their mean burnup was respectively 26.0, 25.4 and 25.8 GW·d/t U.

Owing to the particular nature of the « mother » rod, refabrications of the three segments were very simplified compared to the standard operating way: indeed, once the PWR rod reduced in elemental sub-rods, those were simply controlled and completed with the addition of lower and upper end plugs, without any modification affecting the fuel column and its environment (e.g. no re-pressurization was required).

2.2. Ramp tests conditions

2.2.1. Experimental device

The three rods were irradiated in the ISABELLE1 loop of the experimental reactor OSIRIS at CEA Saclay. This device [1] is designed for experimental irradiation of PWR or BWR fuel under thermo-hydraulic and chemical conditions representative of prototype or commercial power reactors. Its design allows it to be inserted and removed while the OSIRIS reactor is operating. The power variations result from the movement of the ISABELLE1 loop with respect to the reactor core.

The advantage of this procedure is that the thermal neutron flux evolution during power variation is quite representative of what happens during a transient in a commercial reactor. Moreover, the axial power profile in the fuel stack may be considered as constant all along the experiment and can be precisely determined by the γ-spectrometry measurements performed at the end of the test.

The mean heat rate of the rod is determined during irradiation using two independent methods :

a thermo-hydraulic analysis from temperature measurements upstream and downstream of the fuel ;

a neutron analysis from current measurements taken by self-powered neutron detectors located on the periphery of the loop, in the median plane.

Thermo-hydraulic and neutron modelling of the ISABELLE1 loop substantiated the various small corrections applied to the heat balance and a program of inter-comparison with three methods of fission power measurements achieved to qualify the thermal measurements procedure. The combination of the rod mean power and of the axial power profile, both measured for each test, provide an accurate determination of the local power in the fuel stack, with an uncertainty of ± 5.8% (2σ).

Rod failure is instantaneously detected during the test through an elongation sensor fixed to the rod and also by delayed neutron and gamma ray measurements in the coolant.

Each experiment is conducted according to strict quality assurance specifications.

2.2.2. Power ramping specifications

The power histories of the ramps presented here are composed of three steps. First, a pre-heating holding time of about 12 hours at the mean power level of the last PWR cycle underwent by

the rod, in order to re-establish the mechanical state of the rod. Then a power increase at the scheduled ramp rate of 10 kW/m/min. And finally a hold time at maximum power for a specific duration. The characteristics of J12/2, J12/4 and J12/5 tests are gathered in Table I.

TABLE I. J12/2, J12/4 AND J12/5 POWER RAMP SPECIFICATIONS

	J12/2	J12/4	J12/5
Pre-heating phase:			
– holding time	16h 11min	13h 35min	12h 42min
– max. power level	19.9 kW/m	20.0 kW/m	21.0 kW/m
Power increase:			
– duration	118s	120s	123s
– max. Ramp Terminal Power (RTL)	41.5 kW/m	40.7 kW/m	39.5 kW/m
Holding time at RTL	0s	16min 26s	12h 19min

The three rods underwent very similar power transient conditions, except for their holding times at Ramp Terminal Level (RTL) which range from zero (J12/2) to 12 hours (J12/5), through about 16 minutes (J12/4). So, they provide complementary data to study the influence of the hold period on cladding deformation during a power transient .

2.3. Results

Non-destructive examinations were performed on the three rods before and after ramping (visual examination, neutron radiography, eddy current testing, diameter measurement along eight lines and axial γ-scanning). Destructive examinations were only performed on the J12/4 and J12/5 rods (SEM examination of the cladding, fission gas release analysis, fuel density measurements, radial and axial metallographies). Indeed, the J12/2 rod was preserved to undergo a second power ramp sequence in a future experiment.

2.3.1. Rod integrity

No failure was detected during the three power ramp tests. This result was confirmed by the visual examination and the eddy current testing performed on the three rods after the tests, which show them to be in a good condition with no abnormal features.

2.3.2. Radial and axial metallographies

Radial micrographic examinations revealed that fission gas bubbles precipitation occurred in the fuel central area. Although this phenomenon depends on many parameters such as burnup, temperature and hold time, precipitation extent appeared to be close within the J12/4 and J12/5 rods. Still, the gas bubbles precipitation boundary is more distinct for J12/4.

Axial micrographic examinations showed partial filling of dishes at maximum power level in the J12/4 and J12/5 rods. Hold time seems to matter as dish reduction reached respectively 17% and 33% during these two power ramp tests. It is generally assumed that dish filling materialized fuel creep. Yet fuel swelling could also participate, particularly for long hold time. As no elongation of fuel column was observed through γ-scanning before and after ramp experiments, swelling contribution is hard to quantify. Nevertheless, radial metallographies of the J12/4 rod show no evolution in the porosity structure during the ramp test whereas, on the J12/5 rod, slight porosity migration was observed towards grain boundaries, which indicates gaseous swelling early beginning.

It is also to notice that, on J12/5 fuel, fragmentation perpendicularly to the pellet axis has been observed facing secondary ridges.

2.3.3. Cladding diametral deformation and axial power profile

During power transients, fuel thermal expansion triggered a global increase of cladding diameter and hard pellet to cladding contact caused interface ridges to grow. Secondary ridges also increased with transient duration, sometimes as much as interface ridges when hold time at RTL and local power were sufficient.

Diameter changes during transients are gathered in Table II. Figures 1 to 3 plot the axial profile of cladding deformation during the J12/2, J12/4 and J12/5 power ramp tests along with the axial power profiles determined by γ-scanning.

TABLE II. CLADDING DEFORMATION DURING POWER RAMP TESTS ON A THREE PELLETS AREA CORRESPONDING TO THE MAXIMUM POWER LEVEL.

Variations induced by the power transient (μm) on :	J12/2 rod	J12/4 rod	J12/5 rod
- cladding outer diameter off ridges	4	11.3	23
- cladding outer diameter on interface ridges	5	15.5	28.5
- cladding outer diameter on secondary ridges	4.5	14.7	30.3
- interface ridges diametral height	1	4.2	5.5
- secondary ridges diametral height	0.5	3.4	7.3

2.4. Discussion

Figures 1 to 3 demonstrate that the axial profile of diameter changes perfectly coincides with the axial power profile all along the plastically deformed area of the three rods. This shows, in these cases, that the cladding deformation can be expressed as an affine function of the local power reached at RTL.

It also clearly appears that deformation increases with hold time at RTL (cf. Table II, Fig. 4 and 1 to 3). This statement is proved correct on off ridges cladding outer diameter as well as on interface and secondary ridges heights. Nevertheless, the dependency of ridges height towards hold time seems to be much more important as far as secondary ridges are concerned. Indeed, when hold time varies from 0s (J12/2) to 16min (J12/4) then 12h (J12/5) interface ridges height at maximum power level increases respectively of 0%, 40% and 40% during transient whereas secondary ridges height raises by over 50%, 150% and 350%. Some of the mechanisms proposed to explain secondary ridges build-up involve fuel swelling, which in our case seems coherent with the metallographic observation trends

3. POST-CALCULATIONS OF THE EXPERIMENTS: ANALYSIS OF CLADDING DEFORMATION

3.1. Presentation of the modelling code: TOUTATIS

Post-calculations of the experiments have been carried out with the 2D version of TOUTATIS computer code [2], developed by the CEA to calculate the local thermo-mechanical behaviour of PWR fuel rods during normal and incidental conditions. This code consists of a specific module of the

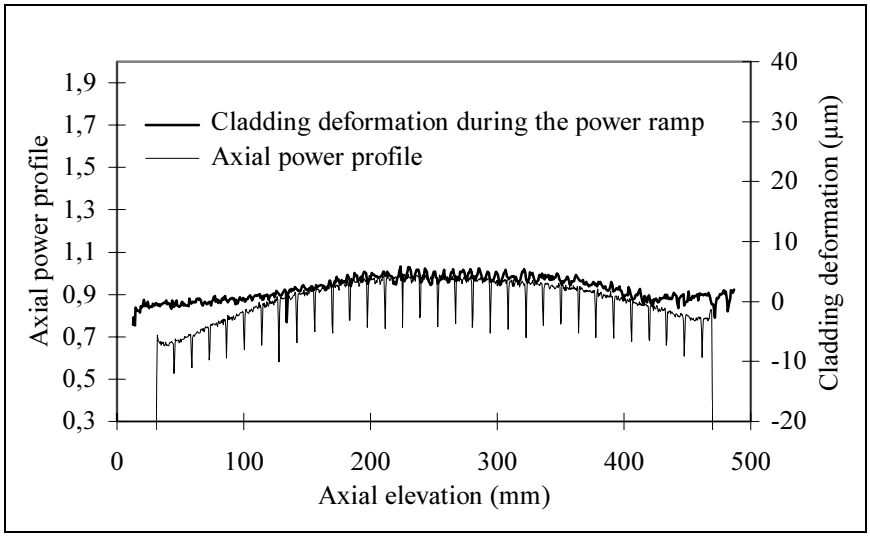

FIG. 1. Cladding diameter change of the J12/2 rod due to power ramping along with the axial power profile determined by γ-scanning.

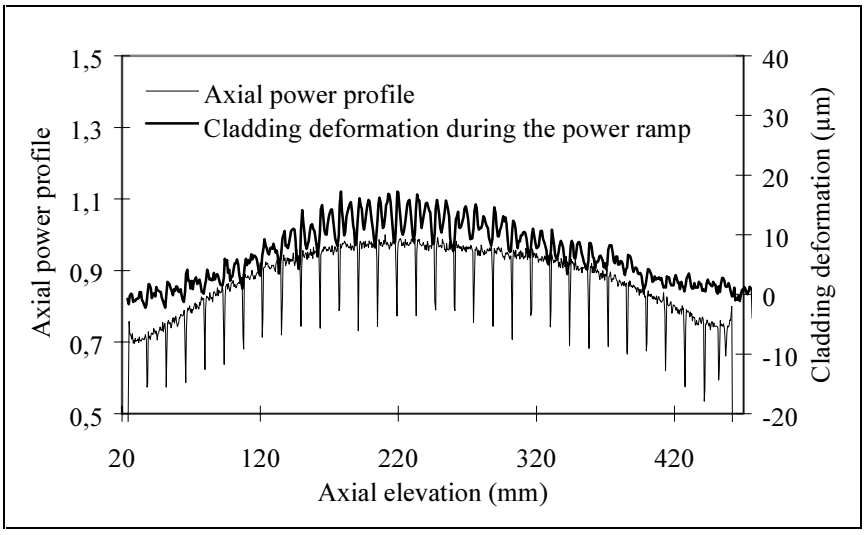

FIG. 2. Cladding diameter change of the J12/4 rod due to power ramping along with the axial power profile determined by γ-scanning.

general purpose CASTEM 2000 code, using the finite element method. It is developed in the framework of the CEA research and development project METEOR, as well as the 1D1/2 thermo-mechanical code METEOR/TU [3] which is used to describe the global behaviour of a fuel rod.

Considering symmetry conditions and in order to reduce computation time, the fuel rod axial modelling is limited to a half pellet and the associated cladding portion. The boundary conditions and mechanical loads applied are synthesized on Fig. 5.

The main phenomena taken into account within TOUTATIS code 2D version are:

in base irradiation conditions : in-pile densification and swelling of the fuel, creep of the cladding under the effect of coolant / rod differential pressure, evolution of the fuel-cladding gap

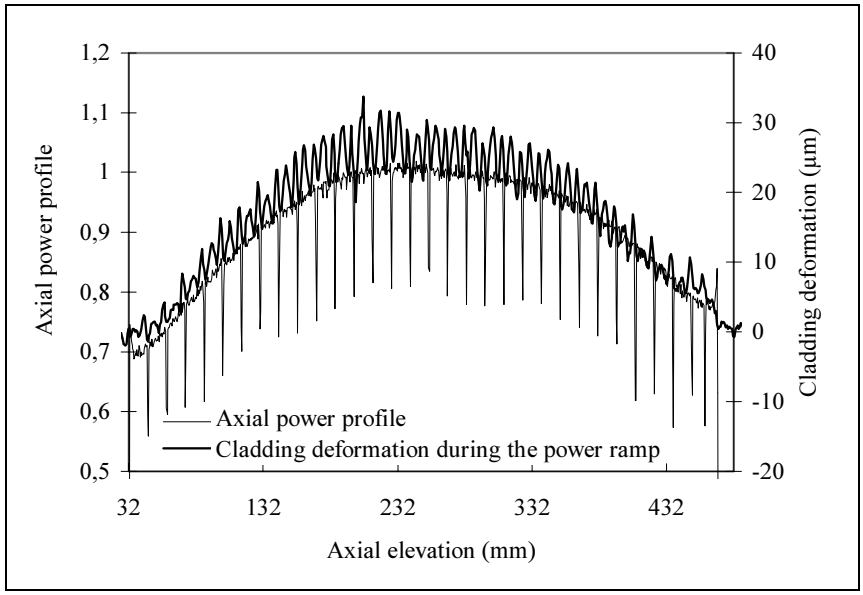

FIG. 3. Cladding diameter change of the J12/5 rod due to power ramping along with the axial power profile determined by γ-scanning.

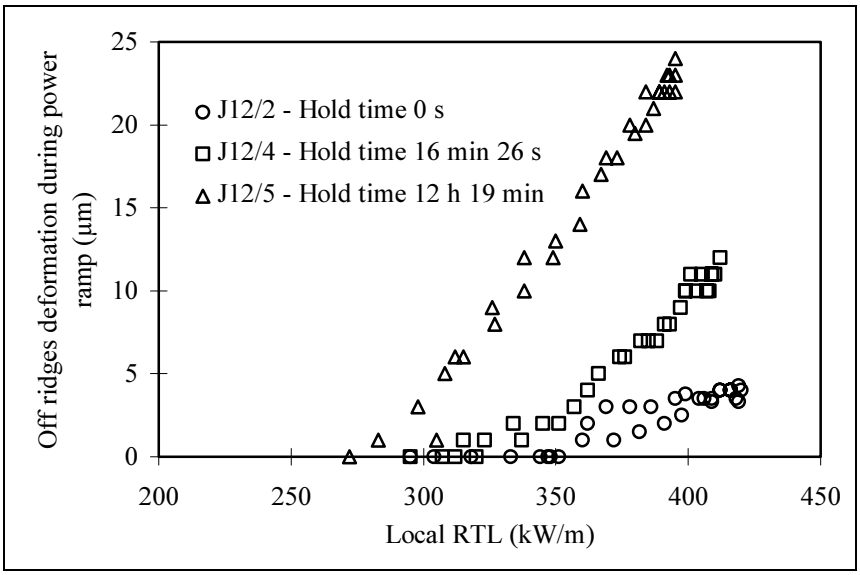

FIG. 4. Cladding deformation during J12/2, J12/4 and J12/5 power ramp tests at edges of interface ridges against local RTL.

thermal conduction, formation of ridges on the cladding at the pellet interfaces due to Pellet-Cladding Mechanical Interaction (PCMI);

in transient conditions : intensification of the PCMI due to the fuel temperature increase, creep of the fuel and viscoplasticity of the cladding under high stresses.

Up to now, the TOUTATIS code has been oriented towards the modelling of the PCMI failure risk of relatively low irradiated fuels, which thus contain little gaseous fission products. Moreover, for what concerns the cladding failure in stress corrosion conditions, only the few minutes preceding failure are of interest - which means the first minutes at RTL. In such conditions, gaseous swelling

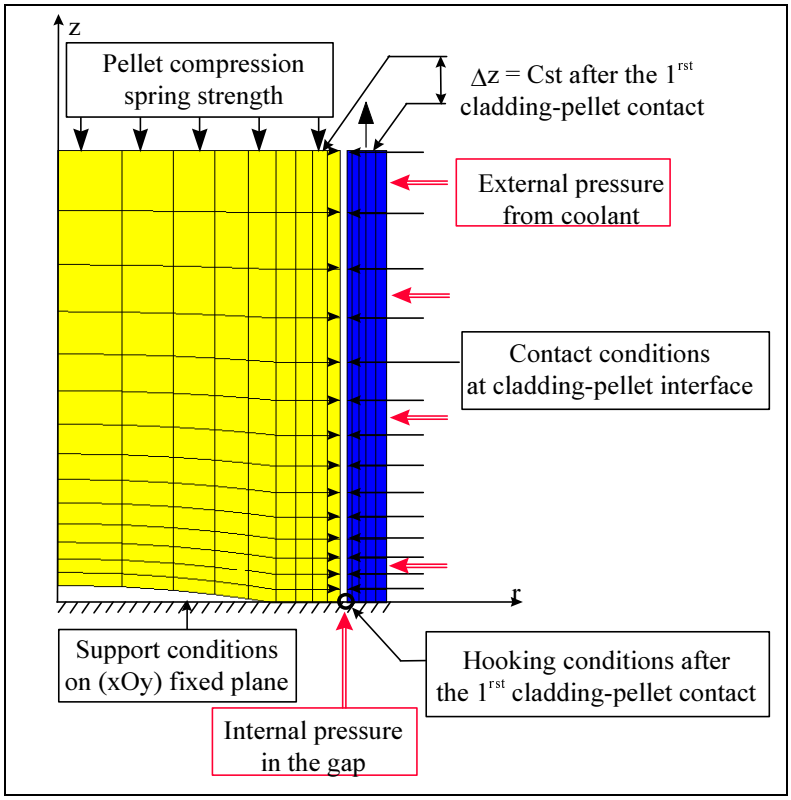

FIG. 5. Boundary conditions and mechanical loads applied on the half pellet and the associated cladding portion modelled by TOUTATIS code.

influence has been considered as negligible. This is the reason why creation and behaviour of fission gas within the fuel pellet are not yet taken into account within TOUTATIS code.

3.2. Simulations of PWR pre-irradiation

Post-calculations of the J12/2, J12/4 and J12/5 experiments required the preliminary computation of the « mother » rod irradiation up to two cycles in a French PWR. Indeed, the acquaintance of thermal history and cladding strains undergone by the «mother » rod up to the experiment is necessary to obtain a realistic representation of the refabricated rods at the beginning of the power ramp tests.

Moreover, the 2D version of TOUTATIS code does not consider any fragmentation within the fuel, which leads calculations to more or less underestimate fuel expansion and thus cladding deformation, especially at the end of PWR pre-irradiation. An adjustment method was adopted to ensure

3.2. Simulations of PWR pre-irradiation

Post-calculations of the J12/2, J12/4 and J12/5 experiments required the preliminary computation of the « mother » rod irradiation up to two cycles in a French PWR. Indeed, the acquaintance of thermal history and cladding strains undergone by the «mother » rod up to the experiment is necessary to obtain a realistic representation of the refabricated rods at the beginning of the power ramp tests.

Moreover, the 2D version of TOUTATIS code does not consider any fragmentation within the fuel, which leads calculations to more or less underestimate fuel expansion and thus cladding deformation, especially at the end of PWR pre-irradiation. An adjustment method was adopted to ensure

the consistency of calculated and measured off ridges cladding outer diameters after PWR irradiation. For each rod, two calculations of base irradiation were performed. The first one allowed to quantify the difference between measurements and rough computations. The rod geometry used in the second calculations was then adjusted to compensate this difference ; fuel radius were reduced of 3-5μm for the J12/2, J12/4 and J12/5 rods. The final stresses and strain fields at the end of this last computation were introduced as initial state for the power ramp calculation.

As shown in Table III, the results provided by the adjusted computation of the PWR pre-irradiation showed reasonably good agreement compared with most of the «mother » rod measurements. Nevertheless, calculation overestimates the interface ridges height. Indeed, during PWR irradiation, creep of the oxide contributes to straighten up fuel fragments which lowers PCMI at pellets interface levels. When fuel fragmentation is not taken into account, this phenomenon is weakened and oxide thrust on the cladding is undervalued at pellets interface levels.

TABLE III. COMPARISON BETWEEN MEASUREMENTS AND TOUTATIS 2D CALCULATIONS AT THE END OF THE PWR PRE-IRRADIATION OF THE « MOTHER » ROD.

	Post-irradiation Examinations	Calculation results
Outer cladding diameter off ridges :	corrected from zircon thickness	with diameter adjustment
on floor 2	9407 μm	9408 μm
on floor 4	9402 μm	9402 μm
on floor 5	9406 μm	9404 μm
Interface ridges diametral height	5 to 6 μm	9 μm
Pellet-clad gap at zero power	15 μm	16 μm

3.3. Calculations of the J12/2, J12/4 and J12/5 power ramp tests : results and discussion

The TOUTATIS code calculates the local thermo-mechanical behaviour of a fuel rod segment along which the linear power density is constant. Thus, in order to reproduce the axial profile of cladding deformation, calculations were achieved for each tested rod on four different axial levels, including of course the maximum power level.

During the power ramp calculations, clad external temperature was imposed. Its value had been calculated as a function of linear power density from temperature measurements in the coolant during the experiment, considering a clad-coolant exchange coefficient responding to the Colburn relation [4-5].

For what concerns calculation results, the analysis focuses more especially on deformation off ridges and on pellets interface level. The calculation results are reported and confronted to the experimental data on Figures 6 to 8.

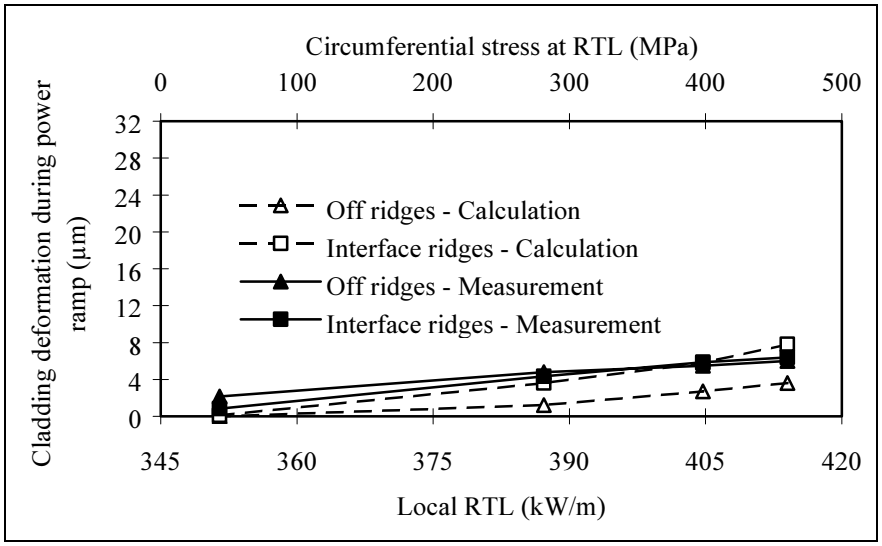

FIG. 6. Cladding deformation of the J12/2 rod during the power ramp against local Ramp Terminal power Level (RTL) and inner cladding circumferential stress on pellet interface levels. The uncertainties on outer cladding diameter measurements are ± 3µm.

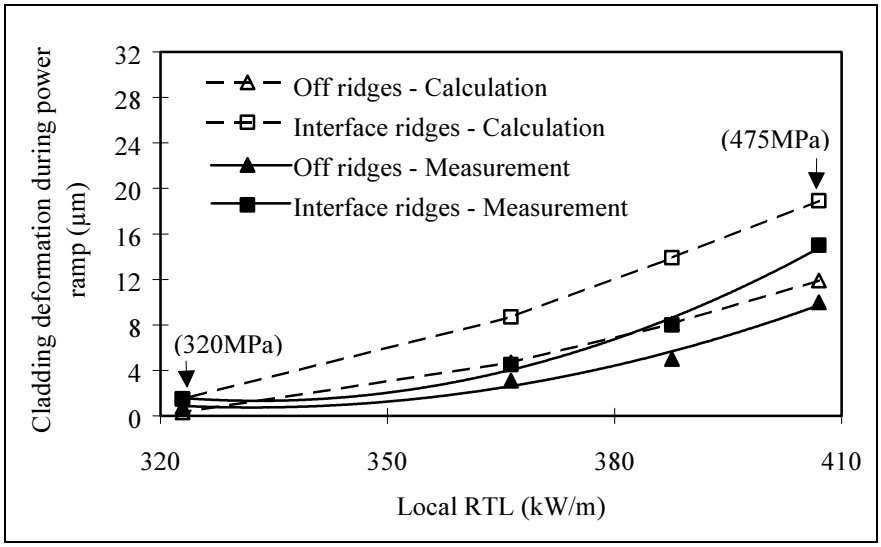

FIG. 7. Cladding deformation of the J12/4 rod during the power ramp against local Ramp Terminal power Level (RTL). Inner cladding circumferential stress on pellet interface levels is indicated in brackets. The uncertainties on outer cladding diameter measurements are ± 3µm.

Computations properly reproduce the influence of axial power profile on cladding variations during the three power transients. They also satisfactorily simulate the influence of hold time ; an especially good agreement is obtained for the J12/2 and J12/4 experiments, with hold times enclosing the failure times experimentally observed for power ramp tests, which stand in the order of a few minutes.

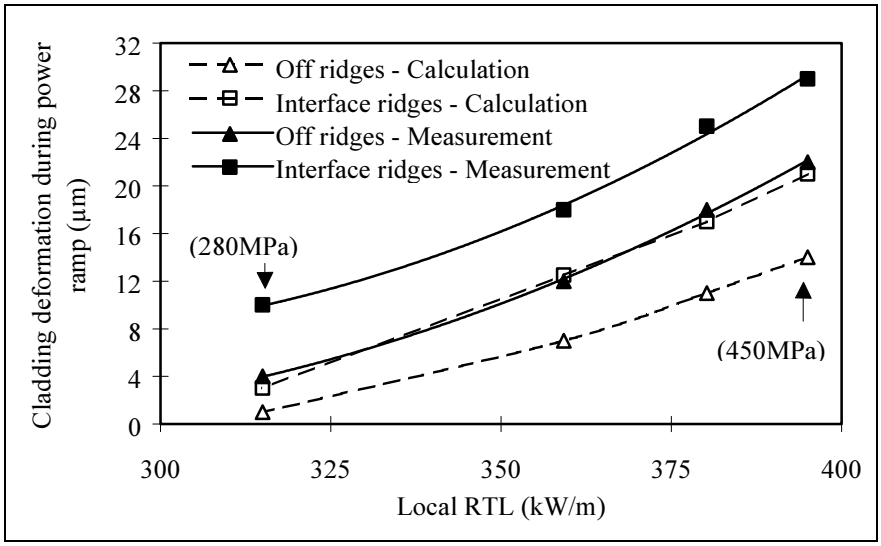

FIG. 8. Cladding deformation of the J12/5 rod during the power ramp against local Ramp Terminal power Level (RTL). Inner cladding circumferential stress on pellet interface levels is indicated in brackets. The uncertainties on outer cladding diameter measurements are ± 3µm.

The J12/2 experiment does not allow to discriminate between Zircaloy time dependent relaxation and instantaneous plasticity to explain the irreversible deformation created during transient but, according to calculation, both mechanisms participate in an equivalent way when the inner cladding circumferential stress calculated at RTL, on the pellets interface level, reached 490 MPa. For information, the corresponding values are respectively 475 and 450 MPa for J12/4 and J12/5 cases.

In the case of the J12/5 test, cladding deformation is perceptibly underestimated although the axial profile is correctly simulated. Indeed, this experiment presents a long hold time at RTL compared to the others (12h against 0s and 16 min), which could have allowed fuel gaseous swelling to occur. As this phenomenon is not taken yet into account within TOUTATIS code, its missing contribution leads to underestimate the cladding deformation of this rod. The fact that experimental data differ from calculation results in a very regular manner together with micrographic examinations (which indicates a weak but noticeable gaseous swelling) supports this assumption.

4. CONCLUSION

The J12/2, J12/4 and J12/5 ramp tests were achieved with the respective hold times of zero at 41.5 kW/m, 16 min 26s at 40.7 kW/m and 12h 19min at 39.5 kW/m; no rod failure occurred during or after these experiments.

For all cases, a good correlation was observed between the local power during experimental irradiation and the cladding deformation measured after the ramp tests. Inter-comparison of post-irradiation measurements performed on the three rods also clearly demonstrates that the cladding deformation increases with the hold time at RTL. This parameter influences more particularly the evolution of secondary ridges.

An analysis of the cladding deformation has been achieved concerning the J12/2, J12/4 and J12/5 rods by carrying out post-calculations of the three experiments with the 2D fuel modelling code TOUTATIS. Diameter changes calculated during the tests satisfactorily reproduce measurements, especially for the J12/2 and J12/4 experiments with hold time at RTL enclosing the failure times

experimentally observed for power ramp tests. But a noticeable effect of gaseous swelling appears for the longer hold time, in accordance with the metallographic examinations.

REFERENCES

[1] ALBERMAN, A., ROCHE, M., COUFFIN, P., BENDOTTI, S., MOULIN, D.J., and BOUTFROY, J.L., Nucl. Eng. Design 168 (1997) 293-303.

[2] BROCHARD, J., BENTEJAC, F., and HOURDEQUIN, N., "Nonlinear finite element studies of the Pellet Cladding Mechanical Interaction in a PWR fuel", Structural Mechanics in Reactor Technology (Proc. Int. Conf. Lyon,1997).

[3] STRUZIK, C. , MELIS, J.C., and FEDERICI, E., Light Water Reactor Fuel Performance (Int. Topical Meet.West Palm Beach, 1994).

[4] WONG, H.Y., LONGMAN (eds), Handbook of essential formulae and data on heat transfer for engineers.

[5] KREITH, F., MASSON (eds), Transmission de la chaleur et thermodynamique.

FINITE ELEMENT SIMULATION OF THE THERMOELASTIC BEHAVIOUR OF A FUEL ROD

A. SOBA, A. DENIS
Depto. Combustibles Nucleares,
Comisión Nacional de Energía Atómica,
Buenos Aires, Argentina

Abstract

In 1986 the irradiation of the first prototypes of MOX fuels fabricated in Argentina started. The experiment's description, the results of the PIEs and the comparison with the output of the BACO code were published in 1996. In particular, Eddy current testings were performed before and after irradiation. The latter yielded wavelike signals whose amplitude variations can be easily correlated with the pellet distribution through the fuel rod and with the power profile. The present work attempts to give a thermomechanical interpretation of this experimental fact. The pellet and the cladding are simulated by a finite element scheme. Although the results are still preliminary, the tendency of the system to expand preferentially in the vicinity of the pellet's edge is well represented and the results correlate properly with the experimental observations.

1. INTRODUCTION

The first Argentine prototypes of Pressurized Heavy Water Reactor (PHWR) UO_2 (MOX) fuel rods were fabricated and controlled in the α-Facility of the U.A.Combustibles Nucleares of the Comisión Nacional de Energía Atómica (CNEA). The irradiation experiments were carried out in the High Flux Reactor (HFR) of Petten, The Netherlands. The preirradiation destructive examinations of one of the rods and the postirradiation examinations of the others were performed in the Kernforschungszentrum (KfK), Karlsruhe, Germany. Two of the rods included Iodine doped pellets, one of them with elemental Iodine and the other one with CsI, to simulate a starting burnup of about 14-15 GWd/ton(M). Two other non-doped rods were irradiated together for a long period at an average linear power of 230 W/cm to a final burnup of 15 GWd/ton(M). After that, one of them was submitted to a power ramp until an increase of activity in the coolant water was detected, indicating that a failure in the rod had occurred. The detailed description of this experiment is given elsewhere [1].

All the rods were examined after irradiation. Besides the visual inspections, dimensional determinations were performed in both non-doped rods after the base irradiation and in one them also after the power ramp. To this end, Eddy current testings and absolute diameter measurements were carried out. The linear power profiles are shown in Fig. 1. The dimensional results are shown in Figs. 2 and 3, that correspond to the rods labeled A.1.2 and A.1.3 respectively in Ref. [1].

The dimensional characteristics of the fuel rods are:

Pellet height	1.12±0.01 cm
Pellet radius	1.040±0.001 cm
Pellets number	21
Enrichment	1.25%
Cladding inner radius	0.5225 cm
Cladding outer radius	0.5825 cm
Gap thickness	0.0025 cm

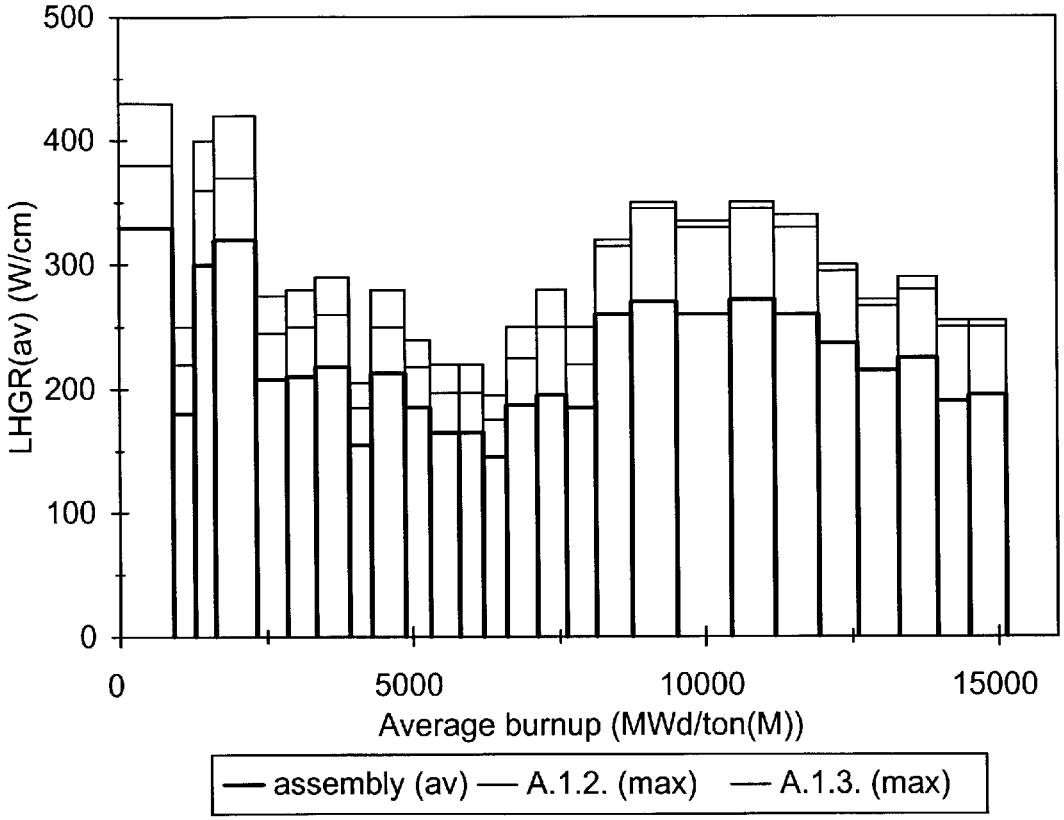

FIG. 1.a. Linear heat generation rate during stationary irradiation of rods A.1.2 and A.1.3.

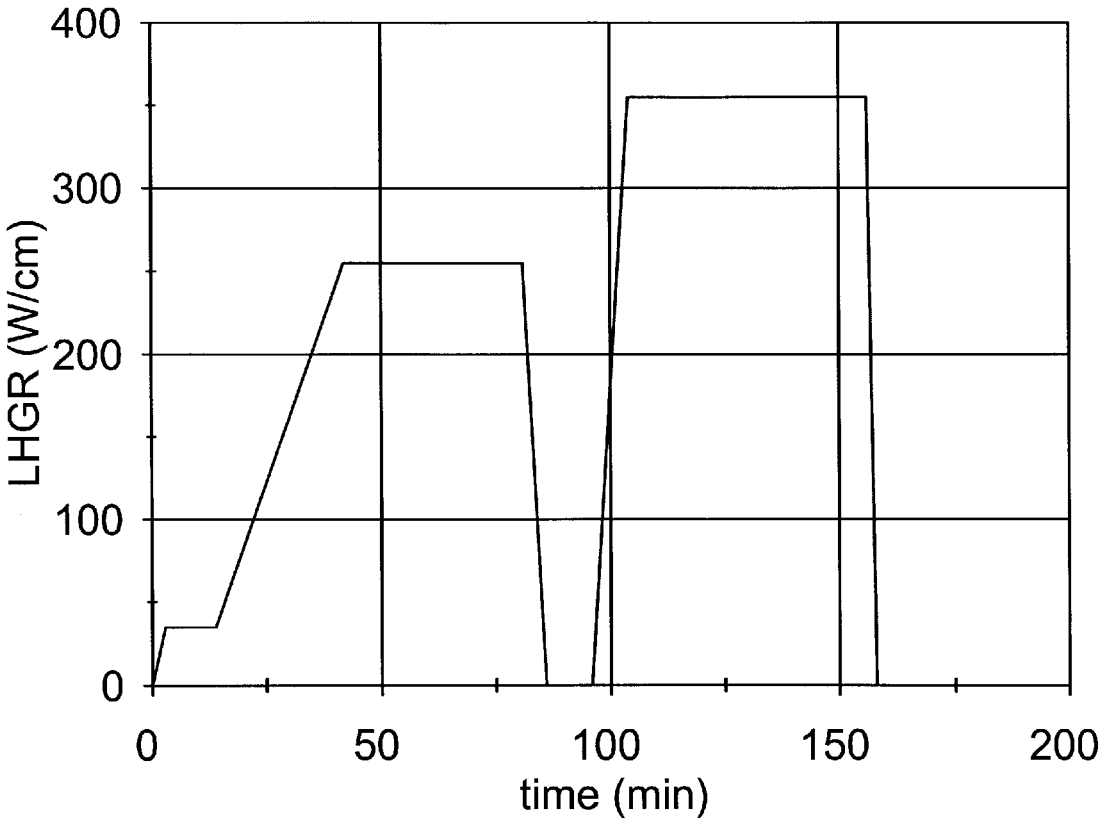

FIG. 1. b. Linear power ramp applied to rod A.1.3 after the stationary irradiation of a.

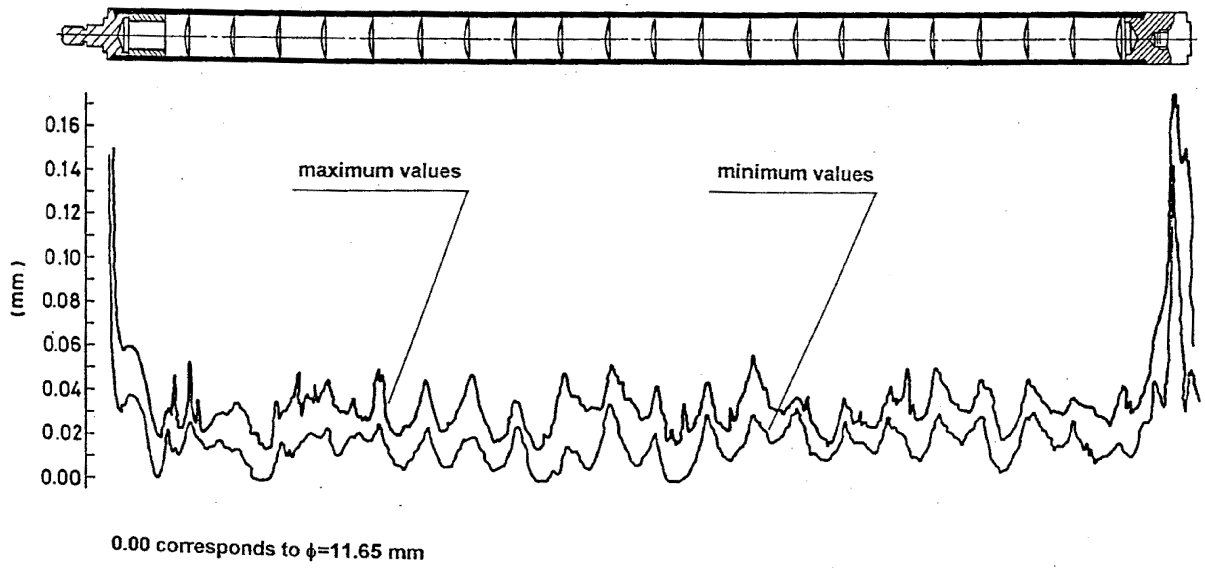

FIG. 2. Dimensional profile of rod A.1.2 after stationary irradiation.

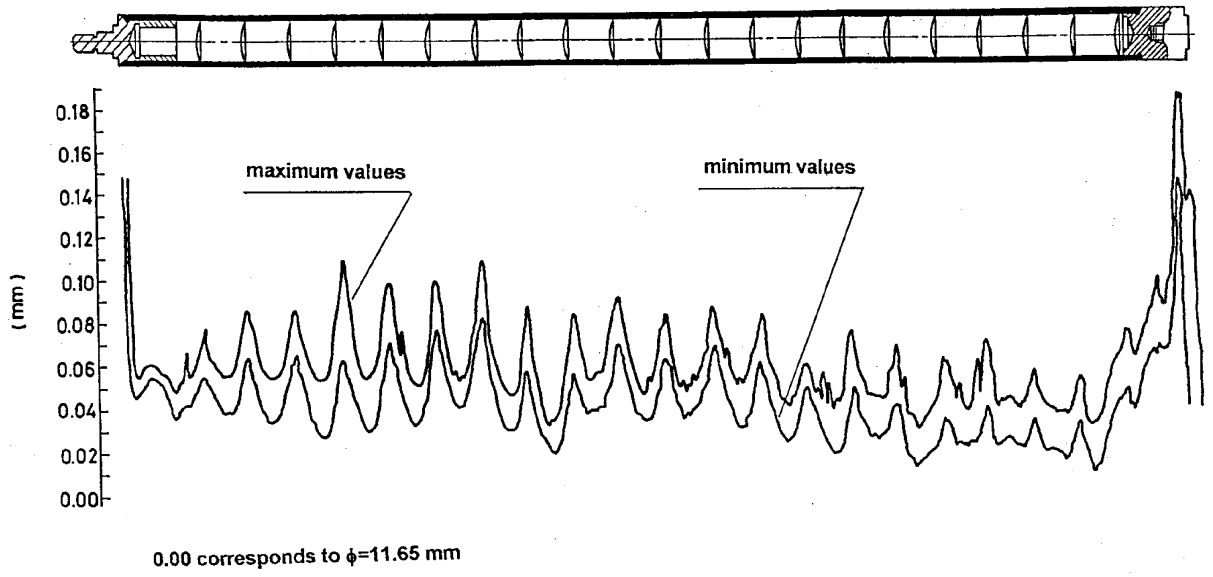

FIG. 3. Dimensional profile of rod A.1.3 after stationary irradiation and power ramp.

2. PROPOSED MODEL

The pellet, the cladding and the gap between them are simulated by the finite element method. A scheme of the system representing a longitudinal section of the fuel rod is shown in Fig. 4.

Due to the high temperatures developed within the pellet, particularly at its center line, and to the strong temperature gradient that consequently appears, the cylindrical pellet surface distorts: it bends outwards, the top and bottom faces being displaced further than the central belt [2]. The dimensional changes in the fuel rod provoked by thermal expansion may induce pellet-cladding interaction (PCI) and the consequent plastic cladding strain [3].

To simulate this problem the thermal and elastic coupled equations have to be solved.

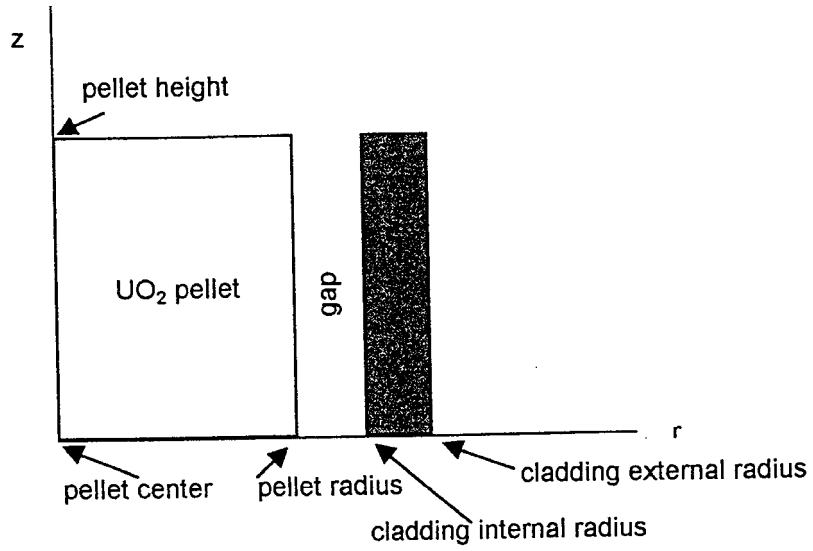

FIG. 4. Scheme of the longitudinal section of the pellet-gap-cladding system.

2.1. The thermal problem

Since the system has axial symmetry, cylindrical coordinates are employed. The temperature depends on r and z only. If T represents the temperature, Q is the volumetric heat generation rate, $\kappa=\kappa(T)$ is the thermal conductivity and assuming steady-state heat transfer conditions, the temperature distribution in each material is obtained by solving the differential equation:

$$\kappa\left(\frac{1}{r}\frac{\partial}{\partial r}\left(r\frac{\partial T}{\partial r}\right)+\frac{\partial^2 T}{\partial z}\right)+Q=0$$

with the boundary conditions: T=300°C at the cladding external radius (Dirichlet condition) and ∇T=0 (Neumann condition) at the remaining portion of the system boundary.

Application of the finite element method involves definition of a mesh, which in this case is chosen of triangular elements, definition of the corresponding shape functions, approximation of the continuous unknown function T by a linear combination of the shape functions. A system of linear equations is finally obtained, one equation for each unknown nodal value. The matrix formulation of the problem is:

$$[k^e]\{\Phi^e\}=\{f_Q^e\}-\{I^e\} \qquad \text{(A)}$$

where the superscript e indicate a magnitude referred to an element, $[k^e]$ is the element stiffness matrix defined as

$$[k^e]=2\pi\bar{r}A[B]^T[D][B], \qquad \text{(B)}$$

$\bar{r}$ is the radial distance to the centroid of the element, A is the element area, the coefficients in the matrix B are obtained differentiating the shape functions relative to r and z,

$$D=\kappa\begin{bmatrix}1 & 0\\ 0 & 1\end{bmatrix},$$

the column vector $\{\Phi^e\}$ contains the nodal values of the unknown function,

$$\{f_Q^e\}=\int_V Q[N]^T dV,$$

the row vector $[N]$ contains the shape functions and the column vector $\{I^e\}$ contains the Neumann boundary conditions, which in the present case are zero.

The solution of the heat transfer problem becomes the input to the stress analysis problem and the same discretization is used to solve both.

2.2. The constitutive equations

Given the axial symmetry of the system, neither the geometry nor the surface loading depends on the angular coordinate. The displacements, strains and stresses are functions of r and z only. Let us represent with u and w the displacements in the r and z direction, respectively. The strain-displacement relations are [4]:

$$e_{rr} = \frac{\partial u}{\partial r} \;\; ; \;\; e_{\theta\theta} = \frac{u}{r} \;\; ; \;\; e_{zz} = \frac{\partial w}{\partial z} \;\; ; \;\; e_{rz} = \frac{\partial u}{\partial z} + \frac{\partial w}{\partial r} \;\; ; \;\; e_{r\theta} = 0 \;\; ; \;\; e_{z\theta} = 0$$

The four non-zero components of the strain are placed in the column vector $\{e\}$:

$$\{e\}^T = [e_{rr} \quad e_{\theta\theta} \quad e_{zz} \quad e_{rz}]$$

The strain components are separated into elastic ($\{\varepsilon\}$) and thermal ($\{\varepsilon_{th}\}$) strains:

$$\{e\} = \{\varepsilon\} + \{\varepsilon_{th}\}$$

where:

$\{\varepsilon\}^T = [\varepsilon_{rr} \quad \varepsilon_{\theta\theta} \quad \varepsilon_{zz} \quad \varepsilon_{rz}]$ and $\{\varepsilon_{th}\}^T = [\alpha\Delta T \quad \alpha\Delta T \quad \alpha\Delta T \quad 0]$

and α is the thermal expansion constant.

According to the elasticity theory, for small deformations, the stresses depend linearly on deformations. This is the Hooke's law which in matrix form is expressed as:

$$\{\sigma\} = [D]\{\varepsilon\}$$

where the vector of stress components is

$\{\sigma\}^T = [\sigma_{rr} \quad \sigma_{\theta\theta} \quad \sigma_{zz} \quad \sigma_{rz}]$

and $[D]$ is the material matrix given by:

$$[D] = \frac{E}{1+\mu}\begin{bmatrix} d & b & b & 0 \\ b & d & b & 0 \\ b & b & d & 0 \\ 0 & 0 & 0 & 1/2 \end{bmatrix} \quad \text{with} \quad d = \frac{1-\mu}{1-2\mu} \quad \text{and} \quad b = \frac{\mu}{1-2\mu}$$

The constants E and μ are the Young's modulus and the Poisson's ratio, respectively.

When the finite element method is applied, the unknown displacements u and w are written in terms of the element nodal values and the shape functions. The above differential equations are thus transformed to linear equations:

$$\begin{Bmatrix} u(r,z) \\ w(r,z) \end{Bmatrix} = [N]\{U^e\}$$

The strain-displacement relationships yield:

$$\{e\} = [B]\{U^e\}$$

The matrix formulation of the problem is:

$$[k^e]\{U^e\} = \{f^e\} - \{I^e\}$$

which is formally identical to that employed for the thermal problem (1) , the matrix $[k^e]$ is defined as in (2) with the corresponding expressions for matrices [*B*] and [*D*]. The term $\{f^e\}$ contains the contributions of the thermal force and of the external pressure:

$$\{f^e\} = \int_V [B]^T [D]\{\varepsilon_{th}\} dV + \int_\Gamma [N]^T \begin{Bmatrix} p_r \\ p_\theta \\ p_z \end{Bmatrix} d\Gamma$$

where Γ is the external element surface of volume *V*. The term $\{I^e\}$ contains the Neumann boundary conditions, which are zero as in the thermal problem [4].

The physical constants employed in the present calculations are listed in Table I.

TABLE I.

Young's modulus *E* (N cm^{-2})	
UO_2:	$2.065 \times 10^7 (1+1.091 \times 10^{-4} T)$ [5]
Zry:	$1.236 \times 10^7 - 6.221 \times 10^3 T$ [5]
Poisson's ratio μ	
UO_2:	0.316 [5]
Zry:	0.32 [5]
Thermal expansion α (K^{-1})	
UO_2:	$(-4.972 \times 10^{-4} + 7.107 \times 10^{-6} T + 2.583 \times 10^{-9} T^2)/\Delta T$ [5]
Zry:	$(-2.07 \times 10^{-3} + 6.72 \times 10^{-6} T)/\Delta T$ [5]
Thermal conductivity κ (W $cm^{-1}K^{-1}$)	
UO_2:	$\left[\frac{40.4}{464+T} + 1.216 \times 10^{-4} \exp(1.867 \times 10^{-3} T)\right]$ [5]
Zry:	$7.51 \times 10^{-2} + 2.09 \times 10^{-4} T - 1.45 \times 10^{-7} T^2 + 7.67 \times 10^{-11} T^{-3}$ [5]
He:	$3.366 \times 10^{-3} T^{0.668}$ [5]
temperatures T in K.	

3. CALCULATION PROCEDURE

3.1. The numerical method

The domain discretization in performed by means of linear triangular elements. The mesh employed in the calculations contains 179 nodes and 311 elements divided into three groups, corresponding to each material of the system: UO_2 pellet, gaseous gap and Zry cladding. A non uniform mesh is chosen in order to have a more detailed description in the region where the greater variations are expected. To this end, an element side length of 0.2 cm is chosen at the pellet center and of 0.05 cm at the pellet outer radius, in the gap and in the cladding wall. The discretization was carried out with the bidimensional mesh generator DELAUNAY 2.0 developed at CAB-CNEA; the result is shown in Fig. 5.

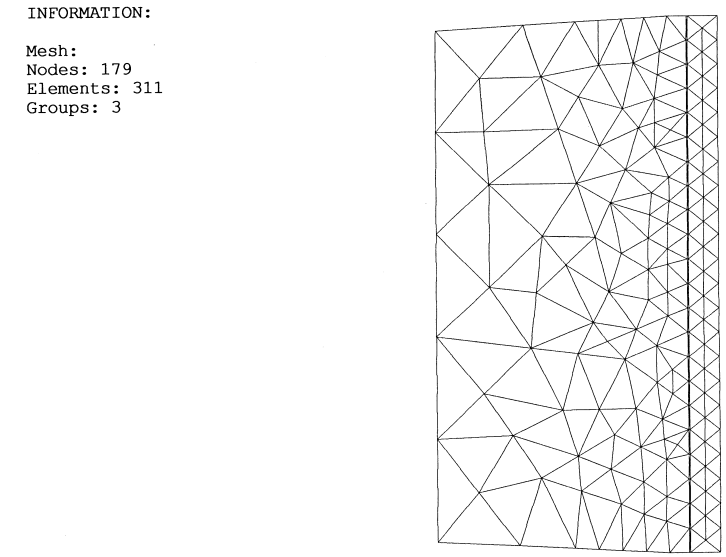

FIG. 5. Finite element discretization of the system.

3.2. The calculation program

The calculation program was written in FORTRAN and consists of approximately 1300 statements. The graphical inputs and outputs were developed in C.

The power history and the boundary conditions constitute the data entry. The code solves the heat transfer equation by the finite element method and gives the temperature distribution in the 3-phases system in each step. Then, the elasticity equations are solved, where the term $\alpha \Delta T$ contains the temperature variation between two consecutive steps. The elastic problem is also solved by the finite element method, the displacements U in each node and in each direction (r and z) are determined, the new coordinates of the nodes are evaluated and the calculation procedure restarts. The stress and strain state at each element are also obtained in each power step.

The output of the thermal problem is visualized by means of the program CONTOURS elaborated at CAB-CNEA while that of the elastic problem is obtained with MATLAB.

The equations systems are solved by the diagonalization method of Gauss. The calculation time required is of about 10 s per step, for the mesh dimensions employed in the present work and using an equipment PC of 32Mb RAM with a Pentium processor of 200 MHz. The power histories involved contain 27 steps of nearly constant power (rod A.1.2) or 90 steps when a final power ramp is included (rod A.1.3).

4. RESULTS AND DISCUSSION

The temperature distribution within the system before deformation is represented in Fig. 6. The isothermal lines run parallel to the axial direction; slight departures due to the discretization process are observed near the pellet center, where the element's size is larger.

Thermal expansion induces dimensional changes in the radial direction, particularly in the pellet. This expansion is more pronounced near the pellet's edges. A magnification of the outer region of the rod is seen in Fig. 7 where the curved shape of the cladding and the pellet is evident. The plot was obtained by simulating the power history of rod A.1.3 (stationary irradiation followed by final power ramp). Although only the elastic behaviour is considered in the model, a permanent deformation is achieved.

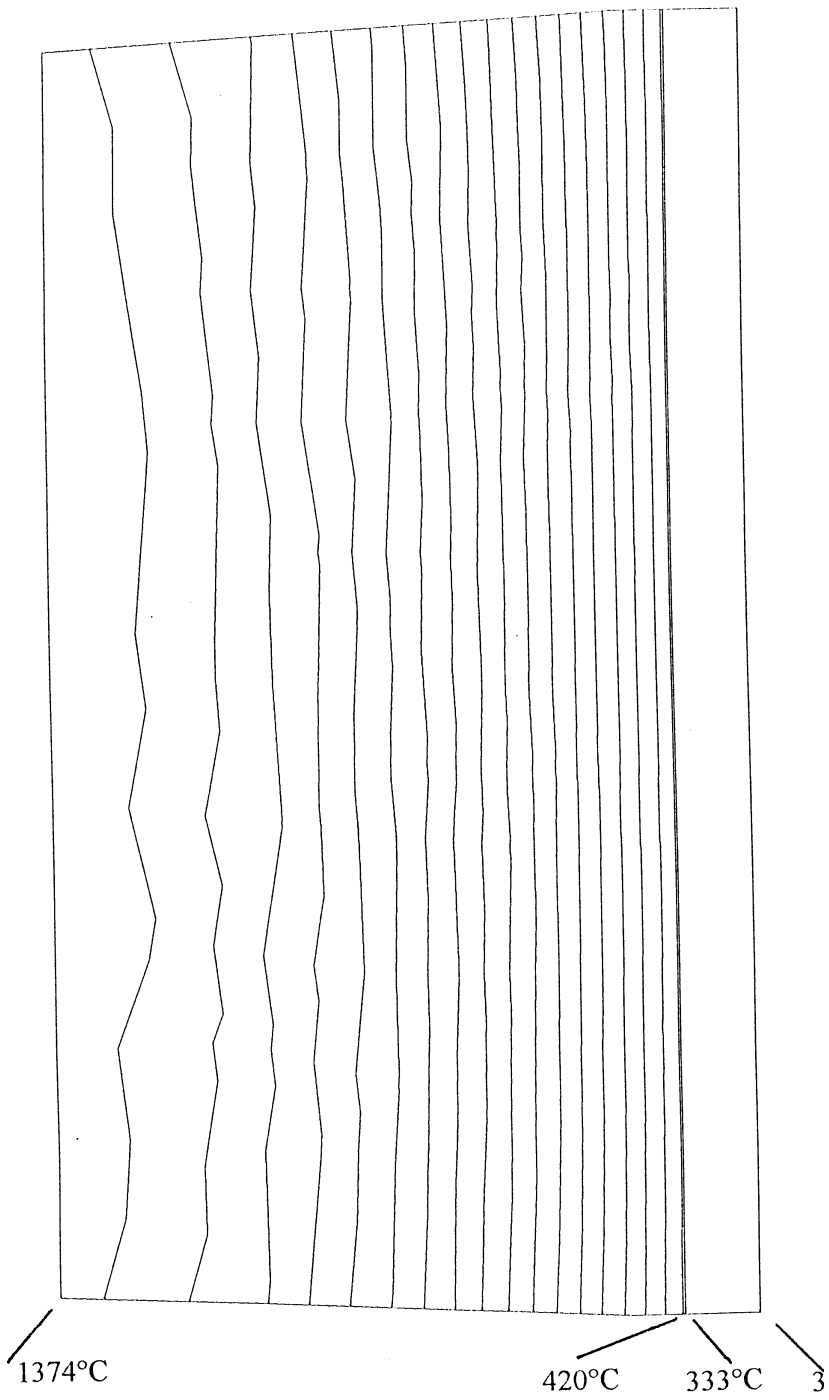

FIG. 6. Temperature distribution in the undeformed system under a linear power of 380W/cm.

This feature becomes clear from Fig. 8 where the evolution of the pellet outer and the cladding inner radii are compared. The apparent inversion between both indicates that the code predicts solid pellet-cladding contact. When this condition appears, a contact pressure between both materials is applied, which effect is to push the cladding outwards.

In Figures 9 and 10 the magnification of the outer cladding boundary after irradiation is shown. The former corresponds to the calculation results obtained with the maximum power and the latter, with the average power. The results obtained after stationary irradiation (rod A.1.2) and after stationary irradiation followed by power ramp (rod A.1.3) are superimposed for comparison. The more remarkable feature is the presence of ridges on the external surface of the cladding accompanying the pellets' distribution. Both rods have experienced a general radius increase, as can

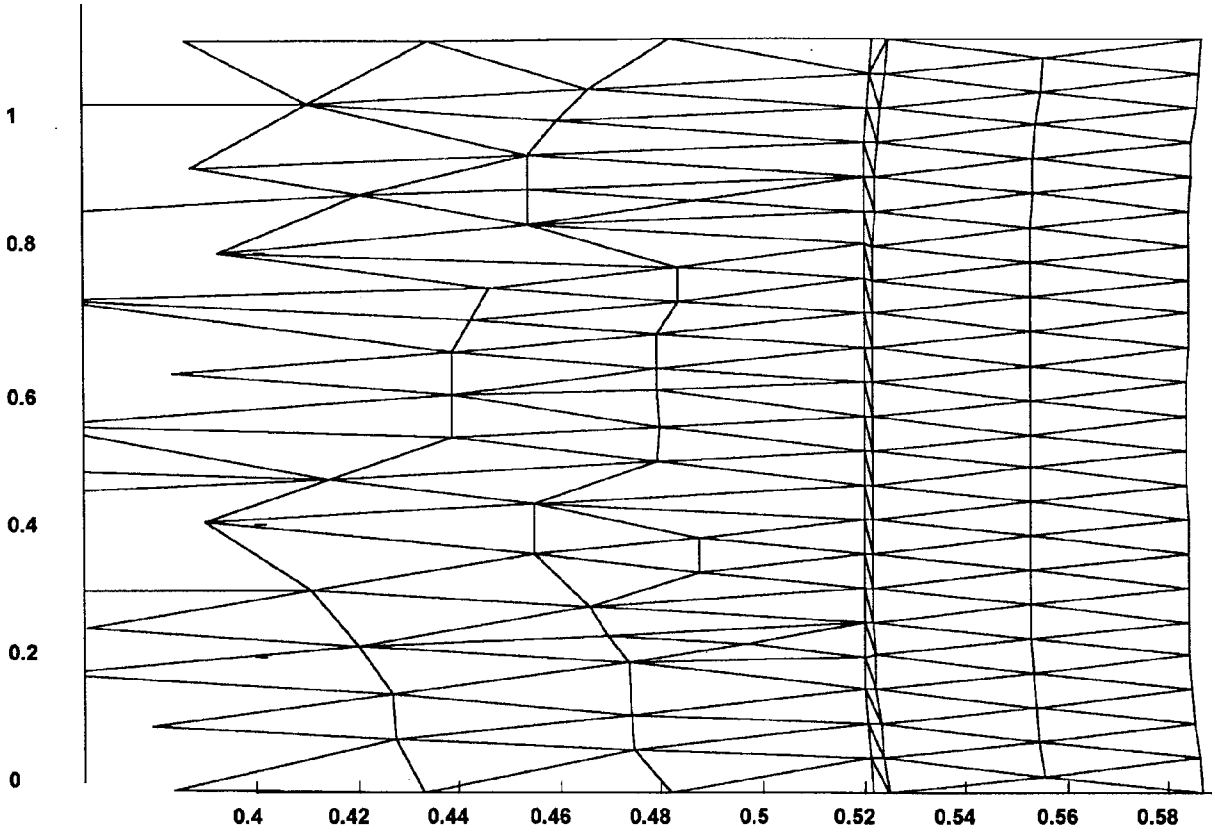

FIG. 7. Effect of irradiation with average power on the pellet and cladding shape of rod A.1.3 after power ramp.

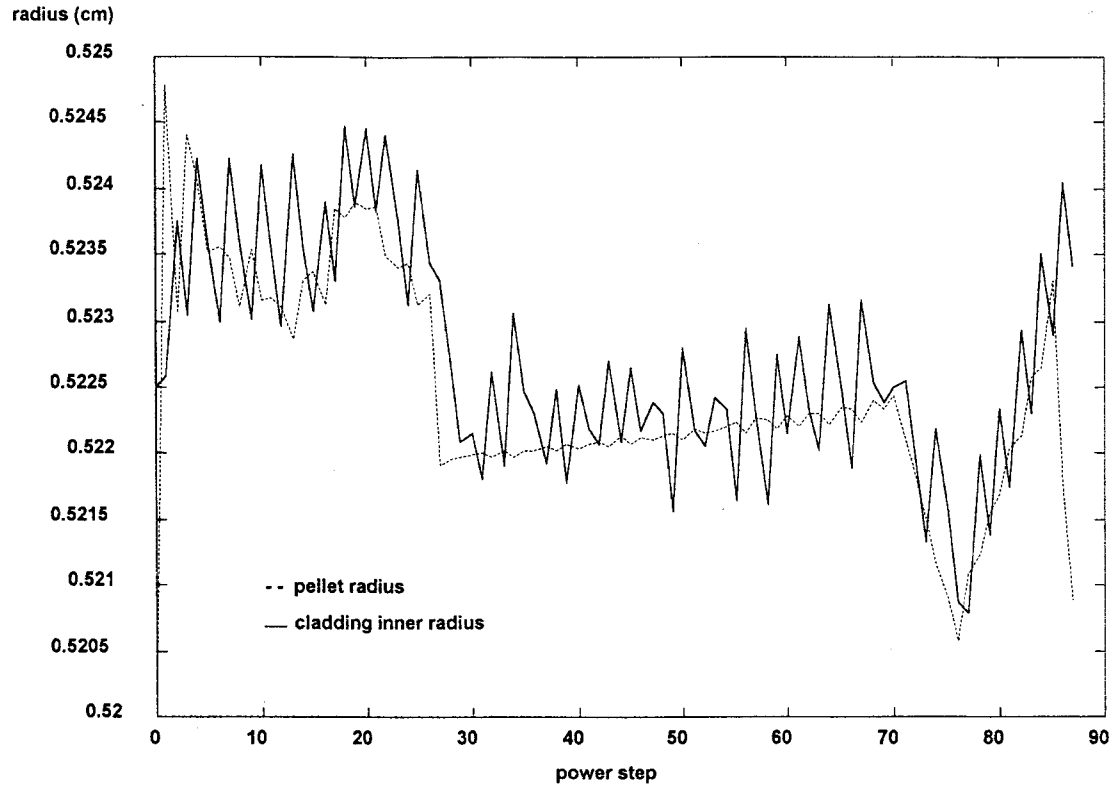

FIG. 8. Evolution of the radius in the belt region of rod A.1.3 during irradiation with maximum power followed by power ramp.

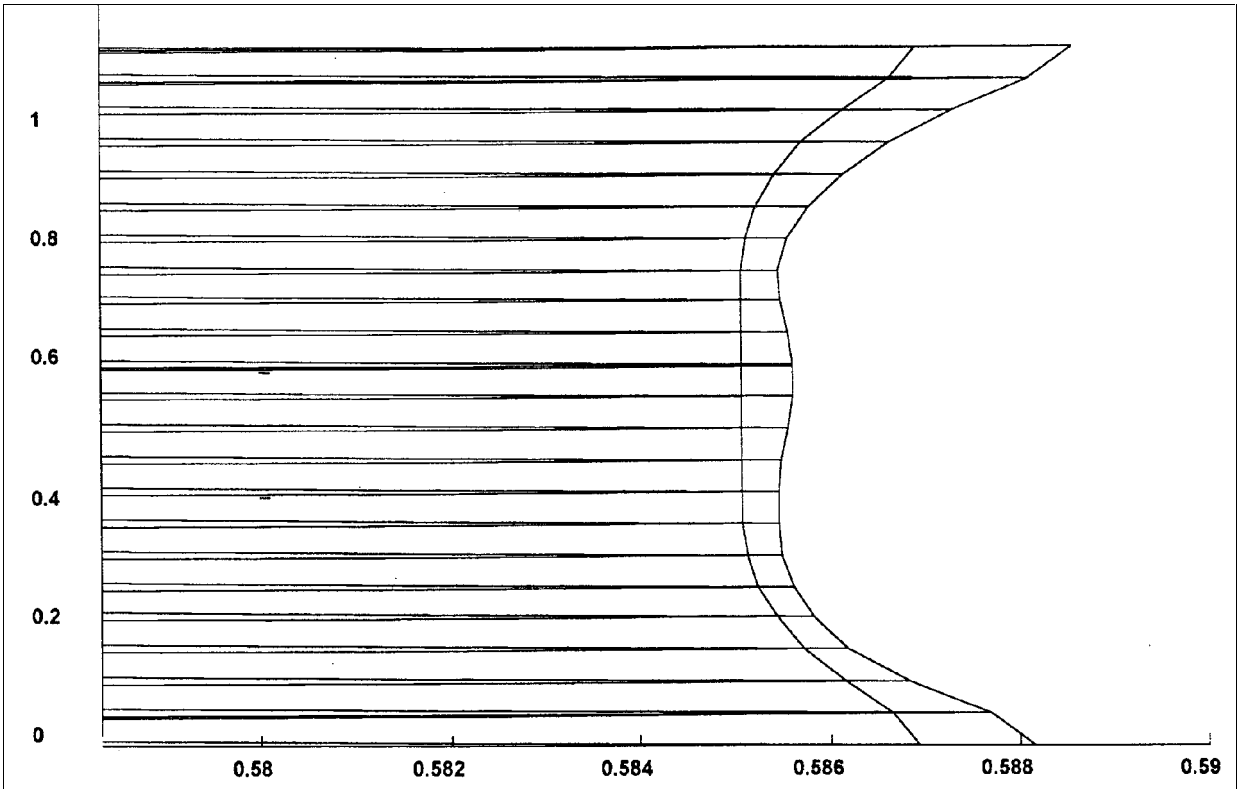

FIG. 9. Comparison between the external boundary final shapes of rods A.1.2 and A.1.3 with maximum power.

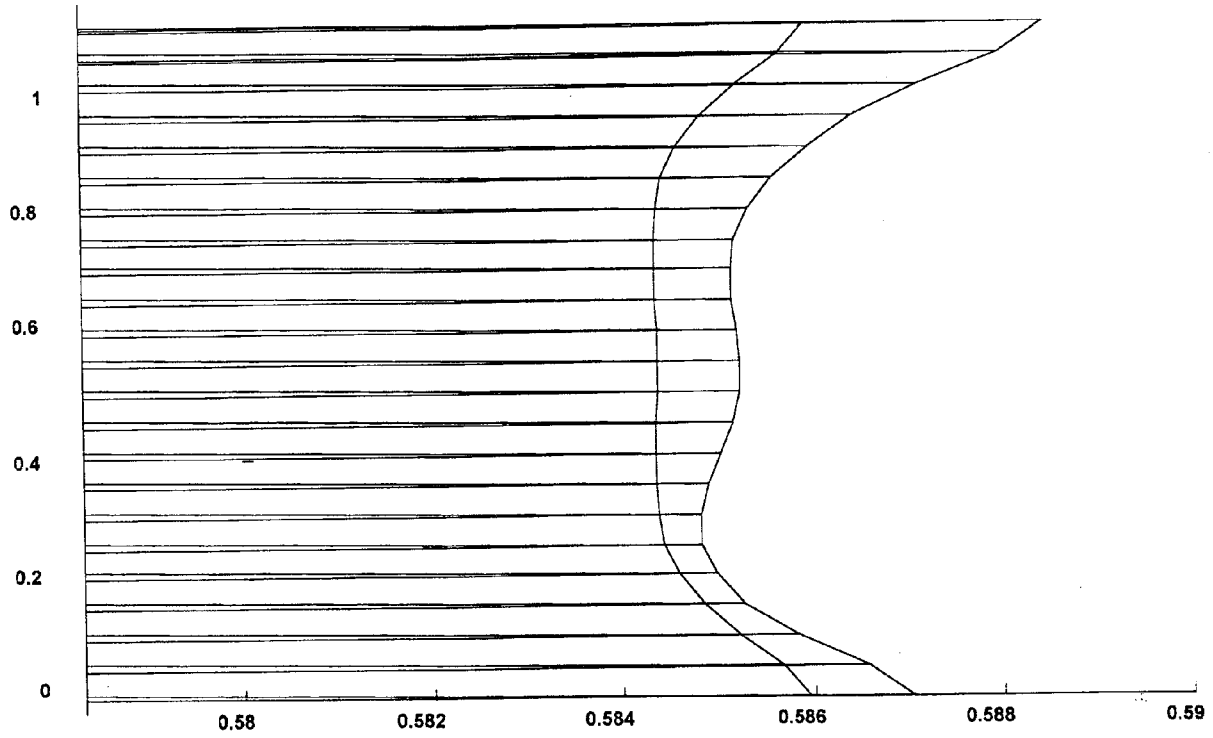

FIG. 10. Comparison between the external boundary final shapes of rods A.1.2 and A.1.3 with average power.

be seen by comparing the clad belt radii with the initial radius of 0.5825 cm. It is visible that the power ramp has a strong effect on the cladding permanent deformation, which is of 0.3% for the rod A.1.2 and 0.55% for the rod A.1.3. This effect is more significant on the crests, where the deformation is of about 0.6% and 1%, respectively.

The experimental results shown in Figures 2 and 3 reveal that for rod A.1.2 the crests' height ranges between 18 and 30 μm and for rod A.1.3, between 28 and 55 μm. The calculations performed in the present work predict values in the ranges 16 to 18 μm in the first case and 29 to 33 μm in the second, the band being due to using the average or the maximum power as input.

5. CONCLUSIONS

The thermoelastic code developed in this work is able to reproduce with reasonable accuracy the deformation of a fuel rod that has undergone either a stationary power history or a power ramp. The results agree with those obtained with the BACO code [1].

As the results presented in the previous section reveal, the calculated figures fall within the lower end of the experimental results range. Given that the model only contains the elastic effects, this seems to indicate that incorporation of the inelastic effects, which will be the next step in the work, will improve the results. The phenomena of creep and swelling will be also incorporated in the near future.

ACKNOWLEDGEMENTS

The authors wish to thank Lic. Pablo Adelfang for his continuous interest on this work and for the contribution of the experimental data.

REFERENCES

[1] MARINO, A.C., PÉREZ, E.E., ADELFANG, P., Journal of Nuclear Materials 229 (1996) 169-186.

[2] MATHEWS, J.R., The quantitative description of deformation and stress in cylindrical fast reactor fuel pins, in Advances in Nuclear Science and Technology, Vol.6 (1972), Academic Press.

[3] CAILLOT, L., LINET, B., LEMAIGNAN, C., Pellet clad interaction in PWR fuel. Analytical irradiation experiment and finite element modelling, (Proc. SMIRT 12, Stuttgart, Germany, 1993).

[4] SEGERLIND, L.J., Applied finite element analysis, 2nd Ed., Wiley (1984).

[5] Handbook of materials properties for use in the analysis of light water reastor fuel behaviour, MATPRO version 11, NUREG/CR-0497, TREE-1280 (1979).

CLADDING FAILURE MECHANISMS AT HIGH BURNUP
(Session 3)

Chairpersons

C. MAURY
France

G. LYSELL
Sweden

PCI PERFORMANCE OF PWR RODS WITH EXCESSIVE OXIDE SPALLING AND LARGE HYDROGEN CONTENT

P. RUDLING, H. PETTERSSON

Abstract

It is well known that hydrides in Zircaloy materials may embrittle the material and deteriorate its mechanical performance. It has also been argued in the open literature that hydrides in Zircaloy materials may impact the stress corrosion cracking, SCC, mechanism resulting in pellet cladding interaction, PCI, failures at lower rod power levels. This paper describes a study to assess if, and in such a case to what degree, hydrides in Zircaloy may lower the PCI resistance. Five fuel rod segments were manufactured from 2 PWR Zr-4 rods irradiated to a rod average burnup of about 35 MWd/kgU. The segments showed excessive oxide spalling resulting in local concentration of the cladding hydrides. Five of these segments were ramp tested in the Studsvik R-2 research reactor to power levels ranging from 45 to 50 kW/m. The paper discusses the ramp results and more specifically the potential role of hydrides/thick oxide layers on PWR fuel cladding PCI performance.

1. INTRODUCTION

Operation limit tests of light water reactor fuel were conducted in the GE test reactor, GETR, in 1964 [1]. At these tests, two fuel rods failed by a mechanism of what subsequently became to be known as pellet-cladding-interaction, PCI. Subsequent tests in the GETR enabled GE to correlate fuel failure tendency with degree of power increase. Fuel failures in commercial BWRs preferentially occurred in the peripheral rods adjacent to the control rods where the local power increase become largest when the control rods are being pulled out [2]. Since power regulation in PWRs results in smoother changes in fuel rod powers compared to that in BWRs, PCI induced failures tends to be unusual in the PWR reactor type. However, PCI-failures in PWRs could happen in conjunction with a severe power transient.

Soon after the first incidences of PCI failures researchers around the world intitiated R&D programs to understand the failure mechanism. It became clear that, stress-corrosion-cracking, SCC, was the principal cladding failure mechanism when PCI events occurred during either normal or off-normal operating conditions [2].Fracture surface characteristics in both BWR and PWR fuel rods were typical of SCC fractures produced in laboratory iodine SCC tests. This indicated that the fission-product iodine might be at least one of the responsible chemical species of PCI failed BWR and PWR fuel rods.

The mechanism of iodine-assisted SCC in Zircaloy consisted of at least two steps: crack initiation and crack propagation [4]. Shortly after the cladding has been subjected to large enough tensile stresses the protective zirconium oxide at the cladding inner surface may crack. Through the cracks the aggressive fission products may attack the fresh Zircaloy material. Cubicciotti et al. suggested that other elements such as Cs and Te in addition to iodine was probably also involved in the formation of SCC cracks in Zircaloy cladding materials [5]. This suggestion was put forward since they found deposits containing CsI, Cs, Te and Cs-U oxides at the clad inner diameter of a failed PWR rod preferentially at the position of the cladding SCC cracks. They did not find this type of deposits on unfailed rods. The deposits where found on the Zircaloy surfaces containing locally higher-than normal concentrations of alloying additives (Fe, sometimes Cr) and impurities (Al, Si possibly others). Crack propagation then occurs via intergranular and/or transgranular cracking.

Yield strength, texture and grain size are the most important material parameters influencing the I-SCC tendency of Zircaloy [4]. Decreasing grain size reduced the SCC tendency. The transgranular cracks propagate mainly in planes that are oriented about 30° to the basal planes. Thus, tubes with strongly radially oriented basal poles have a high resistance against I-SCC.

Pellet geometry, the maximum rod power level, the rod power increase level, and the friction between fuel and cladding may all impact the level of stress in the cladding. Another prerequisite for PCI failures to occur, is that the duration of the power transient is long enough [6,7]. The SCC and PCI mechanisms in Zircaloy materials were thoroughly reviewed by Cox [8,9].

The fuel cladding material picks up hydrogen during the corrosion reaction between Zircaloy and water/steam during reactor operation. The solubility of hydrogen in Zircaloy is low, and hydrides precipitate after the Zircaloy-4 matrix becomes supersaturated with hydrogen. These precipitated hydrides reduce Zircaloy ductility [10].

J. Bai found that for unirradiated Zircaloy-4 tensile sheet specimens at room temperature there is a ductile-brittle transition when the hydrogen concentration is higher than a certain threshold (about 600 wtppm for Zr-4 in stress-relieved condition) [11]. However, the corresponding result at 350°C showed no deterioration of the Zr-4 SRA ductility at the highest tested hydrogen concentration of 1100 wtppm. In this study, it was also shown that not only the hydrogen concentration at room temperature impacts the ductility but also the orientation of the hydrides are important.

Also the fracture toughness of unirradiated SRA and RXA Zircaloy-2 is reduced by the presence of hydrides [12]. A ductile-brittle transition was observed at hydrogen concentrations at 600-700 wtppm at room temperature. In the same study, no ductility deterioration was however found at 300°C up to hydrogen concentrations of 900 wtppm. On the other hand Kreyns et al., observed a continous fracture toughness decrease from 0 to 1500 wtppm H in irradiated Zr-4 [13]. This observation was true for temperatures ranging from room temperature up to 204°C. The fracture toughness also increases with temperature for all hydrogen levels.

In a study made by Cox, specimens from one batch of Zircaloy fuel cladding that had been partially cracked in iodine vapour at 300°C showed small fractured hydrides at the initiation sites of the stress corrosion cracks [14]. These radial hydrides were present at the inside surface of the original tubing and the study showed that these fractured at the start of the SCC test. Therefore Cox proposed that radial hydrides at the inside surface could facilitate the initiation of stress corrosion cracks.

To assess if fuel cladding tubes with such a thick outside surface oxide layer that it has locally spalled, resulting in localisation of hydrides, will deteriorate the PCI performance a ramp test program was initiated.

2. EXPERIMENTAL PROCEDURE

2.1. Materials and irradiation conditions in Ringhals 2

The cladding tubes were manufactured by AB Sandvik Steel and were characterised by relatively small second phase particles, SPPs. It is believed that the small SPPs are responsible for the nonoptimised corrosion properties. Rods manufactured by KWU/Siemens and irradiated in Ringhals 2 between 1983 and 1987 were taken to the hot cell laboratory at Studsvik. The manufacturing and irradiation data are provided in Table 1.

2.2. Ramping in Studsvik

Test rod manufacturing

After the base irradiation of the two rods from Ringhals 2 interim examinations were performed prior to ramp segment manufacturing to ensure that the rods would be acceptable for ramping. These examination included:

- Visual inspection
- Axial gamma scanning

TABLE I. MANUFACTURING AND IRRADIATION DATA OF FATHER RODS IN RINGHALS 2

	Rod no. 09222	Rod no. 08863
Cladding outer diameter (mm)	10,75	10,75
Cladding inner diameter (mm)	9,30	9,30
He-fill pressure (MPa)	2,25	2,25
Fuel density (g/cm^3)	10,4	10,4
Enrichment (%)	3,20	3,20
Pellet height (mm)	11	11
Irradiation data (MWd/kgU)	35,2	35,2
Fission gas release (%Xe)	0,41	0,24

Fuel segments, about 700 mm in length were cut from the two full-size fuel rods and short rods were manufactured for ramp testing, see Fig. 1. The new rodlets were filled with pure He at a pressure of 2,3 MPa. The short rodlets were subsequently examined non-destructively once again to check that no defects were introduced during the refabrication. Figs. 2 to 6, shows the typical appearance of the part of the rodlet that showed maximum oxide spalling.

Test facility

The power ramping of the test rods were performed in the R2 reactor in the pressurised water loop No.1 [15]. Fuel rod power during performance of ramp tests in loop No 1 is controlled by variation of He-3 gas pressure in a stainless steel double mini-coil screen which surrounds the rod test section. The principle of operation of this system is based on the fact that He 3 absorbs neutrons in proportion to its density, that can be varied by changing the pressure. The efficiency of the He-3 neutron absorber system makes it possible to increase test rod power by about a factor of two. Fuel rod failures in the loop No 1 are detected by a Cerenkov-type radiation sensor which monitors the activity of the loop coolant water. The instant of failure could also be revealed by the rod elongation detector. A sudden shortening of the failed fuel rod after a power ramp is considered to be a reliable signal of coolant ingress through the cladding [16]. Fuel rod failures were in some cases detected be a small thermal spike of very short duration, registered by the power measurement system, probably caused by a sudden improvement of the gap conductance when a crack penetrates the cladding.

The following loop data were chosen for the tests:

- Loop pressure 146 bar
- Coolant inlet temperature 315ºC

Ramp program

The power ramp test were performed as follows:

1. A conditioning phase, with a rather slow increase of the linear heat generation rate, LHGR, from the initial values to the conditioning values of 25 kW/m and holding at this values for 4 hours.

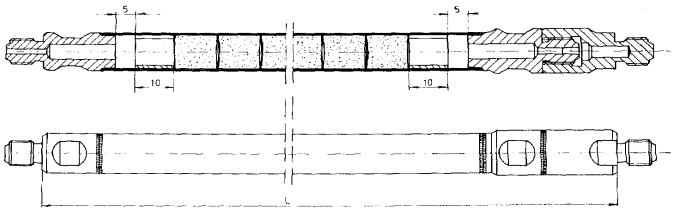

FIG. 1. Drawing of refabricated rods for ramp testing. All numbers in mm. The length of the short rod designated by L is about 700 mm.

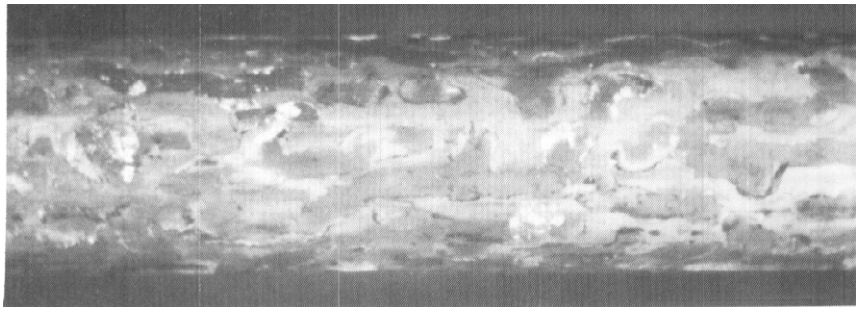

FIG. 2. Rodlet No. 1. This part of the rod was taken between spacer grids no. 5 and 6, from the bottom end plug, of Ringhals 2 rod no. 09222.

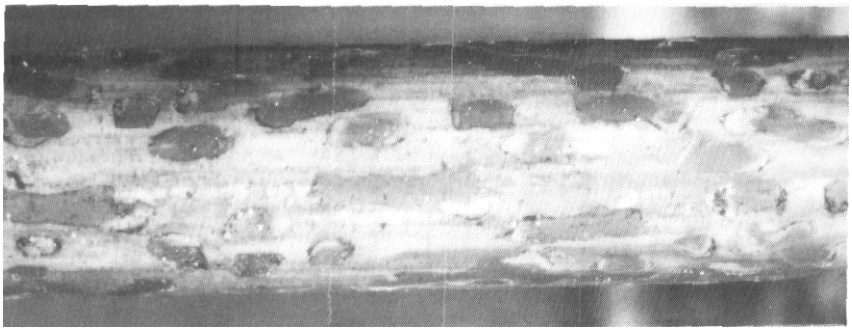

FIG. 3. Rodlet No. 2. This part of the rod was taken between spacer grids no. 4 and 5, from the bottom end plug, of Ringhals 2 rod no. 09222.

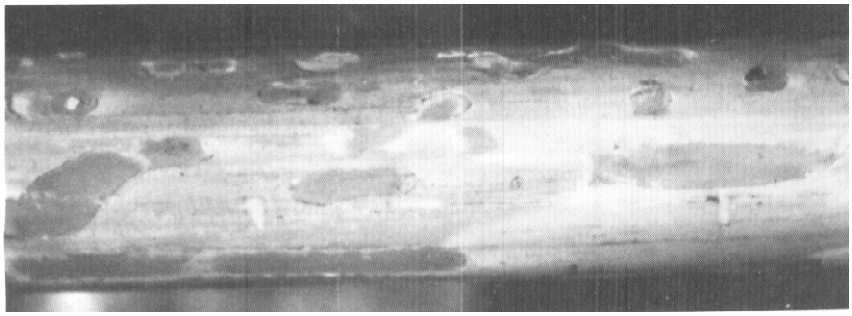

FIG. 4. Rodlet No. 3. This part of the rod was taken between spacer grids no. 3 and 4, from the bottom end plug, of Ringhals 2 rod no. 09222.

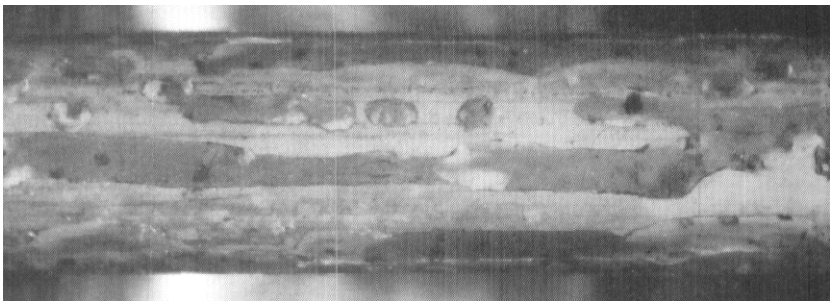

FIG. 5. Rodlet No. 4. This part of the rod was taken between spacer grids no. 5 and 6, from the bottom end plug, of Ringhals 2 rod no. 08863.

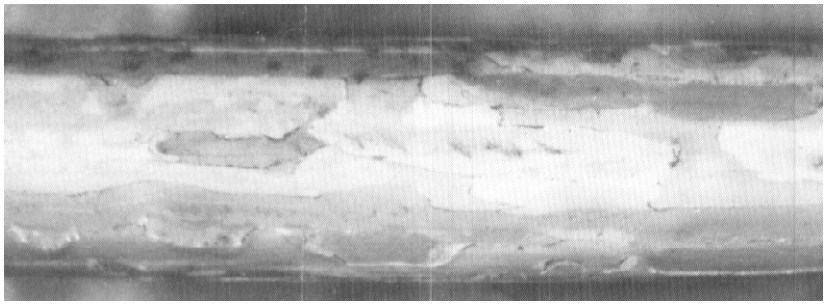

FIG. 6. Rodlet No. 5. This part of the rod was taken between spacer grids no. 4 and 5, from the bottom end plug, of Ringhals 2 rod no. 08863.

2. A ramping phase, involving a rapid increase from the conditioning level up to the preselected terminal level, as follows:

2.1. Ramp no. 1 of test rodlet no. 1 was performed as a step-by-step ramp up to 45 kW/m. The hold time at the final ramp terminal level was 6 hours. Each step had the following characteristics: (i) ramp rate of 100W/(cm·min), (ii) ramp step 5 kW/m and, (iii) hold time of each step 30 minutes.

2.2. Ramps no. 2 - 5 of test rodlets no. 2 - 5 was performed as an one-step ramp up to 45 (rodlets 2-3) and 50 kW/m (rodlets 4-5) with a ramp rate of 100W/(cm·min). The hold time at the final ramp terminal level was 6 hours.

Ramp test results

The axial distribution of the rod power was calculated with due regard to the control rod position and to the axial burnup distribution established by gamma scanning. The results are presented in Figure 7. The detailed ramp data are provided in Fig. 8.

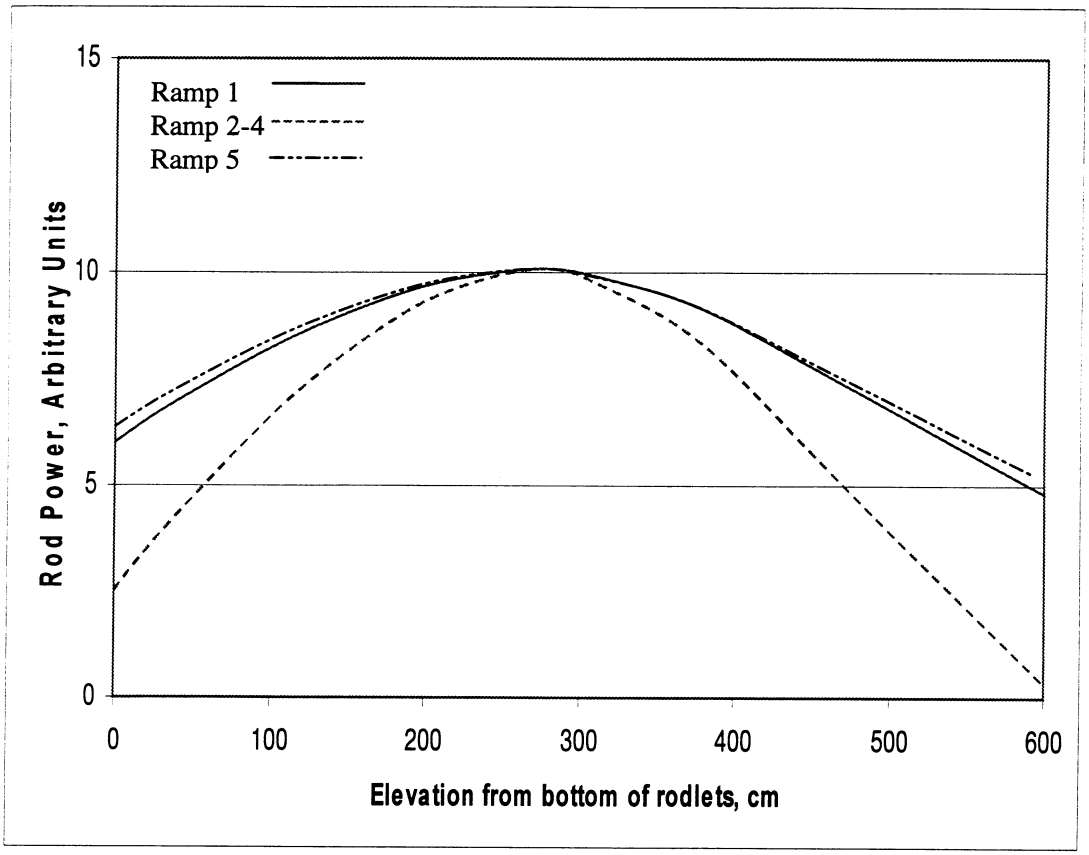

FIG. 7. Axial distribution of power during ramping.

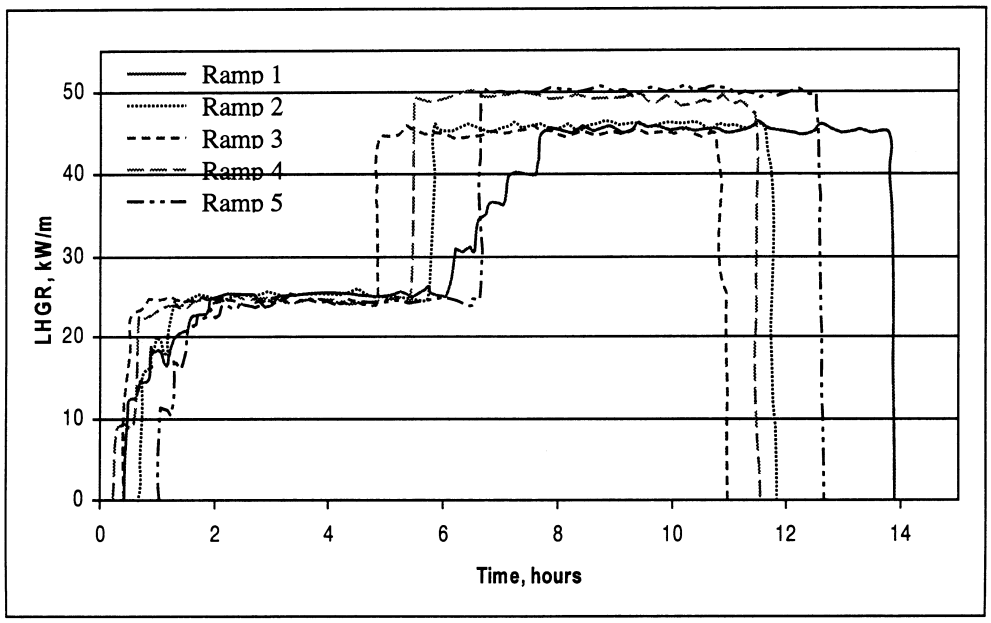

FIG. 8. Irradiation history of ramped rodlets.

The ramp test data and results are summarised in Table 2. None of the rods failed, which leads to the conclusion, that the abnormally thick outside surface oxide layer of the cladding did not imply an inferior ramp resistance of these rods compared to other rods with a normal oxide thickness.

TABLE II. RAMP TEST DATA AND RESULTS

Rod No.	Test No.	Conditioning		Ramping				Failure/ Nonfailure
		Power level, kW/m	Hold time, h	No. Of steps	Ramp rate, W/cm min	RTL, kW/m	Hold time at RTL	
2243	1	25,2	4,0	4	100	45,3	6,2	NF
2244	2	25,2	4,2	1	100	45,5	6,0	NF
2245	3	24,9	4,0	1	100	45,5	6,0	NF
2246	4	25,2	4,1	1	100	50,0	6,0	NF
2247	5	24,7	4,0	1	100	50,7	6,0	NF

The different test rodlets were after ramping subjected to different examinations such as:

- Eddy-current testing
- Profilometry
- Fission gas release
- Metallography and ceramography

EC-testing indicated no cracks even though cracks were identified at the cladding outer diameter in the destructive examination. Profilometry showed that the cladding had plastically deformed during the ramptesting and that the rodlet subjected to the highest RTL showed the largest deformation (Table 3).

TABLE III. MAXIMUM CLADDING DEFORMATIONS RESULTING FROM RAMP TESTING THE DATA OF A NONRAMPED RODLET IS ALSO PROVIDED AS A REFERENCE

Rodlet No.	RTL, kW/m	Mean diameter increase at midpellet location[a], mm	Mean diameter increase at pellet-pellet interface location[b], mm	Maximum cladding diameter increase	
				mm	%
2	45,5	88	140	140	1,3
3	45,5	101	146	170	1,6
5	50,7	150	210	220	2,1
Reference rod	-	~20	~20	~30	~0,3

The maximum cladding diameter increase obtained in this test program is much larger than e.g. the ones reported by J. Joseph et al. in a similar ramp program [19]. The maximum cladding diameter increase was 0,2 % of a rod with a burnup >50 MWd/kgU and subjected to a ramp terminal level of 44 to 51 kW/m with a power increase from the conditioning level of 38 kW/m. Mogard reported that ramped nonfailed PWR rods that had the highest burnup, and survived power ramps up to 49 kW/m, showed the largest incremental clad deformation. This was on the average 100 microns at mid pellet positions and 135 microns at ridges [17]. All the other rods exhibited considerably smaller deformation.

The ramped rodlets no. 1 and 4 in this study were subjected to fission gas analysis. The Xe fission gas release was 5,5 and 9,3 % with the larger release for the rodlet subjected to the highest RTL (rodlet no. 4). The rod internal pressure prior to puncturing of the rodlets were 2,39 and 2,80 MPa for rodlets no.1 and 2, respectively.

Samples for metallography and ceramography were also taken from these rodlets from about the middle part of the rodlets (that had been subjected to the highest RTL). The oxide thickness at the cladding OD was measured on 12 micrographs of each rodlet. The oxide thickness ranged from 38 to 90, and 5 to 101 microns, on rodlet no. 1 and 4, respectively. One has to keep in-mind that the hypothetical maximum oxide thickness would have been significantly larger, if the thick oxide would not have spalled. The metallographic samples were etched to reveal the hydride distribution. Examples of oxide structure and hydride distribution at the middle part of the rodlets no. 1 and 4 are provided in Figs. 9 and 10. Based upon the visual appearance of the etched cladding cross section, the average hydrogen content in each microghraph was estimated [18]. The micrographs show that the hydride concentration is significantly larger at the clad OD, and furthermore that the largest concentration can be found in the areas were the oxide has spalled off.

In samples from rodlet no. 1, only one crack was detected (no micrograph presented here shows that crack). However, rodlet no. 4, that had been ramped to 50 kW/m, showed 3 cracks at the outer part of the cladding was observed. The crack depth varies from 40 to 110 microns. In the deepest crack, the hydride orientation has been redistributed due to the plastic deformation and/or the stress enhancement ahead of the crack tip. It is interesting to note that no crack had initiated at the cladding ID, that would have indicated PCI.

[a] Measured at the cladding corresponding to the 5 mid-pellet locations in the part of the rod subjected to the highest power during the ramp.
[b] Measured at the cladding corresponding to the 5 pellet-pellet interface locations in the part of the rod subjected to the highest power during the ramp.

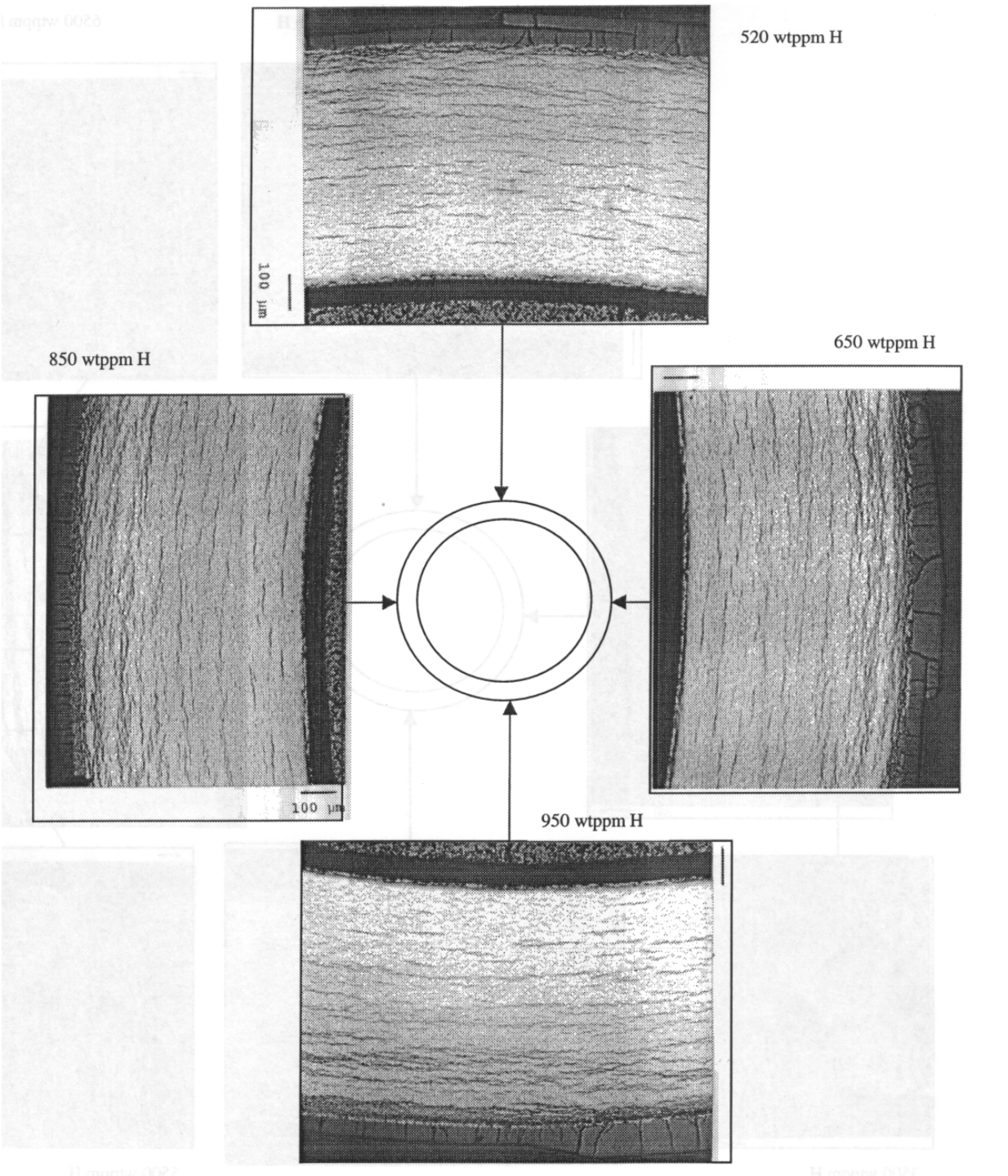

FIG. 9. *Typical micrographs showing oxide thickness and hydride structure in rodlet No. 1. The scale mark indicate 100 microns.*

.

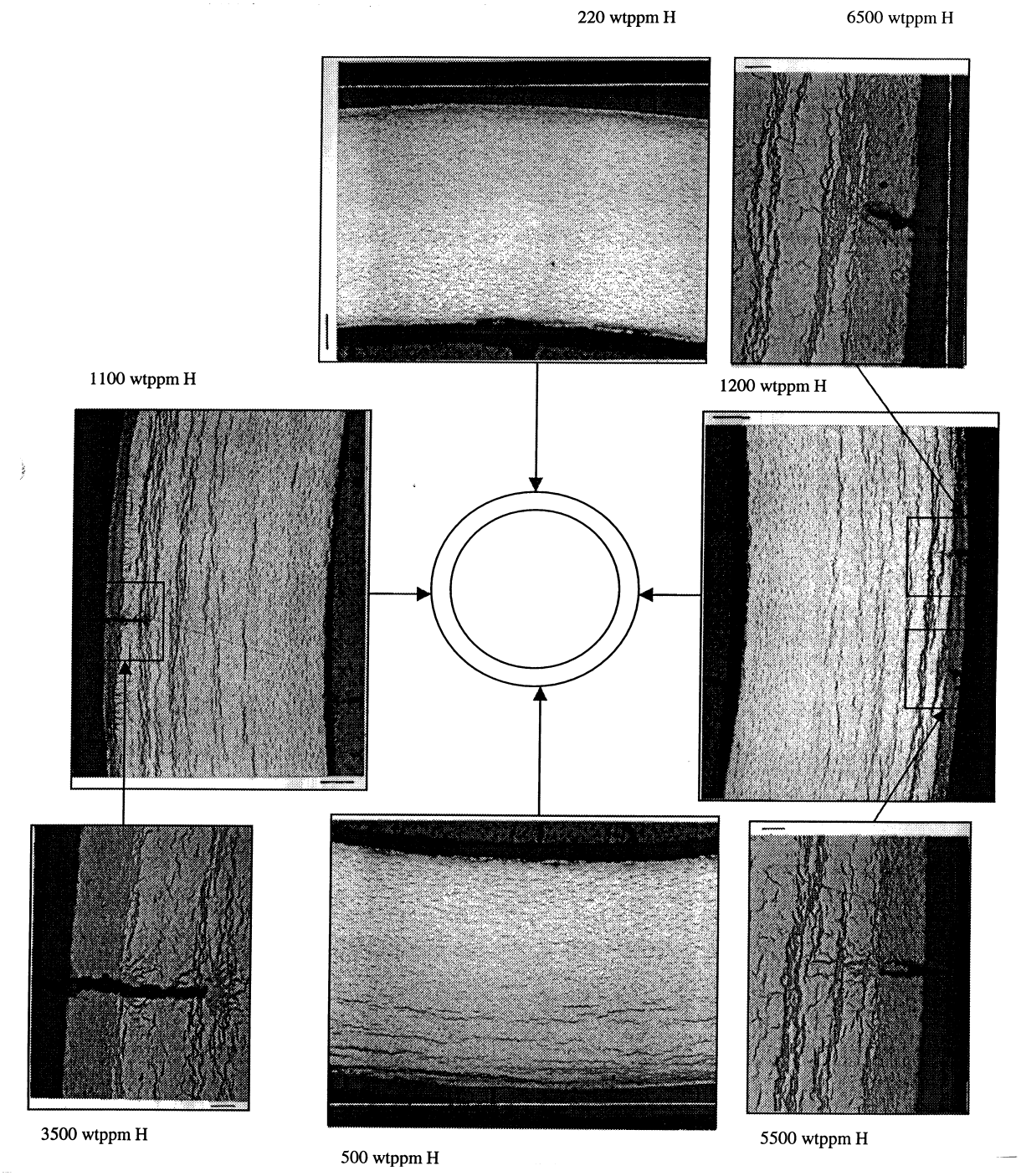

FIG. 10. *Typical micrographs showing oxide thickness and hydride structure in rodlet No. 4. The scale mark indicates 100 microns and 20 microns in enlargements.*

Also the fuel samples were etched and the results are provided in Figs. 11 and 12.

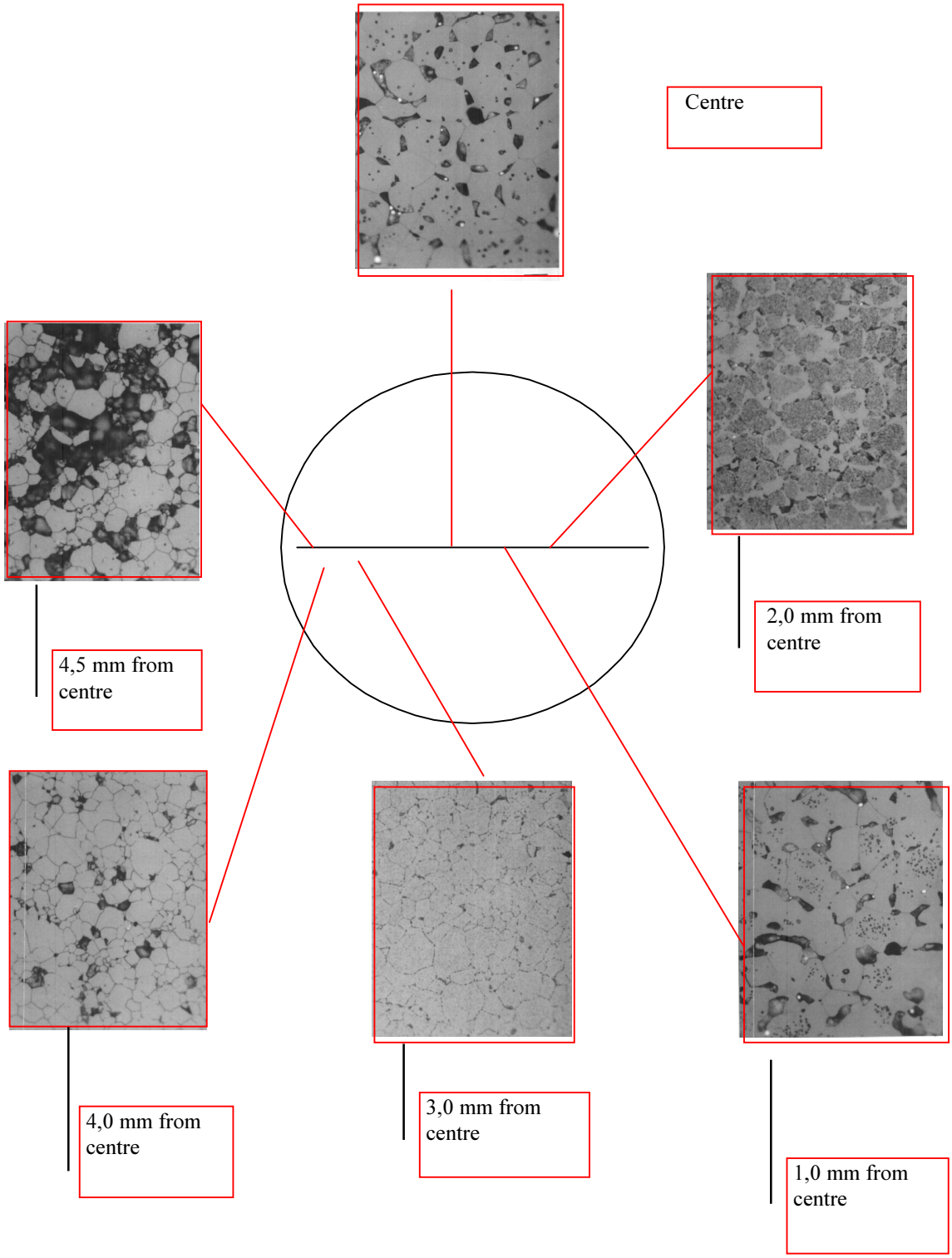

FIG. 11. Ceramographis cross section at various radial positions in rod no. 1. The scale mark in the top ceramograph of 10 microns is representative of all the ceramographs.

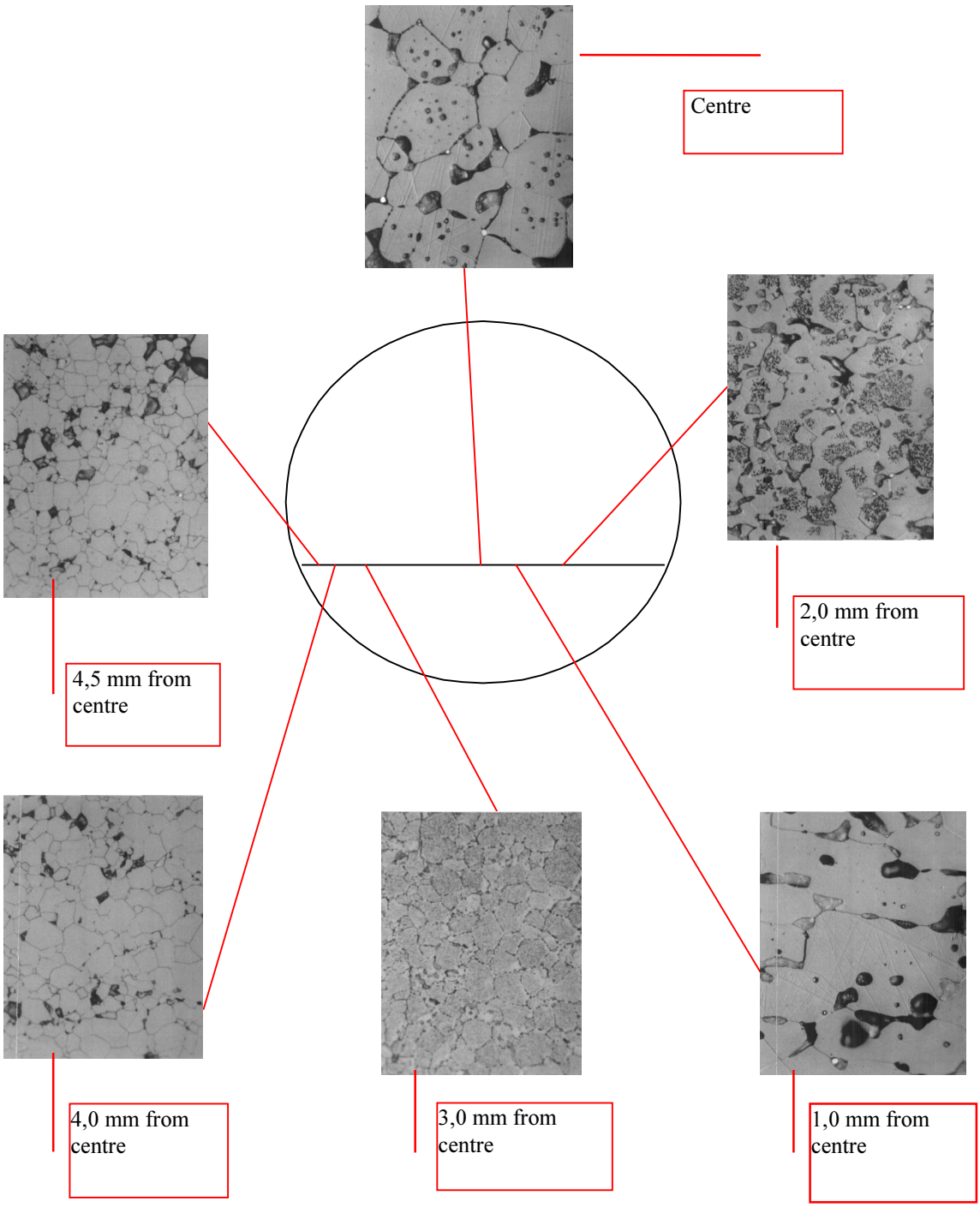

FIG. 12. *Ceramographis cross section at various radial positions in rod no. 4. The ceramographs have the same enlargement as in fig. 12 .*

The ceramographs showed the same type of characteristics as earlier presented by J. Joseph et al. [19], Figs. 11 and 12. The inner part of the fuel consists of grains that are almost completely free of fine intragranular bubbles, while the number of intergranular bubbles has increased. Ceramographs taken 2 to 3 mm from the centre show a large number of pores inside the grains. Specifically on the ceramographs taken at 2 mm from the centre, the difference in pore density areas become very pronounced. The pore deficient areas is a result of grain boundary sweeping due to grain growth. The grain size at different fuel pellet radius are plotted in Fig. 13.

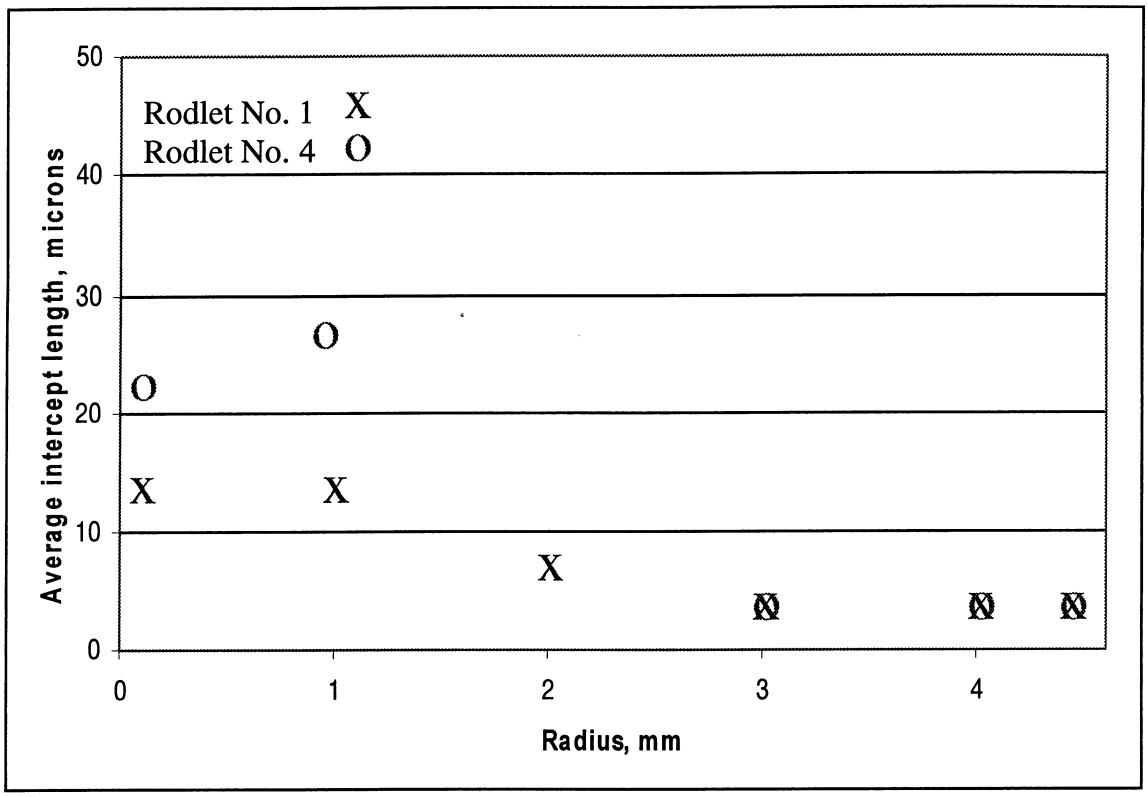

FIG. 13. Fuel grain size at various radial positions in the fuel pellet from rodlets no. 1 (x) and 4 (o).

3. DISCUSSION

In the Fig 14, the ramp data in this study are compared to that obtained in the Super-ramp [18] and Trans-Ramp II [8] projects indicating a PCI threshold of about 36 kW/m.

In the paper presented by J. Joseph et al. the PCI failure threshold of commerical Fragema fuel rods with burnups ranging from 20-60 MWd/kgU range and ramped in a french test reactor was about 42 kW/microns [19]. The discrepency in PCI threshold between the Swedish Super-Ramp and Trans-Ramp II projects on the one hand and the French project reported by J. Joseph et.al. may be related to differences in ramp characteristics and differences in fuel rod design.

The results obtained in Trans-Ramp II and by J. Joseph et al. indicated a relationship between rod power and the time to failure in ramp tests performed at very fast speed. They showed that the rods may survive the type of transients performed, provided that the duration of the transient is short enough

The rods in this study were specifically selected for ramping since they showed excessive oxide spalling. In the Super-Ramp, Trans-ramp II program and in the study presented by J. Joseph et al., no cladding oxide thickness and hydrogen concentration data were presented. One may however assume that, the major part of the ramped rods in the these programs showed less oxide thickness and less

hydrogen concentrations than the rods in this program. This since the rods in this study were specifically selected due to their excessive oxide spalling. If one then assumes that the local hydrogen concentration was much lower in the other programs, the rampdata in this study indicate that an average hydrogen concentration of about 1200 wtppm in the cladding thickness does not impact the PCI performance. The ramped rods in this study survived ramps up to 45 and 50 kW/m that are higher than the PCI failure threshold of 36 kW/m. Also, the micrographs show that no PCI crack was seen at the clad inner diameter, supporting this conclusion.

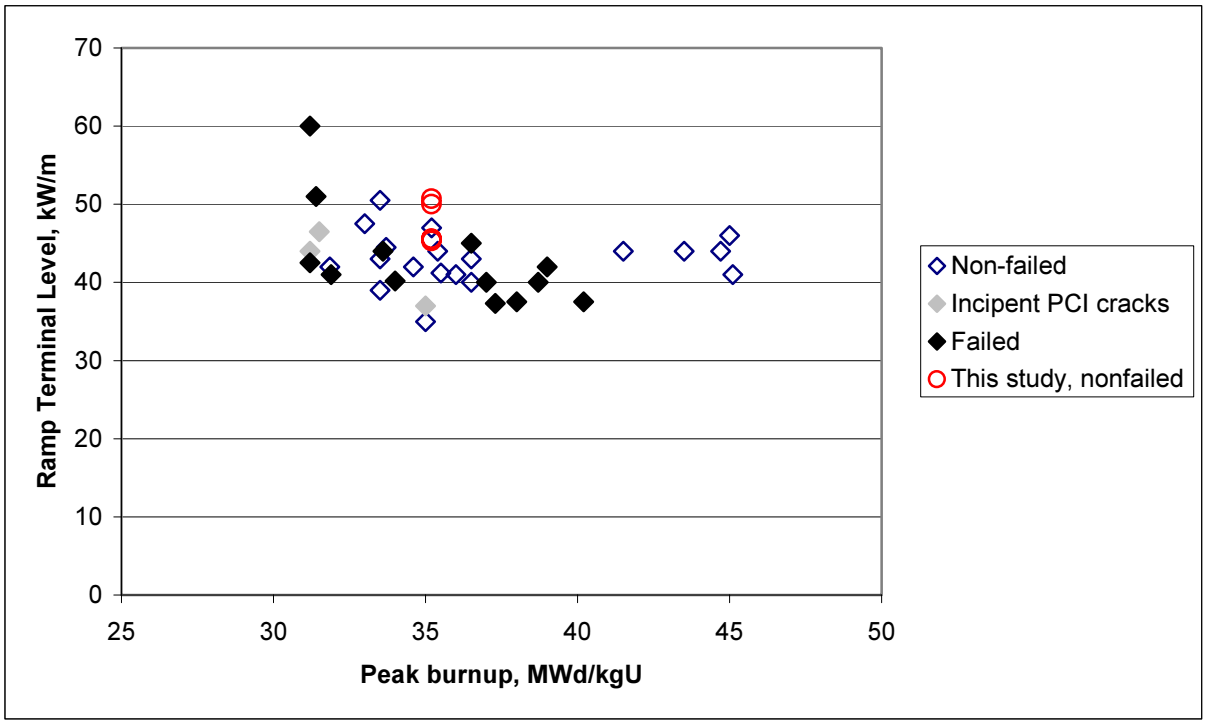

FIG. 14. Comparision of ramp data from this study with that obtained in the international PWR rampprojets Super-Ramp and Trans-Ramp II.

Garde et al. investigated the influence of hydrides on irradiated Zircaloy ductility by conducting tube burst, tube tensile and ring tensile tests at various temperatures [20]. For samples irradiated to the same fluence level and containing the same amount of hydrides, the ductility obtained in the burst tests was significantly lower compared to that obtained in the other two types of tests. The total plastic circumferential elongation at these tests at 315°C ranged from 1 to 6 % of samples containing 200-600 wtppm H. However, one burst and one ring tensile test sample with spalled oxide tested at 315 and 300°C, respectively, containing 731 (burst test sample) and 760 wtppm H (ring tensile test sample), showed only cirumferential elongation values of 0,58 and 0,44 %, respectively. Examination of fracture surfaces indicated ductile failure in the metallic ligaments separating the hydride precipitates that appeared to have failed in a brittle fashion. The hydride distribution in the fuel cladding in our study, Figs. 9 and 10, correlates with that reported by Garde. Garde showed that the hydrides were circumfentially oriented but that the hydride concentration increased closer to the cladding outer surface. This situation occurs due to that hydrogen diffuses down thermal gradients and will concentrate at the colder regions [21,22]. A sample with spalled oxide was also investigated by Garde and it was clear that the hydrogen had concentrated even more in this case at the cladding outer diameter. This because the spalling of the oxide will form a cold spot at this position due to that the resistance of the zirconium oxide to the surface heat flux will be smaller at this position. This nonuniform distribution of the hydrides in the cladding cross section is the probable cause that the samples with spalled oxide showed so small ductility values. The reason for our higher ductility data compared to that of Garde, despite that our claddings had higher hydrogen contents may be related to differences in stress state during the ramp and burst tests. In addition, the fuel claddings were delivered by two different fuel vendors and may have inherently different ductility properties. Also, the temperature in the fuel cladding during ramping was significantly larger than that in the tests reported by Garde. At a linear

heat generation rate of 50 kW/microns, the clad temperature at inner and outer surface is 434 and 350°C, respectively, [23], compared to the test temperatures of 300-315°C used in Gardes study.

It is however surprising that the spalled fuel claddings in our study could sustain as large plastic deformation of 2,1 % without showing any indication of stress corrosion cracking. Normally, one may get SCC cracking at the point when plastic deformation in the material occurs, i.e., when the stress exceeds the yield strength. The factors that may explain this observation are as follows:

1. Large plasticity of the fuel pellets and a fuel cladding that show a large creep rate may reduce the stresses in the cladding below the yield strength at RTL.

2. The existence of a thin tenacious zirconium oxide at the cladding inner surface that would not crack during the ramp.

The cracks observed at the cladding outer surface is probably related to the situation that the thick oxide and the locally hydrided areas are brittle compared to the Zr-metal matrix. Since the oxide contain many types of defects such as pores and small cracks, the oxide will become more brittle with increasing oxide thickness. Thus, the thin zirconium oxide at the cladding inner surface would not show the same tendency for cracking compared to the cladding outer surface oxide. Due to the fact that the surface heat flux will drive the hydrogen to the outer cladding surface, the hydrides will not be able to facilitate PCI crack initiation .

4. CONCLUSIONS

This study show that an average hydrogen concentration in the cladding thickness of up to 1200 wtppm will not affect the fuel cladding PCI performance. This is probably related to the fact that the surface heat flux will drive the hydrogen to the outer cladding surface where they will not be able to facilitate formation of PCI cracks at the cladding inner surface.

ACKNOWLEDGEMENT

The authers would like to acknowledge the following persons at Studsvik for carrying out this ramp program: Bengt-Åke Nilsson, Ulla-Britt Eklund, Anders Brisling, Per Ekberg and Tord Jonsson and Seved Djurle. We would also like to thank Gunnar Lysell and Bertil Josefsson for reviewing the paper.

REFERENCES

[1] ARMIJO, J.S., COFFIN, L. F., ROSENBAUM, H. S., ”Development of Zirconium-Barrier Fuel Cladding”, Zirconium in the Nuclear Industry: Tenth International Sypomosium, ASTM STP 1245, A. M. Garde and E. R. Bradley, Eds., American Society for Testing and Materials, Philadelphia, 1994, 3–18.

[2] LAMBERT, J. D. B. and STRAIN R., in: Material Science and Technology, Volume 10 A, Eds. R. W. CAHN, P. HAASEN, E. J. KRAMER, Volume editor, B. R. T. Frost,Wurzburg, Germany, VCH Verlagsgesellschaft, 1994, Chapter 3.

[3] ROBERTS, J. T. A, JONES, R. J., CUBICCIOTTI, D., MILLER, A. K., WACHOB, H. F., SMITH, E. and YAGGEE, F. L., ”A Stress-Corrosion Cracking Model for Pellet-Cladding interaction Failures in Light-Water Reactor Fuel Rods”, Zirconium in the nuclear industry: Eleventh International Symposium, ASTM STP 681, American Society for Testing and Materials, 1979, 12–32.

[4] GARZAROLLI, F., STEHLE, H. and STEINBERG, E., ”Behaviour and properties of Zircaloy in power reactors: A short review of pertinent aspects in LWR fuel”, Zirconium in the nuclear industry: Eleventh International Symposium, ASTM STP 1295, E. R. Bradley and G. P. Sabol, Eds., American Society for Testing and Materials, 1996, 12–32.

[5] CUBICCIOTTI, D., JONES, R. L. and SYRETT, B. C., ”Stress corrosion cracking of Zircaloys”, EPRI report no. NP-1329, 1980.

[6] MOGARD, H., BERGENLID, U., DJURLE, S., LYSELL, G. and RÖNNBERG,G., ”The international TRANS-RAMP I fuel project”, IAEA Technical Committee on Fuel Rod Internal Chemistry and Fission Products Behaviour, Karlsruhe, FR Germany, 11–15 November, 1985.
[7] MOGARD, H., HOWL AND, D. A., GROUNES, M., ”The international trans-ramp II project – A study of the effects of rapid power ramping on PCI resistance of PWR fuel” ANS Topical Meeting on LWR Fuel Performance, Williamsburg, Virginia, USA, 17–20 April 1988, 232–244.
[8] COX, B., Journal of Nuclear Materials, 170 (1990) 1–23.
[9] COX, B., Journal of Nuclear Materials, 172 (1990) 249–292.
[10] COLEMAN, C.E. and HARDIE, D., J. Less-Common Metals Volume. 2, (1966), 168–185.
[11] BAI, J., PRIOUL, C., PELCHAT, J. and BARCELO, F., ”Effect of hydrides on the ductile-brittle transition in stress-relieved, recrystllised nad beta-treated Zircaloy-4”, ANS Topical Meeting on LWR Fuel Performance, Avignon, France, 21-24 April 1991, 233–241.
[12] GRIGORIEV, V., JOSEFSSON, B. and ROSBORG, B., ”Fracture toughness of Zircaloy cladding tubes”, Zirconium in the nuclear industry: Eleventh International Symposium, ASTM STP 1295, E. R. Bradley and G. P. Sabol, Eds., American Society for Testing and Materials, 1996, 431–447.
[13] KREYNS, P. H., BOURGEOIS, W. F., WHITE, C. J., CHARPENTIER, P. L., KAMMENZIND, B. F. and FRANKLIN, D. G., ”Embrittlement of reactor core materials”, Zirconium in the nuclear industry: Eleventh International Symposium, ASTM STP 1295, E. R. Bradley and G. P. Sabol, Eds., American Society for Testing and Materials, 1996, 758–782.
[14] COX, B., "Hydride cracks as initiators for stress corrosion cracking of Zirealoys," Zirconium in the Nuclear Industry (Fourth Conference), ASTM STP 681, American Society for Testing and Materials, 1979, 306–321.
[15] RÖNNBERG, G., BERGENLID, U. and TOMANI, H., ”Power Ramp Technique at Studsvik”, Proc. KTG/ENS/JRC Meeting on Ramping and Load Following Behaviour of Reactor Fuel, Petten, Netherlands, Nov 30- Dec 1, 1978, EUR 6623 EN, 37–51.
[16] BERGENLID, U., MOGARD, H. and RÖNNBERG, G., ”Experimental Observations of the PCI Failure Occurence on Power Ramping”, IAEA Specialists Meeting on Pellet-Cladding Interaction in Water reactors”, Risö, Denmark, 22–26 September 1980.
[17] MOGARD, H. and HECKERMAN, H., ”The international super-ramp project at Studsvik”, ANS Topical Meeting on LWR Fuel Performance, Orlando, Florida, USA, 21–24 April 1985, Section 6, 17–33.
[18] SCHRIRE, D. and LYSELL, G., private communication.
[19] JOSEPH, J., ROYER, J. and GROSGEORGE, M., ”Transient behaviour of Fragema fuel rods previously irradiaited under commerical reactor operating conditions” ANS Topical Meeting on LWR Fuel Performance, Williamsburg, Virginia, USA, 17–20 April 1988, 225–231.
[20] GARDE, A. M., SMITH, G. P., and PIREK, R. C., "Effects of Hydride Precipitate Localization and Neutron Fluence on the Ductility of Irradiated Zircaloy-4", Zirconium in the Nuclear Industry: Eleventh International Symposium, ASTM STP 1295, E. R. Bradley and G. P. Sabol, Eds., American Society for Testing and Materials, 1996, 407–430.
[21] MARKOWITZ, J. M.,Transactions of the Metallurgical Society of AIME, Volume. 221, 1961, 819–824.
[22] KAMMENZIND, B. F., FRANKLIN, D. G., PETERS, H. R. and DUFFIN, W. J., "Hydrogen pickup and redistribution in alpha-annealed Zr-4", Zirconium in the Nuclear Industry: Eleventh International Symposium, ASTM STP 1295, E. R. Bradley and G. P. Sabol, Eds., American Society for Testing and Materials, 1996, 338–370.
[23] LYSELL, G., private communication.

TESTING CLADDING INTEGRITY AT HIGH BURNUP

D. SCHRIRE, G. LYSELL, V. GRIGORIEV, B. JOSEFSSON
Studsvik AB, Nyköping, Sweden

Abstract

LWR fuel cladding has a tendency to reduced ductility and fracture strength at high burnup due to irradiation hardening, corrosion and hydriding. At the same time, the effective fuel-clad gap available to take up pellet expansion in the event of a power increase is greatly reduced due to cladding creepdown, and fuel swelling and crack healing. There is therefore a need for reliable tests to demonstrate that cladding integrity is maintained at high burnup during normal operation and anticipated transients. Studsvik has performed such testing for several years, combining in-pile power ramp tests, mechanical testing of irradiated cladding, and extensive post-irradiation examination (PIE). Many of the tests have focused on the effect of cladding hydriding at high burnup. Power ramping is an integral test of the fuel rod integrity under realistic conditions. The rod to be tested is either a short rodlet from a segmented stringer rod, or refabricated in the hot-cell from a full-length rod, which has been pre-irradiated in a power reactor. Suitable sections of a fuel rod for refabrication can be selected based on non-destructive PIE such as neutron radiography (to locate regions with different hydrogen levels in the cladding) or eddy current lift-off oxide thickness measurements. Of several possible mechanical testing methods (such as burst, expanding mandrel, axial tensile and ring tensile testing), a specially adapted ring tensile testing technique has been found to be most suitable for highly irradiated cladding. This method combines ease of defuelling and relatively low radiation levels with the advantage of being able to test very locally, for instance at locations with increased hydrogen contents (for example due to oxide spalling or pellet interfaces). Finally, detailed examination after ramping or mechanical testing is essential to analyse the fracture behaviour. In particular, scanning electron microscopy (SEM) of the cladding cross-section has proven invaluable for fracture path analysis, measurement of the local hydrogen concentration and oxide thickness in the vicinity of the crack, and assessment of localised plastic deformation. At sufficiently high levels of cladding hydriding and strain, fracture by a hydride cracking mechanism has been observed in both ramp and mechanical testing. In both types of testing, the fracture process has shown the same types of features and behaviour. The cracks initiate at the outer surface of the cladding, where the hydride level is highest. They appear to start from radial cracks in the oxide layer, continuing into the underlying material if there happens to be a hydride opposite an oxide crack. Within the cladding itself, radial cracks may sometimes occur in individual hydrides at high local stress and strain levels, without the matrix material (metal) cracking. Ultimately, at sufficiently high strains a crack can penetrate through the entire wall thickness by a combination of hydride cracking and overload fracture of the non-hydrided material. A combination of ramp testing and mechanical testing, followed by scanning electron microscopy, provides the most complete information for determining the fuel rod failure criteria.

1. INTRODUCTION

Higher discharge burnup levels lead to increased mean in-reactor residence times and neutron fluences, and more severe cumulative service conditions for cladding corrosion and hydrogen pickup. One consequence of this is that Zircaloy cladding has a tendency to reduced ductility at high burnup due to a combination of irradiation hardening, corrosion and hydriding [1]. At the same time, the effective fuel-clad gap available to take up pellet expansion in the event of a power increase is greatly reduced due to cladding creepdown, and fuel swelling and crack healing.

Of the factors affecting the cladding mechanical properties of interest for fuel rod integrity under pellet-cladding mechanical interaction (PCMI) loading conditions, hydriding is probably the most complex, and frequently limiting. Hydrogen diffuses readily in cladding material at normal operating temperatures in response to a temperature, concentration or stress gradient. High hydrogen concentrations may thus arise as a result of generally high levels of corrosion-related uptake, or locally due to a combination of cold spots (e.g. at interpellet gaps, pellet interfaces, spalling oxide, etc.) and sufficient time and mean hydrogen concentration to build up high local hydrogen concentrations. There is also generally a pronounced radial hydrogen concentration profile through the cladding wall due to the lower temperature at the outer surface. The effect of hydriding on the cladding integrity is additionally complicated by the strong dependence on the hydride morphology and other factors [2].

There is therefore a need for reliable tests to demonstrate that cladding integrity is maintained during normal operation and anticipated transients with the levels of corrosion and hydriding which can occur at high burnup. Studsvik's extensive experience with in-pile PCI (pellet-cladding interaction) ramp testing and fuel examination has also led to the testing of the cladding integrity of high burnup fuel with relatively high levels of waterside corrosion and/or hydriding under PCMI loads representative of normal operation and anticipated transients. Corresponding testing of the behaviour in (off-normal) reactivity insertion accidents (RIA) is normally carried out at dedicated pulse-type test reactors.

The results and details of most of the tests performed at Studsvik are proprietary, so the focus of this paper is on some common features and mechanisms of fuel cladding fracture initiation and propagation under PCMI load conditions, when the cracking is associated with cladding corrosion and hydriding.

2. EXPERIMENTALS METHODS

The experimental techniques employed fall into three main areas: in-pile power ramp tests in the Studsvik R2 reactor, mechanical testing of irradiated cladding, and post-irradiation examination (PIE).

2.1. Ramp testing

Power ramping is an integral test of the fuel rod integrity under realistic conditions. The rod to be tested is either a short rodlet from a segmented stringer rod, or refabricated in the hot-cell from a full-length rod using the STUDFAB procedure, which has been pre-irradiated in a power reactor.

The R2 reactor is a 50 MW(th) tank-in-pool testing reactor. The reactor core is contained within an aluminium vessel located at one end of a large open pool, which also serves as a storage for spent fuel elements and irradiated experimental equipment. Power ramp testing as well as medium and long-term irradiation of LWR fuel rods are performed in two test loops which can reproduce PWR and BWR coolant conditions. The in-pile part of the loops are designed as U-tubes, occupying two adjacent R2 core positions. The in-pile part of the loop is thermally insulated from the reactor primary coolant by a gas gap containing CO_2. Heat losses from the hot loop pressure tube to the reactor coolant are consequently quite small thereby facilitating accurate calorimetric power measurements.

The ramp test facility in the test loops consists of a sample exchange device, a ramp test rig with a reloadable ramp capsule, a ^{3}He absorber system for power control and instrumentation for rod power and elongation measurement. Fission product detectors are a part of the permanent installation in the test loops. The fuel rod power during ramp tests and long term instrumented irradiation in the R2 reactor loops is controlled with the ^{3}He screens and by variation of the R2 reactor power, separately or in combination. The ^{3}He neutron absorber system makes it possible to increase the test rod power by about a factor of 2 at constant reactor power. In order to achieve higher power increase factors, the reactor power is increased before or simultaneously with the ^{3}He-ramping.

Since the R2 core height is only 60 cm, there is an appreciable axial power profile in the test fuel rod if its length exceeds approximately 30 cm. This is exploited in order to assess the fuel rod behaviour at different local power levels, such as cladding permanent hoop strain or fuel swelling.

Test fuel rod power measurement is accomplished by a fast acting calorimetric technique. The temperature increase over the test section is measured by means of 2 or more pairs of thermocouples (situated at the inlet and the outlet). The coolant flow rate and pressure are also measured. The test fuel rod power is obtained by correcting the total power generated in the rig for the experimentally

determined external gamma heating in the rig structure, the rod end fittings, the ramp capsule and the coolant.

A rod elongation detector (LVDT) is located at the bottom of the ramp rig below the R2 core. The elongation movements of the test rod are transmitted by a push-rod, which is built in at the bottom guide plug of the ramp capsule. Fuel rod failures in the R2 reactor loops are detected by a Cerenkov-type radiation sensor, which monitors the β-decay of fission products in the loop coolant water. The delay time of the system, from in-core to detector chamber, is approximately 155 seconds. The exact time of rod failure following a power ramp is usually revealed by a sudden change in the rod elongation as a result of coolant ingress through cladding crack(s) leading to a change in the gap conductance. In most cases, with significant fission gas contamination of the gap, a sudden shortening of the rod is seen. A corresponding small transient calorimetric power spike is also observed in some cases, resulting from the improvement in the gap conductance causing a slight decrease in the amount of stored energy in the test rod.

All the relevant reactor and experimental loop instrument data are recorded by a Hewlett-Packard 9000 computer at a frequency of 1 to 2 Hz. In addition, ramp test data are also acquired at a higher frequency on a PC-based system.

Suitable sections of a fuel rod for refabrication can be selected based on non-destructive PIE such as neutron radiography (to locate regions with different hydrogen levels in the cladding) or eddy current lift-off oxide thickness measurements. The STUDFAB procedure entails cutting the rod section to the pre-determined length, preparing the ends for welding on a new (unirradiated) lower end plug and upper plug and extension (including plenum), welding on these parts, determining the rod internal volume, evacuating and filling (with the gas composition and pressure as required), and sealing/welding. The refabricated rod is then subjected to helium leak testing, visual weld inspection, gamma-scanning or neutron radiography (fuel stack control), eddy current testing and other non-destructive examinations (NDE) as required.

2.2. Mechanical testing

Of several possible mechanical testing methods (such as burst, expanding mandrel, axial tensile and ring tensile testing), a specially adapted ring tensile testing technique has been found to be most suitable for highly irradiated cladding. This method combines ease of defuelling and relatively low radiation levels with the advantage of being able to test very locally, for instance at locations with increased hydrogen contents (for example due to oxide spalling or pellet interfaces).

The modified ring tensile testing technique enables bending of the specimen gauge length during loading to be avoided [3]. To establish the relationships between the experimentally measured global force and the hoop stress in the specimen, and between the load-line displacement measured by means of LVDT sensors fixed close to the specimen and the hoop strain in the specimen, two master curves are derived from 3-D FEM analyses. All main parameters affecting the master curves are included into the analysis, such as friction between the specimen and the fixture, and clearances between the specimen and different parts of the fixture. Finally, the stress-strain curve for each tested ring is determined from the experimental force-displacement data with the help of the master curves.

2.3. Post-irradiation testing

Finally, detailed post-irradiation examination is essential to analyse PCMI-induced cladding fracture. Several non-destructive examination techniques are routinely employed both before and after ramp testing. Neutron radiography is generally used to locate regions with different hydrogen levels in the cladding, and to assess the pellet stack geometry. Visual inspection and eddy current lift-off measurements are used to characterise the fuel rod surface oxide. Gamma spectrometry is used to determine the axial burnup profile, and to confirm the power profile during ramp tests; gamma

spectrometry is also sometimes used for non-destructive fission gas release determination (by measurement of the Kr-85 in the plenum).

"Gap squeeze" measurements are used to non-destructively assess the pellet-clad mechanical gap in the cold state, by elastically compressing the cladding and measuring the resistance force as a function of cladding deformation. This technique enables the gap to the relocated (fragmented) pellet as well as the gap to the compressed pellet to be determined with high experimental precision, providing valuable data for benchmarking PCMI models.

Profilometry measurements are used to measure the fuel rod outer diameter with high accuracy before and after ramp testing, enabling the permanent cladding hoop strain due to the power ramp to be determined. Since the hoop strain and stress are not measured in-pile during the ramp testing, unlike in the case of mechanical testing, where both the strain and stress are determined over the entire test, one way to assess the cladding stress in the PCMI situation is to determine the permanent strain following a short ramp (with too short a hold time to allow significant creep). The axial variation in the cladding strain can be used to find the onset of plastic deformation, approximately corresponding to the yield stress in the absence of significant creep strain.

Of the destructive PIE techniques available, optical microscopy (OM) and scanning electron microscopy (SEM) provide the most valuable information for assessing the PCMI fracture mechanisms at high burnup. Metallography of fuel and cladding cross sections are used to visualise PCMI-induced cracks in the cladding and their relation to other features such as pellet cracks, surface oxide cracks and cladding hydrides. In these examinations the fracture path can be analysed, and localised plastic deformation can be assessed, and also allows the measurement of the local oxide thickness and hydrogen concentration in the vicinity of the crack. Backscattered electron imaging (BEI) of polished cladding in the SEM is used together with image analysis [4] to determine the local hydrogen concentration and radial hydrogen profile through the cladding wall (see Figure 1).

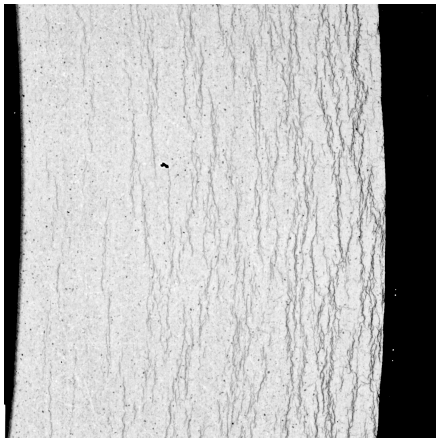

FIG. 1a. SEM (BEI), as-polished cladding wall

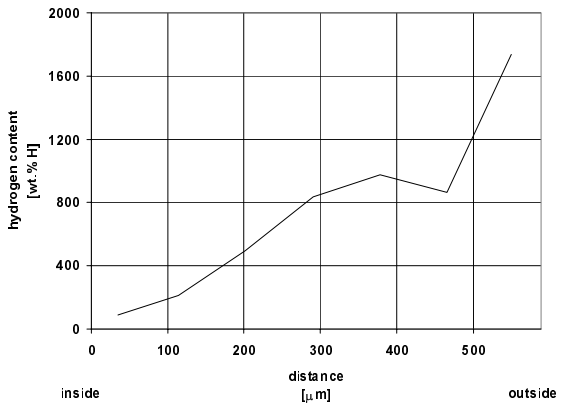

FIG.1b. Hydrogen concentration profile through

Radial hydrogen concentration profile determined by quantitative image analysis of BEI image.

3. CLADDING FAILURE MECHANISMS

3.1. PCI

Pellet-cladding mechanical interaction (PCMI) loads arise from an increase in the local linear heat rating of a fuel rod, leading to pellet thermal expansion which in turn results in cladding tensile stresses. The most common cause of cladding failure under PCMI loads which arise from normal operation (power ascension, BWR control blade motion, etc.) or anticipated transients is ”pellet-clad interaction” (PCI), a form of stress corrosion cracking where volatile fission products (presumably iodine) released during the power ramp act as the stress corrosion agent [5].

This type of failure is characterised by intergranular crack initiation at the inner surface of the cladding, followed by crack propagation which usually occurs by a mixture of quasi-cleavage (transgranular) and ductile tearing (fluting). PCI failures frequently occur some time after achieving the maximum power (i.e. the crack initiation or propagation is time dependent). Such features have been seen in BWR and other power reactor fuel rods which fail during or immediately after rapid power ramps as a result of control rod manoeuvres or fuel shuffling at power, and also in short fuel rods intentionally subjected to power ramps in Studsvik’s R2 reactor and other test reactors [6]. Cladding fractures with similar features have also been obtained out of pile, with both irradiated and unirradiated cladding specimens, by subjecting the cladding to a high stress intensity while exposing it to a stress corrosion agent (usually iodine).

3.2. Hydride assisted cracking

Two different basic forms of hydride assisted fracture mechanisms have been observed experimentally in LWR cladding at high burnup. In the first form the crack propagates fairly rapidly, initially in the comparatively brittle hydride phase, and then as the stress level locally exceeds the yield stress of the irradiated zirconium alloy, both in the hydrides and by ductile tearing of the metal ligaments between the hydrides. The other form of hydride assisted cracking is fairly slow, and includes the formation of radially oriented hydrides ahead of the crack tip; this mechanism is essentially the same as the delayed hydrogen cracking observed in CANDU components [7].

3.3. Rapid hydride assisted cracking (hydride embrittlement)

Rapid cladding failure due to hydride embrittlement at high burnup under in-pile PCMI loadings has been observed in RIA simulation tests in pulse-type reactors [8, 9]. By their very nature, such tests are too short (with significant cladding straining occurring over a time of less than 0.1s) and the cladding temperatures too low (frequently below normal cladding operating temperatures for the duration of the peak stress-strain transient) for hydrogen diffusion to play a role in the fracture process; only those hydrides existing at the start of the transient affect the crack initiation and propagation. In a number of high burnup RIA tests the cladding fracture has been found to be situated at regions with locally enhanced hydriding associated with oxide spalling. In at least two cases, HBO-5 and HBO-6, non-penetrating cracks were clearly observed to have started at the outside surface of the cladding. In both cases, the cracks had penetrated through the heavily hydrided outer part of the cladding wall, and in both cases the cracks were associated with (i.e. appeared to be continuations of) radial cracks in the surface oxide layer [8].

At Studsvik, non-penetrating incipient cracks have also been seen in high burnup fuel rods with significant local hydriding, which have been subjected to power ramps with a short duration (hold time at ramp terminal power level of less than 1 minute), to simulate certain types of anticipated transient (Figure 2a). The cracks typically appear to have initiated at the outer surface of the cladding wall, and have penetrated a certain distance into the cladding, in the heavily hydrided part of the wall (Figures 2b and 2c). The cracks have then arrested in the relatively hydride-free metal further into the

cladding. No radially oriented hydrides have been seen ahead of the crack tip in the case of short-duration ramp tests.

This type of crack seems to always coincide with a radial crack in the surface oxide layer; however, not all radial cracks in the oxide layer have corresponding cracks in the underlying cladding (typically there are several tens of radial cracks in the waterside oxide around the circumference of a

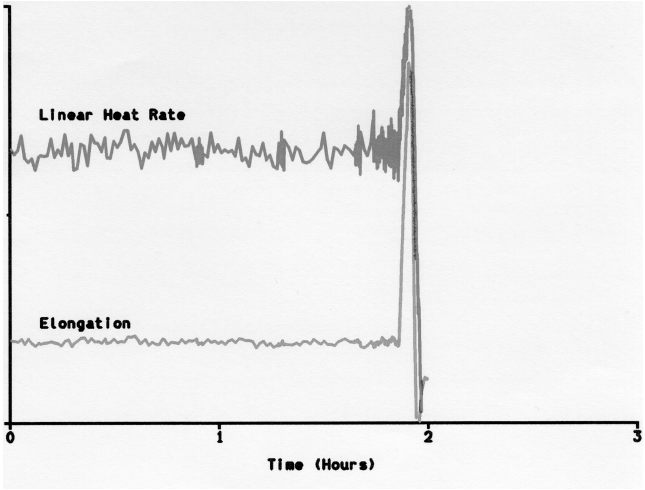

FIG. 2a. Ramp test with short hold time at peak power.

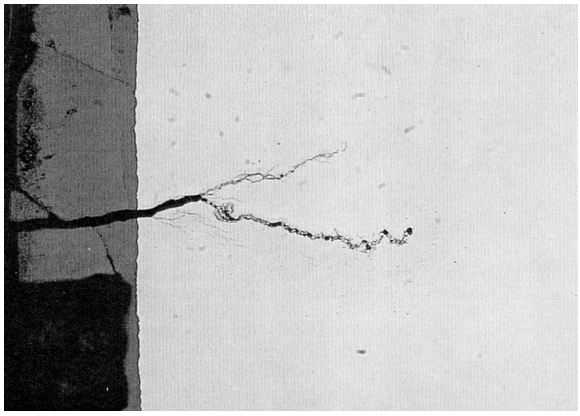

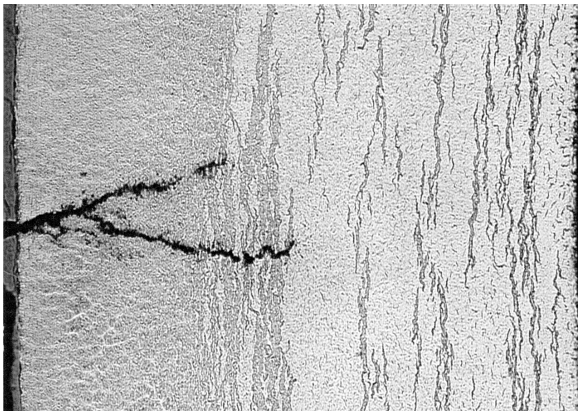

FIG. 2b. As polished condition *FIG. 2c. Hydride etched condition*
Incipient crack appearance after short ramp test, optical microscopy

power ramped fuel rod, depending on the power ramp amplitude and oxide layer characteristics, but only one or two cracks in the underlying hydrided metal).

Constant strain rate mechanical testing to failure (such as the ring tensile test) resembles the short-duration PCMI situation inasmuch as there is no hold at constant or reducing load (which would simulate the situation with a power ramp followed by a holding time at constant power). The features seen in mechanically tested irradiated cladding with significant local hydriding are very similar to those seen in the ramped fuel rods: crack initiation apparently starting at a radial crack in the surface oxide layer, followed by propagation inwards (initially in the heavily hydrided outer part of the cladding, finally by a combination of relatively brittle cracking of the hydrides and tearing of the metal ligaments between the hydrides). These features are illustrated below for ramp tested and ring tensile tested cladding from similar fuel (Figures 3-5). Of particular interest is the fact that cracks can form in the hydrides in a direction normal to the tensile stress axis, irrespective of the hydride

orientation; however, the total crack length is naturally far greater in a hydride with the same orientation as the crack propagation direction. It should also be noted that the crack can be arrested when entering a less hydrided region. The large local plastic strain in the metal phase can be inferred from the crack width and blunting.

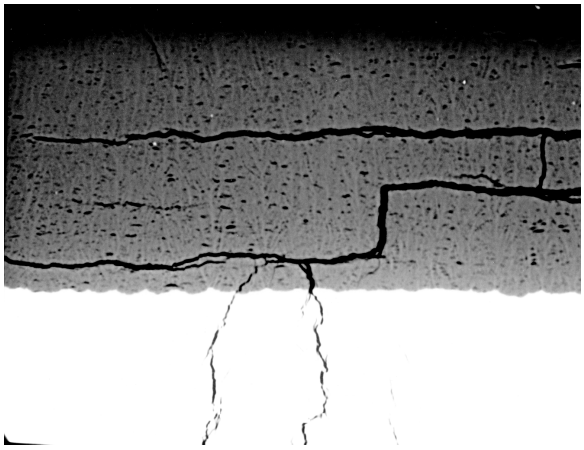

Fig. 3a. SEM, ramped *Fig.3b. SEM, mechanical test*
Crack initiation at outer surface opposite radial cracks in oxide layer

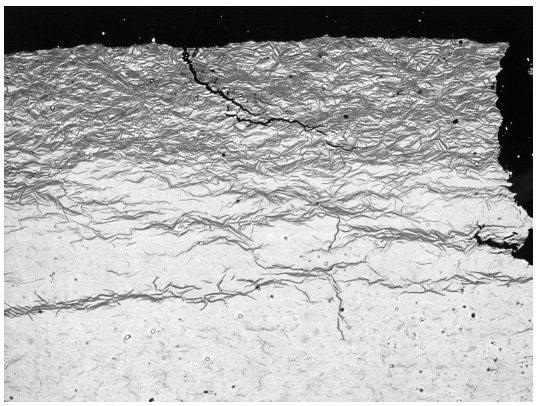

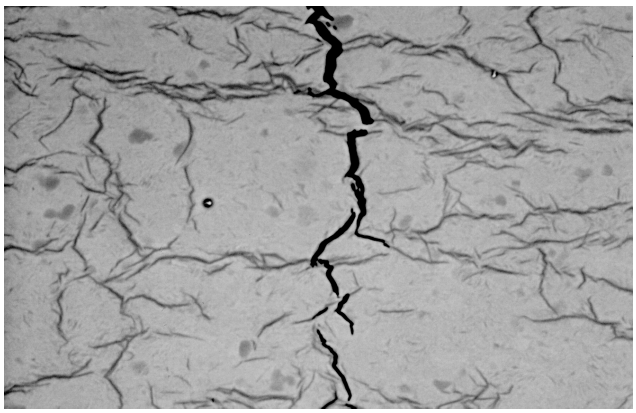

FIG. 4a. SEM, ramped *FIG. 4b. SEM, mechanical test*
Crack propagation in hydrides oriented normal to tensile stress direction

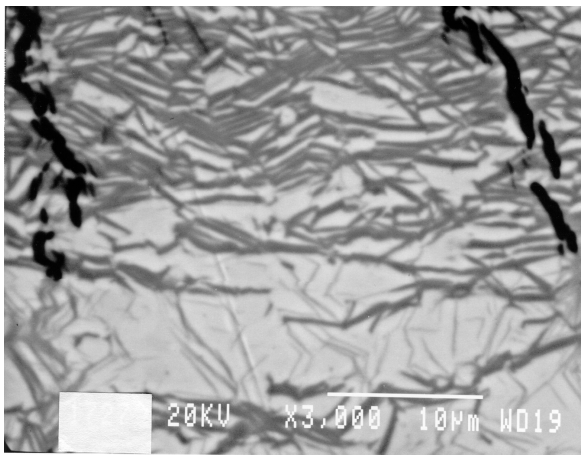

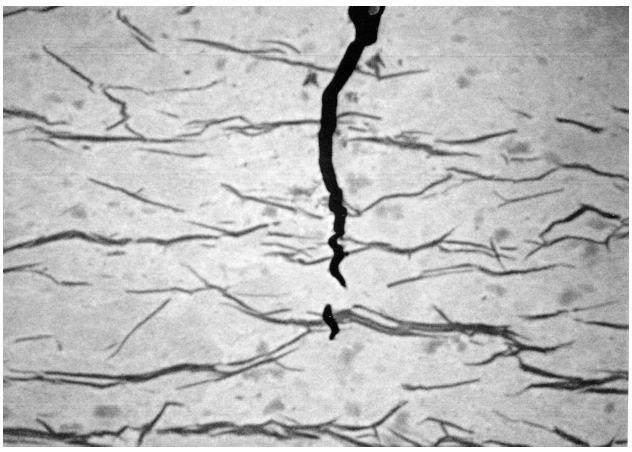

FIG. 5a. SEM, ramped *FIG. 5b. SEM, mechanical test*
Crack propagation in hydrides oriented parallel to tensile stress direction

3.4. Slow hydride assisted cracking (hydride assisted delayed cracking)

In some ramp tests of high burnup fuel with significant corrosion and/or hydriding, the fuel rod has failed after a significant time at constant power (typically tens of minutes at the ramp terminal level). An example of this type of behaviour is shown in Figure 6a, where the cladding has failed (as seen by the drop in the cladding elongation signal) approximately 40 minutes after reaching the ramp terminal level, and fission product release has started (as a puff) several minutes later. The crack is shown in cross-section in Figure 6b, at an axial position where it does not penetrate through the entire cladding wall.

In other cases, fuel rods have survived ramp tests with significant hold times at the ramp terminal level; however, non-penetrating (incipient) cracks in the outer part of the cladding have been found in the peak-power position [10]. An example of such a ramp and the ensuing incipient crack are shown in Figures 7a and 7b. In this case, unlike in the short duration ramp test case, radially oriented hydrides are seen ahead of the crack tip. Since there are no such radial hydrides to be seen anywhere else in the cladding, it may be assumed that these hydrides formed during the ramp test, as a result of the crack and the resulting stress gradient at its tip.

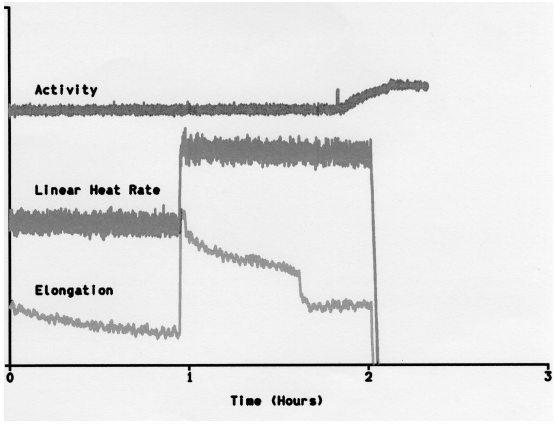

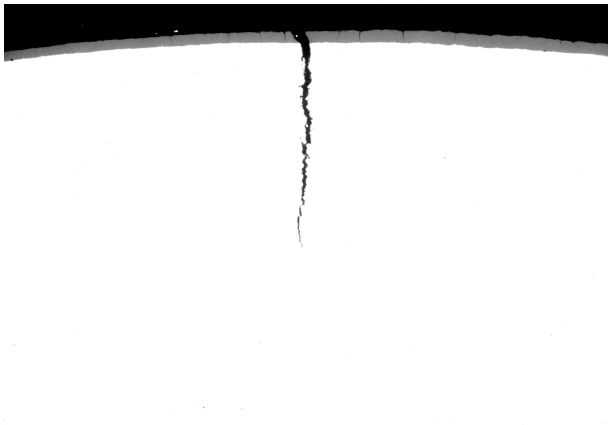

FIG. 6a. Ramp with failure after significant hold time. FIG. 6b. SEM, non-penetrating part of crack.

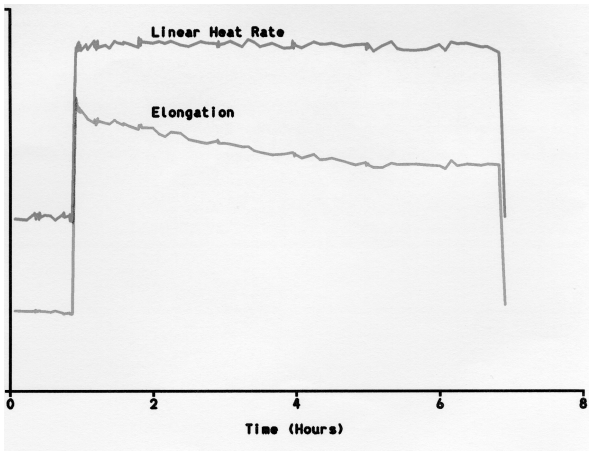

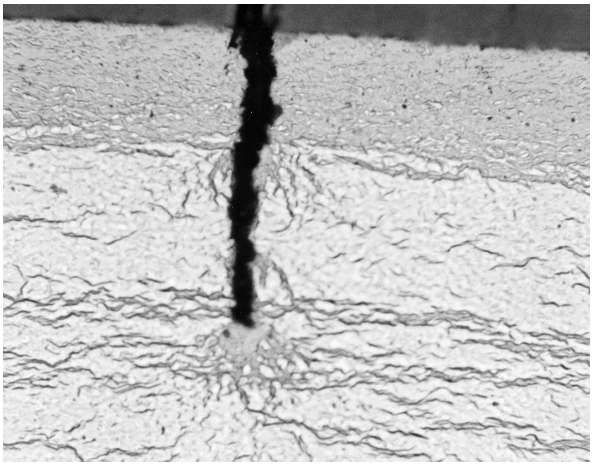

Fig. 7a. Ramp without failure after significant hold time.

Fig. 7b. OM, hydride etched, incipient crack.

The formation of hydrides ahead of the crack tip, and aligned with the direction of crack propagation, are strongly reminiscent of the features of delayed hydride cracking (DHC) observed in Zr-Nb pressure tubes and other zirconium alloys [7]. In this case, however, the crack has not penetrated through the cladding wall, presumably because of either insufficient stress intensity (the cladding hoop stress is reduced by creep relaxation during the constant power hold), the increasing temperature and decreasing hydrogen concentration further into the cladding, insufficient time, or fabrication or materials properties.

Again, the crack in the hydrided metal is associated with a radial crack in the surface oxide layer, suggesting that the crack initiation process is the same in both the rapid and the slow hydride assisted cracking mechanisms.

Experience with delayed hydride cracking testing of the axial propagation of through-wall cracks in irradiated Zircaloy cladding, conducted by constant loading of pre-cracked cladding halves [11], suggests that it may be possible to simulate the hydride assisted delayed PCMI cracking mechanism observed in-pile with out-of-pile mechanical tests.

4. CONCLUSIONS

Hydride embrittlement and hydride assisted delayed cracking mechanisms have been identified in high burnup LWR fuel cladding tested under PCMI conditions in the R2 reactor and in out-of-pile mechanical testing. The fracture features are very similar to those recently observed in simulated RIA tests on some high burnup fuel rods. In all cases, the cracks appear to have initiated at radial cracks in the waterside oxide layer, and then propagated inwards into the cladding. In many cases, extensive ductility has been seen in the metallic phase, resulting in significant local plastic deformation, and frequently leading to crack arrest in the less hydrided region further into the interior of the cladding wall. The radial hydride concentration gradient in fuelled cladding, with the highest density of hydrides occurring at the cooler outer surface of the cladding wall, apparently plays an important role in determining the rate and extent of the crack propagation into the cladding. The hydrides are preferential fracture sites, while the metal phase withstands significant local plastic strain before failing. Given sufficient time with applied PCMI load, radial hydrides can sometimes form ahead of the tip of an arrested non-penetrating crack. Through wall fracture (rod failure) due to hydride assisted PCMI in ramp tests, identified by cladding contraction and activity release from the rod, frequently occurs some time after reaching the ramp terminal power, suggesting that at least part of the crack propagation is time dependent in these cases.

In order to obtain a good qualitative and quantitative understanding of the mechanisms involved in hydride assisted PCMI fracture, it has been necessary to employ a number of experimental techniques. Eddy current lift-off measurements and neutron radiography are powerful non-destructive techniques for identifying the most heavily oxidised and hydrided local sections of fuel rods, in order to prepare specimens for ramp or mechanical testing. Finally, detailed examination after ramping or mechanical testing is essential to analyse the fracture behaviour. In particular, scanning electron microscopy (SEM) of the cladding cross-section has proven invaluable for fracture path analysis, measurement of the local hydrogen concentration and oxide thickness in the vicinity of the crack, and assessment of localised plastic deformation.

REFERENCES

[1] GARDE, A.M., SMITH, G.P., PIREK, R.C., Effects of hydride precipitate localization and neutron fluence on the ductility of irradiated Zircaloy-4. ”Zirconium in the Nuclear Industry: 11th Int. Symposium”, ASTM STP 1295, 407–430 (1996).

[2] COLEMAN, C.E. HARDIE, D., The hydrogen embrittlement of α-zirconium- a review. J. Less-Common Metals 11, 168 (1968).

[3] ARSENE, S., BAI, J., A new approach to measuring transverse properties of structural tubing by a ring test — Experimental investigation. Journal of Testing and Evaluation, 26, 1, January 1998, 26–30.
[4] SCHRIRE, D., PEARCE, J., Scanning electron microscope techniques for studying Zircaloy corrosion and hydriding. "Zirconium in the Nuclear Industry: 10th Int. Symposium", ASTM STP 1245, 98–115 (1994).
[5] ROBERTS, J.T.A., et al., A stress corrosion cracking model for pellet-cladding interaction failures in light water reactor fuel rods, in "Zirconium in the Nuclear Industry: 4th Int. Symposium", ASTM STP 681(1979).
[6] BERGENLID, U., MOGARD, H., RÖNNBERG, G., Experimental observations of PCI failure occurrence on power ramping. IAEA Specialists Meeting on Pellet-Clad Interaction in Water Reactors, Risø, 1980.
[7] NORTHWOOD, D.O., KOSASIH, U., Hydrides and delayed hydride cracking in zirconium and its alloys. Int. Metals Review 28, (2), 92 (1983).
[8] FUKETA, T., et al., NSRR/RIA experiments with high burnup PWR fuels. Proc. Int. Top. Mtg. On LWR Fuel Performance, Portland, Oregon, March 1997.
[9] MENUT, P., LESPIAUX, D., TROTABAS, M., Cladding and fuel modifications of a 60 GW·d/tM irradiated rod during a power transient performed in the CABRI reactor. CSNI Specialist Mtg. on Transient Behaviour of High Burnup Fuel, Cadarache, Sept. 12–14, 1995.
[10] RUDLING, P., PETTERSSON, H., PCI performance of PWR rods with excessive oxide spalling and large hydrogen content. This Technical Committee Meeting.
[11] EFSING, P., Delayed hydride cracking in irradiated Zircaloy. Ph D Thesis, Royal Institute of Technology, Stockholm, 1998.

A PWR PCI FAILURE CRITERION TO BURNUPS OF 60GW·d/t U USING THE ENIGMA CODE

A.P. CLARKE, P.A. TEMPEST, J.H. SHEA
British Energy, Reactor Analysis Group,
Gloucester, United Kingdom

Abstract

A fuel performance modelling code (ENIGMA) has been used to analyse the empirical PCI failure criterion in terms of a clad failure stress as a function of burnup and fast neutron dose. The Studsvik database has been analysed. Results indicate a rising and then saturating failure stress with burnup and fast neutron dose. Using the PCI failure limits, equivalent to 95/95 confidence limits, an ENIGMA stress-based methodology is used to derive PWR PCI failure limits up to 60 GW·d/t U using a conservative assumption that the failure stress does not increase at high burnup and neutron dose. In addition experimental ramp data on gadolinia-doped fuel rods do not indicate any increased susceptibility to PCI failure implying that the UO_2 criterion can be used for gadolinia doped fuel.

1. INTRODUCTION

Power transients in PWRs may lead to fuel failure from strong Pellet Clad Interaction (PCI). In order to limit the possibility of PCI induced failures, restrictions are imposed on the allowable power uprates during normal operation and fault transients. The magnitude of the uprates are defined by a PCI failure criterion which was derived from an experimental database of ramped fuel prototypic for BNFL fuel loaded in Sizewell B. A statistical analysis of the failure/survivor distribution as a function of fuel conditioning power and burnup was performed [1].

The analysis enabled lines to be defined above which 95% of the fuel ramped to this level would survive with 95% confidence (refered to as 95/95 lines). Originally in the safety case for the first and second fuel loadings at Sizewell B this empirical PCI criterion was used. The main limitation of this approach was the burnup range of applicability (<35 GW·d/t U) which was defined by the experimental database used in the criterion derivation. Although the experimental database in Ref. [1] contains survivors at a burnup of 45 GW·d/t U and a failure at 38 GW·d/t U the conservative view was taken to restrict the high burnup limit to 35 GW·d/t U.

The experience of Siemens with fuel, which has been made available to British Energy for the licensing of Siemens fuel for Sizewell B power station, varying in burnup from 35GW·d/t U to about 45GW·d/t U reveals no failures [2]. Further examples include recent PCI tests conducted by Babcock and Wilcox on three rods at 62.3 GW·d/t U [3] and Siemens fuel ramped at 61 GW·d/t U. It is a feature of high burnup ramped fuel that it is difficult to fail through PCI. However, the problem with high burnup survivors is that they cannot be used in isolation to derive a *failure* criterion at high burnup without some failures to help define a failure/survivor boundary.

Using the ENIGMA code [4],[5], which is a fuel performance code principally developed by British Energy, a methodology has been developed for extending the PCI criterion to burnups of 60GW·d/t U by conducting a detailed analysis [6] of the entire Studsvik ramp database, including non-prototypic fuel. Use has also been made of additional data from Siemens. The methodology uses ENIGMA to calculate the clad hoop stress of identified rods in the PCI database.

2. THE EFFECTS OF HIGH BURNUP ON PCI MECHANISMS

A PCI failure is thought to be driven by Stress Corrosion Cracking (SCC) at the pellet ends where clad ridging occurs due to pellet wheatsheafing. The corrodent is assumed to be an aggressive fission product, nominally iodine which has been confirmed by out-of-pile tests [7]. The evidence from the ramp database suggests a survivor/failure boundary that is dependent on the final power reached in the ramp which is consistent with an increase in fission product release from the fuel at high power.

The ENIGMA analysis indicates that the propensity to failure by PCI depends on the clad hoop stress reaching a threshold value. The observation of an increase in threshold stress with fast neutron dose has been explained in terms of crack initiation and rapid propagation at surface flaws whose depth decreases during neutron exposure [6]. This argument is supported qualitatively by SEM observations of fresh and irradiated cladding [8]. Rather than degrade with irradiation, some mechanical properties of Zircaloy tend to improve, in keeping with the anisotropy of the mechanical properties decreasing. However, changes in the pellet/clad chemical environment such as the oxidation of the clad inner bore can also be expected to influence localised stress levels. Thus clad surface smoothing would not be expected to operate in isolation of other phenomena.

The basic underlying mechanisms of SCC and threshold stress established up to 50GW·d/t U can be expected to dominate above 50GW·d/t U also. Differential thermal expansion, pellet wheatsheafing, clad ridging, fuel and clad creep relaxations will still determine the clad hoop stress in the ENIGMA calculations. The most obvious material change to the pellet clad interaction zone at burnups above 50 GW·d/t U is the gradual formation of a rim region at the periphery of the pellet. In LWR fuel, the pellet rim starts to become porous at an average burnup of approximately 50 GW·d/t U as supported by Ref. [9] and reviewed by Ref. [10]. Although potentially detrimental in terms of increased fuel temperatures and enhanced fission gas release, the effect on PCI is probably more benign. The loss of pellet rigidity at the point of clad contact would be expected to reduce the pellet driving strain and hence reduce the induced clad stresses. Furthermore localised straining effects over radial fuel cracks would be significantly reduced as the pellet cracking fissures are smeared out over the rim region. Put simply, the fuel becomes more compliant in the rim region and unable to sustain concentrated stresses in contact with the clad.

3. ANALYSIS OF THE AVAILABLE DATABASES

The Studsvik database has been analysed using the ENIGMA code. The database consists of ramp tests from the OVERRAMP [11], INTERRAMP [12], SUPERRAMP [13] and the TRANSRAMP (II & IV) [14, 15] programs. Ranges of specific parameters, from the above programs, are listed in Table I**.** The available current Siemens database, which includes PCA-2a, KWU-SUPER & OVERRAMP and gadolinia cases, [2] has been used to extend a range of parameters from the Studsvik database. The extended parameters are listed in Table II. In order to adequately model Siemens clad and gadolinia doped fuel a new version of the ENIGMA code (version 5.10) was developed [16]. ENIGMA 5.10 gives the same results as that of the ENIGMA 5.9 code except in the cases where Siemens clad or gadolinia doped fuel are modelled.

The available data have been used to calculate peak hoop stresses as a function of fast neutron fluence using ENIGMA 5.10. Survivor and failure cases are plotted in FIG. 1. In addition to these cases the figure also includes hoop stress/fast fluence data points determined for four ramped gadolinia doped rods. The figure shows that the peak hoop stresses increase with fast neutron dose to a maximum peak hoop stress calculated at approximatley 750 MPa which occurs at a fast fluence of 8×10^{25} n/m^2.

TABLE I. A TABLE SHOWING THE RANGE OF PARAMETERS AVAILABLE FROM THE STUDSVIK DATABASE

Pellet length L	11.0–15.24mm
Pellet diameter D	8.19–10.71mm
L/D	1.2–1.66
Fuel grain size	4.5–22 μm
Fuel density	10.27–10.47 g/cm^3
Enrichment	2.82–8.26 %
Burnup	9.4–41.6 GW·d/t U
Clad type	Zircaloy 2 & 4, CW-SR, RX & PRX.
Clad yield stress	363–610 MPa
Clad Temperatures	291–363°C
Fast fluence	1.16–6.94 × 10^{25} n/m^3 (E>1MeV)

TABLE II. A TABLE SHOWING THE INCREASED RANGE OF PARAMETERS WHEN THE SIEMENS DATABASE IS INCLUDED

Pellet length L	10.62–15.24mm
L/D	1.1–1.64
Burnup	9.4–62.5 GW·d/t U
Clad Temperatures	291–372°C
Fast fluence	1.16–11.3 × 10^{25} n/m^3 (E>1MeV)
Gadolinia fuel	0–8wt%

The observation of a rising threshold failure stress with fast neutron dose using ENIGMA was instrumental in forming an alternative perception of the PCI failure criterion. This approach was developed in Ref. [6] where the rising threshold failure stress was associated with the smoothing of incipient clad inner bore surface flaws by processes stimulated by fast neutron bombardment.

Equally plausible as a mechanism to promote surface smoothing during irradiation is the effect of fission damage. Here the relevant parameter is burnup rather than fast neutron dose. FIG. 8.2 shows the variation of threshold stress as a function of burnup and a similar trend to that seen with fast neutron dose is apparent although discrimination between failures and survivors appears not so distinct. On this evidence there is a broader-based root cause associated with the observation of an increasing hoop stress for failure with burnup and/or fluence irrespective of any proposed mechanism. Fission damage could play a major role in enhancing surface smoothing processes.

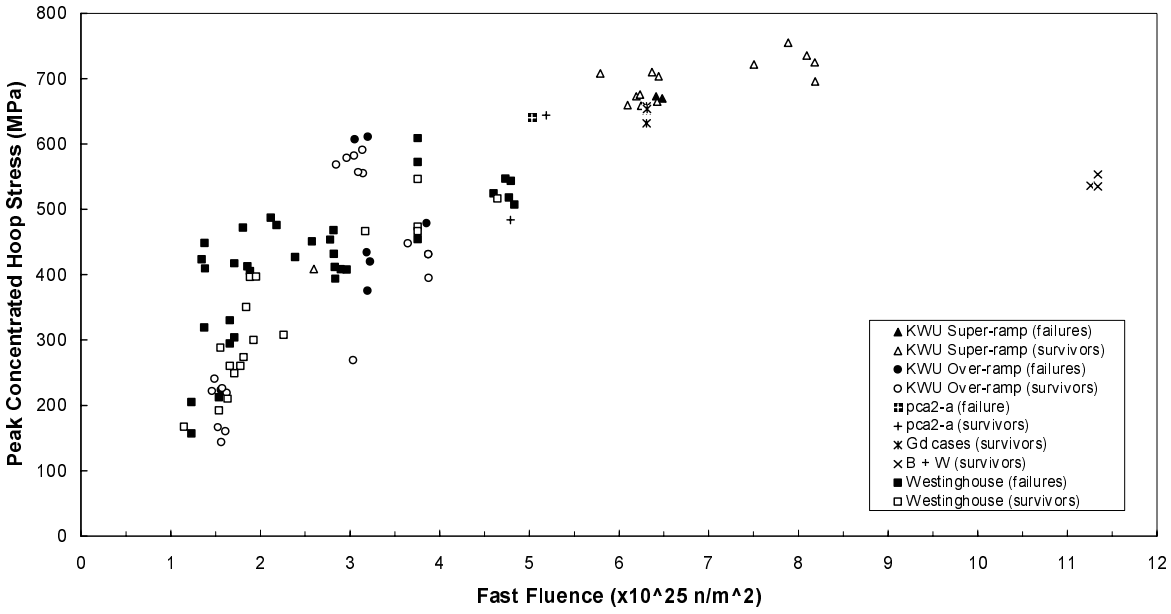

FIG. 1. Peak concentrated hoop stress as a function of fast fluence using ENIGMA 5.10.

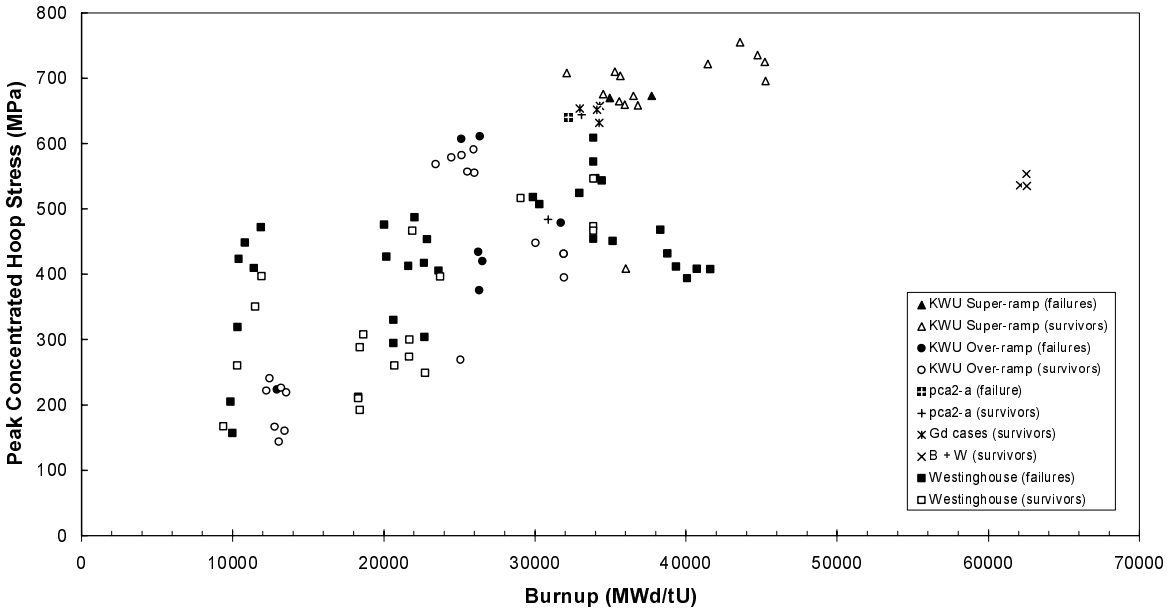

FIG. 2. Peak concentrated hoop stress versus burnup using ENIGMA 5.10.

4. METHODOLOGY AND RESULTS

4.1. Conditioning period

The methodology used to extend the PWR PCI failure criterion to higher burnups utilised power histories that modelled the irradiation conditions experienced by fuel rods in the Sizewell B reactor. The methodology ensures that PCI has occurred and that the pellet and clad are fully conditioned prior to the transient by imposing the following condition: the hoop stress is positive and approximately constant:-

$$\frac{d\sigma_\theta}{dt} \sim 0 \qquad (1)$$

where σ_θ is the hoop stress.
Typically, when equation (1) is satisfied the hoop stress is of order 50±20 MPa.

4.2. Hoop stress calculation of the 95/95 criterion

In order to determine concentrated hoop stresses for the empirical failure criterion, power histories were constructed for fuel rods with burnups of 15, 25 and 35GW·d/t U and conditioning powers of 20, 25 and 30kW/m. The power histories consisted of three parts:

a long base irradiation period at 24kW/m (peak average)
a conditioning period (such that equation 1 is satisfied)
a final ramp at a rate of 30kW/m/min.

A ramp rate of 30 kW/m/min was chosen so that clad stresses are influenced by pellet strains and not primary creep of the clad. The allowable power uprate, from the 95/95 failure lines, is then used to derive a stress due to the uprate, the results of which can be seen in Table III. It can be seen that the criterion relates to a lower hoop stress at the higher conditioned powers. More interestingly the implied 'failure' stresses (implied since the 95/95 lines are assumed in the safety case to define failure) are largely insensitive to burnup. When these stress levels are plotted on the stress-fluence plot of the actual fuel failure database in FIG. 9 it can be seen that they fall some way below the experimental rod failure stresses. By conservatively assuming that the 95/95 stress levels remain constant at higher burnups it is possible to reverse the ENIGMA calculational route and derive allowable uprates.

4.3. Extensions to higher burnups

The extension of the PWR PCI failure criterion to burnups above 35GW·d/t U involves calculating a stress at each of the conditioned powers (20, 25 and 30kW/m) from the 95/95 lines at 15, 25 and 35 GW·d/t U and averaging the stresses over the three burn ups. The derived hoop stresses are listed in Table IV. Due to the hoop stress being relatively insensitive to burnup an average of the hoop stresses at each conditioned power is used to set a failure stress for burnups above 35GW·d/t U. These failure stresses are approximately 418, 332 and 216 MPa for conditioning powers of 20, 25 and 30kW/m respectively (Table IV). In order to determine a power uprate from a transient above 35GW·d/t U power histories were constructed as described in Section 4.2. The power at which the failure stress is reached (E_f) is defined as the failure power equivalent to a new point on a high burnup 95/95 line. The power uprate (ΔP) is defined as:

$$\Delta P = E_f - P_c \qquad (2)$$

where P_c is the conditioned power. Results are listed in Table IV. Figure 4 shows the PWR PCI failure criterion up to burnups of 60GW·d/t U. Note, if the stresses are not averaged over burnup but are linearly extrapolated the results would change by only about 0.7kW/m at 60GW·d/t U.

TABLE III. A TABLE CONTAINING FUEL BURNUPS (15 TO 35GW·D/T U), CONDITIONING POWERS AND POWER UPRATES USED TO DETERMINE CONCENTRATED HOOP STRESSES

Burnup (GW·d/t U)	Conditioned Power (kW/m)	Power Uprate (kW/m)	Hoop stress (MPa)
15	20	15.0	—— 419.8
	25	11.5	—— 341.6
	30	8.0	—— 226.4
25	20	14.0	—— 428.4
	25	10.5	—— 329.4
	30	7.0	—— 223.8
35	20	13.0	—— 406.1
	25	9.5	—— 323.8
	30	6.0	—— 198.2

TABLE IV. A TABLE CONTAINING FUEL BURNUPS (40 TO 60GW·D/T U), CONDITIONING POWERS AND POWER UPRATES THAT WERE DETERMINED FROM AVERAGES OF CONCENTRATED HOOP STRESSES, AT GIVEN CONDITIONED POWERS, FROM TABLE III

Burnup (GW·d/t U)	Conditioned Power (kW/m)	Power Uprate (kW/m)	Hoop stress (MPa)
40	20	11.9	—— 418.1
	25	8.9	—— 331.6
	30	6.0	—— 216.1
50	20	11.0	—— 418.1
	25	8.3	—— 331.6
	30	5.9	—— 216.1
55	20	10.6	—— 418.1
	25	8.1	—— 331.6
	30	5.4	—— 216.1
60	20	10.0	—— 418.1
	25	7.9	—— 331.6
	30	5.4	—— 216.1

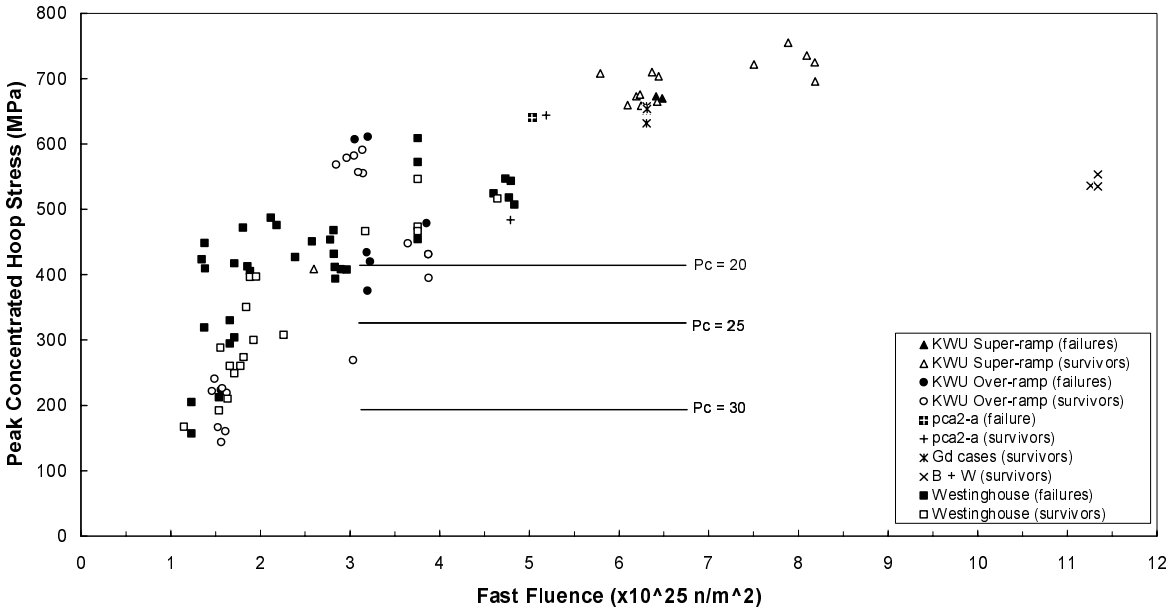

FIG. 3. Peak concentrated hoop stress as a function of fast fluence using ENIGMA 5.10 with conditioned powers indicated.

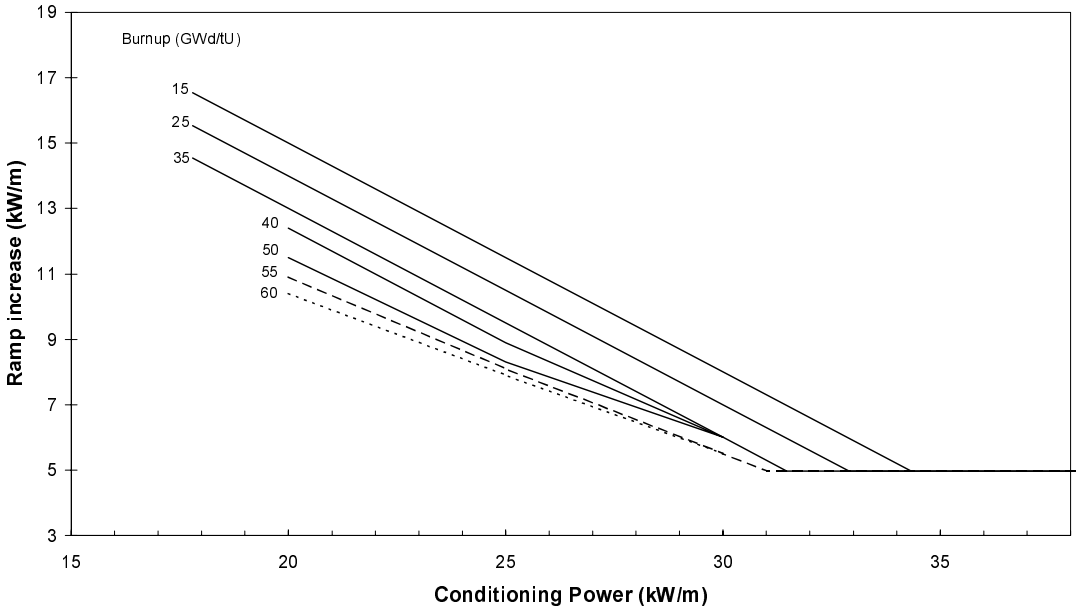

FIG. 4. The PWR PCI failure criterion to 60GW·d/t U.

The trend of decreasing uprate with conditioning power for burnups of 40GW·d/t U and above is similar to that for burnups ≤35GW·d/t U between conditioning powers of 20 and 30kW/m. Also the power uprates, calculated using the ENIGMA code up to a conditioning power of 30kW/m, decrease with burnup above 35 GW·d/t U in a manner similar to the decrease seen in the empirical criterion between 15 and 35 GW·d/t U. Above a conditioning power of 30kW/m the ENIGMA high burnup lines converge to meet the burnup independent portion of the criterion above 31 kW/m.

Above conditioned powers of 30kW/m, the 55GW·d/t U failure threshold has been linearly extrapolated to higher conditioned powers until the high conditioned power 95/95 criterion limit of 4.97kW/m is reached. Because the 55 and 60 GW·d/t U lines are coincident at 30 kW/m they have been conservatively extrapolated to be coincident at the point of the intersection of the 55GW·d/t U line with the 4.97kW/m horizontal line.

4.4. Lower conditioning powers

In order to extend the failure criterion to lower conditioned powers Murfin, Rippon and Turnbull [17] considered the criterion as a final power criterion independent of conditioned power. They argued that as there is no change in the mechanisms that induce/relax stresses in the clad as a function of conditioned power that the empirical best estimate failure lines can be extrapolated, without modification, to lower conditioning powers. By similar reasoning, therefore, as the 95/95 PCI failure lines are derived from the best estimate criterion, they can also be extrapolated below 20kW/m.

4.5. Sensitivity investigations and conservatisms

A sensitivity study has been made of the effect of changes in the power history on conditioned stresses and the choice of concentrated or mean calculated clad stress. Results indicate that if the current methodology is adopted, i.e. the concentrated hoop stress is approximately constant and is between 30 and 70 MPa prior to the final transient, then the derived failure limit lines at burnups above 35 GW·d/t U are relatively insensitive to these parameters.

To check the sensitivity of the ramp rate chosen (30kW/m/min) an investigation of ramp rate at 60 kW/m/min and 10 kW/m/min was performed. This produced an increase of only 10 MPa and a decrease of 30 MPa respectively in a threshold stress of 425 MPa for a conditioned power of 20 kW/m implying that the sensitivity is very low.

The proposed criterion extension can be regarded as conservative in 3 respects as follows:
the 95/95% confidence level PCI criterion on which the extrapolation is based
the threshold stresses to failure for conditioned powers above 20 kW/m are chosen conservatively with respect to the stress versus fluence trend derived from the ramp tests
it is observed that fuel above 35 GW·d/t U is difficult to fail through PCI

5. HIGH BURNUP AND GADOLINIA DATA

5.1. PCI ramp data at high burnup

Additional high burnup data (29 rods at burnups above 35 GW·d/t U) from the Siemens database are presented in FIG. 11. Eleven rods were ramped at a burnup in excess of 40GW·d/t U (highest 61.0GW·d/t U) and did not fail. All survivors and the one failure at 36.7GW·d/t U lie comfortably above the 35 GW·d/t U 95/95 line. The highest burnup rods subjected to PCI ramp tests were Babcock and Wilcox rods which were ramp tested in the Studsvik R2 test reactor at 62.3GW·d/t U [3]. Again none of these rods failed even though they were ramped well in excess of the 95/95 line.

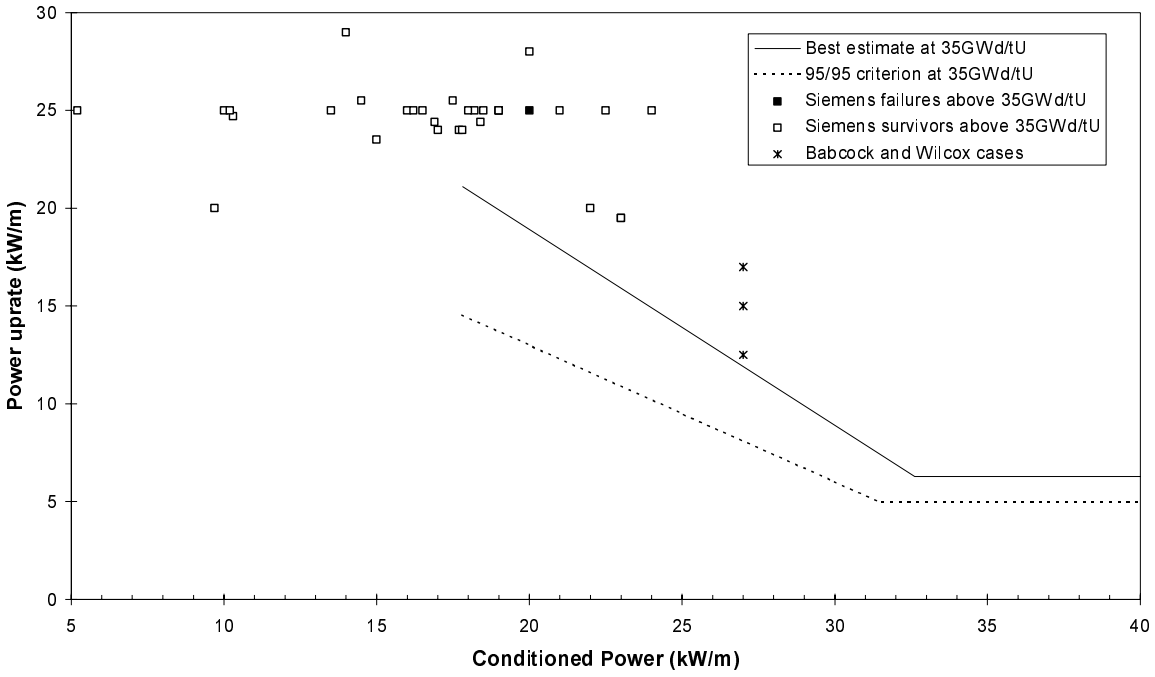

FIG. 5. High burnup cases above 35GW·d/t U with the PWR PCI best estimate and the 95/95 failure line indicated.

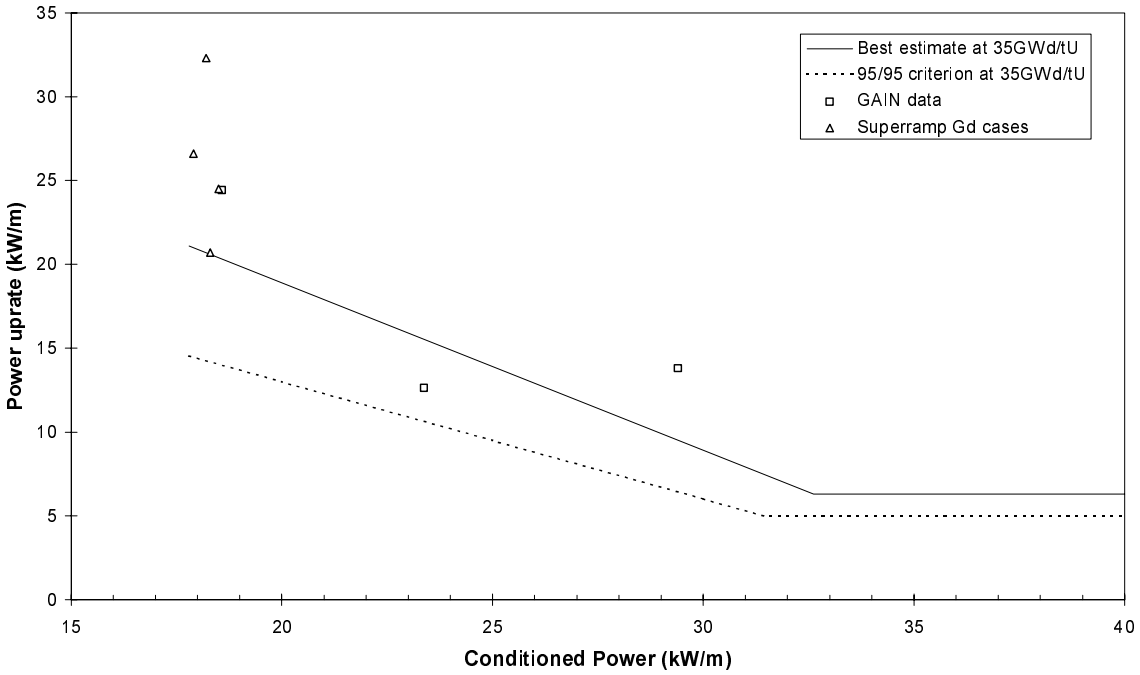

FIG. 6. Gadolinia cases with the best estimate and the 95/95 failure line at 35GW·d/t U indicated.

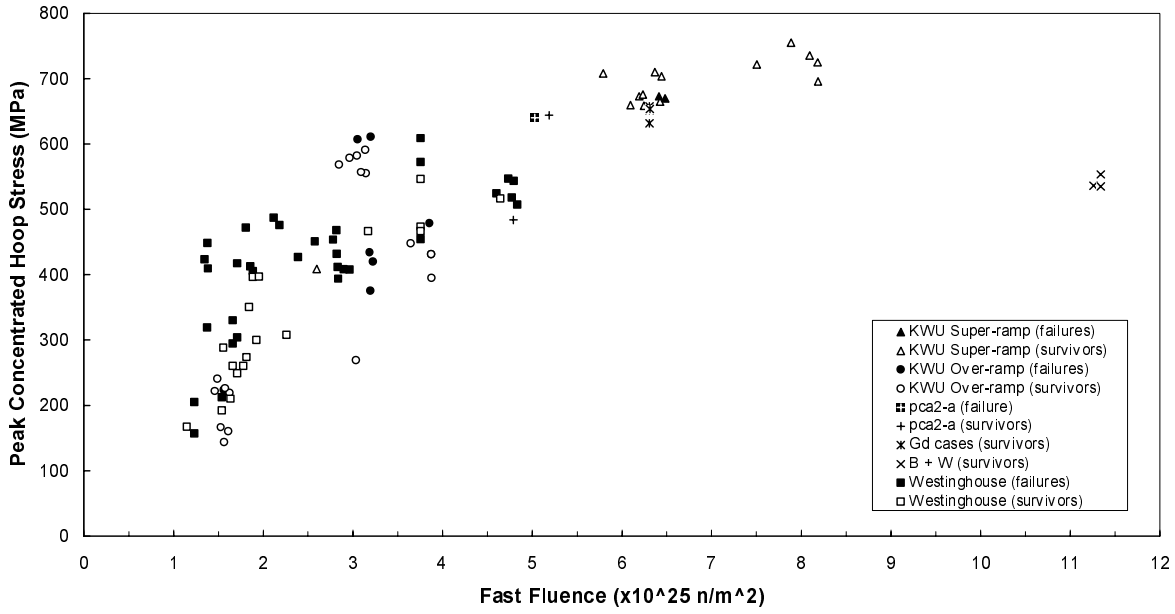

FIG. 7. Peak concentrated hoop stress as a function of fast fluence using ENIGMA 5.10.

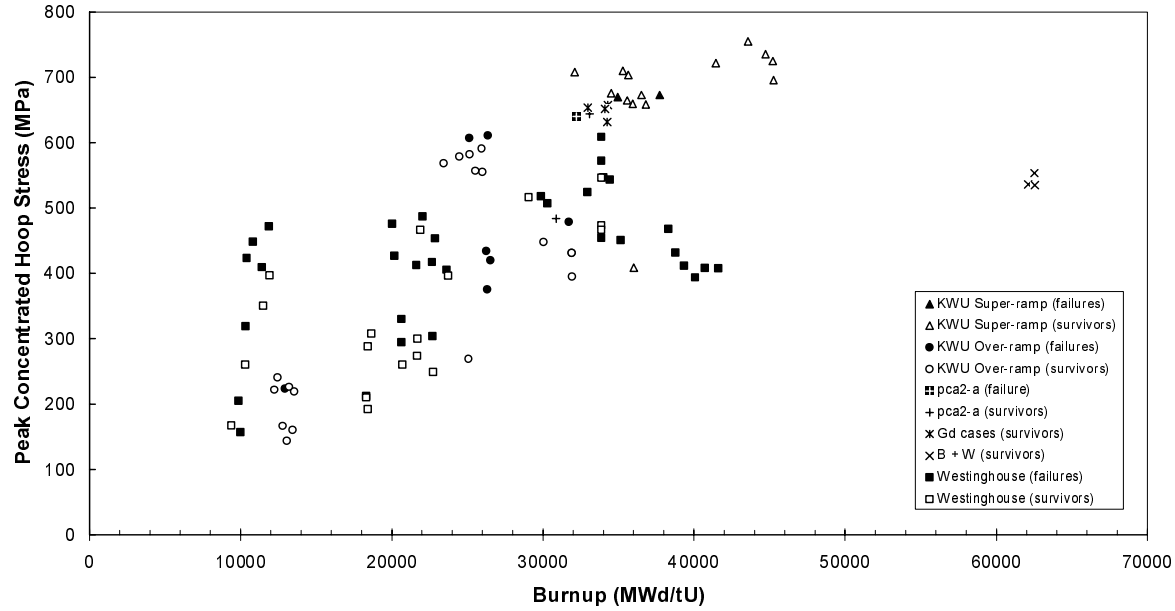

FIG. 8. Peak concentrated hoop stress versus burnup using ENIGMA 5.10.

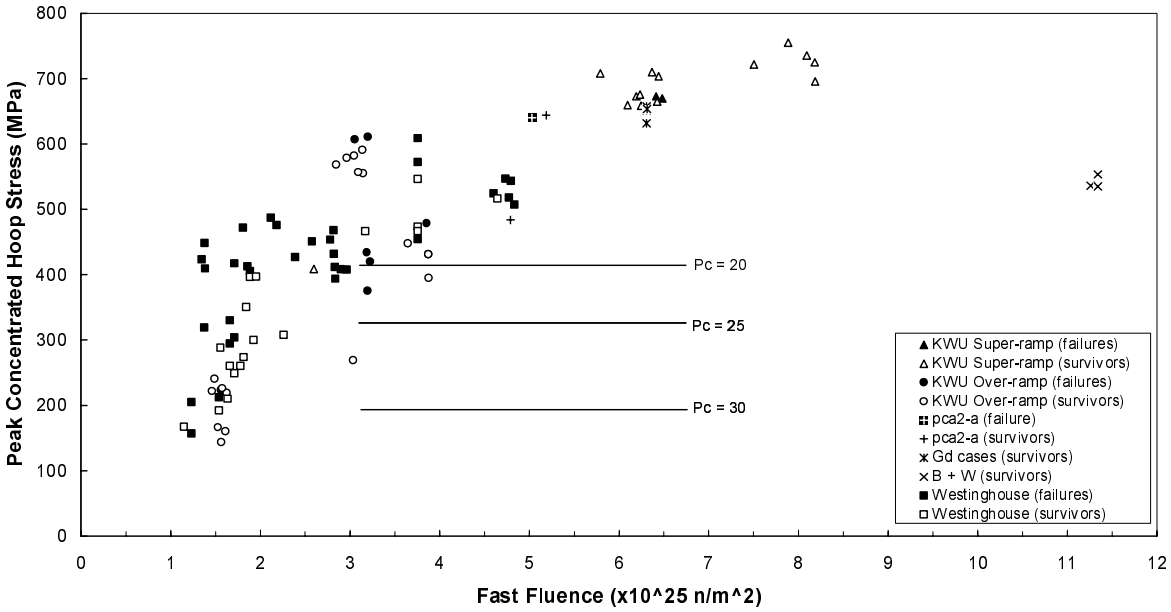

FIG. 9. Peak concentrated hoop stress as a function of fast fluence using ENIGMA 5.10 with conditioned powers indicated.

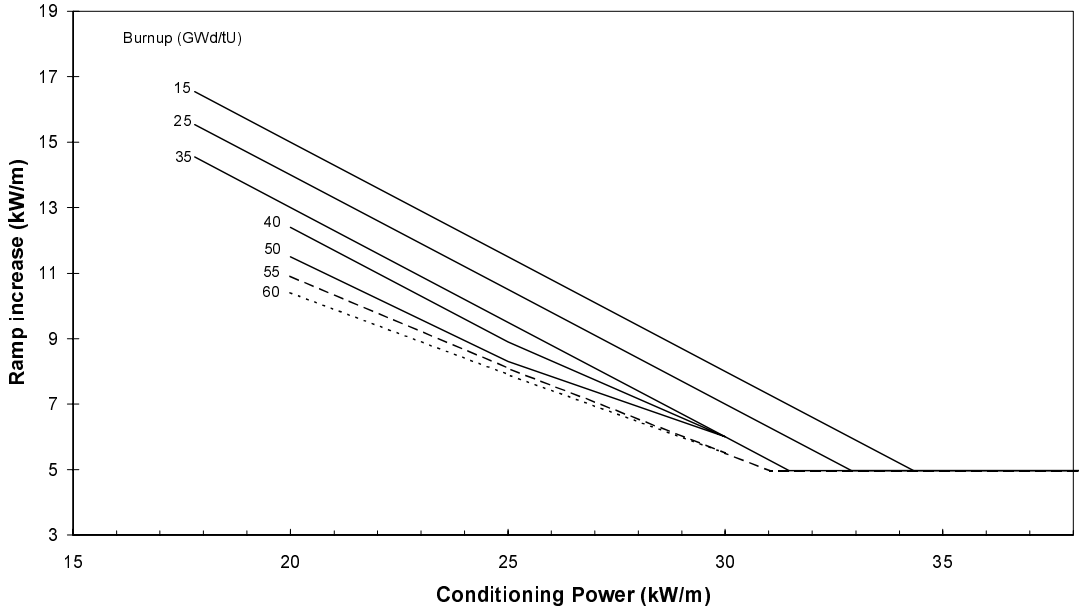

FIG. 10. The PWR PCI failure criterion to 60GW·d/t U.

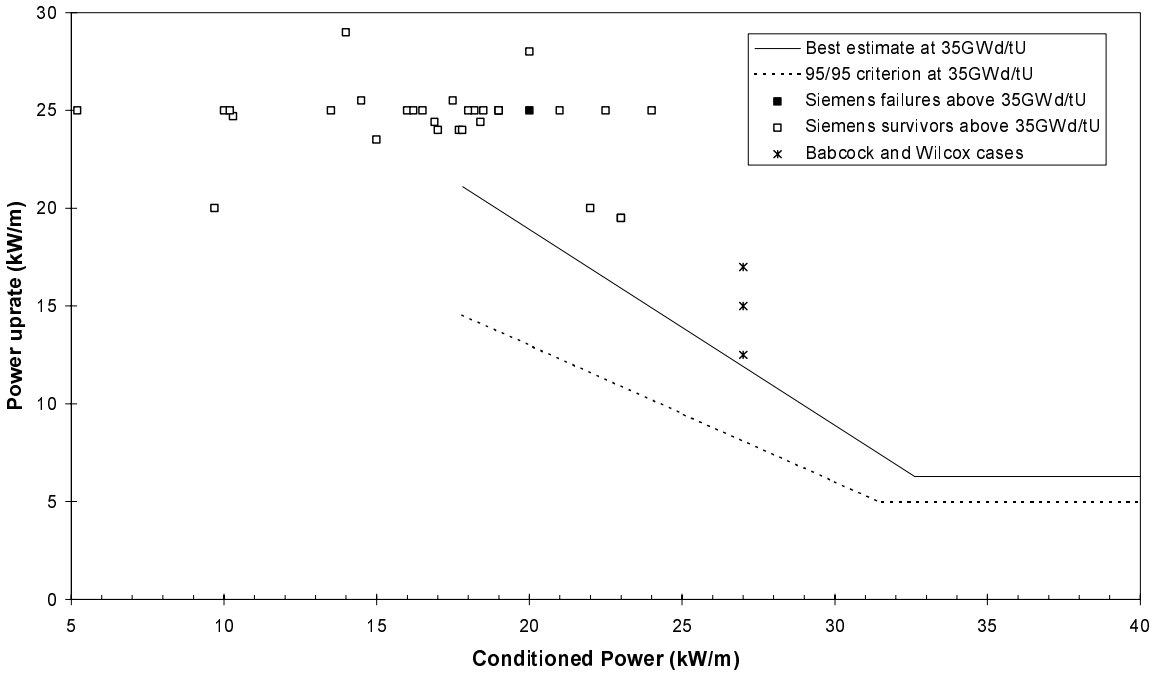

FIG. 11. High burnup cases above 35GW·d/t U with the PWR PCI best estimate and the 95/95 failure line indicated.

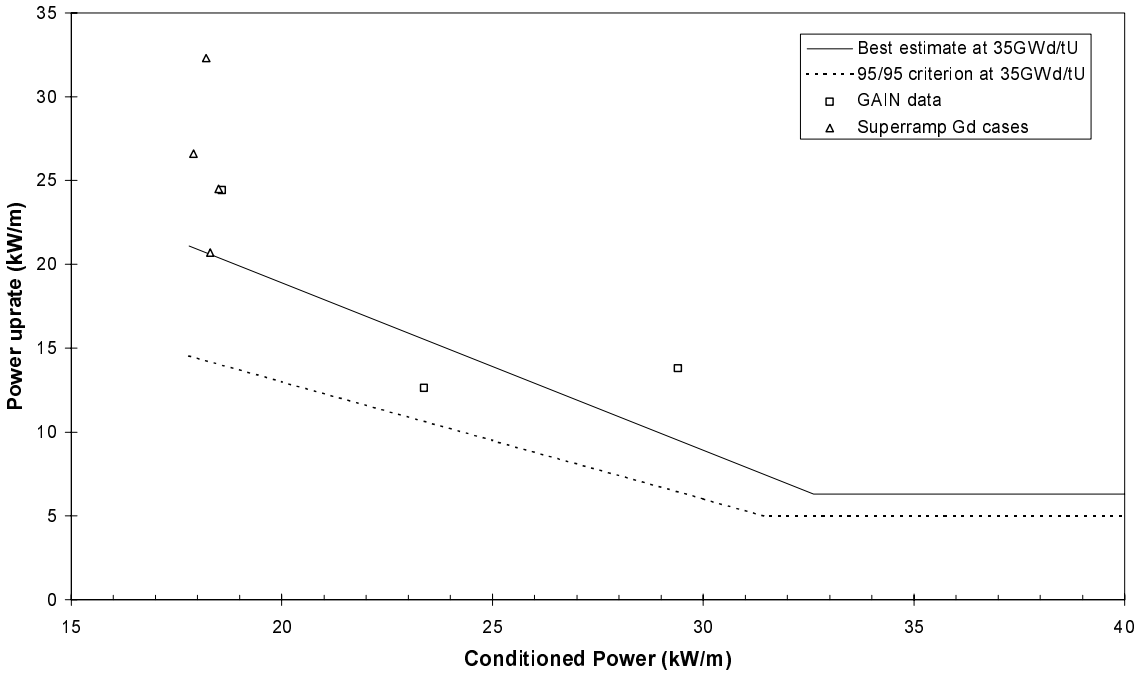

FIG. 12. Gadolinia cases with the best estimate and the 95/95 failure line at 35GW·d/t U indicated.

The difficulty in failing rods at high burnup is reflected in the data, the highest burnup failure occurring at 38 GW·d/t U for Westinghouse clad fuel and 37 GW·d/t U for Siemens clad fuel.

5.2. PCI ramp data on gadolinia - doped fuel

Since PCI induced clad stress is driven primarily by differential thermal expansion between the pellet and the clad, it might be expected that gadolinia-doped fuel (because of its reduced thermal conductivity) would be more susceptible to PCI failure than standard fuel when ramped from the same conditioning power for the same uprate. The data for Siemens fuel and from the GAIN programme [2], however, although limited to seven rods, does not reveal any vulnerability of the fuel to PCI failure. FIG. 12 shows the data for the seven rods, none of which failed. The burnup range covered by the Siemens rods is around 33–34 GW·d/t U and the GAIN rods 20–40GW·d/t U. The Siemens data covered very high final powers as high as 50 kW/m and yet did not fail. Interestingly these rods reached a fast neutron dose of 6.3×10^{25} n/m^2 which would imply a low probability to failure according to the stress-fluence plot in FIG. 7.

As there are data for only seven gadolinia doped rods and none of them failed it is not possible to derive a PCI criterion specifically for gadolinia rods. However, as none of the gadolinia rods failed despite being ramped above failure thresholds defined by the UO_2 rod PCI criterion, the UO_2 criterion can be used for gadolinia doped fuel.

6. CONCLUSIONS

- An ENIGMA based analysis of an enlarged experimental PCI ramp database including additional data from Siemens rods has shown that there is a threshold peak clad stress to failure which increases with fast neutron dose and burnup.
- The conservative assumption that the failure stress does not increase at high burnup has been used to derive PCI limits at high burnups using the ENIGMA methodology.
- PCI failure limits equivalent to 95/95 confidence limits have been derived for burnups up to 60 GW·d/t U.
- Experimental ramp data on gadolinia-doped fuel rods do not indicate any increased susceptibility to PCI failure implying that the UO_2 criterion can be used for gadolinia doped fuel.

REFERENCES

[1] CHESTNUTT, M.M., Development of a Pellet-clad Interaction Failure Criterion for PWR fuel of the Standard Westinghouse Design for Use in safety Analysis. SXB-IP-096146, Feb 1992.

[2] Private communication from Siemens.

[3] WESLEY, D.A., MORI, K., INOUE, S., Mark-BEB Ramp Testing Program. International Topical Meeting on LWR Fuel Performance, West Palm Beach, Florida, USA, April 1994.

[4] GATES, G.A., TEMPEST, P.A., WHITE, R.J., The ENIGMA 5.9 Code Documentation, EPD/GEN/REP/0152/96, August 1996.

[5] BROHAN, P., The ENIGMA Fuel Performance Code Description: Version 5.10 EPD/GEN/REP/0304/98, March 1998.

[6] WHITE, R.J., HUTT, P.K., KILLEEN, J.C., Extension of the Empirical PWR PCI Failure Criterion to Higher Burnups, EPD/SXB/REP/0087/96.

[7] VIDEN, K., LUNDE, L., BOTROS, S.W.S., Influence of Iodine Content on Stress Corrosion Crack Growth Rate of Zircaloy. Paper presented at Enlarged Halden Programme Group Meeting, Loen, Norway, May 1993.

[8] SAH, D.N., VISWANADHAM, C.S., SAHOO, K.C., PURUSHOTHAM, D.S., RAMAKUMAR, M.S., Computer Code 'PROFESS' and its Application to IAEA CRP on FUMEX. Paper presented at the IAEA FUMEX Project, Bombay, India, April 1996.
[9] UNE, K., NOGITA, K., KASHIBE, S., TOYONAGA, T., AMAYA, M., Effects of Irradiation Microstructural Evolution on High Burnup Fuel Behaviour, International Topical Meeting on Light Water Reactor Fuel Performance, Portland, Oregon 1997.
[10] GOMME, R.A., The Rim Effect in High Burnup Uranium Dioxide, AEA Report AEAT 0201 for HSE/IMC, March 1996.
[11] The Studsvik OVERRAMP Project, Final Report, STOR-37, May 1981.
[12] The Studsvik INTERRAMP Project, Final Report, STIR-53, August 1.
[13] The Studsvik SUPERRAMP Project, Final Report, STSR-32, December 1984.
[14] The Studsvik TRANSRAMP-II Project, Final Report, STTRII-14, March 1987.
[15] The Studsvik TRANSRAMP-IV Project, Final Report, STTRIV-25, November 1994.
[16] BROHAN, P., BECK, W., SCHUH, K., Validation of ENIGMA 5.10, EPD/SXB/REP/0275/98.
[17] MURFIN, RIPPON AND TURNBULL, SXB-IP-096393.
BROHAN, P., Validation of ENIGMA 5.10 against data from the GAIN Program, EPD/SXB/REP/0301/98.

POWER RAMP PERFORMANCE OF SOME 15 × 15 PWR TEST FUEL RODS TESTED IN THE STUDSVIK SUPER-RAMP AND SUPER-RAMP EXTENSION PROJECTS

S. DJURLE
Studsvik Nuclear AB,
Nyköping, Sweden

Abstract

This paper presents results obtained from the STUDSVIK SUPER-RAMP (SR) and SUPER-RAMP EXTENSION (SRX) projects. As parts of these projects test fuel rods of the same PWR type were base irradiated in the Obrigheim power reactor and power ramp tested in the STUDSVIK R2 reactor. Some of the rods were ramped using an inlet coolant water temperature 50°C below the normal one. As fabricated data on the test fuel rods are presented as well as data on the base irradiation, interim examination, conditioning irradiation, power ramp irradiation and results of the post irradiation examination. The data on the change of diameter at ridges due to power ramping have shown that a lower clad temperature during ramping leads to smaller deformations. Most likely this may be explained as due to a smaller creep rate in the cladding at the lower temperature, resulting in a more severe stress situation. The combination of low cladding temperature, high ramp terminal level and the presence of a stress corrosion agent may have caused the failure of one of the test rods.

1. INTRODUCTION

This paper presents results obtained from the STUDSVIK SUPER-RAMP (SR) and SUPER-RAMP EXTENSION (SRX) projects. As parts of these projects test fuel rods of the same PWR type were base irradiated in the Obrigheim power reactor and power ramp tested in the STUDSVIK R2 reactor. Some of the rods were ramped using an inlet coolant water temperature 50°C below the normal one.

A general overview of the SR project has been given in [1]. The main observations were highlighted but no analyses of the data were given - in accordance with the project agreement.

The SRX project has not been the subject of any public report and therefore a summary of scope and objectives are given. The project was a continuation of the SR project and comprised three parts with different objectives.

The first part consisted of a complementary post-irradiation examination (PIE) of six PWR and four BWR type test fuel rods, all being part of the SR project, and had the objective to identify possible characteristic differences, which could explain the different pellet clad interaction (PCI) failure propensities experienced.

The second part consisted of power ramp testing four PWR type test fuel rods in the R2 reactor, after base irradiation in the Obrigheim power reactor to a burnup in the range of 31 to 36 MWd/kgU. The objective of this program was to study the influence of a reduced clad temperature on the rod behaviour during fast, single step, power ramping.

The third part consisted of power ramping eight BWR type test fuel rods in the R2 reactor, after base irradiation in the Oskarshamn 2 power reactor. The objective of this program was to study the effect of rod pre-pressurization on the critical safe ramp rate.

2. TEST FUEL RODS

Fuel rod segments of the same design (standard ”A”) were delivered by KWU (now Siemens) to the SR project (rod groups PK1 and PK2) and to the SRX projekt (rod group PK1X). All the segments (test fuel rods) had been irradiated in the nuclear power plant Obrigheim prior to the transport to Studsvik.

The data of the five test fuel rods of each group are given in Table I. It is seen that the main difference between the groups is the size of the as-fabricated gap between fuel and clad.

TABLE I. TEST FUEL ROD DATA

Rod group designation			PK1	PK1X	PK2
Rod Nos.		Accuracy	D452-D456	D396-D399,D414	D168-D172
Overall rod length	mm	± 0.1	387.9-388.1	387.9	390.1-390.3
UO_2 pellet column length	mm	± 0.1	309.8-311.5	311.1-313.6	317.2-319.0
Total stack length[1)]	mm	± 0.1	325.4-325.6	325.6	327.0
Pellet-clad gap[2)]	mm	± 0.015	0.191-0.200	0.185-0.191	0.145
UO_2 fuel weight	g	± 0.5	205-206	206-209	209-210
Fission gas plenum length[3)]	mm	± 0.1	32.0-32.4	32.0-32.3	32.5-33.0
He fill pressure	bar	± 1.0	22.5	22.5	22.5
Rod internal atmosphere	% He		≥ 99.8	≥ 99.8	≥ 99.8
Rod moisture content	ppm		≤ 5	≤ 5	≤ 5

1) Including Al_2O_3 spacer pellets
2) Average diametrical
3) Evaluated from X-ray image of plenum.

TABLE II. FUEL PELLET DATA

Rod group designation			PK1,PK1X	PK2
UO_2 powder[1)]			AUC	AUC
U-235 enrichment of Uranium		%	3.2	3.21
Pellet diameter[2)]		mm	9.110 ± 0.006	9.138 ± 0.003
Pellet length		mm	11.35 ± 0.60	11.34 ± 0.40
Density of green pellet compact		g/cm^3	5.5-5.8	5.60
Sintering temperature/time		°C/h	1710/2.4	1700/2.2
Final pellet density		g/cm^3	10.360 ± 0.012	10.340 ± 0.019
Density increase[3)]		%	0.4	0.7
Average grain size[4)]		µm	6.0	5.5
O/U ratio			2.00 ± 0.01	2.00 ± 0.01
Portion of open porosity:				
of overall porosity		%	50 ± 5	55.8 ± 3.1
of pellet volume		%	2.7 ± 0.3	3.16 ± 0.27
Residual gas content:				
altogether	mm^3	STP/g	9.2	7.5
Hydrogen portion	mm^3	STP/g	3.3	4.3
Moisture (H_2O equivalent)		ppm	2.7	3.5

1) AUC = Ammonium-Uranyl-Carbonate
2) The pellet diameter of rod PK1X/S (D396) was 9.150 ± 0.005 mm
3) After standard thermal densification test at 1700°C for 2.2 hours
4) A smaller grain size, in the range of 3.6 to 5.4 µm, was measured in the metallographic examinations, see Table XI.

The fuel pellets had the same design. The cylindrical surface was ground and the ends of the enriched fuel pellets were dished with a total combined dish volume of 16 mm^3. Two batches of fuel have been used for the fuel pellets, one for the PK1 and PK1X pellets and another for the PK2 fuel pellets. Data of the fuel pellets are given in Table II. It is seen that there is a difference in the densification test between the two batches and also a difference in the average grain size.

The Zircaloy 4 cladding of the test fuel rods was manufactured from very similar tube lots for each of the PK1, PK1X and PK2 groups. The final heat treatment was for all a temperature of 530°C during 2.5 hours. The variation of the mechanical properties and grain size is shown in Table III. and the cladding tube dimensions for each of the test fuel rods are given in Table IV.

It may be noted that the cladding inside of the fuel rod PK1X/S was finally electropolished in addition to the normal surface treatment of the cladding.

TABLE III. CLADDING TUBE DATA

Rod group designation		PK1	PK1X	PK2
Ultimate tensile strength				
at room temperature	N/mm^2	720	704	708
at 400°C	N/mm^2	425	410	402
Yield strength				
at room temperature	N/mm^2	548	542	592
at 400°C	N/mm^2	317	317	318
Elongation[1)]				
at room temperature	%	17.6	17.7	21.3
at 400°C	%	20.3	17.3	20.0
Creep strain (400°C, 150 N/mm^2 (σ_{hoop}), 240h)	%	0.7	0.7	0.55
Uniform burst strain (400 ± 3°C, 50 bar/min)[2)]	%	4.1	3.7	4.1
Grain size (No. of ASTM E 112) after heat treatment 610°C, 2.0 h	µm	10.5	10.0	9.5

[1)] Measuring length 50 mm
[2)] 20 mm away from rupture end.

3. BASE IRRADIATION OF TEST FUEL RODS

The test fuel rods were base irradiated in the commercial pressurized water reactor Obrigheim (KWO) either for three operation cycles (rod groups PK1 and PK1X) or for four cycles (rod group PK2). The reactor was operated at an average system pressure of 145 bar. The temperature of the coolant was 283°C at the inlet and 312°C at the outlet.

The test fuel rods were irradiated as the five middle members of seven rodlets, one on top of the other, which together formed a stringer rod. In evaluating the irradiation history it was found that the stringer rod containing the PK1X group of rods was irradiated upside down during the second and third irradiation cycles.

TABLE IV. CLADDING TUBE DIMENSIONS

Rod designation	Rod No.	Outer diameter average[1)] mm	Inner diameter average[1)] mm	Ovality maximum [2)] mm
PK1/4	D452	10.762	9.309	0.012
PK1/3	D453	10.762	9.308	0.010
PK1/2	D454	10.762	9.308	0.012
PK1/1	D455	10.763	9.310	0.010
PK1/S	D456	10.766	9.301	0.008
PK1/E1[3)]	D457	10.763	9.307	
PK1X/4	D414	10.776	9.295	0.011
PK1X/3	D399	10.773	9.298	0.013
PK1X/2	D398	10.777	9.301	0.013
PK1X/1	D397	10.775	9.298	0.012
PK1X/S	D396	10.775	9.337	0.011
PK2/4	D168	10.751	9.283	0.008
PK2/3	D169	10.752	9.283	0.005
PK2/2	D170	10.752	9.283	0.006
PK2/1	D171	10.753	9.283	0.006
PK2/S	D172	10.754	9.283	0.005
PK2/E1[3)]	D174	10.752	9.283	

1) Circumferential average, accuracy ± 0.003 mm
2) Accuracy ± 0.002 mm
3) E1 = lower end segment of the stringer rod.

The evaluation of the power and burnup history of the test fuel rods was based on two-dimensional neutron-physics calculations and aeroball measurements of the axial neutron flux profile. The axial and time average values of the linear heat generation rates (LHGR), as well as the effective full power days (EFPD), have been reported for each month of irradiation for each of the test fuel rods. The cycle average and the maximum values of the axial average LHGR, and the axial average burnup at the end of each cycle for all the test fuel rods are put together in Table V. The individual rod linear heat rating versus burnup is depicted in Figures 1-3 (periods of zero power removed).

The average fast neutron fluence after irradiation in KWO was the following:
5,8 x 10^{21} n/cm^2 for PK1 rods
5,3 x 10^{21} n/cm^2 for PK1X rods
8,1 x 10^{21} n/cm^2 for PK2 rods.

4. POWER IRRADIATION OF TEST FUEL RODS

The power ramping of the test fuel rods was performed in the R2 reactor in the pressurized water loop No. 1 with forced-circulation cooling at a system pressure of 146 bar. The temperature of the inlet water was normally 314-315°C, however four of the ramp tests were performed at an inlet temperature 50°C lower.

The facilities used for the power ramping included the loop system, a sample exchange device, a He-3-absorber system for power control, and instruments for power measurements, fission product monitoring, and rod elongation measurements. The R2 ramp facilities and test techniques have been described in detail elsewhere [2].

TABLE V. BASE IRRADIATION DATA OF TEST FUEL RODS

Rod designation	Rod No.	Cycle 1				Cycle 2			
		Segment axial position[1]	Rod average linear heat rating Time average w/cm	Maximum w/cm	Rod average burnup at end of cycle MWd/kgU	Segment axial position[1]	Rod average linear heat rating Time average w/cm	Maximum w/cm	Rod average burnup at end of cycle MWd/kgU
PK1/4	D452	VI	237	343	11.8	VI	207	211	23.2
PK1/3	D453	V	254	268	12.6	V	217	227	24.6
PK1/2	D454	IV	258	270	12.8	IV	216	225	24.7
PK1/1	D455	III	255	261	12.6	III	213	219	24.4
PK1/S	D456	II	241	248	11.9	II	210	219	23.6
PK1X/4	D414	VI	210	216	10.4	II	273	282	23.0
PK1X/3	D399	V	226	233	11.2	III	275	296	23.9
PK1X/2	D398	IV	228	235	11.3	IV	264	298	23.5
PK1X/1	D397	III	228	235	11.3	V	253	274	23.0
PK1X/S	D396	II	213	233	10.8	VI	208	250	20.4
PK2/4	D168	VI	183	188	9.6	VI	229	234	20.9
PK2/3	D169	V	207	216	10.9	V	245	259	23.0
PK2/2	D170	IV	209	219	11.0	IV	249	262	23.3
PK2/1	D171	III	209	219	11.0	III	248	255	23.3
PK2/S	D172	II	194	199	10.2	II	239	246	22.0

		Cycle 3				Cycle 4			
PK1/4	D452	VI	193	205	33.1				
PK1/3	D453	V	207	224	35.2				
PK1/2	D454	IV	211	219	35.6				
PK1/1	D455	III	214	218	35.4				
PK1/S	D456	II	209	216	34.4				
PK1X/4	D414	II	214	222	34.3				
PK1X/3	D399	III	221	225	35.6				
PK1X/2	D398	IV	213	225	34.8				
PK1X/1	D397	V	207	223	33.0				
PK1X/S	D396	VI	191	201	30.5				
PK2/4	D168	VI	208	221	32.5	VI	173	184	41.4
PK2/3	D169	V	218	237	35.1	V	185	201	44.6
PK2/2	D170	IV	218	237	35.4	IV	189	196	45.1
PK2/1	D171	III	216	230	35.3	III	192	195	45.2
PK2/S	D172	II	214	218	33.9	II	188	195	43.4

1) VII = Top segment, I = Bottom segment

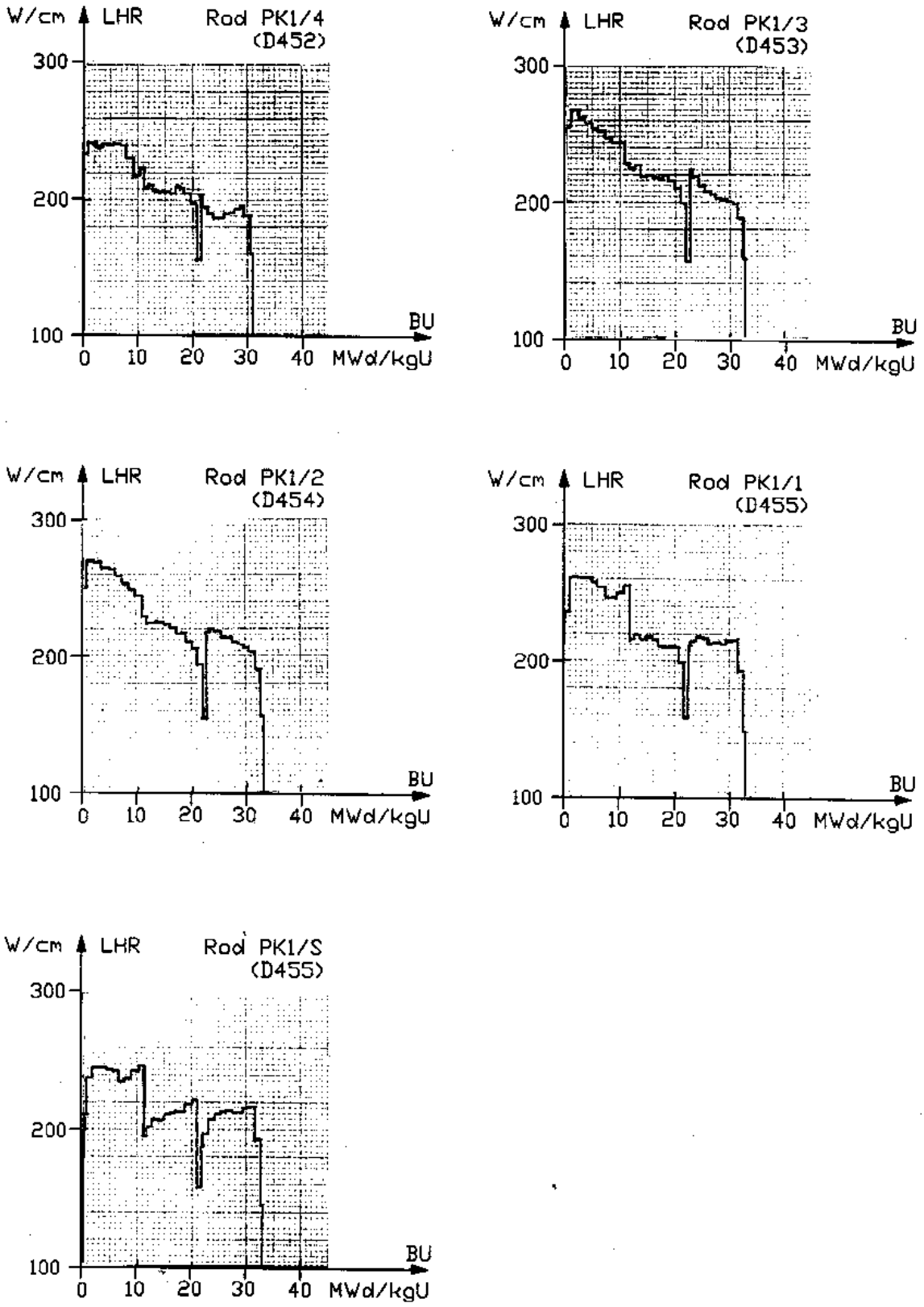

FIG. 1. Base irradiation history of PK1 test fuel rods. Linear heat rating versus burnup.

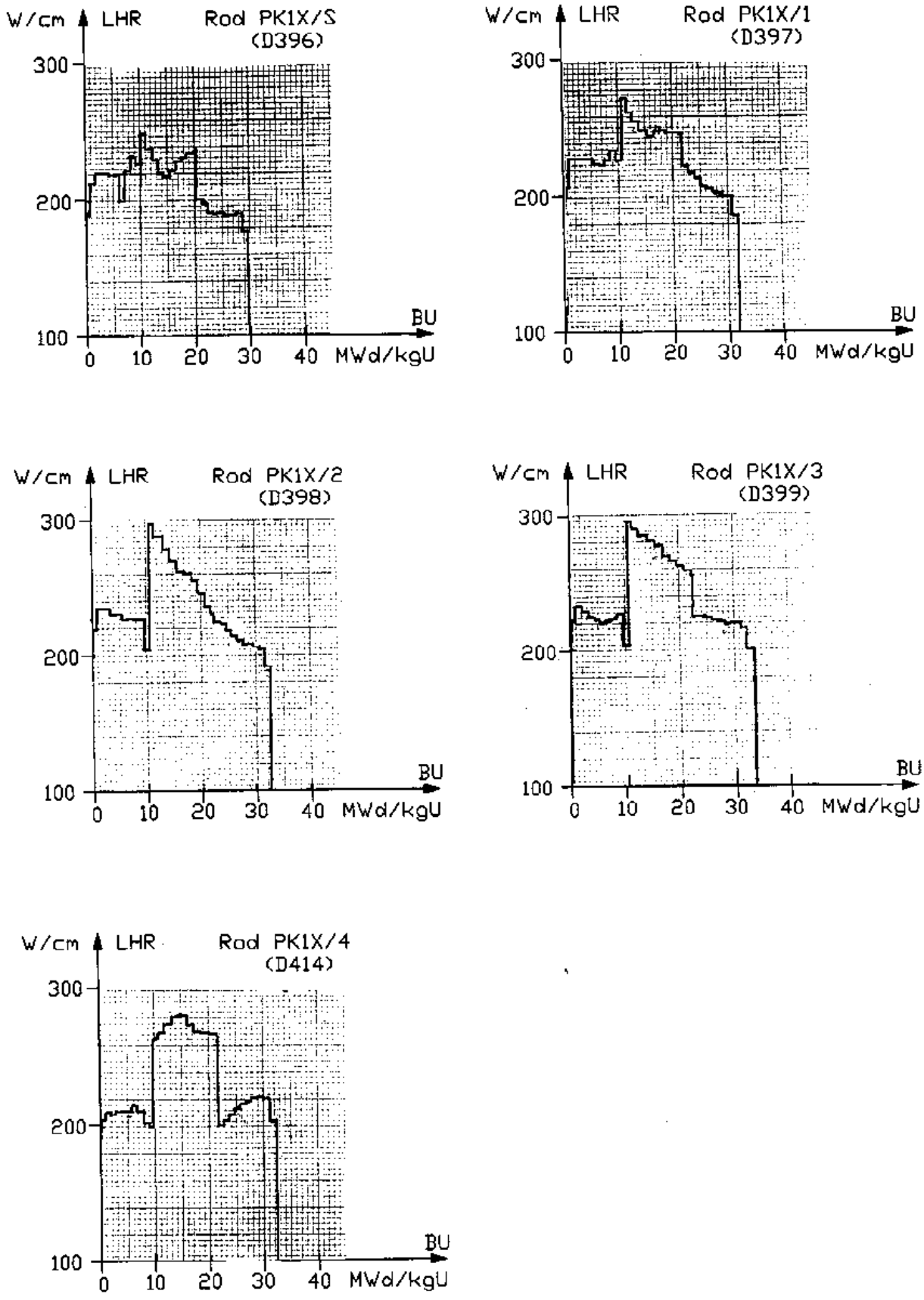

FIG. 2. Base irradiation history of PK1X test fuel rods. Linear heat rating versus burnup.

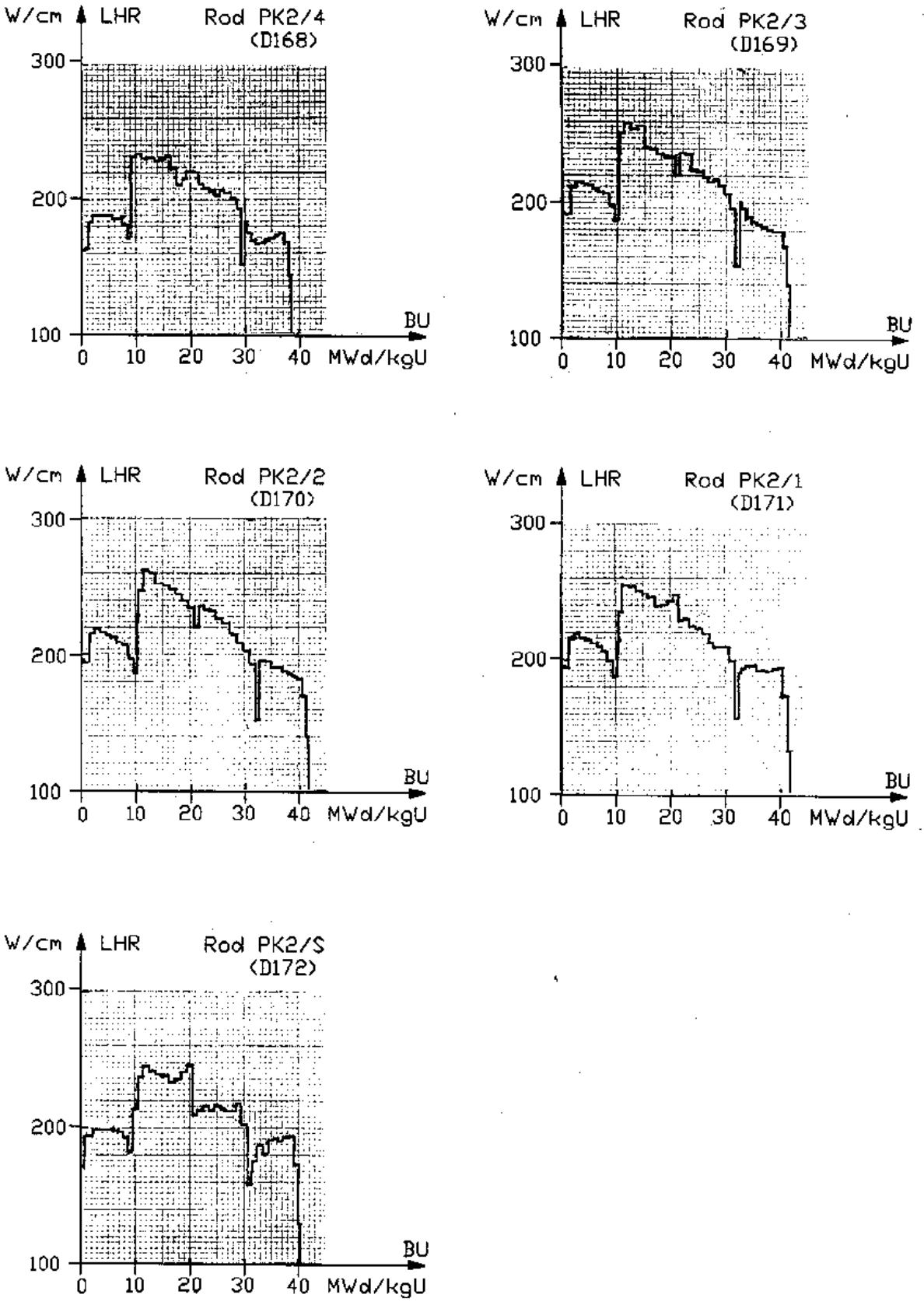

FIG. 3. Base irradiation history of PK2 test fuel rods. Linear heat rating versus burnup.

The power ramp tests were performed as fast rate, single step ramps according to a general scheme, characterized by three consecutive phases as follows:

Conditioning, with a moderate power ramp rate up to a steady power level, normally 250 W/cm, where the power was held for 24 hours.
Ramping, with a rapid power increase to a predetermined ramp terminal level. The ramp rate was normally about 100 W/cm,min.
Holding, with power being held constant at the ramp terminal level for normally 12 hours or until the occurrence of an increase of fission product activity in the coolant.

In order to be able to separate effects of the fuel from effects of the cladding, the data for temperature of the coolant, conditioning power level, and power ramp step were chosen to yield about the same fuel center temperature level for the rods PK1X/2 and PK1X/3.

The power ramp irradiation data are summarized in Table VI.

TABLE VI. CONDITIONING AND POWER RAMP IRRADIATION DATA OF TEST FUEL RODS

Rod designation	Rod No.	Inlet temperature of cooling water °C	Conditioning		Ramping					
			Power level W/cm	Hold time h	Reactor control rod level cm	Power ramp rate W/cm, min	Ramp terminal level W/cm	Hold time min	Failure (F) or no failure (NF)	Rod elongation measurements
PK1/4	D452	314	250	24	55	95	475	720	NF	X
PK1/3	D453	314	250	24	54	85	475	720	NF	X
PK1/2	D454	314	250	24	52	80	440	720	NF	X
PK1/1	D455	314	250	24	50	90	415	720	NF	X
PK1/S	D456	314	250	24	52	60	420	720	NF	X
PK1X/3	D399	265	250	24	54	100	435	720	NF	X
PK1X/2	D398	315	225	24	57	100	420	720	NF	X
PK1X/1	D397	265	250	24	61	100	410	720	NF	X
PK1X/S	D396	265	250	24[1)]	51	100	460	15.2	F[2)]	X
PK2/4	D168	314	250	24	48	85	440	1[3)]	NF	
PK2/3	D169	314	250	24	53	85	490	720	NF	X
PK2/2	D170	314	250	24	50	95	460	720	NF	X
PK2/1	D171	314	250	24	59	85	410	720	NF	X
PK2/S	D172	264	250	24	56	85	440	720	NF[4)]	

1) Due to a reactor scram the holding time was interrupted for 3 hours.
2) The time to a sudden rod shortening was 9.3 min. The time to fission product activity increase was 11.3 min.
3) Intentionally interrupted
4) A small incipient (non-penetrating) crack was observed only in the cldding of rod PK2/S (D172) at post irradiation examinations of the PK1 and PK2 rods.

5. POST IRRADIATION EXAMINATION OF TEST FUEL RODS

Non-destructive examinations after the base irradiation respectively after the power ramp testing were performed either at the hot cells at Karlstein or in the R2 pool-side facility at Studsvik. The destructive examinations were performed in the hot cells at Karlstein. An overview of the examinations is given in Table VII. The main results of the examinations are given in Tables VIII through XI.

TABLE VII. OVERVIEW OF POST-IRRADIATION EXAMINATION OF TEST FUEL RODS

Project Rod No.	Supplier Rod No.	Examination after base irradiation				Examination after ramp irradiation									
		VI	ECT	PROF	GSCAN	NRAD	ECT	PROF	FGA	GAP	MET	CII	SEMC	SEMF	BU
PK1/4	D452	X	X			X	X		X						
PK1/3	D453	X	X	X		X	X	X	X						
PK1/2	D454	X	X			X	X		X		X	X	X		
PK1/1	D455	X	X	X		X	X	X	X						
PK1/S	D456	X	X			X	X								
PK1/E1[1)]	D457									X	X	X	X	X	
PK1X/4[1)]	D414		X	X					X						
PK1X/3	D399		X	X		X	X	X	X	X	X	X			
PK1X/2	D398		X	X		X	X	X	X	X	X	X			
PK1X/1	D397		X	X			X	X							
PK1X/S	D396		X	X		X	X	X		X	X				
PK2/4	D168	X	X		X				X	X	X	X	X		
PK2/3	D169	X	X	X	X	X	X	X	X						
PK2/2	D170	X	X		X	X	X		X		X	X	X		X
PK2/1	D171	X	X	X	X	X	X	X	X						
PK2/S	D172	X	X	X	X	X	X	X	X	X	X	X	X		
PK2/E1[1)]	D174				X					X	X	X	X	X	X

VI = Visual inspection
ECT = Eddy current testing
PROF = Profilometry
GSCAN = Gamma scanning (axial)
NRAD = Neutron radiography
FGA = Fission gas analysis
GAP = Gap measurement by compression testing for PK1 and PK2 rods, by metallography for PK1X rods
MET = Metallography
CII = Clad inside inspection
SEMC = Scanning electron microscopy of clad
SEMF = Scanning electron microscopy of fuel replica
BU = Burnup analysis

[1)] Not ramped.

TABLE VIII. ORDER OF INCREASING FUEL DISH FILLING FOR TEST FUEL RODS ACCORDING TO NEUTRON RADIOGRAPHY

$$Rod \left\{\frac{PK1X/2}{PK1X/3}\right\} < PK2/S < \left\{\frac{PK1/1}{PK1/S}\right\} < \left\{\frac{PK1/2}{PK1/4}\right\} < PK1/3 < PK2/1 < PK2/2 < PK2/3$$

Note that all the rods above were ramped and held at the ramp terminal level for the same time (720 min).

TABLE IX. SUMMARY OF DIAMETRAL MEASUREMENTS OF TEST FUEL RODS

Project Rod No.	Supplier Nod No.	Pre-ramp Mean ridge-height[1] µm	Post-ramp Mean ridge-height[1] µm	Mean diameter change between ridges[2] µm	at ridges[3] µm
PK1/3		4	34	36	68
PK1/1		3	25	26	28
PK1X/3		4	20	< 0	13
PK1X/2		5	25	7	30
PK1X/1		3	12	2	10
PK1X/S		4	21	< 0	14
PK2/3		6	37	107	138
PK2/1		10	41	39	71
PK2/S		10	33	11	36

1) Mean of the eight ridges around the position of axial power maximum at ramping
2) Mean of the nine positions covering the eight ridges defined in[1]
3) Mean of the eight positions defined in[1].

TABLE X. SUMMARY OF TEST FUEL ROD DATA ON FISSION GAS ANALYSIS AND ON GAP SIZE AFTER IRRADIATION.

Project Rod No.	Supplier Rod No.	Measured Gas Quantities[1] Total ml	He ml	Kr ml	Xe ml	Release of Kr+Xe %	Radial gap[2] to relocated pellet µm	compressed pellet µm	Radial gap based on metallography µm
PK1/4	D452	92.0	68.3	2.2	21.3	13.0			
PK1/3	D453	109.9	67.1	3.6	38.8	22.1			
PK1/2	D454	91.8	65.3	3.1	23.3	13.6			22-40
PK1/1	D455	85.1	68.6	1.9	14.5	8.5			
PK1/E1[3]	D457						30	59	25-44
PK1X/4[3]	D414	69.2	67.3	0.2	1.7	1.0			
PK1X/3	D399	83.4	69.0	1.5	12.9	7.4			27-52
PK1X/2	D398	82.4	68.6	1.4	12.3	7.2			38-44
PK1X/S	D396								7-14
PK2/4	D168	99.1	77.1	2.5	19.5	9.5	6	22	27
PK2/3	D169	169.3	57.6	10.4	101.3	44.9			
PK2/2	D170	150.5	69.7	8.2	72.6	32.1			22-30
PK2/1	D171	136.7	66.1	7.2	63.4	28.0			
PK2/S	D172	68.9	43.8	2.5	22.6	10.4	9	18	25
PK2/E1[3]	D174						24	35	27

1) At 760 torr and 0°C
2) Measured at about the position of rod power maximum
3) Not ramped.

TABLE XI. SUMMARY OF METALLOGRAPHIC EXAMINATIONS OF TEST FUEL RODS

Project Rod No.	Supplier Rod No.	Section L/T [1]	Distance from rod bottom mm	Local RTL [2] W/cm	Hold time at RTL min	F NF [3]	Ratio R_E/R_F [4]	UO_2 grain size Pellet periphery μm	Pellet center μm
PK1/2	D454	L	197	440	720	NF	0.76	4.8 [7]	36
PK1/E1	D457	T	306	222	[5]	NF	0.31 [6]	4.4	5.9
PK1X/3	D399	T	231	430	720	NF	0.71	5	11
PK1X/2	D398	T	198.5	419	720	NF	0.72	4	10
PK1X/S	D396	T	127	445	15.2	F	0.68	5	7
PK2/4	D168	L	196	438	1	NF	0.66 [6]	3.8	8.3
PK2/2	D170	L	252	435	720	NF	0.785	4.4	12.8
PK2/S	D172	L	181	438	720	NF	0.69	5.4	11.8
PK2/E1	D174	T	306	226	[5]	NF	0.33 [6]	3.6	6.2

1) L = Longitudinal Section; T = Transversal section.
2) Local ramp terminal level or in case of PK1/E1 and PK2/E1 local maximum linear heat rating during the base irradiation.
3) F = failure; NF = no failure.
4) R_E = radius of increased etching susceptibility, and of fission gas bubbles on grain boundaries becoming visible.
R_F = radius of fuel pellet
5) Not ramped
6) As reported by KWU
7) Columnar grains (≥ 50 μm) had been developed at the center of the fuel pellet to a radius of 0.8 mm at the positions about ¼ and ¾ of the pellet length.

Neutron radiography confirmed that the rods were sound except rod PK1X/S (D396) for which failure was confirmed by the presence of hydride.

Inter-pellet dishes were essentially closed over a middle zone and partially filled at the ends of the fuel stack. The rods have been compared as to the degree of dish filling and put in order of increasing dish filling in Table VIII. It has to be remarked that for this comparison due regard has to be taken to the variation of the axial power profile with the R2 control rod position, as illustrated in Figure 4. The order of increasing dish filling may be considered as a rough indication of order of increasing fuel temperature.

Diametral measurements were performed on some of the test fuel rods after the base irradiation as well as after the ramp irradiation. The results are summarized in Table IX.

Analysis of fission gas content was performed on twelve test fuel rods. The quantities of He, Kr and Xe and the calculated release fraction of Kr + Xe are summarized in Table X.

Radial gaps were measured on some of the rods, see Table X.

Metallographic examinations were performed on longitudinal or transverse sections of two rods after base irradiation and seven rods after power ramping. A summary of data is given in Table XI. Local ramp terminal level has been calculated for the studied sections by using data about control rod position, and the maximum ramp terminal level, see Table VI, and the axial power distribution for the specific control rod level, which is illustrated in Figure 4.

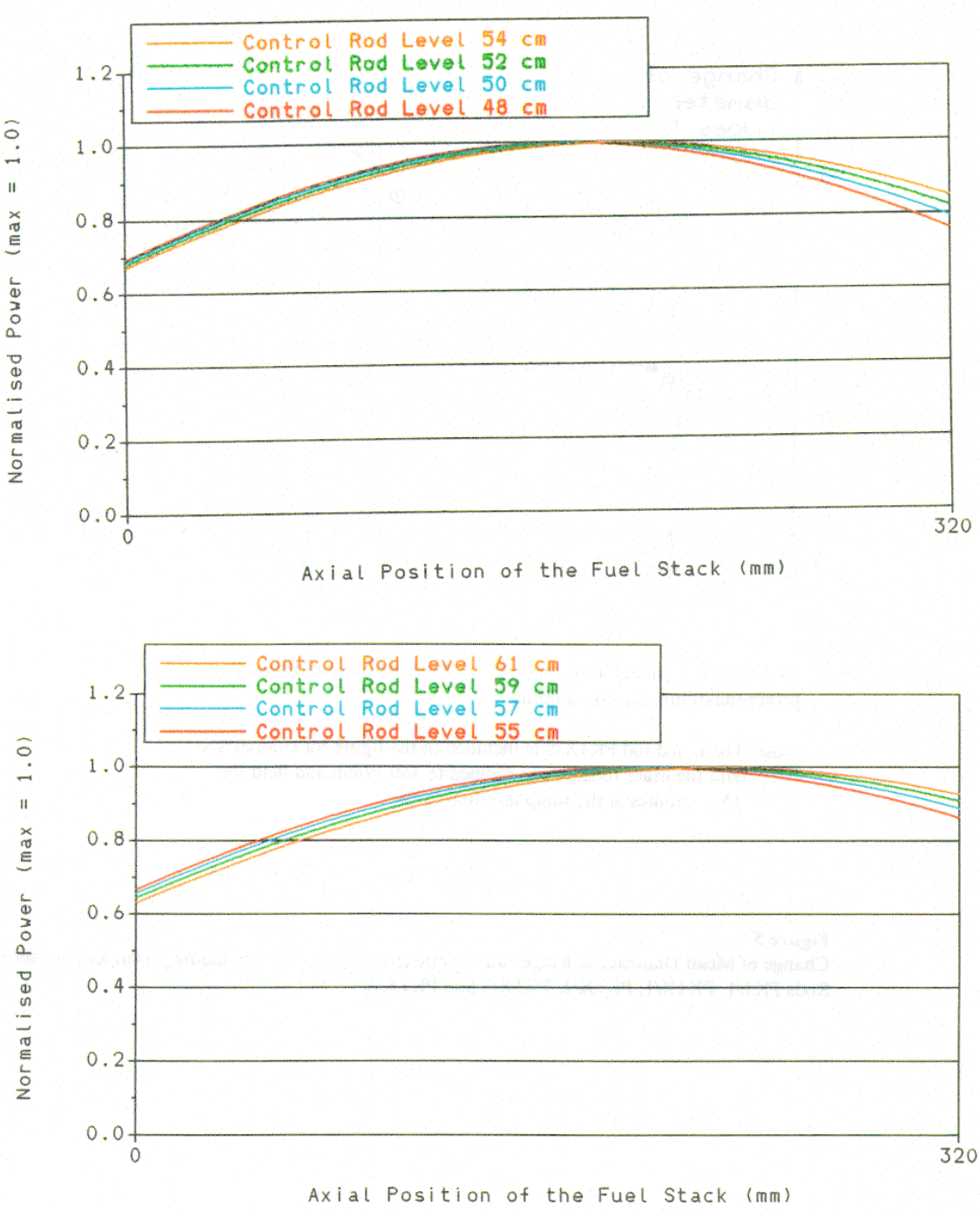

FIG. 4. Axial power distribution for various reactor control rod levels

Cladding inside studies were performed on the non-ramped rods PK1/E1 and PK2/E1 and on the ramped rods PK1/2, PK1X/3, PK1X/2, PK1X/S, PK2/4, PK2/2 and PK2/S to various extent. Oxide thickness, interaction layers and fuel particles bonded to the cladding were studied in the metallographic examinations. The clad inside was optically inspected after splitting the cladding into halves, and part of this cladding was examined by SEM.

In summary: The non-ramped rod PK1/E1 showed a coherent thin oxide layer at the inside. The oxide layer on rod PK2/E1 was very thin. There were no pellet-clad interaction layers on these two rods. Particles less than 10 μm were spread over the internal surface. These particles contained, besides uranium and zirconium, also the fission products cesium and technetium.

For the ramped PK1 and PK2 rods thickness of the oxide layer on the inner surface and the extent of surface coverage were as follows:

PK1/2	0.5-12 μm	100 %
PK2/2	2-12 μm	45 %
PK2/4	1-8 μm	22 %
PK2/S	2-10 μm	40 %

The clad inside of these rods was covered with interaction layers containing uranium and fission products, heavily on the rods PK1/2 and PK2/2, less heavily on PK2/S, and on PK2/4 only at the pellet interface positions.

The visual examination of the inside of cladding halves of the rods PK1X/3 and PK1X/2 revealed that the cladding sections were very similar and pellet-pellet interfaces and pellet cracks showed up clearly. This agrees with the metallography of these rods and of rod PK1X/S, which gave the following values for the thickness of the inside oxide layer: PK1X/3 0.5-8 μm (generally 0.5 μm), PK1X/2 0.5-4 μm (generally < 0.5 μm) and PK1X/S 0-2 μm. These three rods had pellet-clad interaction layers and bonded fuel only on local areas.

6. DISCUSSION

6.1. Fission gas release

Comparison of rods in order of increasing dish filling given in Table VIII may be compared with the order of rods for increasing fission gas release. The order is the same except for rod PK2/S and PK1/1. The cause of this is not known, however, the quantity of He measured after irradiation is remarkably low compared to the other rods (see Table X).

6.2. Diametrical data

Some results of the diametral measurements have been presented in Table IX.

The data on the diametral height after the base irradiation are commented on as follows: The larger ridges for the PK2 rods compared to the other rods may be due to the smaller as-fabricated gap and the higher burnup.

The influence of cladding temperature on the diametral changes due to power ramping is studied by plotting these data, see Figure 5, using test fuel rods with low center temperature (low ramp terminal level, low fission gas release and small dish filling) and with fuel from the same batch (rod groups PK1 and PK1X). That the cladding changes are smaller at the lower cladding temperature may be explained as due to a smaller creep rate in the cladding at the lower temperature. This may result in a more severe stress situation, increasing the failure probability.

6.3. Failure of rod PK1X/S

Rod PK1X/S was the only rod that experienced failure due to the power ramping. The cladding temperature was low, and the ramp terminal level was the highest one for the PK1X group of rods. The failure of rod PK1X/S may be due to the combination of these data and the presence of a stress corrosion agent.

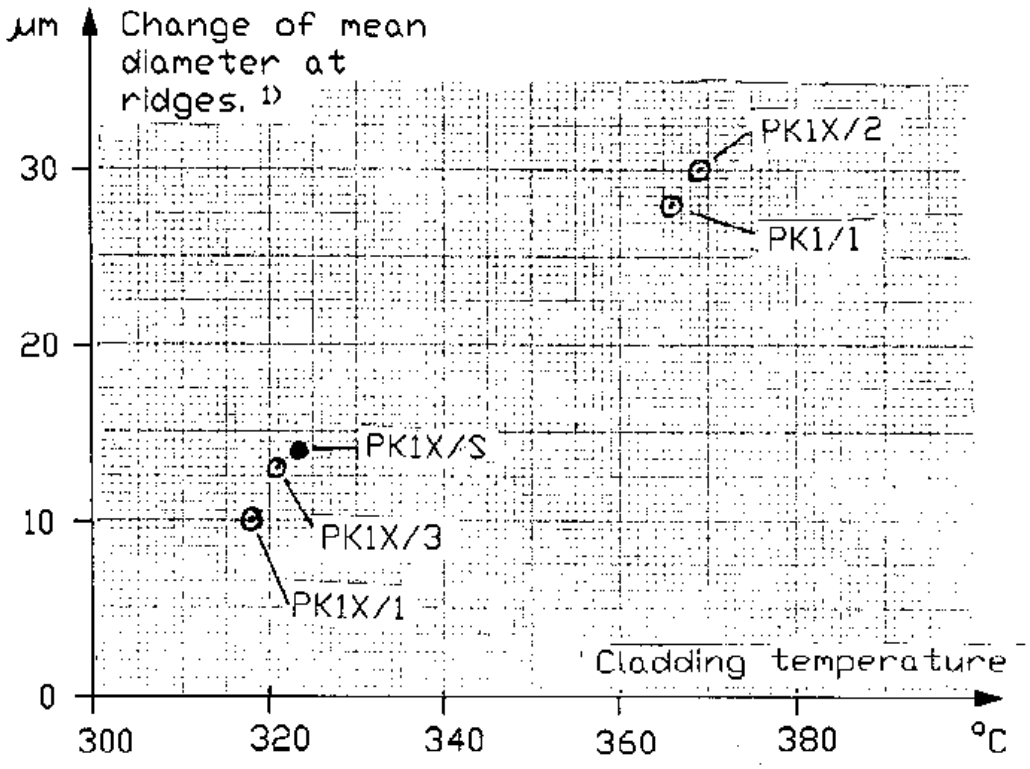

1) Mean of the diameter at the eight ridge positions around the axial power maximum during ramping.

Note: The failed rod PK1X/S is included in the figure for comparison with the other rods. It was ramped to 460 W/cm and held for 15.2 minutes at the ramp terminal level

FIG. 5. Change of mean diameter at ridges due to power ramping versus cladding temperature for the Rods PK1/1, PK1X/1, PK1X/2, PK1X/3 and PK1X/S.

REFERENCES

[1] MOGARD, H., HECKERMANN, H., The International SUPER-RAMP Project at Studsvik. ANS Topical Meeting on LWR Fuel Performance, April 21-24 1985, Orlando, Florida, USA.

[2] RÖNNBERG, G., BERGENLID, U., TOMANI, H., Power Ramp Test Technique at Studsvik. Proceedings of the KTG/ENS/JRC Meeting on Ramping and Load Following Behaviour of Reactor Fuel. Petten, Netherlands, November 30-December 1, 1978.

A PCI FAILURE IN AN EXPERIMENTAL MOX FUEL ROD AND ITS SENSITIVITY ANALYSIS

A.C. MARINO
Grupo Diseño Avanzado y Evaluación Económica,
Centro Atómico Bariloche, Comisión Nacional de Energía Atómica,
Bariloche, Argentina

Abstract

Within our interest in studying MOX fuel performance, the irradiation of the first Argentine prototypes of PHWR MOX fuels began in 1986 with six rods fabricated at the α Facility (CNEA, Argentina). These experiences were made in the HFR-Petten reactor, Holland. The goal of this experience was to study the fuel behaviour with respect to PMCI-SCC. An experiment for extended burnup was performed with the last two MOX rods. During the experiment the final test ramp was interrupted due to a failure in the rod. The post-irradiation examinations indicated that PCI-SCC was a mechanism likely to produce the failure. At the Argentine Atomic Energy Commission (CNEA) the BACO code was developed for the simulation of a fuel rod thermo-mechanical behaviour under stationary and transient power situations. BACO include a probability analysis within their structure. In BACO the criterion for safe operation of the fuel is based on the maximum hoop stress being below a critical value at the cladding inner surface; this is related to susceptibility to stress corrosion cracking (SCC). The parameters of the MOX irradiation, the preparation of the experiments and post-irradiation analysis were sustained by the BACO code predictions. We present in this paper an overview of the different experiences performed with the MOX fuel rods and the main findings of the post-irradiation examinations. A BACO code description, a wide set of examples which sustain the BACO code validation, and a special calculation for BU15 experiment attained using the BACO code including a probabilistic analysis of the influence of rod parameters on performance are included.

1. INTRODUCTION

Within our interest in studying MOX fuel performance, the irradiation of the first Argentine prototypes of PHWR MOX fuels began in 1986 with six rods fabricated at the α Facility (CNEA, Argentina) [1]. These experiences were made in the HFR-Petten reactor, Holland. The goal of this experience was to study the fuel behaviour with respect to PMCI-SCC.

An experiment for extended burnup was performed with the last two MOX rods. During the experiment the final test ramp was interrupted due to a failure in the rod. The post-irradiation examinations indicated that PCI-SCC was a mechanism likely to produce the failure [2]. That analysis was predicted with the calculated stresses [3].

In a nuclear reactor, the materials at the fuel are at relatively large temperatures and suffer the effect of an aggressive chemical and radiation environment. Therefore, mechanical solicitation might sometimes be near the limits of materials endurance. Design, within engineering concepts, has to consider parts performance as well as their in-service mechanical coupling. This coupling requires computer codes for valid results to be obtained.

At the Argentine Atomic Energy Commission (CNEA) the BACO code was developed for the simulation of a fuel rod thermo-mechanical behaviour under stationary and transient power situations [4]. Our modelling approach is based on using simple models, which are however sustained on physically sound ideas. BACO include a probability analysis within their structure covering uncertainties in input, fabrication, parameters and models and, therefore, output ones may include statistical dispersion [5]. In BACO the criterion for safe operation of the fuel is based on the

maximum hoop stress being below a critical value at the cladding inner surface. This is related to susceptibility to stress corrosion cracking (SCC) [6].

The BACO code validation is sustained for a wide set of irradiation. We select some examples of BACO validity tests. The complete benchmarking is done with each new improvement included in the code. The selection made in this paper corresponds to exigent and very well known international blind tests and open literature.

The parameters of the MOX irradiation, the preparation of the experiments and post-irradiation analysis were sustained by the BACO code predictions [7].

This paper presents an overview of the different experiences performed with the MOX fuel rods and the main findings of the post-irradiation examinations. A BACO code description, and a special calculation for BU15 experiment attained using the BACO code including a probabilistic analysis of the influence of rod parameters on performance are included.

2. BACO CODE

2.1. BACO code description

The BACO code structure and models in its present versions are described by Marino et al., including steady state and transient thermal analysis. The number of instructions is at present (version 2.40) around one thousand FORTRAN 77 sentences. Data post-processing improves the code's performance and analysis of results.

On modelling the UO_2 pellet, elastic deformation, thermal expansion, creep, swelling, densification, restructuring, cracks and fission gas release are included. While for the Zry cladding, the code models elastic deformation, thermal expansion, anisotropic plastic deformation, and creep and growth under irradiation. The modular structure of the code easily allows the incorporation of different material properties. It can be used for any geometrical dimensions of cylindrical fuel rods with UO_2 pellets (either compact or hollow and with or without dishing) and Zry cladding.

Fuel rod power history and either cladding or coolant external temperatures are inputs to the program. Rod performance is numerically simulated using finite time steps. The code automatically selects time steps according to physical criteria. Temperature distribution in the pellet and cladding, main stresses at pellet and cladding, radial and axial crack pattern in the pellet, main strains and hot geometry of pellet and cladding, change in porosity, grain size and restructuring of the pellet, fission gas release to the free volume in the rod, trapped gas distribution in the fuel and in the UO_2 grain boundary, internal gas pressure and current composition of the internal gas, are calculated. The output contains the distribution along the rod axis of these variables.

2.2. Numerical treatment

We assume cylindrical symmetry for the fuel rod; our model is bidimensional and angular coordinates are not considered. However, angular dependent phenomena, as radial cracking, are simulated via some angular averaging method. For the numerical modelling the hypotheses of axial symmetry and modified plane strains (constant axial strain) are adopted. With respect to the axial dependence of the fuel rod behaviour, arising mainly from the axial dependence of power generation in the reactor, the fuel rod is divided in axial sections.

The mechanical and thermal treatment and the pellet, cladding and constitutive equations are very well described in Reference [4].

2.3. BACO code validity tests

2.3.1. Experimental irradiation at the NRX reactor

The work reported by Notley [9] was used for testing the BACO code and results were reported in References [4, 8]. In Notley's work six Zircaloy-sheathed UO_2 fuel elements were irradiated at power outputs between 760 and 600 W/cm to a burnup of about 5500 MWd/tonU. Then two of them and another two new rods were irradiated at lower powers for a further 1250-1700 MWd/tonU. The experiment was irradiated in the X-2 loop of NRX reactor. All elements were destructively examined and some of them were measured during the irradiation. The predicted and measured rod radius change $\Delta R/R$, fission gases released, columnar and equiaxed grains and central hole are provided by Notley [9] and calculated with BACO [4, 8].

We find that, although the predictions of $\Delta R/R$ and the gas released are approximately correct, the measured rod dimension changes are somewhat larger than predicted at low power and low burnup and are overpredicted by the code at high power and burnup. We discussed in reference [8] that this might be related to burnup and power ranges to which the code parameters have been fitted.

2.3.2. CANDU fuelograms

In CANDU reactors, fuel reshuffling is done under reactor operation. During reshuffling, the fuel undergoes a power ramp due to the power distribution along the fuel channel. For this reason, it is interesting to study the behaviour of a CANDU fuel under fast (10-20 min long) power ramps. The Linear Heat Generation Rate (LHGR) before the ramp, the burnup at which the ramps occurs, and the ramp height, cover a wide range. AECL has published bounds for safe operation, based on actual experience of power ramping due to fuel reshuffling in nuclear power stations. Usually [10, 11], the maximum power increase and maximum power such that fuel operation below those values present no failures, are given as a function of burnup.

The experimental bounds for power increase and maximum power corresponding to the Pickering Stations are plotted by Penn et al. [12]. Power histories simulating reshuffling were simulated with the BACO code. In the Code, the criterion for safe operation was based on the maximum hoop stress at the cladding inner surface. This is related to susceptibility to stress corrosion cracking. BACO results are in good agreement with AECL data; even the mispredictions can be explained on a physical basis [7]. A CANDU fuel rod simulation including statistical analysis was included in the Reference [13].

2.3.3. A classical blind test (EPRI NP-369)

The cases reported at the EPRI NP-369 [14] were a set of classical blind tests for fuel codes. The new versions of codes have evolved since then. The idea of this point is to show how the BACO code solves now the problem of relocation and compares with experiments.

Relocation of pellet fragments into the gap has an important effect on gap conductance. We use Broughton and MacDonald correlation [15] and a phenomenological model that includes circumferential cracks models relocation. Case C of EPRI [14] benchmarking is simulated and the experimental result satisfactorily reproduced.

In case C of the EPRI report on fuel code benchmarking, all codes predicted a central temperature larger than the experimental one. This fact agrees with the Broughton and Mac Donald (BMD) [16] observation that the fuel temperature calculated with large hot gaps gives poor agreement with experiments when the Ross and Stoute [17] or similar models are used for gap conductance. Case C of EPRI is then used for testing whether including a model of partial gap closing by pellet relocation proposed by BMD provides a better agreement between predictions and experiments.

In Figure 1 the EPRI benchmarking temperature for case C is plotted against burnup. The good agreement between experiments and BACO code predictions can be seen by using either the BMD model or its modifications when two cracks are included. We also include the performance of the COMETHE III J code. It can be seen that it overpredicts the central temperature. The same happens if in the BACO code the modified BMD model is not included.

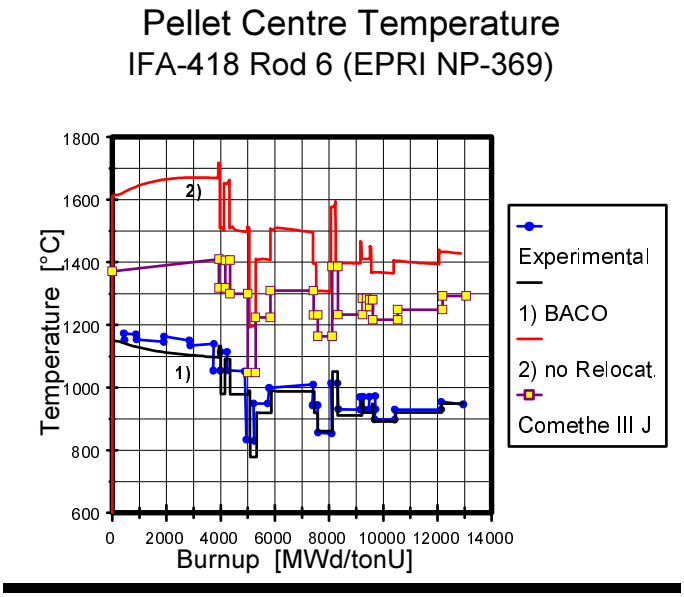

FIG. 1. Pellet centre temperature measurement and BACO calculations for the EPRI Case C.

It is shown that allowing for pellet relocation in the pellet-cladding gap provides gap heat conductance expressions that fit better to experiments than usual laws based on Ross-Stoute [17]. The perfect agreement obtained in the cases studied must however be taken with care. The gap conductance parameters are taken from BMD [16] model, which does not include a full pellet relocation model as proposed by us above. Then, although we found those values were sensible, a proper fit to experiment should be done for obtaining the best available model of gap conductance within our modified version of BMD model.

2.3.4. Co-ordinated research project on fuel modeling at extended burnup

The IAEA's CRP FUMEX (Co-Ordinated Research Project on Fuel Modelling at Extended Burnup) is a blind-test consisting of a set of experiments in order to compare fuel performance with code predictions. The OECD-HALDEN reactor (Norway) provided data. A set of instrumented fuels allowed to follow the evolution of some parameters (pellet centre temperature, inner pressure of the rod, cladding elongation, fission gas release, cladding diameter). The experiments include PIE analysis. The final burnup reached for the fuels were intermediate (25 MWd/kgU) and high (50 MWd/kgU) [18, 19].

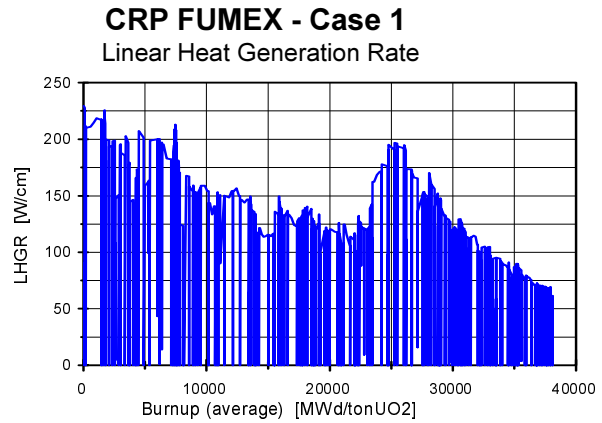

FIG. 2. Linear Heat Generation Rate (power history) as a function of the averaged burnup of the fuel rod.

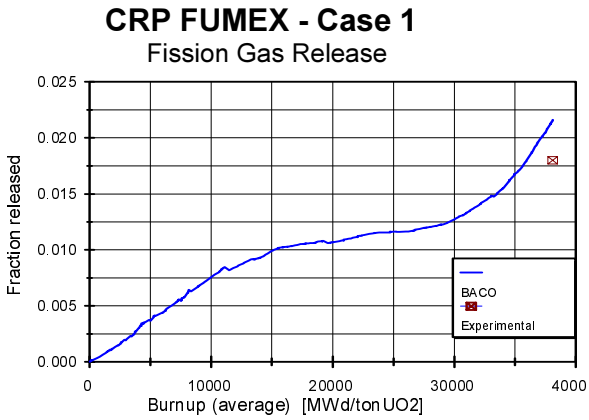

FIG. 3. Fraction of fission gas released as a function of averaged burnup of the fuel rod.

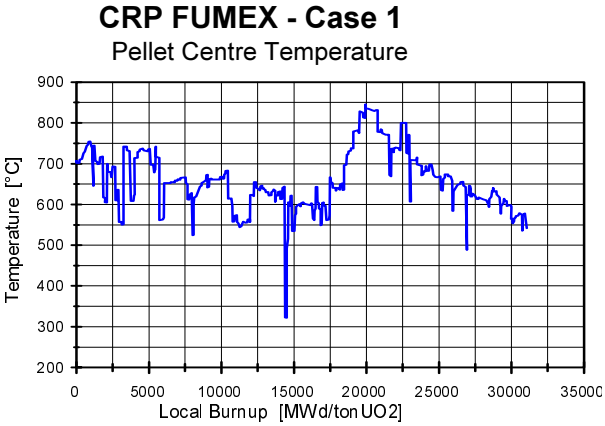

FIG. 4. Pellet centre temperature. CRP FUMEX Case 1. "On line" temperature measured at the OECD Halden Reactor.

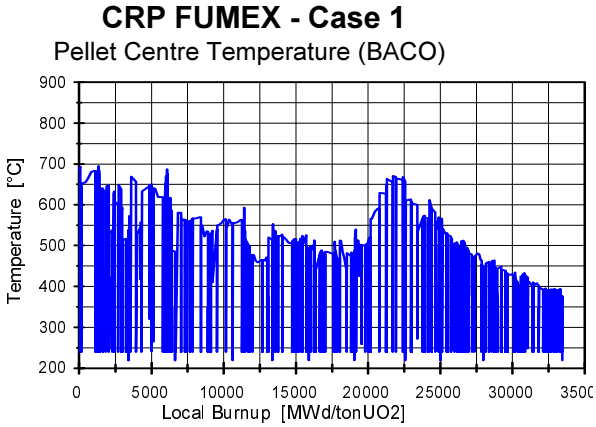

FIG. 5. BACO output for the pellet centre temperature. CRP FUMEX Case 1.

As an example of the BACO Code performance during the CRP FUMEX we include some of our results for the first exercises (FUMEX Case 1). Figure 2 shows the power history (input data) for that case. The calculated fraction of fission gases released at EOL (End Of Life) is 2.2 % (and the predicted value during the "blind test" stage was 2.5 %). The experimental value was 1.8 % (see Figure 3).

Figure 4 shows the measurement during irradiation of the temperature at the pellet centre (top of the nuclear fuel rod). The temperature monitoring was made every 15 minutes during all the irradiation. The measurement error was ± 50 °C. Figure 5 includes the BACO code calculation [20].

2.4. Sensitivity analysis with BACO

The uncertainties in the results of a validated fuel computer code with an experimented user are due to different sources:

(1) Input data of the codes:
  (a) Neutronic and reactor data,
  (b) Power history of the irradiation,
  (c) Fuel data:
    (i) Dimensional data
    (ii) Material properties

(2) Internal data of the code (and code structure):
  (a) Code parameters,
  (b) Modelling,
    (i) Physical constants,
    (ii) Parameters of the model,
    (iii) Field of application of the model.

Also, we can join these data around the point of view of its influence on the uncertainties:

- Modelling and its empirical or theoretical parameters,
- Data provided by direct measures due to in reactor irradiation and fuel test, and
- Fuel manufacturing data and fuel design data.

We can request the best models for our codes and then we solve the first point. We can request the best measurements during irradiation, material testing and reactor parameters. This means that an improvement of code results due to modelling and reactor and material data is possible.

The same does not happen with the parameters of the fuel due to the manufacturing process. The tolerances of fuel dimensions are a consequence of that process and they are sustained by the basic design. Then we must include the treatment of this source of uncertainties.

The first and easy way to analyse these topics is the definition of a set of worst cases. Those cases are the coupling of the variations of fuel parameters taking account of the tolerances in order to produce the worst situations (as maximum stress, maximum strains, extreme temperatures, etc.).

Some fuel performance codes include a probability analysis within their structure covering uncertainties in input, fabrication, parameters and models [21, 22, 23]. The BACO code (version 2.4) includes statistical analysis including statistical dispersion of the fuel rod parameters.

A BACO´s statistical analysis of power fuel reshuffling in the Atucha I NPP (an Argentinean PHWR) is included in the Reference [24], where we analyse the susceptibility of hoop stress during fuel reshuffling at different powers and burnups. Here we reproduce the recommendation of the designer for fuel reshuffling with simplified rules. The fuel for the Atucha I NPP are analysed in the Reference [5] and, the fuel for the EMBALSE NPP (CANDU type, Argentina), are analysed in Reference [13]. These exercises show, on the one hand, the sensitivity of the predictions concerning such parameters and, on the other, the potentiality of the BACO code for a probability study.

3. MOX FUEL IRRADIATIONS

3.1. MOX fuel description

The original design of the rods was made for utilization of the MZFR reactor (Karlsruhe, Germany). Due to the decommissioning of that reactor another place to make the irradiation tests had to be found. We carried out the experiments in the HFR-Petten reactor. Figure 6 shows the basic rods (rod A.1.2 and rod A.1.3). We intended to emulate extended burnup with Iodine doped pellets. Figure 7 shows the rods A.3 and A.4 and indicates the position of the doped pellets. Table I presents the characteristics of the rods taking into account the parameters specified by usual design. Those data are a coupling of MZFR, Atucha I and Petten fuel parameters. The Pu of these MOX fuels and the extension in burnup are compatible with our PHWR NPPs and they imply an increment of three times the actual burnup.

The fuel rod tolerances included in the Table 1 are provided by basic design. The real process at the α Facility Laboratory (CNEA, Argentine) allows a most detailed performance for those fuel rod parameters. Finally, the labs lead to a narrow band within tolerance and we can analyse the

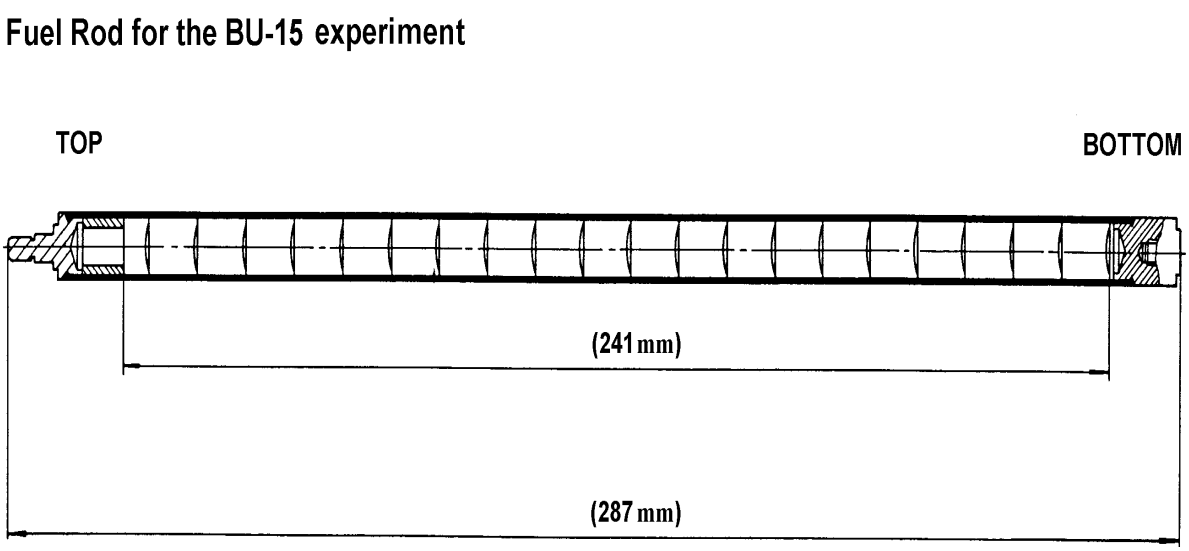

FIG. 6. MOX fuel rod type A.1 for the BU15 experiment.

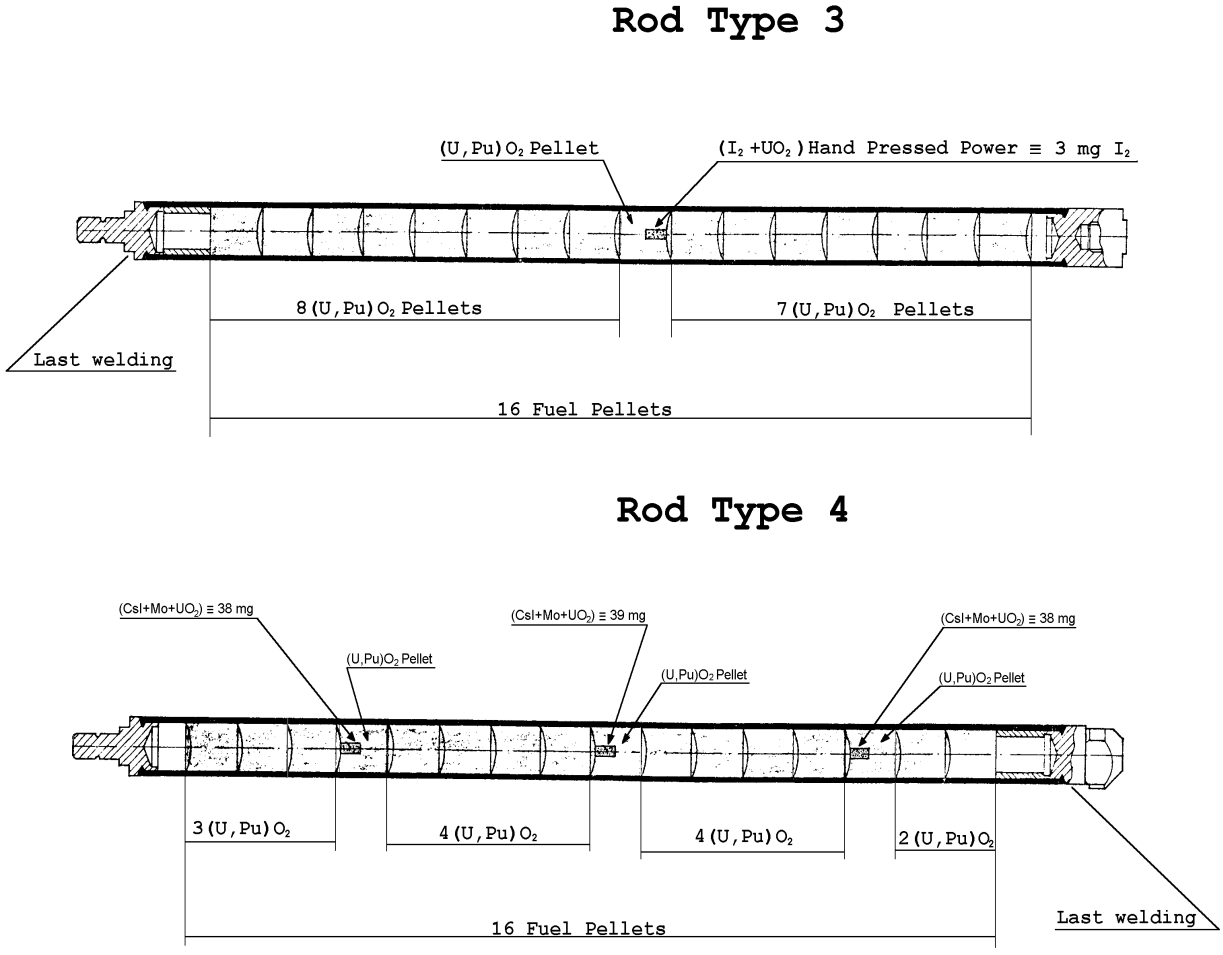

FIG. 7. MOX fuel pins type A.3 and A.4.

TABLE I. MOX FUELS IRRADIATED AT PETTEN REACTOR AS-FABRICATED FUEL RODS PARAMETERS FUEL RODS TYPE A.1, A.3 Y A.4

Rod	A.1	A.3	A.4
Length [cm]	24.1 cm	17.9	17.95
Number of rods	4	1	1
Pellets number	21	16	16
Compensating pellets number	1	-	-
Doped pellets number	-	1	3
Dope material	-	I	CsI Mo
Dope material (mg)	-	3	6.604 ± 0.170 1.373 ± 0.036
Simulated burnup (MWd/ton(M))	-	13761 ± 4933	14800 ± 390
Filling gasses	He	He	He
Filling pressure (atmospheres)	1.15	1.15	1.15

PELLETS

Pellet diameter	1.040 ± 0.001 cm
Pellet height	1.12 ± 0.01 cm
Density	10.52 ± 0.04 gr/cm^3
$Pu_{fiss}/U+Pu_{met}$	0.53 %
Enrichment (U^{235}+Pu)	1.25 %
O/M relation	2.00
Dishing volume	25. ± 5. mm^3

CLADDING

Cladding material	Zry-4
Cladding inner diameter	1.17 cm
Cladding thickens	0.06 cm

TABLE II. MOX FUELS IRRADIATED AT PETTEN REACTOR. SOME STATISTICAL PARAMETERS OF THE FUEL RODS

PELLETS	Main Value (or specification)	Standard Deviation	Minimum Value	Maximum Value
Pellet diameter (cm)	1.0402	0.0005	1.0390	1.0414
Pellet height (cm)	1.1217	0.0204	1.1000	1.3000
Density (gr/cm^3)	10.522	0.048	10.350	10.650
…	…	…	…	…
CLADDING				
Cladding inner diameter	1.170 cm	…	1.166	1.174
…	…	…	…	…

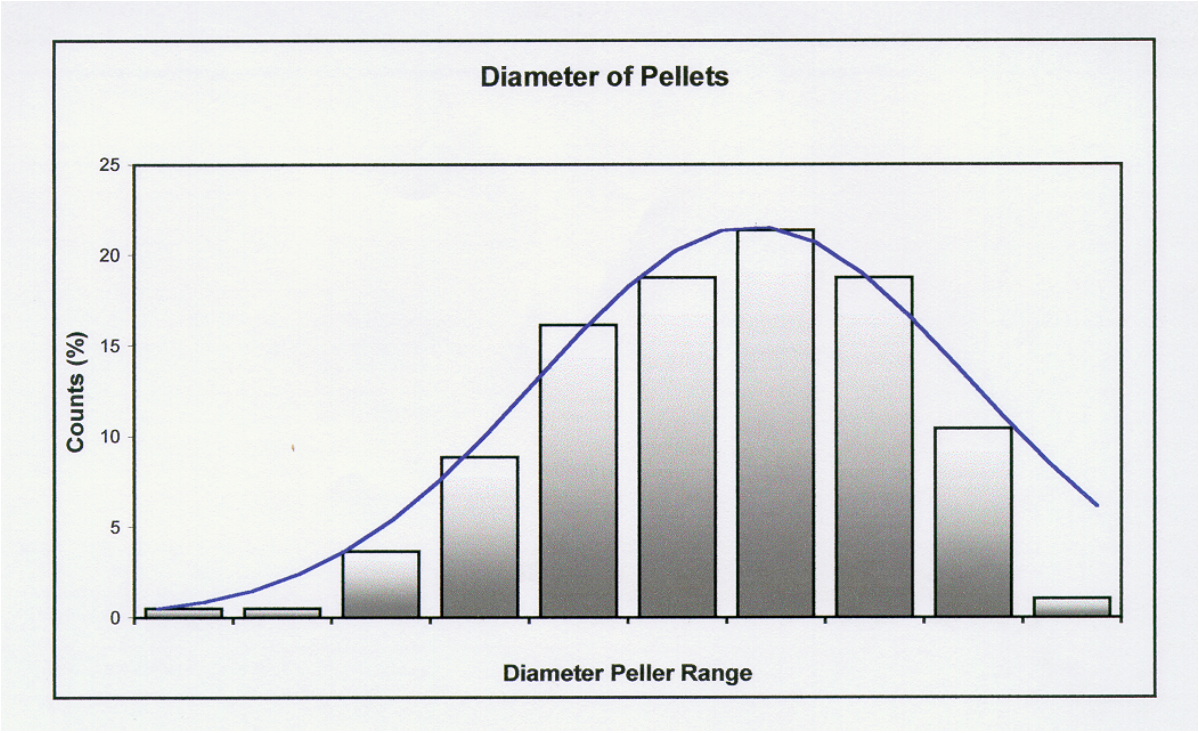

FIG. 8. Histogram of the pellet diameters. The columns are between the maximum and minimum specified values [$Ø_p$ = (1.040 ± 0.001) mm]. The curve is the associated Gauss distribution.

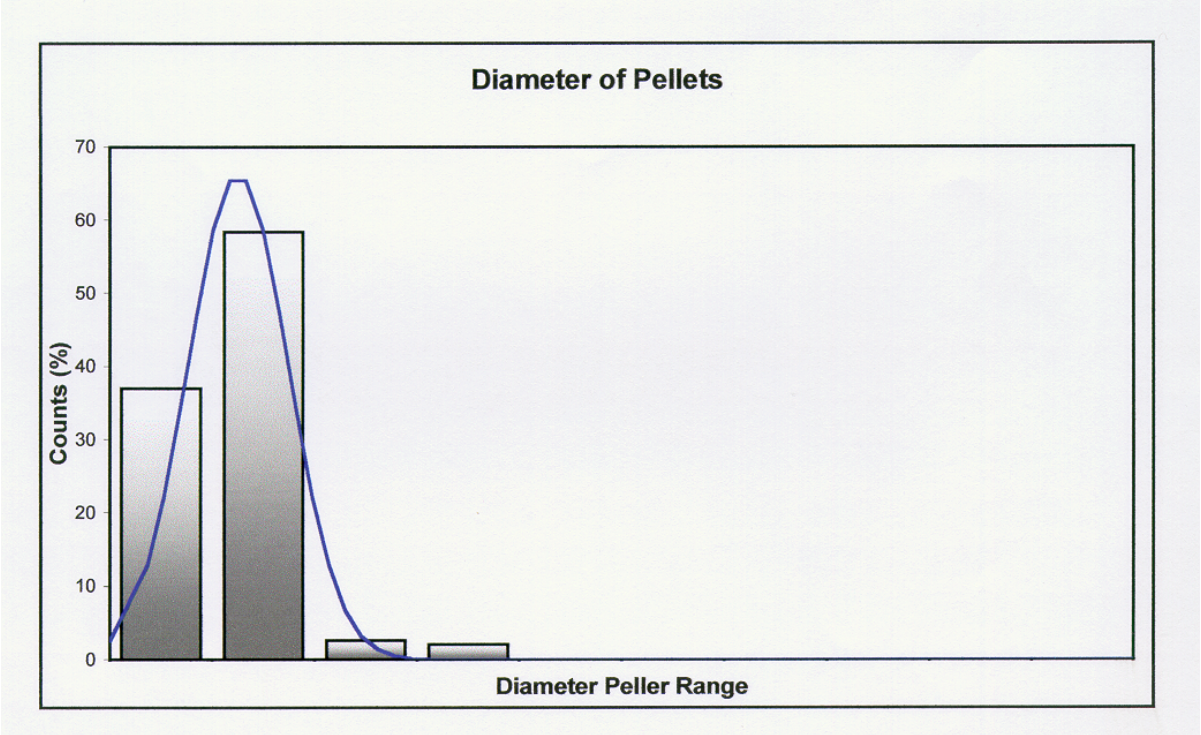

FIG. 9. Histogram of the pellet heights. The ten columns are between the maximum and minimum specified values [h_p = (11. ± 1.) mm]. The curve is an approximated Gauss distribution.

probability distribution of the fuel parameters with a big sample (pellet density, dishing volume, etc) or taking the measurements of all the pellets (pellet diameter, pellet height, etc.). Table II includes some statistical parameters of the fuel and maximum and minimum values found. Figure 8 shows the histogram for the pellet diameter distribution. Figure 9 includes the histogram for the pellet height. Both histograms are between the specified maximum values. The figures include the Gauss distribution curves.

The first irradiation was with the A.1.4 rod. We intended to calibrate the HFR reactor instruments. That experience verified the response of the HFR reactor detection systems with our MOX rod.

3.2. Doped MOX fuel rods A.3 (with Iodine) and A.4 (with CsI)

The experiment started with the irradiation of two fuel rods similar to pathfinder, both containing Iodine compounds as dope to simulate the effect of extending burnup [26].

Fuel rods A.3 and A.4 have been employed for this second experiment. This irradiation, carried out during 15 days consisted in a power cycling between 120 and 290 W/cm and a final ramp to reach 400 W/cm [27]. This final power level lead to a “hoop stress” of about 170 MPa which is likely to induce microcracks in the inner surface of the cladding, representing an incipient defect produced by stress corrosion cracking, without reaching the failure threshold of the tubing.

Rod A.4: CsI and Mo were mixed with UO_2, the mixture was introduced in central holes drilled in three pellets and hand pressed.

Rod A.3: Pure iodine was introduced in one pellet with the aim of comparing its effect on the cladding with that of combined iodine (CsI).

BACO code was employed to design the power history. The experimental power history was in good accordance with the proposed power history. Rod A.3 and A.4 behaved as expected:

- There were no failures in the cladding,
- No fabrication defects have been detected, and
- Microcracks in the inner surface of the cladding were detected during PIE.

There were good agreements between post-irradiation and BACO code output especially about stress analysis and gap dimension [3].

3.3. BU15 experiment

The third irradiation experiment was carried out with fuel rods A.1.2 and A.1.3, both similar to the pathfinder. A burnup of approximately 15 000 MWd/ton(M) was reached in both rod lets. This required 531.5 irradiation days. Rod A.1.3 was submitted to EOL power ramp.

Rods A.1.2 and A.1.3 behaved during the stationary phase as it was expected:
- No rod failures were detected,
- No fabrication defects were evident.

During the EOL power ramp, rod A.1.3 behaved as follows:
- A maximum power of 390 W/cm was reached,
- The power ramp had to be finished earlier than planned due to an increase in activity in the coolant circuit,

- Visual inspection of the fuel rod revealed the existence of a small circular hole in the cladding,
- This kind of failure is likely to be produced by SCC.

The aim of this step of the experiment was to study the stresses in the rod submitted to the power transient in order to determine the causes of the failure.

3.3.1. Irradiation power history

The BU15 irradiation experiment was carried out with fuel rods A.1.2 and A.1.3, both similar to the pathfinder. The power history for this irradiation test was proposed upon calculations made with the BACO code. The target duration of the irradiation was an average burnup of 15 000 MWd/ton(M), more or less twice the final burnup for Atucha I fuel. After the steady state irradiation at an average power level of 230 W/cm one of the rods was submitted to a power ramp [28].

During the steady state irradiation both rods were assembled together through a threaded coupling. This system permits an easy disassemble of the two rods in any irradiation stage.

The average burnup of 15 000 MWd/t(M) was reached in two main steps:

a) Up to a burnup of 8100 MWd/t(M) the rods were irradiated in different locations of the HFR core. The irradiation device consisted of an aluminium fuel rod capsule located in either of two different carriers. The first of these consisted of an aluminium structure in the core section while the other had a hollow stainless steel structure having the possibility of containing pressurized BF_3 gas for power control purposes. The primary pressure in the fuel rod capsule was kept at 145 bar, and
b) Up to a burnup of 15 000 MWd/t(M) both rods were irradiated in the Pulse Side Facility (PSF) of the reactor. The irradiation device consisted of an aluminium fuel rod capsule located in a special PSF capsule carrier which can be translated parallel to the HFR core box wall. Also the primary pressure in the fuel rod capsule was kept at 145 bar.

After termination of the bulk irradiation phase both fuel rods were disassembled in the Petten hot cells and the A.1.3 rod was prepared for insertion into a standard LWR fuel testing capsule consisting of an aluminium capsule located in a similar carrier as described in *b*), which allowed to adjust it to a specified power level. In this case the primary system pressure in the fuel rod capsule was kept during the ramp test phase at 115 bar (e.g. PHWR system pressure).

The ramp proposed consisted of two parts:
1) A short period of pre-irradiation power level in the PSF position which will be used for the ramp test in order to determine the experiment power versus PSF position characteristics, and
2) The ramp test starting with a ramp rate of 50 $Wcm^{-1}min^{-1}$ from nearly zero power to maximum 420 W/cm linear fuel rod power and followed by a 6 hours steady state holding at this maximum power.

The ramp test was performed following the proposed schedule. However, instead of the anticipated high power level of 420 W/cm the maximum fuel power reached only a maximum ramp power level of approximately 380 W/cm, due to the low quantity of remaining fissile material in the fuel rod.

Rods A.1.2 and A.1.3 behaved during the stationary phase as it was expected:
- No rod failures were detected,
- No fabrication defects were evident.

During the EOL power ramp, rod A.1.3 behaved as follows:

- A maximum power of 390 W/cm was reached,
- The power ramp had to be finished earlier than planned due to an increase in activity in the coolant circuit,
- Visual inspection of the fuel rod revealed the existence of a small circular hole in the cladding.

During operation for the entire experiment the total power production was determined via a heat balance approach by measuring the increase in temperature of the capsule coolant water and then the real power fuel rod production by difference with the measured nuclear heating of an empty capsule structure.

The power history includes the normal cycle operation, which means reactor shutdowns, variations from the planned average power in the fuel rods of approximately 100 W/cm and the final ramp test for the A.1.3 fuel.

The total time for this test was 1020.2 calendar days, corresponding to 26 irradiation periods (531.5 days) and 26 periods on which the fuels rods were not irradiated due to changes of irradiation capsules, reactor shutdowns or non availability of a suitable core position.

After a cooling time of 49 days and 9 hours rod A.1.3 was submitted to a power ramp.

Before the ramp test a preconditioning irradiation was performed, increasing power rate at 7.2 W/cm.min during 42 minutes until an average fuel rod power of 250/260 W/cm was reached. This last power level was held 39 minutes. The fuel rod power was then reduced during 5 minutes at a power rate of 48 W/cm.min until an average fuel rod power of 10 W/cm was attained, after 10 minutes, the power level was increased at a rate of 43 W/cm.min during 8 minutes to a final average rod power of 350/360 W/cm. This power was held during 52 minutes.

At approximately 28 minutes operation at the ramp power level an increase of the activity of the primary water was detected. This activity peak decreased after 6 minutes to its previous level. As this event gave reason for assumption of a fuel rod failure the experiment was 24 minutes after the start of the activity release shutdown at a power rate of 175 W/cm.min during 2 minutes.

It is noteworthy that at the beginning of life, the A.1.2 and the A.1.3 fuel rods reached a maximum peak fuel rod power of 430 W/cm and 380 W/cm, respectively. The average for the assembly was 330 W/cm. These maximum peak power levels, during that pre-irradiation period, where higher or equal than the maximum power reached during the final ramp test for the A.1.3 fuel rod.

3.3.2. Post-irradiation analysis

After finishing the low level irradiation in the HFR, the irradiation device was disassembled and some non-destructive examinations were done on both pins. These examinations were repeated on fuel rod A.1.3. after the transient. Destructive examinations were performed on both rods (for A.1.2 after the low level irradiation and for A.1.3. after the transient). The main findings of the post-irradiation examinations are described in the following paragraphs.

The irradiation-induced effects were studied in detailed post-irradiation-examination, which was performed at the HFR site in Petten, and later at the hot cells of the Karlsruhe Nuclear Research Centre.

We do not give too much detail about this aspect of the experiment because the aim of the report is about BACO code comparison. We indicate only the main post-irradiation analysis made with the pins, as follows (references [2, 25, 29, 30 and 31]):

- Visual inspection
- Eddy current check
- Neutron radiography
- Gamma scanning
- Betatron-radiography
- Dimensional control [32]
- Sectioning diagram
- Ceramography
- Scanning Electron Microscopy (Fig. 17 and 18 show the microcracks of the rod A.1.3)

The analysis of the experiment made with the BACO code and a complete description of the calculation was presented at the IAEA's TCM on "Water Reactor Fuel Element Modelling at High Burnup and Experimental Support" [3]. At that meeting it was suggested that additional post-irradiation examinations and more details of the failure condition would be needed to confirm the failure as being due to PCI. That report was continued in the IAEA's TCM on "Recycling of Plutonium and Uranium in Water Reactor Fuel" [2]. At that meeting we presented a new set of post-irradiation examinations (not available at the previous meeting). The results attained show a PCI-SCC failure in the A.1.3.

3.4. First results for the MOX fuel irradiation and the BACO code performance

The absence of fabrication induced failures in the irradiated rods is an important achievement in our MOX fuel development programme.

The presence of microcracks inside the cladding in the doped rods, the coincidence between the predicted and measured pellet-cladding gap values, the temperature calculated and the microstructure observed, the grain sizes distribution, indicated a good BACO code evaluation.

The defective zone of the A.1.3 rod had the biggest mechanical demands. The calculated hoop stress with BACO 2.20 was enough to indicate that PCI-SCC was the mechanism likely to produce the failure. The maximum hoop stress and pellet-cladding radial contact pressure appears in the axial section corresponding to the failure. That prediction was confirmed with the post-irradiation examinations.

4. BACO CODE SIMULATION OF THE MOX FUEL BEHAVIOUR DURING THE BU15 EXPERIMENT

The reactor's assumed power history which is used here for the fuel rod performance analysis was explained in 3.3.1) and is sketched in Figure 10. We consider five segments for calculation. Bottom axial section suffers the high power during irradiation. However, the biggest demand happens at the final power ramp for the top section due to its inversion at the PSF. We include a BACO code analysis at Reference [3] using an old version (2.20) of the code. There is no substantive difference in the usual calculation.

The calculated temperature corresponds to the post-irradiation. The maximum temperature calculated was 1600°C at the bottom of the fuel rod (See Figure 11).

Compression is generally predicted for the "hoop stress" calculated at the cladding (i.e., tangential stress at the inner surface of the cladding). However, stress reversal happens due to local power increment followed by stress relaxation, i.e. creep of the cladding. The maximum hoop stress

calculated was up to 300 MP during the final ramp test at the top of the fuel (defective section). The maximum calculated radial contact pressure was up to 50 MPa. (See the fill curve in Figure 13).

There is an increment of pressure in the rod with irradiation due to the fission gas release and local variations are induced by power changes. The calculated gas pressure at EOL was 1.6 Mpa (See Figure 15).

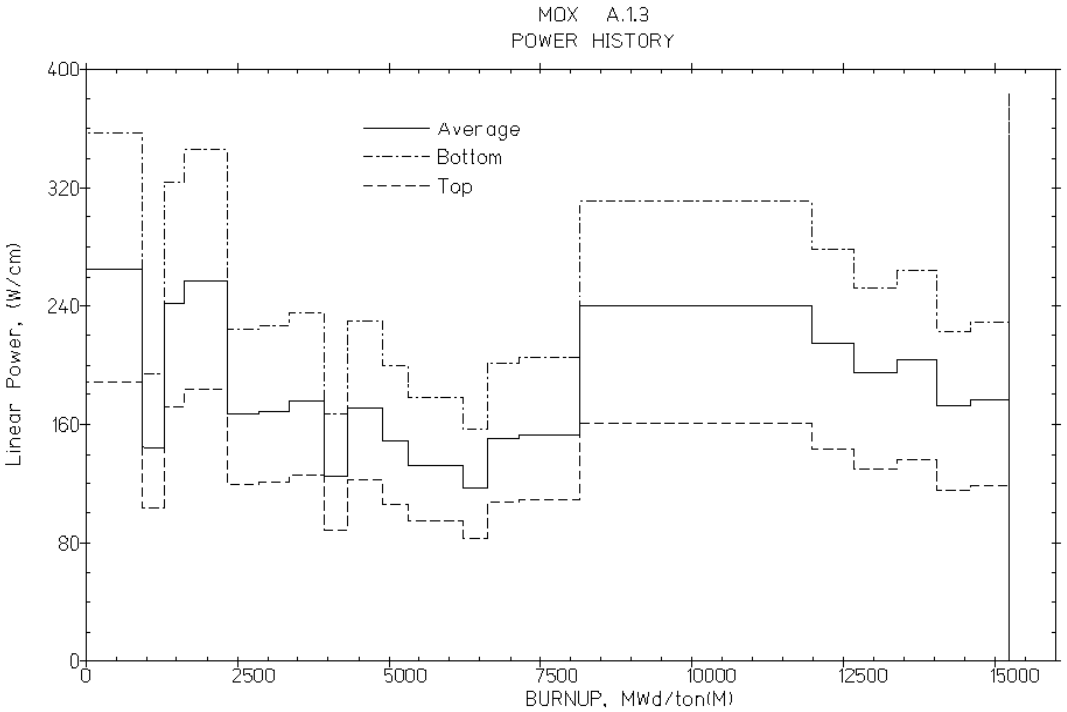

Fig. 10. Linear heat generation rate in function of burnup for the A.1.3 fuel rod. The upper curve corresponds to the top of the fuel, the lower curve corresponds to the defective zone of the rod.

4.3. Parametric analysis of the MOX fuel rod

The purpose of this exercise is to consider how the combination of assumed extreme rod dimension conditions — within reasonable tolerance for its fabrication — can affect performance. We define two extreme situations:

A rod with the largest gap between pellet and cladding compatible with the as-fabricated tolerances, and

A rod with the smallest gap.

The first situation should give rise to the maximum temperature in the fuel, and the second to maximum stress between pellet and cladding.

For the same power history of Figure 10, Figure 11 includes the pellet centre temperature at the maximum gap situation at the bottom of the fuel rod. The largest temperature attained in this case is 1675°C (while the minimum gap situation is 1600°C). Figure 13 includes the BACO calculation of hoop stress with a minimum gap situation. Here we do not see a big change; the wide range between both situations at the middle of life is due to the hard contact that occurs. The calculated curves show a narrow band due to the strict QA in lab conditions.

We obtain a stable solution, with the three parameters mentioned, which proves that the BACO code is a good tool to be used for fuel rod design.

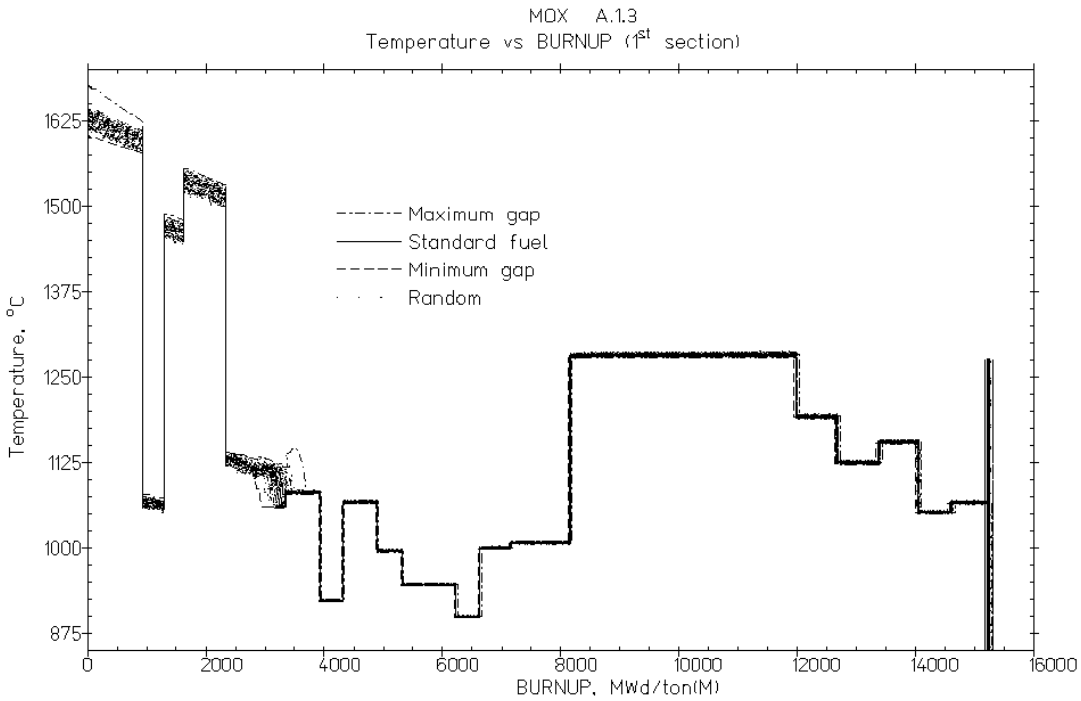

FIG. 11. Pellet centre temperature in the first segment of the fuel rod for the BU15 experiment (A.1.3 rod).

4.4. Sensitivity analysis of the BU15 experiment

As outlined in the Introduction, the flexibility of the BACO code and its speed in computer time allows performing systematic statistical analysis. Using allowed fabrication dimensional limits

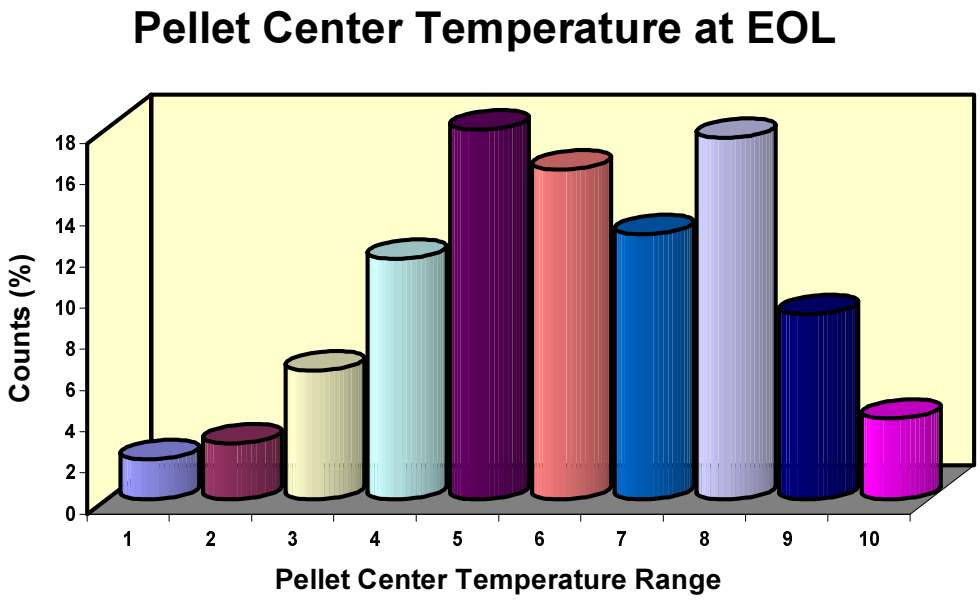

FIG. 12. Histogram of the pellet centre temperature at End of Life (EOL). The columns are between the maximum and minimum calculated values (1275-1278°C).

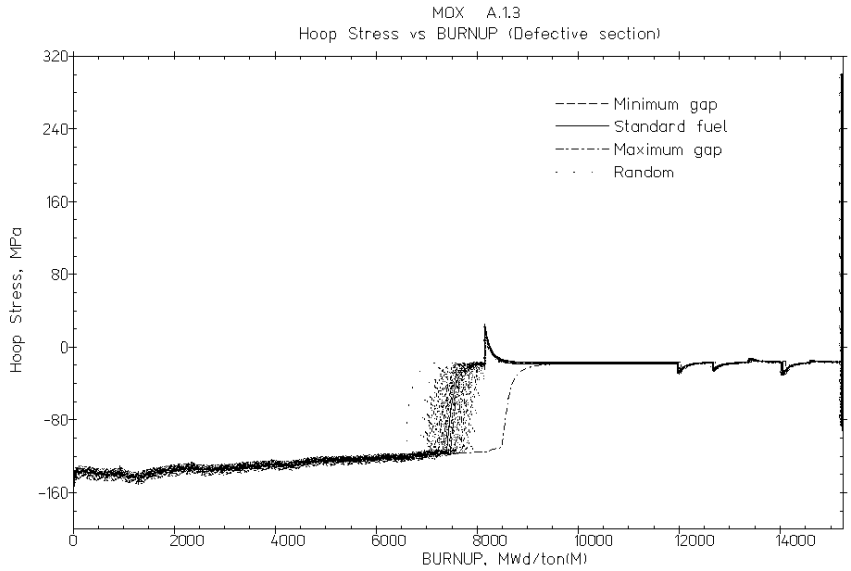

FIG. 13. Hoop stress at the defective segment of the fuel rod for the BU15 experiment (A.1.3 rod).

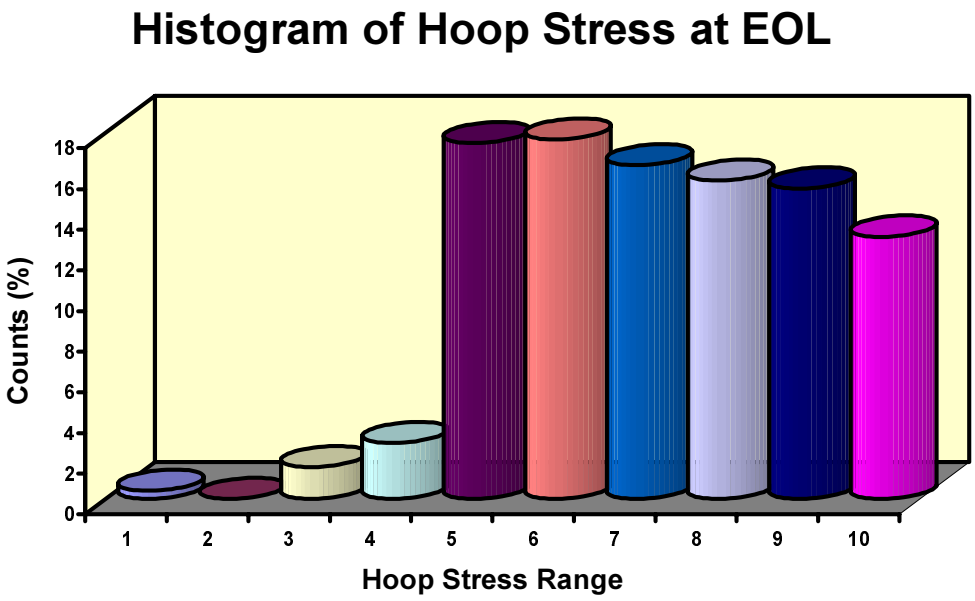

FIG. 14. Histogram of the hoop stress at End of Life (EOL). The columns are between the maximum and minimum calculated values (292-302 MPa).

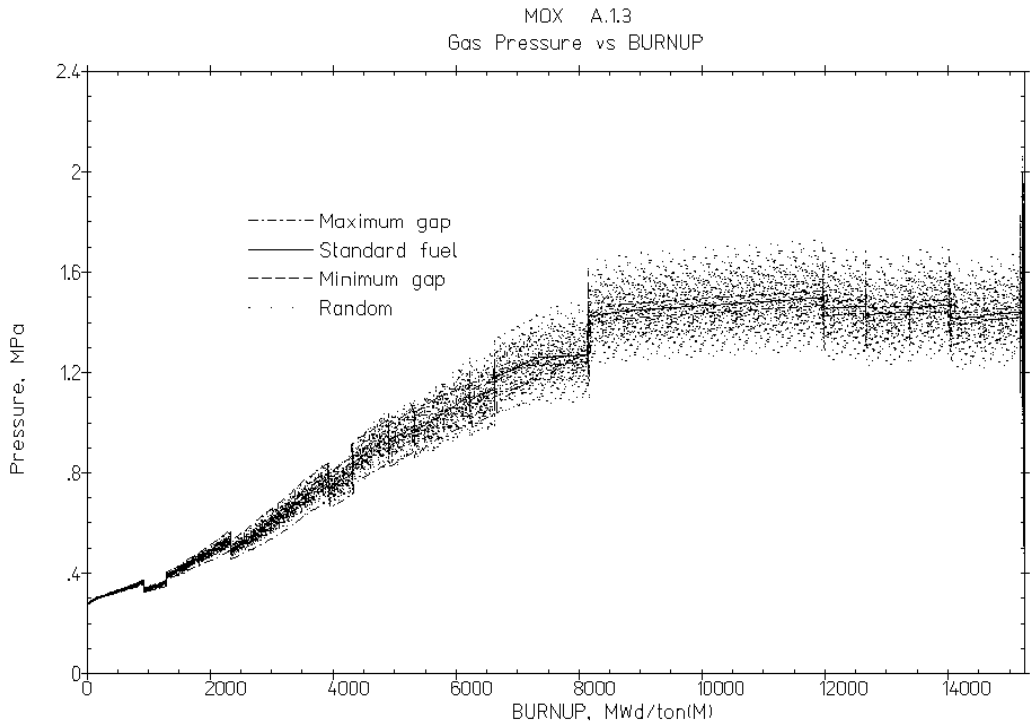

FIG. 15. Gas pressure of the free gases in the fuel rod for the BU15 experiment (A.1.3 rod).

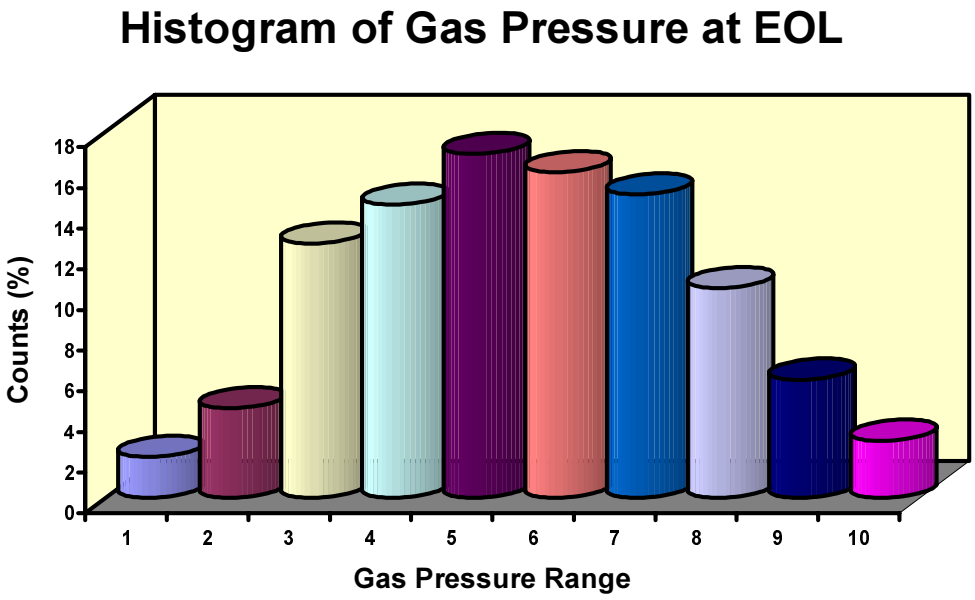

FIG. 16. Histogram of the gas pressure of the free gases in the rod at End of Life (EOL). The columns are between the maximum and minimum calculated values (1.60-2.07 MPa).

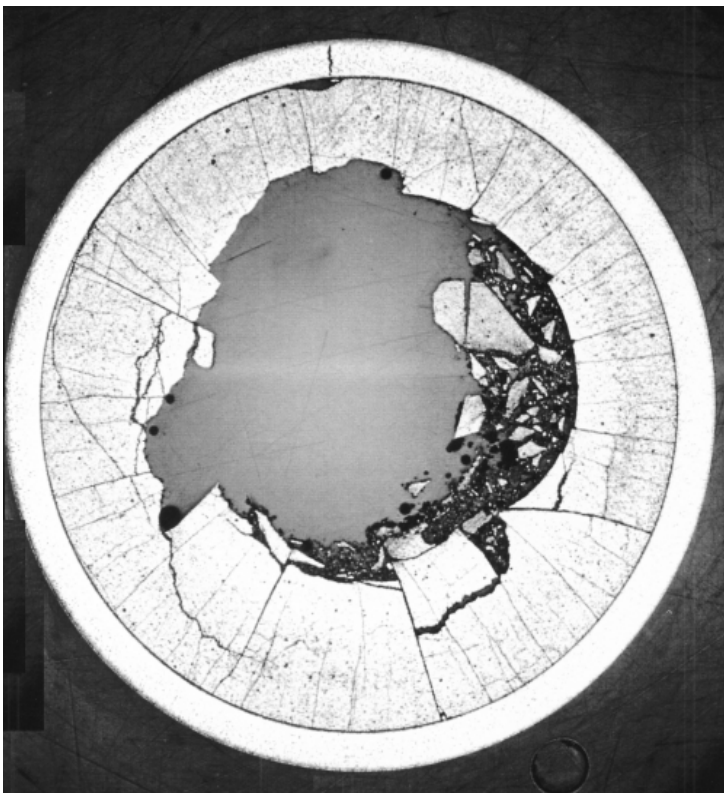

FIG. 17. Micrograph of a cross section near the defect in rod A.1.3. showing the hole. (Coversheet of Journal of Nuclear Material 229 (1996), [25]).

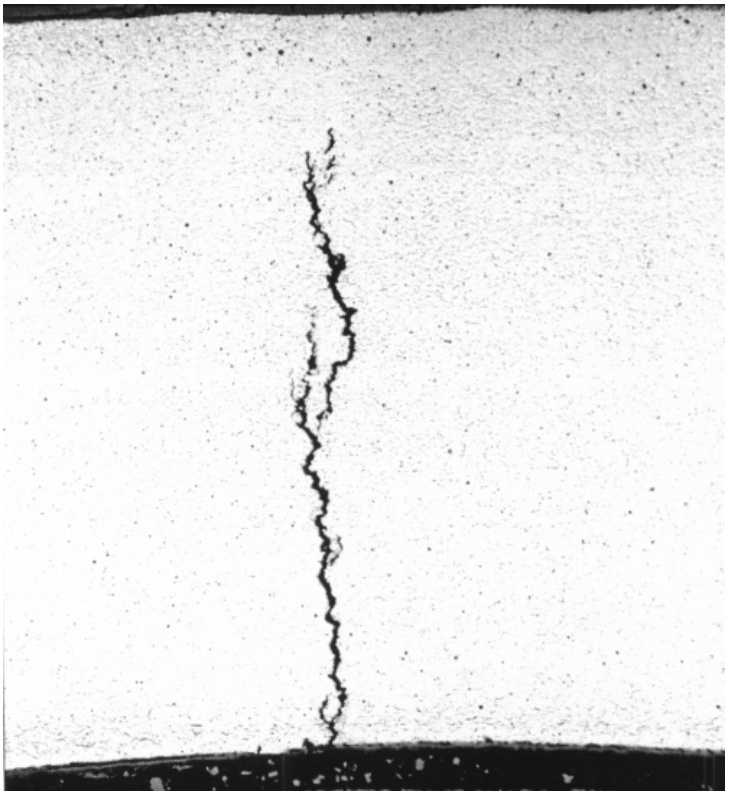

FIG. 18. Micrograph of the defect in fuel rod A.1.3. Cross section over the hole in the fuel.

and a statistical distribution of values within those; several runs (a minimum of 1000) are performed with different sets of initial values for the rod dimensions. We study the predicted variations in:

Pellet centre temperature,
Cladding hoop stress, and
Gas pressure predictions.

The rod input data were randomly selected within assumed deviations for pellet diameter and height, inner and outer diameter of the cladding and pellet density. The random selection of input values was done assuming a Gauss distribution of values between limits. See Table II and Figures 8 and 9.

Figures 11, 13 and 15 represent the BACO code sensitivity analysis of some performance parameters in the MOX fuel rod A.1.3. We plot in the curves:

Standard parameters of input data of the rod,
The parameters of the maximum gap situation,
The parameters of the minimum gap situation, and
The points of the random selection.

Figure 11 is the BACO code calculation of the pellet centre temperature for the same viewer history of Figure 1. All the random points calculated are between the extreme values in as-fabricated tolerances, taken at approximate realistic values. There is convergence of dots at EOL (End of Life) due to pellet-clad contact. Figure 12 shows a histogram of the pellet centre temperature at EOL, after the final ramp.

Figure 13 shows the dispersion in the cladding hoop stress with the same inputs as the previous plot. The points show a great dispersion at the middle of life due to the pellet-cladding contact situation. There are points out of the extreme limits of the previous analysis. The calculation shows that the hoop stresses converge during the irradiation that is clearly demonstrated by the small dispersion at EOL previous to the final ramp (see Figure 14).

Figure 15 is the free gas pressure at the fuel rod. The gas pressure calculation takes account of the thermal calculation, dimensional calculation (stresses), fission gas release, etc. That is the coupling of all the fuel rod parameters (input data and behaviour modelling). There is a small dispersion at BOL. The calculated values of pressure diverge during irradiation. Finally, after 4000 MWd/ton(M), there are values both smaller and larger than those predicted at the extreme conditions of the “gap” size situation. Figure 16 is a histogram of the rod gas pressure of the free gases at EOL. The main value agrees with the one calculated for the standard fuel parameters.

A similar detailed work is included in Reference [13] where a CANDU fuel analysis is done. At that situation the dispersion of parameters is relevant.

5. CONCLUSIONS

The schedule sketched in this paper begins with a validated code for the simulation of the fuel rod behaviour under irradiation, almost for internal use in the institution (2.3). The help obtained from international projects such as the CRP FUMEX are relevant at this point (2.3.4). The enhancement of fuel modelling about relocation was sketched with the classical blind test of EPRI (2.3.2). The application of simple rules was included in the CANDU fuelograms analyses (2.3.2). An example of institutional benchmarking of the BACO code was presented with the NRX irradiation (2.3.1).

A MOX fuel rod failure due to PCI-SCC was presented. The BACO code was a computing tool during all the stages of the experiments. The original scope of the MOX irradiation was the correct research, developing and manufacturing of MOX fuels in the α Facility. An additional

developing was the induction of fuel failures due to SCC mechanism and the simulation of burnup extension with synthetic products (CsI and Iodine).

We are showing that a simple running code is not enough in order to simulate the behaviour of a fuel rod. Parametric analysis of extreme cases must be done. But the analysis sketched shows that the study of extreme cases is not enough. The smallest dispersion found in the selected parameters (temperature, hoop stress and gas pressure) is due to the QA procedures in the laboratories. Nevertheless, it is easy to see that the probability distributions of the fuel rod parameters must be known and statistical analysis must be included in order to follow the correct influence of the manufacturing QA procedure of fuel elements. A complete fuel element design must consider the dispersion in rod dimensions due to fabrication. Changes in the design of rod in fabrication parameters can be tested. This exercise shows, on the one hand, the sensitivity of the predictions concerning such parameters and, on the other, the potentiality of the BACO code for a probability study.

REFERENCES

[1] ADELFANG P., MARINO A. C. et al, "Fabricación y control de barras combustibles de óxidos mixtos (U,Pu)O_2 , para ensayo de irradiación en el Reactor HFR-Petten.", XIV annual meeting of the AATN (Asociación Argentina de Tecnología Nuclear), Córdoba, paper 86, October 1986.

[2] MARINO A. C., PÉREZ E. E., ADELFANG P., "Irradiation of Argentine MOX fuels. Post-irradiation results and analysis", IAEA's TCM on Recycling of Plutonium and Uranium in Water Reactor Fuel. Newby Bridge, Windermere, United Kingdom, 3-7 July 1995.

[3] MARINO A. C., PÉREZ E. E. AND ADELFANG P., "Argentine Nuclear fuels MOX irradiated in the Petten Reactor, Experiment analysis with the BACO code". IAEA's TCM on Water Reactor Fuel Element Modelling at High Burnup and Experimental Support, paper 1/6, Windermere, 1994.

[4] MARINO A. C. , SAVINO E. J. AND HARRIAGUE S. , "BACO (BArra COmbustible) Code Version 2.20: a thermo-mechanical description of a nuclear fuel rod", Journal of Nuclear Materials Vol. 229, April II, 1996 (p155-168)

[5] MARINO A. C. , SAVINO E. J., "Sensitivity analysis applied to nuclear fuel performance related to fabrication parameters and experiments", 14th International Conference on Structural Mechanics in Reactor Technology, Paper C01/7, SMiRT 14, August 17-22, 1997, Lyon, France

[6] SPINO J., "Fragilización de la vaina de Zircaloy-4 en elementos combustibles PWR por acción de los productos de fisión volátiles. Fenómeno de corrosión bajo tensiones activado por iodo. Influencia interna de la química interna del combustible.", Ph.D. thesis Instituto de Física Dr. Balseiro, Universidad Nacional de Cuyo, Argentina, February 8, 1988.

[7] MARINO A. C. AND SAVINO E. J., "Power ramp and reshuffling analysis for nuclear fuels using the BACO code", 14th International Conference on Structural Mechanics in Reactor Technology, SMiRT 14, August 17-22, 1997, Lyon, France.

[8] MARINO A. C., SAVINO E. J. AND HARRIAGUE S., "Thermo-mechanical description of a nuclear pin, BACO code version 2.20", 13th International Conference on Structural Mechanics in Reactor Technology, (SMiRT 95), Universidade Federal do Rio Grande do Sul, Porto Alegre, Brazil, August 13-18, 1995.

[9] NOTLEY M., "Zircaloy-sheathed UO_2 fuel irradiated with a declining power history to determine its effect on fission product gas release", Atomic Energy of Canada Limited, AECL-6585 (1980).

[10] TRUANT P. T., "CANDU Fuel Performance: Power Reactor Experience", IAEA/CNEA International Seminar on Heavy Water Fuel Technology, S. C. de Bariloche, June 27-July 1, 1983,AECL MISC 250 (1983).

[11] HASTING I. J. et al, “CANDU fuel performance: Influence of fabrication variables”, IAEA-CNEA International Seminar on Heavy Water Reactor Fuel Technology, S. C. de Bariloche (1983), AECL MISC 250 (1983).
[12] PENN W. J. et al, “CANDU fuel - Power ramp performance criteria”, Nuclear Technology 34, p. 249 (1977).
[13] MARINO A. C., “Computer simulation of the behaviour and performance of a CANDU fuel rod.”, 5th International Conference on CANDU fuel, Toronto, Ontario, Canada, September 21-24, 1997.
[14] FREEBORN H. et al. 1977. Light Water Reactor Fuel Rod Modelling Code Evaluation. EPRI NP-369 (Project 397-1) Final report, March 1977.
[15] MATPRO-Version 09: A Handbook of materials properties for use in the analysis of LWR fuel rod behaviour. TREE-NUREG-1005, EE.UU. (1976).
[16] BROUGHTON J. AND MACDONALD P. 1976. Gap heat transfer in MATPRO-Version 09.
[17] Ross A. and Stoute R. 1962. AECL 1552.
[18] CHANTOIN P., TURNBULL J. AND WIESENACK W., “Summary of findings of the FUMEX program, IAEA’s TCM on water reactor fuel element modelling at high burnup and its experimental support, Windermere, UK, 19-23 Sept. 1994.”
[19] “Fuel Modelling at extended burnup”, Report of the Co-Ordinated research Programme on Fuel Modelling at Extended Burnup - FUMEX 1993-1996, IAEA-TECDOC-998, January 1998
[20] MARINO A. C., “Proyecto FUMEX (Fuel Modelling at Extended Burnup) de IAEA: Evaluación final de la participación del código BACO (Irradiaciones en el OECD Halden Reactor)”, XXIV annual meeting of the AATN (Asociación Argentina de Tecnología Nuclear), Buenos Aires, Argentina, 10-12 November, 1997.
[21] LASSMANN K. et al., “Probabilistic Fuel Rod Analysis using the TRANSURANUS Code”, IAEA, TCM on "Water Reactor Fuel Element Modelling at High Burnup and Experimental Support", paper 5/2, Windermere, UK, 1994.
[22] BULL A. J., “A probabilistic analysis of PWR and BWR fuel rod performance using the code CASINO-Sleuth”, Nuc. Eng. and Design 101 (1887) 213.
[23] MOSCALU D. R., “CANDU type fuel behaviour – A probabilistic approach”, 4th International Conference on CANDU fuel, Pembroke, Canada, September 1-4, 1995.
[24] MARINO A. C. and Savino E. J., “Applications of simple rules of fuel failure in a computer model simulation for nuclear fuel behaviour and performance”, Log#31, International Topical Meeting on Light Water Reactor Fuel Performance, Portland, Oregon, USA, 2-6 March, 1997.
[25] MARINO A. C., PÉREZ E. E. AND ADELFANG P., “Irradiation of Argentine MOX fuels. Post-irradiation results and experimental analysis with the BACO code.”, Journal of Nuclear Materials Vol. 229, April II, 1996 (p169-186).
[26] MARINO A. C., ADELFANG P. AND SPINO J., "Experiencias con óxidos mixtos $(U,Pu)O_2$. (Irradiaciones en los reactores MZFR y HFR-Petten)", XIV annual meeting of the AATN (Asociación Argentina de Tecnología Nuclear), Córdoba, 1986 (59).
[27] MARKGRAF J. et al., "Technical Memorandum HFR/87/4663"
[28] MARKGRAF J. et al., "Technical Memorandum IT/92/4960"
[29] ADELFANG P., PÉREZ E. E., "Irradiación de BBCC de óxidos mixtos $(U,Pu)O_2$ .Descripción de las experiencias y ensayos posirradiación no destructivos iniciales", XXI Reunión Científica de la AATN, Mar del Plata, 1993 (26).
[30] GEITHOFF D., "CNEA Fuel Pin Experiment A3/A4 Results of the Post-Irradiation-Examination", Primärbericht-PSB-Ber. IV 775 (Kl. IV)
[31] ADELFANG P., RUGGIRELLO G., OBRUTSKY L., "Resultados parciales de los ensayos posirradiación luego de una rampa de potencia, de una BC de óxidos mixtos $(U,Pu)O_2$ con quemado simulado por productos de fisión sintéticos", XVI Reunión Científica de la AATN,
[32] Mendoza, 1988 (62).
[33] DENIS A. et al,” Finite elements simulation of the thermoelastic behaviour of a fuel rod”, this meeting.

THERMAL PROPERTIES
(Session 4)

Chairpersons

M. ICHIKAWA
Japan

D. SCHRIRE
Sweden

A FUEL THERMAL CONDUCTIVITY CORRELATION BASED ON THE LATEST EXPERIMENTAL RESULTS

F. SONTHEIMER, H. LANDSKRON
Siemens AG, KWU,
Erlangen, Germany

M.R. BILLAUX
Siemens Power Corporation,
Richland, Washington, United States of America

Abstract

A new fuel thermal conductivity (ftc) correlation for UO_2 and $(U,Gd)O_2$ is presented, which is based on the relaxation-time theory [1] of Klemens. The correlation is chosen because of its validity in a wide range of defect concentrations as for instance encountered in fuel with a wide range of burnup and gadolinia additions, as has been shown by Ishimoto [2]. The phonon term of the new correlation has the form $\frac{1}{x} \cdot \arctan(x)$, where x is a measure of the defect concentration introduced by burnup and gadolinia additions. For low defect concentrations, this term is identical with the classical form for the phonon term $\frac{1}{(A + B \cdot T)}$. At high defect concentrations, however, when phonon-point defect scattering starts dominating over phonon-phonon scattering, the new correlation deviates from the classical formulation and has a distinctly weaker dependence on temperature and defect concentration than the classical form. The new arctan correlation in combination with an appropriate electronic ftc term is fitted to the Halden data base of fuel centre-line temperature measurements (represented by the "Halden ftc correlation recommendation"). Agreement is very good up to a burnup of about 60 MWd/kgU; beyond, the arctan form has a saturating burnup degradation. The new arctan correlation in combination with an appropriate electronic ftc term is also shown to describe very well our latest ftc measurements [3] on unirradiated gadolinia fuel up to 9% gadolinia content. Application to Halden measurements up to very high burnup is successfull, when combined with the so-called "rim-effect", which counteracts the saturation tendency of the new correlation at high burnup. Latest laser thermal diffusivity measurements on irradiated gadolinia fuel in the frame of the NFIR program, although not yet open for literature and not discussed in the paper, indicate very good agreement with the new arctan correlation.

1. INTRODUCTION

The fuel thermal conductivity (ftc) of the nuclear fuel UO_2 is affected during irradiation due to dissolving and precipitation of fission products in the fuel matrix, but also due to microstructural changes such as an O/M ratio change, bubble formation and irradiation damage accumulation; doping of UO_2 fuel with gadolinia has a similar effect as fission products accumulated with burnup.

Many studies in the low and medium burnup range up to now have shown, that the decrease in thermal conductivity of UO_2 fuel is proportional to the defect concentration introduced by irradiation and doping of the fuel and that the phonon term of the ftc is well described by the classical form $\frac{1}{\left(A + A_{irr} + A_{dope} + B \cdot T\right)}$, where the terms A_{irr} and A_{dope} describe the influence of the defects introduced by irradiation and doping; the term B describes the phonon-phonon interaction (Umklappprozess).

However, at very high burnups and/or gadolinia additions, it has been shown [2] that there is a change in the physical processes causing ftc degradation from mainly phonon-phonon scattering to mainly phonon-point defect scattering, which is accompanied by a reduction in ftc degradation

dependence on temperature and defect concentration. In this region, the above classical form of the phonon term seems no longer valid.

Based on literature and own measurements, it is shown below that a correlation based on the relaxation-time theory [1] of Klemens, which has a phonon term of the form $\frac{1}{x}\cdot\arctan(x)$ where x is a measure of the defect concentration introduced by burnup and doping (e.g. gadolinia additions), describes ftc degradation at large defect concentrations very well. Moreover, it is appropriate for the whole range of defect concentrations from low to high values, because it contains the classical form as a limit.

2. PROPERTIES OF THE ARCTAN FORM OF THE FTC PHONON TERM IN DIFFERENT REGIONS OF DEFECT CONCENTRATIONS

Ishimoto [2] modified the Klemens ftc theory for arbitrary defect concentrations and provides a phonon contribution λ_{Ph} to ftc, which is expressed by the following equations:

$$\lambda_{Ph} = \frac{\lambda_0}{x}\cdot\arctan(x) \qquad x = D\cdot\sqrt{\Gamma}\cdot\sqrt{\lambda_0}$$

Whereas in the Klemens theory, D is a constant, it is slightly temperature dependent at Ishimoto. $\lambda_0 = \frac{1}{B\cdot T}$ is the thermal conductivity for a defect free sample at Klemens (phonon contribution), whereas $\lambda_0 = \frac{1}{(A + B\cdot T)}$ is the ftc for fresh, undoped UO_2 at Ishimoto. For both Klemens and Ishimoto, Γ is the scattering cross section parameter for all the point defects. For different contributions to scattering we have:

$$x = \sqrt{\sum x_i^{\,2}} \text{ , with } \qquad x_i = D_i\cdot\sqrt{\Gamma_i}\cdot\sqrt{\lambda_0}$$

The index i stands for the different contributions to scattering as e.g. fission products, dopants, stoichiometry deviations, irradiation defects, etc.

2.1. Fresh UO_2, x=0

The term $\frac{\arctan(x)}{x}$ is equal to unity, giving $\lambda_{Ph} = \lambda_0 = \frac{1}{A + B\cdot T}$, the ftc phonon term for as fabricated, undoped UO_2.

2.2. Medium burnup UO_2 and/or doping, x<1

The term **Error!** can be expanded to $1 - \frac{x^2}{3}$, yielding $\lambda_{Ph} = \frac{1}{A + B\cdot T + \Gamma\cdot\frac{D^2}{3}}$, which is exactly the classical form commonly used to describe the burnup influence on ftc, when *G* is identified as burnup (see also classical form of phonon term at low to medium defect concentration shown in the introduction). The linear temperature dependence in the denominator is still the same as for fresh UO_2; also the dependence on *G* is linear.

A value for the burnup proportionality factor often found in litearature (e.g. [4]) is 0.003 (mK)/W/(MWd/kgU). The condition x < 1 then leads to a surprisingly low burnup < 15 MWd/kgU in the temperature range of interest, to which the classical form of the phonon term should be restricted; above, the arctan formulation appears to be more appropriate.

As mentioned, the burnup proportionality factor **Error!** has a slight temperature dependence in Ishimoto's formulation (see also description below). This is in agreement with a slight temperature dependence found in the Halden measurements [4].

2.3. High burnup UO_2 and/or doping, x>>1

The term *arctan(x)* approaches *p/2*, giving:

$$\lambda_{Ph} = \frac{\lambda_0 \cdot \pi}{2 \cdot x} = \frac{\pi}{2} \cdot \frac{1}{\sqrt{A + B \cdot T}} \cdot \frac{1}{D \cdot \sqrt{\Gamma}}$$

In contrast to the region of low to medium defect concentrations x < 1, the temperature dependence and the dependence on *G* in the denominator are now no longer linear for x>>1, instead, a square root dependence is observed. For high burnup and gadolinia content, this results in saturation-like effects.

3. CONFIRMATION OF ARCTAN FROM ISHIMOTO

Figures 1 and 2a and b, which are selected to demonstrate the applicability of the arctan formulation of the ftc phonon term in a wide range of defect concentrations, are taken from Ishimotos paper. The measurements performed were laser flash determinations of ftc on pure UO_2 and 6% gadolinia fuel with simulated burnup (SIM fuel) of 30, 60 and 90 MWd/kgU.

The relevance of the SIM fuel laboratory measurements for the selection of an appropriate ftc correlation is high, because the samples are unirradiated and can be precisely characterized and easily measured. An adequate representation of the real burnup effect of the fission products on ftc by SIM fuel methods has been proven earlier [5].

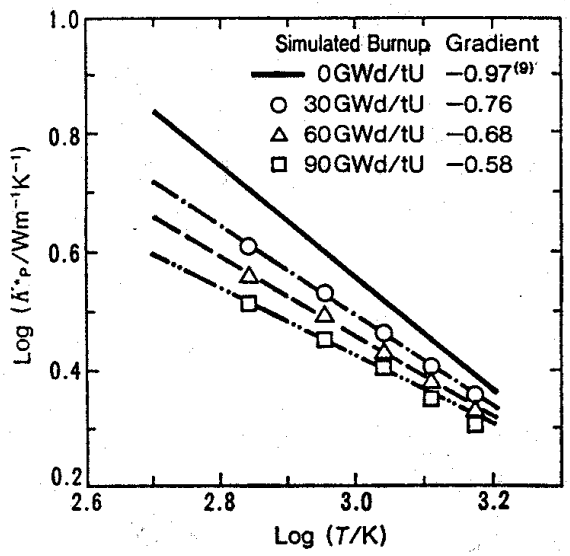

FIG.1. Logarithmic plot of phonon contribution to normalized thermal conductivities in UO_2 with simulated burnup vs. temperature (from [2]).

Figure 1 shows that already at a simulated burnup of 30 MWd/kgU, the temperature dependence of the ftc phonon term (denominator) becomes markedly weaker than linear (slope < 1). This is in agreement with the above statement that at burnups above about 15 MWd/kgU (real burnup!) already, the classical form with the linear temperature dependence in the denominator becomes inappropriate.

At a simulated burnup of 90 MWd/kgU, the slope of the data in Fig. 1 approaches 0.5, confirming the square root temperature dependence found in the high defect concentration approximation of the arctan formulation above.

Because SIM fuel only covers the effect of real burnup on ftc concerning the fission products, a transition of the ftc correlation from the classical form with a linear temperature and burnup dependence in the phonon term denominator to the high defect concentration approximation of the arctan formulation with square root dependencies should occur already well below 90 MWd/kgU.

Comparison of Figs 2a and b shows the different effect of simulated burnup on the ftc of pure UO_2 and 6% gadolinia fuel. Clearly, the effect on ftc of the gadolinia fuel is much smaller, especially in the low to medium temperature range. This is interpreted as the "saturation effect" due to the transition from a linear to a square root dependence on burnup (*G*) described above.

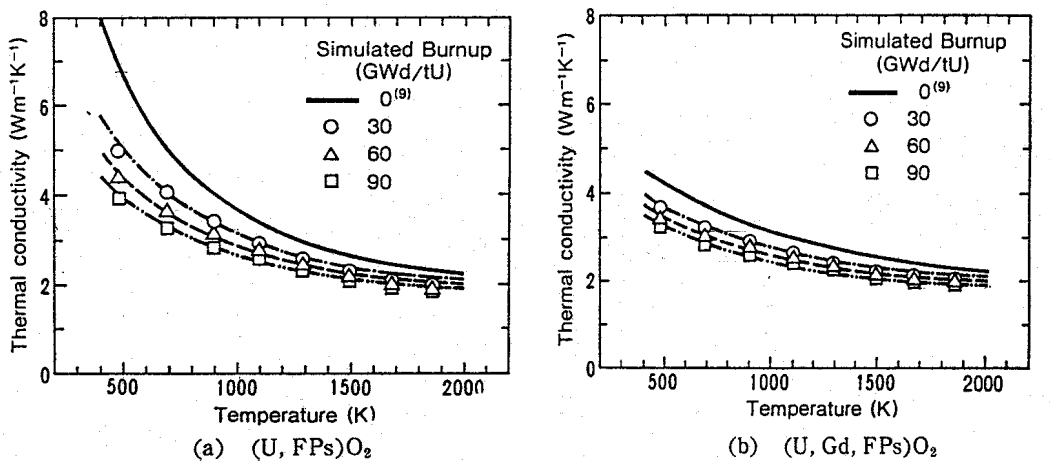

FIG. 2a and FIG. 2b. Thermal conductivities of UO_2 and UO_2/6%Gd_2O_3 with simulated burnup up to 90 MWd/kgU (normalized to 95% TD, from [2]).

The curves drawn are arctan forms of the ftc phonon term (supplemented by a common, burnup independent electronic term), fitting well through the data points.

3.1. Fitting of the arctan form to measurements on rods irradiated in Halden and to unirradiated UO_2/Gd_2O_3 fuel

The full expression for the ftc: $\lambda = \frac{\lambda_0}{x} \cdot \arctan(x) + \lambda_{electronic}$ is fitted to the data. Here λ_0 and $\lambda_{electronic}$ are the ftc phonon term for as fabricated UO_2 and the electronic term used at Siemens, respectively and *x* is a superposition of a burnup term and a gadolinia term:

$$x^2 = x_{bu}^2 + x_{Gd}^2 \text{ with } x_{bu}^2 = D_{bu}^2 \cdot burnup \cdot \lambda_0 \text{ and } x_{Gd}^2 = D_{Gd}^2 \cdot Gd\% \cdot \lambda_0$$

Just like Ishimoto, we assume *D* to have a moderate temperature dependence of the form *exp(-const T)* with the constant in the exponent of the order of 10^{-4} K^{-1}.

3.1.1. Measurements in Halden

In [4], a large data base of in-pile fuel centre-line temperature measurements in Halden and laser flash measurements of thermal diffusivity on irradiated fuel samples is discussed. There, also a formula is recommended which can be regarded as a consensus description of this data base. This Halden recommendation formula was taken as a fitting basis for the new correlation (determining D_{bu}). The fitting range with respect to burnup is limited to a burnup of about 60 MWd/kgU because of the saturation behavior of the new correlation.

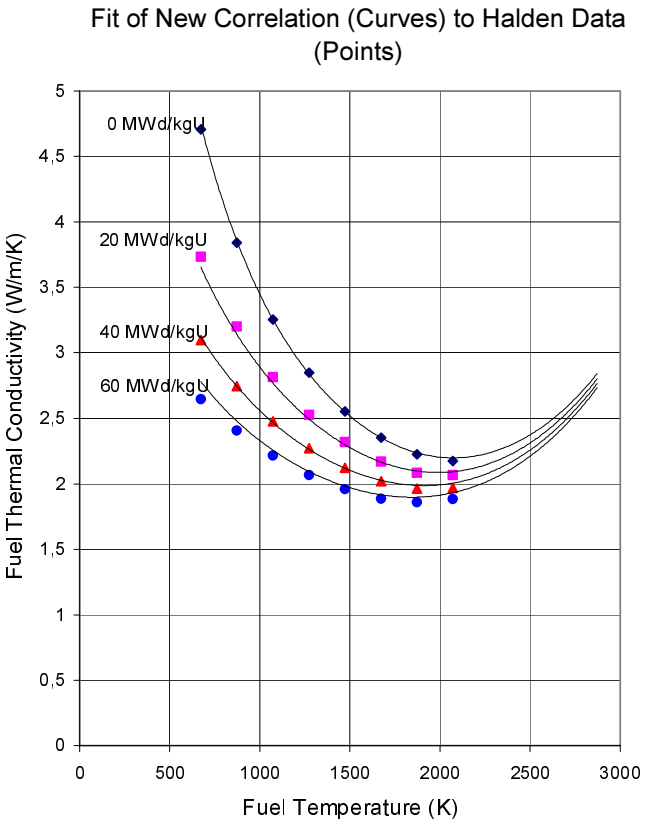

FIG. 3. Arctan correlation fitted to the Halden recommendation formula (Wiesenack [4], ftc at 95% TD).

In Fig. 3 the Halden recommendation (points) and the fitted new correlation (curves) are compared. The Halden recommendation is used only in the temperature range covered in the experiments (up to about 1600°C). Agreement between the new model and the Halden recommendation is very good up to 40 MWd/kgU. At 60 MWd/kgU, the saturation tendency of the new model becomes apparent at low fuel temperature.

3.1.2. Unirradiated UO_2/Gd_2O_3 fuel with up to 9 w% Gd_2O_3

The new Siemens laboratory laser flash measurements [3] were taken to determine the Gadolinia fitting parameter D_{Gd} for the new correlation. It is shown in Fig. 4 that the new correlation

describes the measurements very well. Slight deviations occur for 9% Gd_2O_3, where the measurements (triangles) display a somewhat less pronounced temperature decrease.

Especially, the trend of vanishing Gd influence on ftc at high temperatures above about 1900 K and consequently approaching ftc values for pure UO_2 and UO_2/Gd_2O_3, independent of gadolinia content, is excellently described by the new correlation. Attempts to fit this trend with the old, classical correlation failed; it led to overlapping of the ftc for fresh UO_2 and gadolinia fuel in the high temperature range. The gadolinia data thus also show, that the arctan form is more appropriate than the classical form.

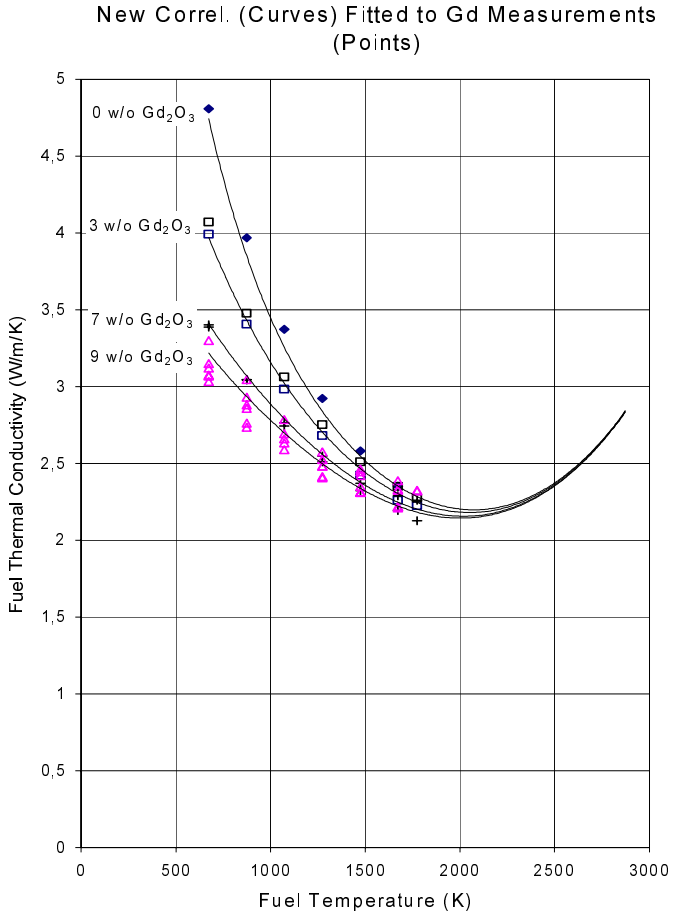

FIG. 4. Arctan correlation fitted to the latest Siemens fuel thermal conductivity measurements (laser flash method) on unirradiated UO_2/Gd_2O_3 fuel (at 95% TD, [3]).

By setting $D_{bu}^2 \cdot burnup \cdot \lambda_0 = D_{Gd}^2 \cdot Gd\% \cdot \lambda_0$, the effect of the Gd dopant on ftc can be compared to the burnup effect. The result in the temperature range of interest is that 1w/o Gd_2O_3 addition corresponds to 4 MWd/kgU.

3.1.3. Saturation of ftc degradation at high burnup and Gd_2O_3 content

In Fig. 5 the relative ftc as a function of burnup is compared for the classical form $\frac{1}{\left(A + A_{irr} + A_{dope} + B \cdot T\right)}$ (points) and the new arctan correlation (curve) at 7w/o Gd_2O_3.

For A_{irr} = 0.0027 · BU (a value used in our fuel rod design code) the degradation of the classical form is much steeper than the arctan function; a reduced burnup dependence in the classical form of A_{irr} □0.0014 · BU comes closer. At very high burnup well above 100 MWd/kgU, however, which becomes relevant in the rim region of the fuel pellet with high burnup, the saturation trend of the arctan form is progressively stronger than in the classical form.

3.2. Application of the arctan form to Halden measurements up to very high burnup

In the Halden Ultra High Burnup (UHB) rig IFA-562, fuel centre-line temperatures are measured up to burnups above 80 MWd/kgU. At such high burnups, the pellet rim effect is known to have a strong influence on fuel temperature (increase).

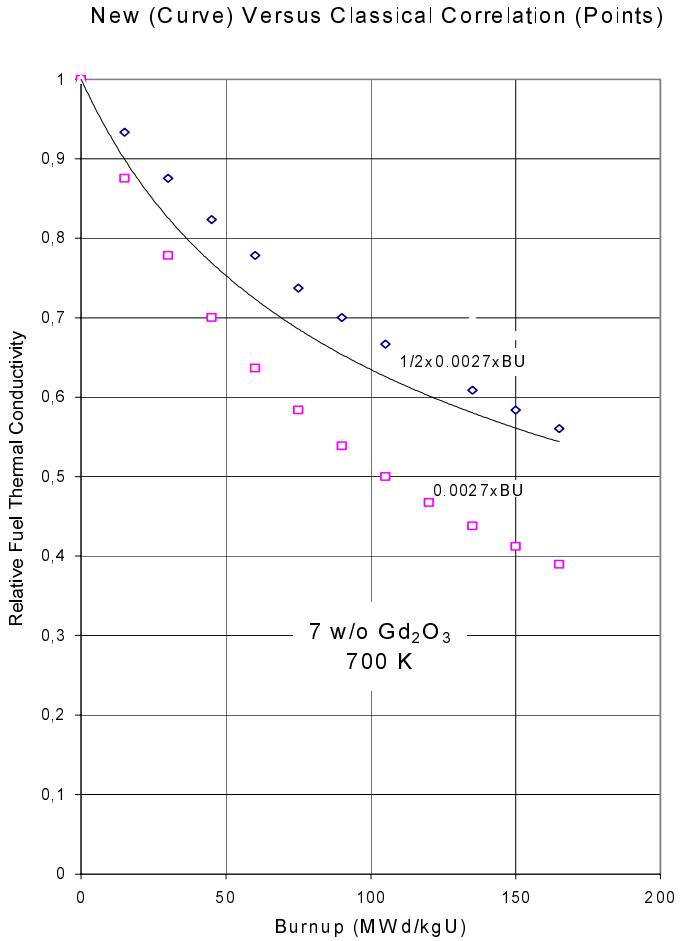

FIG. 5. Relative fuel thermal conductivity degradation for high burnup. Const x 0.0027 is the additive burnup term in the classical phonon term.

The UHB data are central to the Halden recommended ftc correlation described by Wiesenack in [4], which fits the UHB data very well and thus can be used as a representation of the UHB data.

Comparing the UHB ”data” (Wiesenacks correlation) with the classical form and the arctan form, taking the pellet rim effect into account, yields very good agreement for the arctan form and a fuel centre-line overprediction of nearly 100 K for the classical form at 80 MWd/kgU, as shown in Fig. 6. The overprediction of the classical form at burnups above about 50 MWd/kgU is due to the rim effect; in the arctan form, the rim effect is balanced by the saturation in this burnup region.

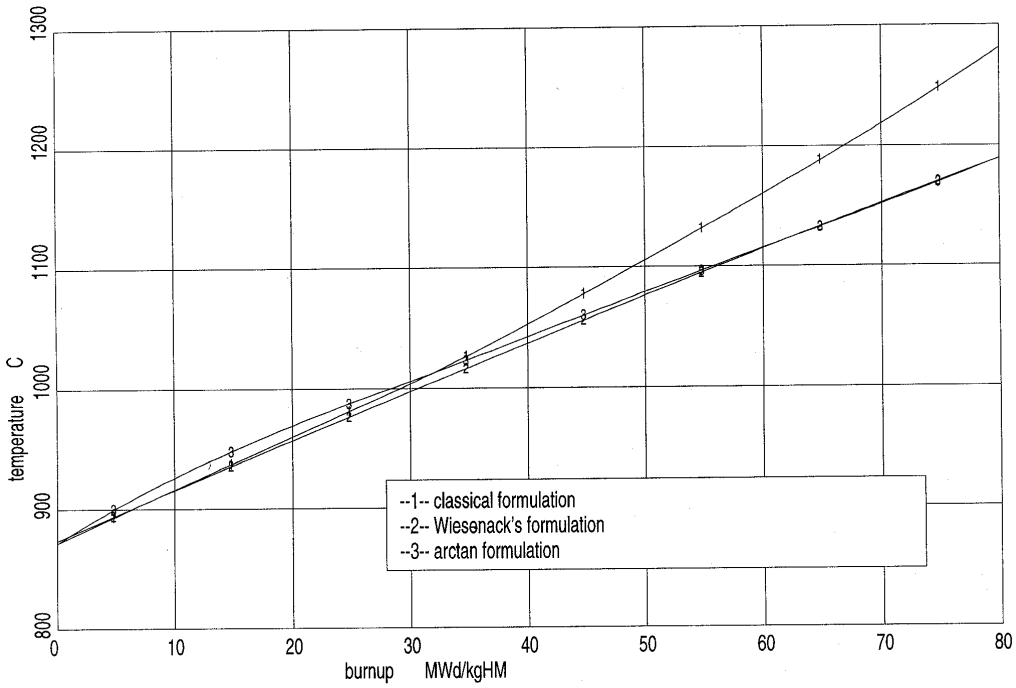

FIG. 6. Pellet centre-line temperature vs. burnup at 250 W/cm calculated with different fuel conductivity correlations with degradation of ftc in the rim region (simplified calculation with flat power profile).

REFERENCES

[1] KLEMENS, P.G.: Phys. Rev., 119, 507 (1960).

[2] ISHIMOTO et al., "Effects of soluble fission products on thermal conductivities of nuclear fuel pellets", J.Nucl. Sci.Technol.31(8), pp.796-802 (August 1994).

[3] JTK 1998 G.GRADEL, W.DOERR, H.GROSS, to be published.

[4] W.WIESENACK et al., "Fuel conductivity degradation assessment based on HBWR data", HWR-469, 96-05.

[5] P.G.LUCUTA et al., "Proc. 2nd Int. Conf. CANDU Fuel", October 1989, Pembroke, Ontario, Canada, Ed. I.J. Hastings, CNS, Toronto (1989) 132.

INFLUENCE OF RIM EFFECT ON FUEL CENTRE TEMPERATURE

N. IKATSU, N. ITAGAKI, K. OHIRA
Nuclear Fuel Industries, Ltd, Tokai-mura, Japan

K. BEKKER
Energy Research Foundation ECN, Petten, Netherlands

Abstract

In recent years the RIM effect in the high burnup region has been discussed in many papers. The RIM effect is characterized by higher burnup, subdivision of grains, and formation of fine pores (porosity increase) at the pellet periphery. In this paper we report the analysis results of the increase of pellet centre temperature by the RIM effect. The pellet centre temperature was calculated using a radial power distribution and the pellet thermal conductivity as a function of the pellet porosity and burnup. The radial porosity distribution was evaluated from SEM images of BWR fuel pellets irradiated up to about 60 GW·d/t. The influence of porosity of pellet thermal conductivity was evaluated by FEM analysis. The thermal conductivity was derived from the measured thermal diffusivity data in a previous report. In the peripheral region of a pellet irradiated to 60 GW·d/t, the maximum porosity was about 15-20%. The correction function for the influence of porosity on pellet thermal conductivity was derived from the results of FEM analysis. The analysis conditions were that the pellet burnup was 60 GW·d/t, the pellet surface temperature was 400'C, and the linear heat generation rate was 300 W/cm. The analysis revealed that the influence of the RIM effect on fuel centre temperature is small, that is to say, about 20°C for the above conditions. In addition, The results of pellet centre temperature analysis showed that the RIM effect influence on pellet temperature was not significant up to 75 GW·d/t. However, the influence of the RIM effect cannot be ignored in the ultra high burnup region close to 100 GW·d/t. Thus, it is necessary that more data for rim growth in the ultra high burnup region will be collected to evaluate fuel performance more accurately.

1. INTRODUCTION

In recent years many reports have been published about the RIM effect observed in high burnup LWR fuels. The effects of RIM were first reported in the 19608. But no longer attention was given then since high burnup was not a topic. In the 1980s, the RIM structure was reported again [l]. Because high burnup fuel was attended in this time, many studies were then performed to clarify the mechanisms of RIM formation, the characteristics of RIM structure, and the degradation in fuel performance. These studies have obtained considerable knowledge about RIM.

The structure of RIM is characterized as grain subdivision and fine pores (porosity increase) in the pellet periphery region. Two mechanisms of formation of the RIM structure are suggested. One is that original grains are divided into submicron grains. The other is that subdivided grains are recrystallized.

The fine pores formed in the RIM region contain fission gas (FP gas). Because the pressure of the FP gas is considered to be very high, FP gas release from the pores was concerned. But a report discloses that FP gas released from the RIM region is not a major contribution to the total FP gas released from the whole pellet. On the other hand, the increase of porosity in the RIM region remarkably decreases thermal conductivity in the peripheral region of pellet. There is concern that the decreasing thermal conductivity may introduce a harmful influence to fuel performance in the high burnup region. That is the increase in pellet centre temperature may result in an increase in the FP gas release rate.

In this study, we evaluated the influence of decreased pellet thermal conductivity that results from the RIM induced porosity increase. The pellet centre temperature increase due to the RIM effect was also examined.

2. PIE RESULTS

The samples for PIE tests were supplied from 9 X 9 fuel irradiated in a German commercial reactor. The enrichment and density Of UO_2 pellets were 4 % and 95 % T.D. The fuels were irradiated for six reactor cycles, poolside and hot cell PIE examinations were executed after the third, fifth, sixth irradiation cycles. SEM, EPMA examination of pellet cross section and measurement of FP gas release rate and so on were performed during the hot cell PIE.

Figure 1 shows SEM images of Pellet cross sections. SEM images show that three-cycle irradiated (about 36 GWd/t) fuel already has fine pores formed in the peripheral region. In the fuels irradiated for five cycles (about 49 GWd/t), porosity increased significantly. The porosity at the pellet edge and the region 0. 1 mm from the pellet edge were obtained by image analysis. The relationship between porosity and burnup is shown in Figure 2.

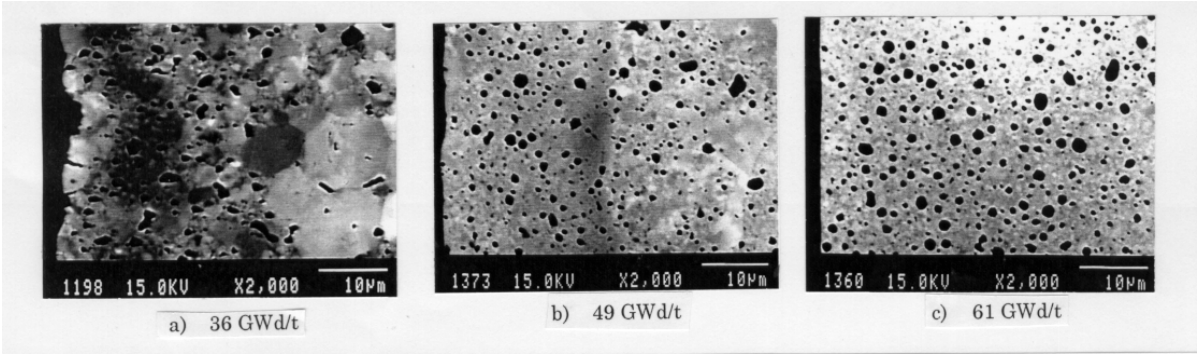

FIG. 1. SEM images of pellet peripheral region.

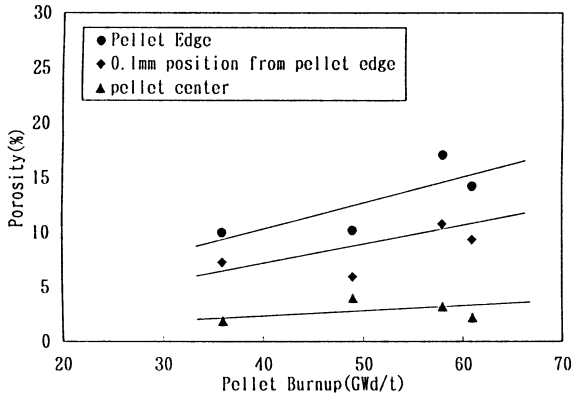

FIG. 2. Porosity dependence on burnup.

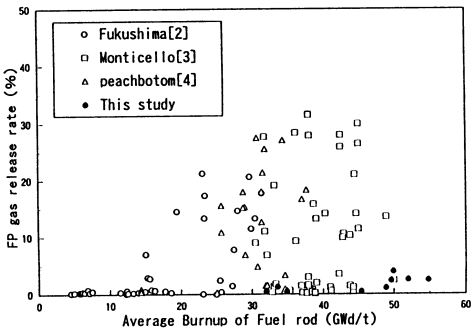

FIG. 3. FP gas release rate.

The porosity in the pellet peripheral region irradiated to about 36 GW·d/t was about 10 %. The growth rate of porosity increases linearly in the region where pellet burnup is over about 36 GW·d/t. For pellets irradiated to about 60 GW·d/t, the porosity reached almost 20%.

The measurements of the FP gas release rate and the Xe/Kr ratio from fuel rods irradiated over 50 GW·d/t are shown in Figure 3 [2–5]. The FP gas release rate of high burnup fuel was about a few percent; a noticeable increase of FP gas release rate was not observed. Moreover, as shown in Figure 4, by analysing the Xe/Kr ratio, the FP gas release from the pellet rim (where the Pu burn ratio is larger) could be negligible when compared with the total FP gas release [5].

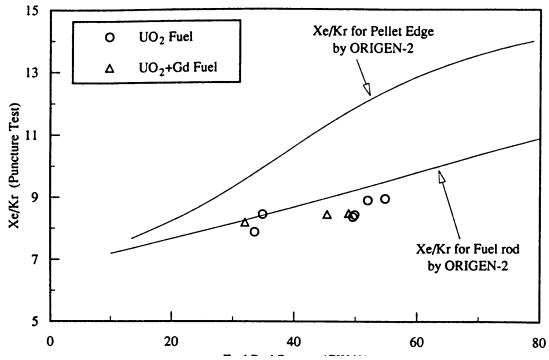

FIG. 4. Calculated result of Xe/Kr ratio [5].

3. EVALUATION OF PELLET THERMAL CONDUCTIVITY IN HIGH BURNUP FUEL

3. 1. Thermal conductivity of high burnup fuel

It is well known that the thermal conductivity of a pellet decreases with burnup. It has been confirmed previously that pellet thermal diffusivity measured using the laser-flush method on fuel irradiated to about 60 GW·d/t in a commercial BWR. A new thermal conductivity model based on the results was developed. This is shown in Figure 5 [6].

On the other hand, because in RIM region the local burnup is very high, the thermal conductivity decreases in the RIM region remarkably.

The pellet temperature was analysed by consideration of the burnup depend model and the burnup distribution in RIM region, and then the calculated pellet temperature was confirmed to correlate well with the measured pellet temperature in operation.

In this study we determined the pellet temperature in the thermal conductivity model. The dependence of thermal conductivity on burnup is shown in Figure 6 [7–9].

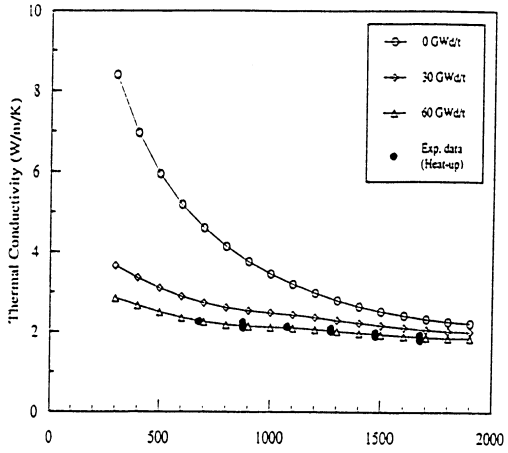

FIG. 5. Thermal conductivity considering irradiation [6].

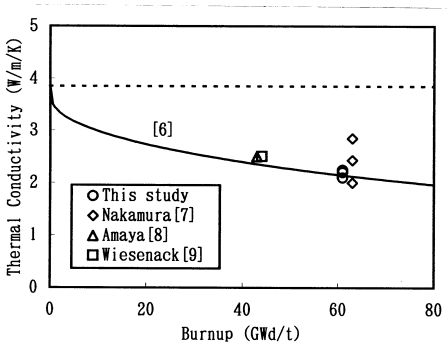

FIG. 6. Thermal conductivity dependence on burnup (at 827K).

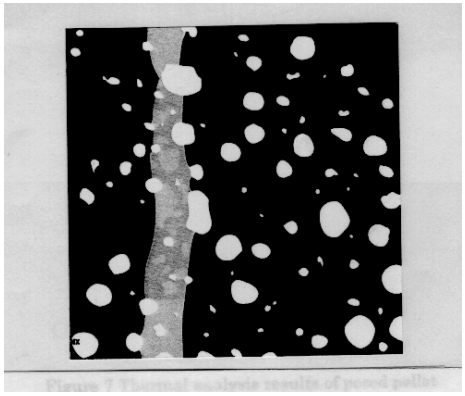

FIG. 7. Thermal analysis results of pored pellet by finite element method.

3. 2. Decrease of thermal conductivity by pores

The decrease of thermal conductivity caused by pellet porosity was analysed by the finite element method (FEM). The FEM code ANSYS was used.

When thermal conductivity was analysed, the actual pore shapes from SEM images were used. For these pores, after two and three-dimensional analyses were performed, the correlation equation for thermal conductivity compared with the 2D analysis and 3D analysis was obtained. Then the thermal conductivity for the 2D cross section of any formed pore was obtained, and the value was correlated into the 3D form's values. Figure 7 shows an example of the thermal analysis result by FEM [10].

Using the above-mentioned method, the following correction equation was obtained:

$$k_{3D} = k_0 \ (1\text{-}P)^{1.6}$$

Where k is the thermal conductivity without porosity, k_{3D} is the porosity corrected thermal conductivity, and P is porosity.

Figure 8 shows the results of this study compared with the results of other studies [11–13]. The results obtained by this study are almost equivalent to Schultz's equation, which assumed a pore was a simple sphere.

The forms of all equations were the same, the only difference was in the exponent of the term "1-P". The exponent has two values, one is about 1.6, formed in this study and by Schultz, and the other is about 2.4, obtained by Shimizu and Loab.

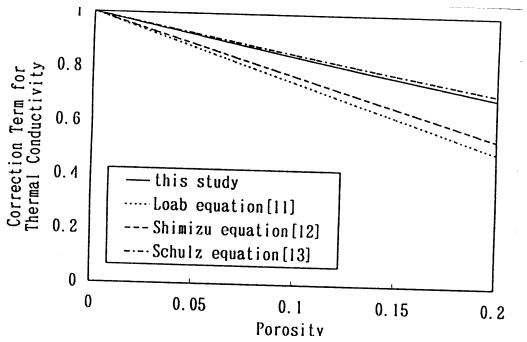

FIG. 8. Thermal conductivity degradation by porosity (compared with other study).

The reason our exponent differs from Loab's is that the actual pore forms at the rim are very close to a simple sphere (shown in Figure 1). On the other hand, Loab's equation and Shimizu's equation were obtained by using pores having irregular shapes.

4. ANALYTICAL RESULTS

The pellet centre temperature was calculated by thermal conductivity while considering the porosity effects.

Figure 9 shows the porosity distribution model for the radial direction. This was obtained from the results of the SEM observations shown in Figure l. In this study, the porosity distribution was modelled as a quadratic fit. Because the porosity measurements did not detect porosity differences in the inner region of the pellet, porosity is constant except in the rim region.

When the pellet temperatures were analysed, the values of the conditions were held constant except porosity, these conditions were:

pellet surface temperature	:	400°C
linear heat rate	:	300 W/cm
pellet radius:	:	4.7 mm

Figure 10 shows analytical results of pellet temperature versus radial position. This shows that the pellet centre temperature increases with an increase of porosity. The dependence of pellet centre temperature increase as a function of burnup is shown in Figure 11. The RIM effect increases with burnup, but the temperature increase is small. For example, in the case of about 60 GW·d/t, the increase in pellet centre temperature is only 20°C.

5. DISCUSSION

The increase of the pellet centre temperature resulting from the RIM effect of fuel irradiated to about 60 GW·d/t was analysed. The analysis confirmed that the influence of porosity is small.

The RIM effect is small at a burnup of about 60 GW·d/t. The porosity may increase significantly at a much higher burnup, as suggested in some reports [14].

Therefore, the influence of the RIM effect to the pellet centre temperature was evaluated assuming the use of higher burnup pellets (greater than 60 GW·d/t). When the analysis was executed, we assumed two cases for the increase in porosity as shown in Figure 12.

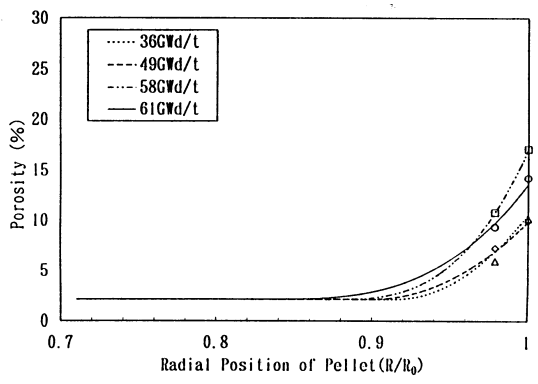

FIG. 9. Radial distribution of porosity.

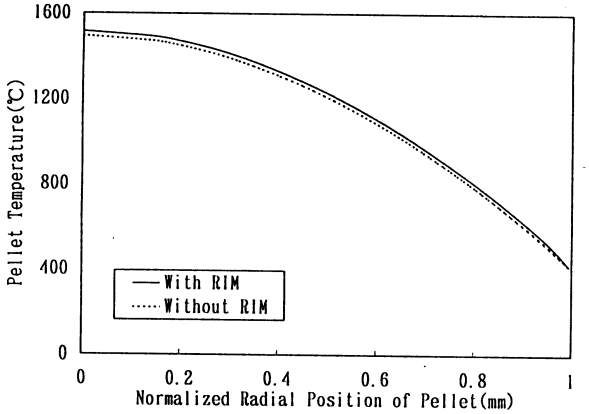

FIG. 10. Analytical results of pellet temperature (at 300 W/cm).

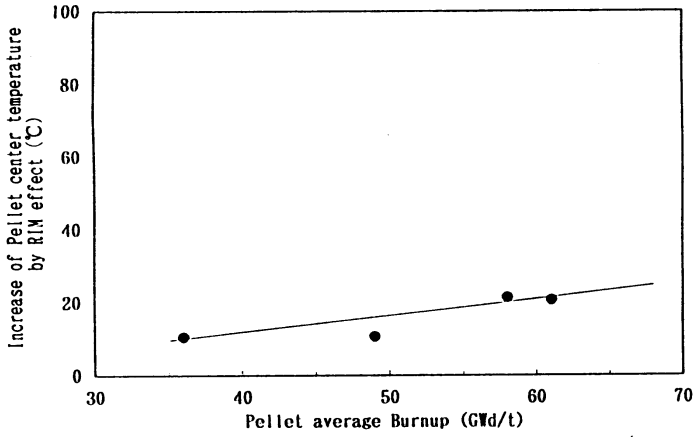

FIG. 11. Pellet center temperature increase vs burnup (at 300 W/cm).

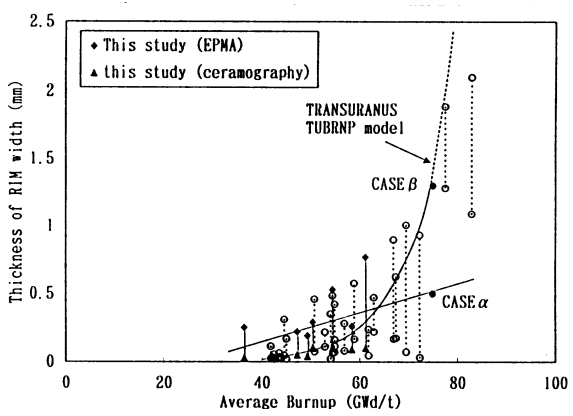

FIG. 12. RIM width by Lassmann report.

One case assumed a constant increase rate for porosity, such as in the lower burnup region. In this study the porosity increases linearly until 60 GW·d/t; thus we assumed the rate of increase does not change at 70 GW·d/t or 80 GW·d/t. (CASE α)

The other assumed case is that the growth rate of porosity is much greater than that at lower burnup. Reported as Lassmann's model, the RIM width rapidly increases over the 60 GW·d/t region and finally the entire pellet becomes RIM structure. In this model, average 75 GW·d/t burnup pellets have a RIM width of l mm. As in the Lassmann model, we assume both the porosity and the rim width to be rapidly increasing. (CASE β)

Figure 13 shows the two cases of porosity. Other parameters remained unchanged.

Figure 14 shows the analytical results of pellet centre temperature versus radial position for 75 GW·d/t.

In CASE α, the increase of pellet centre temperature was about 30ºC at 300 W/cm. Therefore we conclude that the influence of the RIM effect to the pellet temperature is small. But in CASE β, the increase of the pellet centre temperature was about 110ºC at 300 W/cm, 70ºC at 200 W/cm. Figure 14 shows the influence of burnup on the increase of pellet centre temperature. Because the linear heat rate of standard commercial fuel at 75 GW·d/t may be lower than 200 W/cm, we can conclude that the influence of the RIM effect on fuel centre temperature is not significant at 75 GW·d/t.

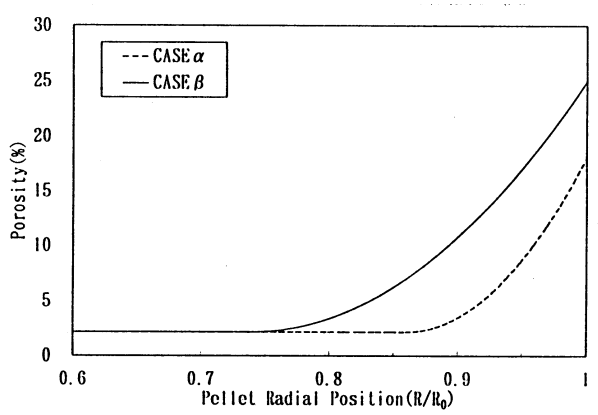

FIG. 13. Porosity model in 75 GW·d/t (assumed).

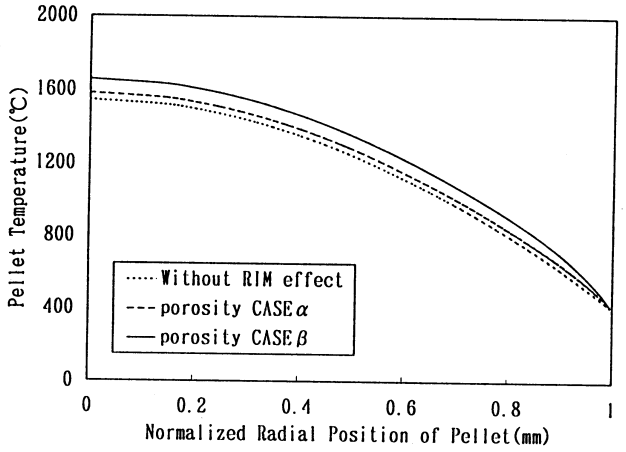

FIG. 14. Pellet temperature vs. radial position for 75 GW·d/t (at 300 W/cm).

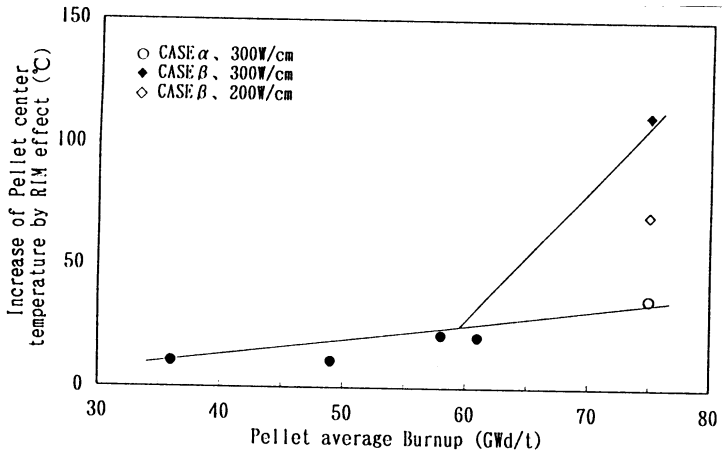

FIG. 15. Pellet center temperature increase by porosity over 60 GW·d/t.

However, from the Lassmann model, the rim effect might alter whole pellets at ultra high burnup (close to 100 GW·d/t) and this influence cannot be ignored. In the case of a RIM effect involvement of a whole pellet, the pellet centre temperature will increase 300°C or more at 200 W/cm in case of 20 % porosity.

6. CONCLUSION

For the fuels irradiated about 60 GW·d/t in a commercial reactor, pellet porosity was evaluated by image analysis. Using this porosity, the thermal conductivity decrease and a correction equation were obtained. The results of pellet centre temperature analysis showed that the RIM effect influence on pellet temperature was not significant up to 75 GW·d/t. However, the influence of the RIM effect can not be ignored in the ultra high burnup region close to 100 GW·d/t. Thus more data for rim growth in the ultra high burnup region need to be collected to evaluate fuel performance more accurately.

ACKNOWLEDGEMENT

The authors wish to thank Mr. R. Manzel of Siemens AG in KWU NBTW, Germany, for his many suggestions and valuable support.

REFERENCES

[1] PATI, S.R., et al., "Fission Gas Release from PWR Fuel Rods at Extended Burnups," ANS Topical Meeting on LWR Light Water Reactor Fuel Performance, Orlando, Florida, 1985.

[2] MISHIMA, Y., et al., "Proving Test on Reliability for BWR Fuel Assemblies", Journal of the Atomic Energy Society of Japan, No.2, Vol.29, 1987.

[3] "BWR Fuel Bundle Extended Burnup Program", DOE / ET / 34031-1~18, 1980-1985.

[4] "BWR Fuel Rod Performance Evaluation Program", EPRI NP-4602, May 1986.

[5] ITAGAKI, N., et al., "Fission Gas Release and Pellet Microstructure Change of High Burnup BWR Fuel," IAEA Technical Committee Meeting, Tokyo, Japan, 1996.

[6] OHIRA, K., et al., "Thermal Conductivity Measurements of High Burnup UO_2 Pellet and a Benchmark Calculation of Fuel Center Temperature," ANS Topical Meeting on LWR Fuel, Portland, USA, 1997.

[7] NAKAMURA, J., et al., "Thermal Diffusivity Measurement of High Burnup UO_2 Pellet," ANS Topical Meeting on LVYT Fuel, Portland, USA, 1997.

[8] AMAYA, M., et al., "Thermal Conductivity Measurements on Power-ramped Irradiated UO_2 Pellets," TopFuel 97 Manchester on 9-11 June 1997.

[9] WIESENACK, W., "Experimental Techniques and Results Related to High Burn-up Investigations at the OECD HALDEN REACTOR PROJECT," IAEA TCM Pembroke Ontario Canada, 28 May, 1992, IAEA-TECDOC-697, p. 118, 1993.

[10] BAKKER, K., et al., "The Contribution of Thermal Radiation to the Thermal Conductivity of Porous UO_2," ECN-RX-94-073.

[11] LOAB, A.L., "J.Am. Ceram. Soc., 37-2, 1954.

[12] SHIMIZU, S., et al., "Thermal Conductivity of Porous UO_2 Pellet," 1993 Annual Meeting of the Atomic Energy Society of Japan, K14.

[13] SHULTZ, B., "Thermal conductivity of porous and highly porous materials," High Temperatures — High Pressures, 1981, vol. 13, 649-660.

[14] LASSMANN, K., et al., "Modeling the high burnup UO_2 structure in LWR fuel," Journal of Nuclear Materials 226 (1995) 1-8.

FUEL BEHAVIOUR IN OFF-NORMAL CONDITIONS
(Session 5)

Chairpersons

K. VALTONEN
Finland

T. JONSSON
Sweden

ASSESSMENT OF CLAD INTEGRITY OF PHWR FUEL PIN FOLLOWING A POSTULATED SEVERE ACCIDENT

B.K. DUTTA, H.S. KUSHWAHA, V. VENKAT RAJ
Reactor Design and Development Group,
Bhabha Atomic Research Centre,
Mumbai, India

Abstract

A mechanistic fuel performance analysis code FAIR has been developed. The code can analyse fuel pins with free standing as well as collapsible clad under normal, off-normal and accident conditions of reactors. The code FAIR is capable of analysing the effects of high burnup on fuel behaviour. The code incorporates finite element based thermo-mechanical module for computing transient temperature distribution and thermal-elastic-plastic stresses in the fuel pin. A number of high temperature thermo-physical and thermo-mechanical models also have been incorporated for analysing fuel pins subjected to severe accident scenario. The present paper describes salient features of code FAIR and assessment of clad integrity of PHWR fuel pins with different initial burnup subjected to severe accident scenario.

1. INTRODUCTION

The integrity of fuel rods under normal, off-normal and accident conditions is an important consideration during fuel design of an advanced nuclear reactor. The fuel matrix and the sheath form the primary barriers in preventing the release of radioactive materials into the primary coolant. An understanding of the fuel and clad behaviour under different reactor conditions, particularly the severe accident conditions, is always desirable for the safe operation of nuclear reactors and mitigation of the consequences of accidents, if any. The severe accident conditions are typically characterized by the energy deposition rates far exceeding the heat removal capability of the reactor coolant system. This may lead to clad failure due to large scale pellet-clad interaction or even clad melting. The fuel rod performance is affected by many interdependent complex phenomena involving extremely complex material behaviour. The versatile experimental data base available has led to the development of powerful analytical models to characterize fuel under extreme scenarios. A number of fuel performance analysis codes have been developed in different parts of the world based on such analytical models. In BARC, the code 'FAIR' has been developed over the last seven years [1]. This code is based on the application of the finite element method for thermo-mechanical modelling and mechanistic modelling of various phenomena affecting the fuel behaviour. The code is capable of analysing the effects of high burnup on fuel behaviour. The code has been validated against a set of data from operating fuel pins subjected to normal and off-normal conditions at high burnup, as a part of the IAEA-Coordinated Research Project (CRP) on FUMEX (FUel Modelling at EXtended burnup). The code 'FAIR' has been subsequently modified to handle fuel pins subjected to extreme accidental scenarios.

During severe accident conditions, the mode of failure of clad is essentially due to clad ballooning. This occurs due to a combination of rod internal pressure and clad temperature. The combination of internal pressure and clad temperature leads to large scale thermal creep in the clad material. The magnitudes of pressure and clad temperature primarily depend upon two input parameters. These are, the amount of energy deposited in the fuel pellet and the coolant heat transfer coefficient. As a part of the present analytical study, a severe accident scenario involving LOCA with the coincidental failure of ECCS has been considered. This is one of the dual failure accidents considered for PHWRs. For such a scenario, the fuel pin failure is characterized by the large scale clad ballooning with the progress of accident time. Based on the data available in published literature, the analytical criterion selected for clad failure is the accumulation of a predefined local creep strain.

The creep strain rates calculated as a function of rod pressure and clad temperature for each time step are integrated with respect to time to obtain the cumulative creep strain. A parametric study has been performed to assess the clad failure time with the burnup of the fuel pin during the course of the accident.

The following sections deal with the description of the code 'FAIR', the accident analysis procedure, the results of the parametric study and the conclusions drawn through the present study.

2. DESCRIPTION OF CODE 'FAIR'

The code 'FAIR' models various physical, chemical and mechanical phenomena occurring in a nuclear fuel during its residence period in a reactor using mechanistic principles. This code is capable of analysing the complex material behavior of fuel pins and the interactive nature of various phenomena affecting the fuel pin behavior. The code is equipped with high burnup modelling capabilities, such as pellet thermal conductivity degradation with burnup, redistribution of radial flux at high burnups, enhanced fission gas release at high burnups. The organisation of this code follows the proven principles of fuel rod modelling, such as, coupling between thermal, mechanical and fission gas release modules, concurrent analysis of different axial sections of fuel rods to consider fission gas mixing. In addition to this, local analysis such as clad ridging can also be performed. The modular nature of the code offers flexibility in incorporating modifications to model fuels of different materials and reactors. A separate module has been incorporated in the code FAIR for performing statistical analysis of fuel pins. Besides the sequential version of the code FAIR, a parallel version is also developed and implemented on a parallel processing system [2]. This parallel version facilitates high speed computation by performing simultaneous analysis of different axial sections of fuel pins for considering axial fission gas mixing.

2.1. Thermo mechanical module of FAIR

The thermo mechanical module of the code FAIR is based on 2-D axisymmetric Finite Element Method [3]. The thermal analysis module can analyse both steady state and transient situations. Both Dirichlette and Neumann boundary conditions can be analysed. The nonlinearities associated with temperature dependent material properties are solved using iterative techniques considering each step as a quasi static state. The convergence of solution is checked by specifying a convergence criterion for the norm of temperatures. Direct integration method (Crank-Nicholson scheme) is employed for analysing transient cases. The mechanical analysis module can analyse thermal visco-plastic loading conditions, which can take care of material nonlinearity of pellet and sheath due to thermal, pressure and creep loadings. The generation of nonlinear characteristic equations is done by Modified Newton-Raphson method. Additional strains on the pellet due to thermal and irradiation induced densification and swelling and strains due to pellet cracking and relocation are treated as initial strains as per standard Finite Element procedure.

The code incorporates three different high temperature creep models for use in severe accident analysis. These models are due to Holt (NIRVANA) [4], Donaldson [5] and Shewelt [6]. These models represent creep rate in an Arhenius type relation as a function of clad temperature and stress.

2.2. Salient fuel models in FAIR

For modelling fission gas release, Standard ANS 5.4 model [7], empirical model based on Halden data [8] and microstructure dependent fission gas release models [9–12] are implemented in the code FAIR. The pellet densification and swelling, grain growth, thermal and mechanical material properties are implemented based on MATPRO [13]. The thermal conductivity degradation of pellet with burnup is modelled using the data available in open literature [14,15]. The variation of flux

profile across pellet radius and the change in this profile with burnup are modelled using RADAR model [16]. The code consists of a separate module for modelling the pellet-clad-interaction (PCI) induced fuel failure [17], which models crack initiation and propagation in clad as a function of the sheath strains and the amount of free Iodine available on the inner sheath surface.

2.3. Statistical analysis module of FAIR

The code FAIR incorporates Probabilistic methods of analysis based on Monte-Carlo technique. The probabilistic methods supplement the mechanistic modelling of fuel behaviour. The effect of variation in the geometry of the fuel due to manufacturing defects, in particular the gap between the pellet and the sheath, the errors in power measurement, the uncertainties in the material properties are studied by varying these parameters in a random fashion. The variations are considered to be following a Gaussian distribution. A number of repetitive analyses are performed considering these variations and the variation of output parameters such as fuel temperatures, fission gas release and fission gas pressure are indicative of the uncertainties involved in the modelling.

3. VALIDATION OF CODE FAIR

The individual models of the code FAIR have been tested and validated against the standard bench mark cases published in the literature. The performance evaluation of FAIR as an integral fuel analysis code has been done against a number of studies. One of the studies was based on an earlier project on fuel rod modelling code evaluation by Electric Power Research Institute [18]. Another study was carried out for simulating analytically the threshold power ramp criteria (P_c, ΔP_c curves) for a Pressurised Heavy Water Reactor (PHWR) fuel rod and comparing the same with the experimental database [19]. The main validation of code FAIR for high burnup fuel pins was carried out during the blind code comparison exercise of IAEA CRP on *FU*el *M*odelling at *EX*tended burnups, FUMEX [20]. The details of these validation studies can be found in References [21–23].

4. SEVERE ACCIDENT ANALYSIS OF PHWR FUEL PINS

During severe accident conditions, the rate of energy deposition exceeds the heat removal capacity of the reactor heat removal system. The likely mode of failure under such conditions is the clad ballooning. This occurs due to a combination of rod internal pressure and clad temperature. The combination of internal pressure and clad temperature leads to a large scale thermal creep of the clad. The variation of pressure and clad temperature with the time of accident basically depend upon three parameters. These are the amount of stored heat energy in the pin at the time of initiation of accident, the amount of heat energy deposited during the accident and the heat transfer conditions at the clad surface. The effect of these parameters on a 220 MW(e) Indian pressurised heavy water reactor (PHWR) fuel pin clad has been studied using the code FAIR.

The accident scenario pertains to the failure of a fuel pin, which is subjected to a power profile and heat transfer conditions similar to those obtained for a LOCA coincident with loss of ECCS. Such an accident is one of the dual failure accidents considered for PHWRs. The thermal hydraulic conditions for such scenario has been obtained using the relevant thermal-hydraulic analysis codes [24]. The analysis has been done to determine the time of clad ballooning after the accident for fuel pins having different burnups at the time of initiation of the accident. Based on the published literature, the analytical criterion selected for clad failure is the accumulation of 75% local creep strain. The calculated creep strain rates as a function of rod pressure and clad temperature for each time step are integrated with time to obtain the cumulative creep strain.

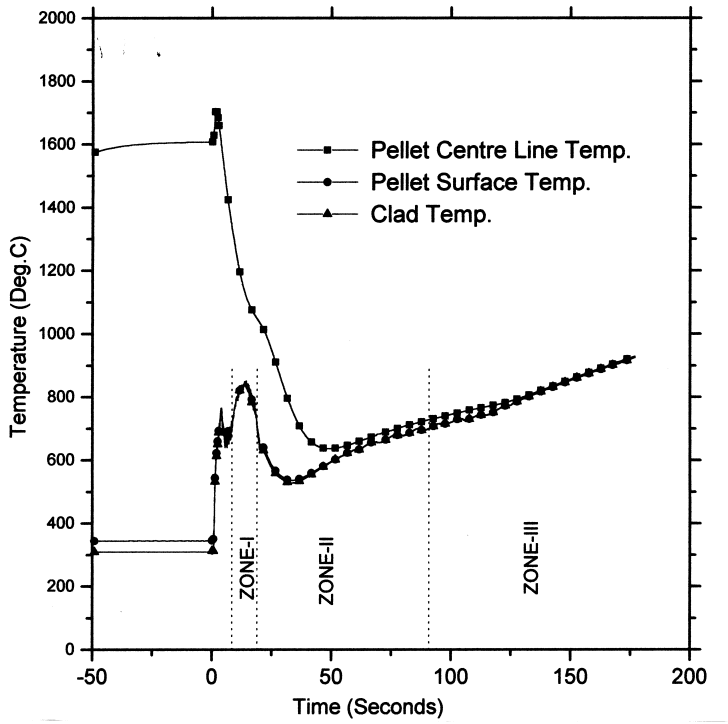

FIG. 1. A typical temperature transient in a PHWR fuel pin subjected to LOCA with ECCS failure.

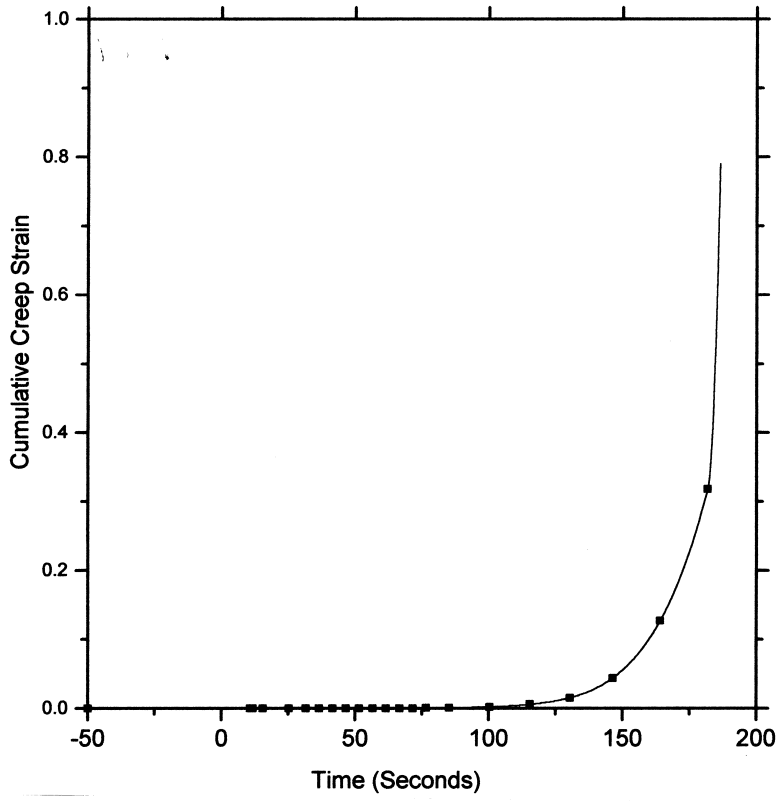

FIG. 2. A typical variation of accumulated local creep strain in a PHWR fuel pin sheath under LOCA with ECCS failure.

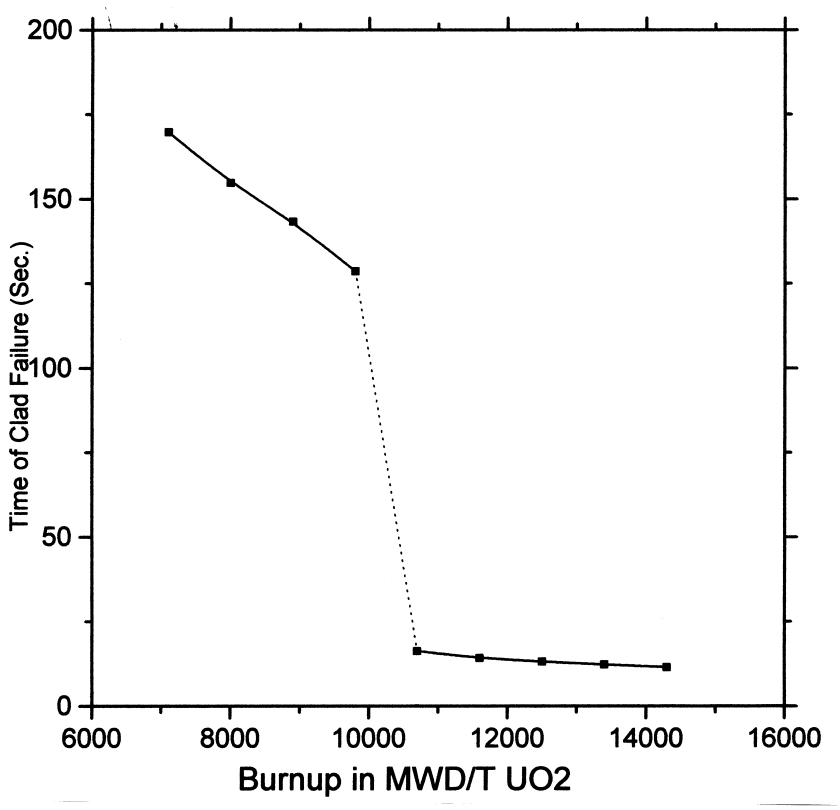

FIG. 3. Assessment of time of clad failure for a furl pin subjected to LOCA with ECCS failure.

5. RESULTS AND DISCUSSIONS

The typical variations of the fuel centre line temperature, the pellet surface temperature and the clad temperature during such an accident for a fuel pin having a burnup of 7000 MWD/T UO_2 are shown in Fig. 1. The transient clad temperature profile in this figure can be divided into three zones along the time scale. These are, the rapid increase in clad temperature just after the initiation of the accident (zone-I), followed by the time interval of moderate clad temperature (zone-II) and finally the slow mode of heating of clad to a high temperature (zone-III). A typical variation of cumulative creep strain with the time of transient is shown in Fig. 2. It may be noted here that the cumulative creep strain increases rapidly once the clad temperature-stress combination crosses a threshold value. The time of clad failure for fuel pins having different initial burnup is shown in Fig. 3. It may be noted here that the failed pins may be put in two distinct groups depending upon the time of clad failure. For the fuel pins having burnup less than 10 000 MWD/T UO_2 , the time to failure is large and these lie in zone-III of Fig.1. On the other hand, the time to failure of fuel pins with burnup more than 10 000 MWD/T UO_2 is much less and these lie in zone-I.

This is essentially because the fission gas pressure available for clad ballooning increases with the burnup. For high burnup fuel pins, the gas pressure may be enough to cause clad ballooning during the initial rapid heating phase of the clad (zone-I) itself. However, clad ballooning may require more time and temperature for the lower burnup fuel pins having less fission gas pressure. For these fuel pins the time of clad ballooning lies in zone-III.

REFERENCES

[1] SWAMI PRASAD, P., DUTTA, B.K., KUSHWAHA. H.S., KAKODKAR, A., Fuel performance analysis code ‘FAIR’, BARC report no:BARC/1994/E/013, (1994).

[2] SWAMI PRASAD, P., DUTTA, B.K., KUSHWAHA, H.S., MAHAJAN, S.C., KAKODKAR, A., Role of BARC parallel processing system in structural analysis of nuclear components, Structural Mechanics in Reactor Technology (SMiRT-13), Paper No: F11/3, (1995b).
[3] COOK, R.D., MALKUS, D.S., PLESHA, M.E., Concepts and applications of Finite Element Analysis, 3rd ed., John Wiley and sons, (1989).
[4] SILLS, H.E., HOLT, R.A., Predicting high temperature transient deformation from microstructural models, 4th ASTM Conf. on Zirconium in nuclear industry.
[5] DONALDSON, A.T., HORWOOD, R.A., HEALY, T., Biaxial creep deformation of Zircaloy-4 in the High Alpha phase temperature range, Water reactor fuel element performance computer modelling, 1983.
[6] SCHEWELT, et al., A high temperature creep model for Zr-2.5 wt % Nb pressure tubes, Jl. of Nuclear Materials, 125, 218-235 (1984).
[7] NUREG/CR-2507, Background and derivation of ANS 5.4 standard fission gas release model, (1982).
[8] VITANZA, C., et al., Fission gas release from In-pile Pressure Measurements, Presented at Enlarged HPG meeting on water reactor fuel performance and application of process computer in reactor operation, Loen, Norway (1978).
[9] HARGREAVES, R., COLLINS, D.A., A Quantitative Model for Fission Gas Release and Swelling in Irradiated Uranium Dioxide, J. Br. Nucl. Energy Soc., 15 (1977), 311-316.
[10] NOTLEY, M.J.F., HASTINGS, I.J., A Microstructure Dependant Model for Fission Product Gas Release and Swelling in UO2 Fuel, Nucl. Engg. Design, 56 (1980), 163-175.
[11] WHITE, R.J., TUCKER, M.O., A New Fission Gas Release Model, J. Nucl. Mater., 118 (1983) , 1-38.
[12] NAKAJIMA, T., SAITO, D.H., A Comparison between Fission Gas Release Data and FEMAXI-IV Code Calculations, Nucl. Engg. Design, 101 (1987), 267-279.
[13] HAGRMAN, D.L., REYMANN, G.A., MASON, R.E., MATPRO-Version 11 (Rev.2) - A handbook of material properties for use in the analysis of light water reactor fuel rod behaviour, NUREG/CR-0497, TREE-1280 Rev.2, (1981).
[14] OTT, C., Testing of the Integral Fuel Behaviour Code TRANSURANUS using Halden Test Fuel Data, Presented at the Halden Extended Programme Group Meeting in Storefjell (N), (1993).
[15] LUCATA, P.G. et al, IAEA-TECDOC-697, 165-171, (1993).
[16] PALMER, I.D., HESKETH, K.W., JACKSON, P.A., A model for predicting the radial power profile in a fuel pin, Light Water Reactor Fuel rod Computer Modelling, (Gittus, J.H. Ed.), (1985), 321-335.
[17] JAMES YU-CHEN YAUNG, A model of pellet cladding interaction to simulate operational ramp failure of water reactor fuel, Ph. D Thesis, University of California, Los Angeles, (1983).
[18] EPRI-NP-369, EPRI report on Light water reactor fuel rod modelling code evaluation (1977).
[19] PENN, W.J., LO, R.K., WOOD, J.C., Candu fuel - power ramp performance criteria, Nuclear Technology, 34 (1977), 249-268.
[20] IAEA/IND/7348, Participation Agreement between IAEA and BARC (India) on Coordinated Research Project FUMEX (1993).
[21] SWAMI PRASAD, P., DUTTA, B.K., KUSHWAHA, H.S., KAKODKAR, A., A Development of computer code for PHWR fuel element analysis, Structural Mechanics in Reactor Technology (SMiRT-12), Paper No:C03/4, (1993).
[22] SWAMI PRASAD, P., DUTTA, B.K., KUSHWAHA, H.S., MAHAJAN, S.C., KAKODKAR, A., Fuel Analysis code FAIR and its high burnup modelling capabilities (Invited Paper), Structural Mechanics in Reactor Technology (SMiRT-13), Paper No: C04/1 (1995).
[23] SWAMI PRASAD, P., DUTTA, B.K. , KUSHWAHA, H.S., KAKODKAR, A., Performance of code FAIR in IAEA CRP on FUMEX. BARC report - BARC/1996/E/022, (1996).
[24] GUPTA, S.K. et al., Personal Communication of Thermal Hydraulic data (1998).

CHARACTERISTICS OF AXIAL SPLITS IN FAILED BWR FUEL RODS

G. LYSELL, V. GRIGORIEV
Studsvik AB, Nyköping, Sweden

Abstract

Secondary cladding defects in BWR fuel sometimes have the shape of long axial cracks or "splits". Due to the large open UO_2 surfaces exposed to the water, fission product and UO_2 release to the coolant can reach excessive levels leading to forced shut downs to remove the failed fuel rods. A number of such fuel rods have been examined in Studsvik over the last 10 years. The paper describes observations from the PIE of long cracks and discusses the driving force of the cracks. Details such as starting cracks, macroscopic and microscopic fracture surface appearance, cross sections of cracks, hydride precipitates, location and degree of plastic deformation are given.

1. INTRODUCTION

Secondary cladding defects in BWR fuel sometimes have the shape of long axial cracks or "splits". Due to the large open UO_2 surfaces exposed to the water, fission product and UO_2 release to the coolant can reach excessive levels leading to forced shut downs to remove the failed fuel rods. A spectacular example of clad splits was a sponge-Zr liner rod that failed in Oskarshamn 3 in 1988 and was examined in Studsvik early 1989, [1]. Since then other rods, all of them of standard 8×8 type without liner, have been examined after developing axial splits. Since the introduction of 9×9 or 10×10 fuel types in Swedish reactors, no axial splits have occurred in these types of fuel rods.

2. GENERAL FEATURES OF AXIAL SPLITS

The axial splits are cracks in the cladding which have propagated from a starting crack. This starting crack could either be a primary PCI (iodine-SCC) crack a few mm in length or a crack in a secondary hydride blister usually about 10 mm in length. One rod can have many axial splits originating at different positions along the rod. If two such cracks meet, they will only overlap over a short distance and not propagate any further. For example, the liner rod [1], which was the first to be examined, had five separate splits all originating from secondary hydride blisters. Another rod had two splits, one originating in a primary SCC crack and the other in a secondary hydride blister.

When the splits are longer than a few cm the crack opening will become large enough (>0,5 mm) to allow liquid water to come in contact with the fuel pellets. This leads to rapid washout of fuel by oxidation and erosion of the pellets thus causing the large release of fission products, which is typical of failures with axial splits. The visual appearance of an axial split and the corresponding neutron radiography image show the large removal of fuel at a cladding split (Fig. 1).

3. MACROSCOPIC FEATURE OF CRACKS

When observing the clad splits under a hot cell periscope the large crack opening often makes it possible to directly observe the fracture surfaces. One can then notice a typical striated pattern, which seems to originate at the starting crack and then remains the same over the whole propagation part of the splits.

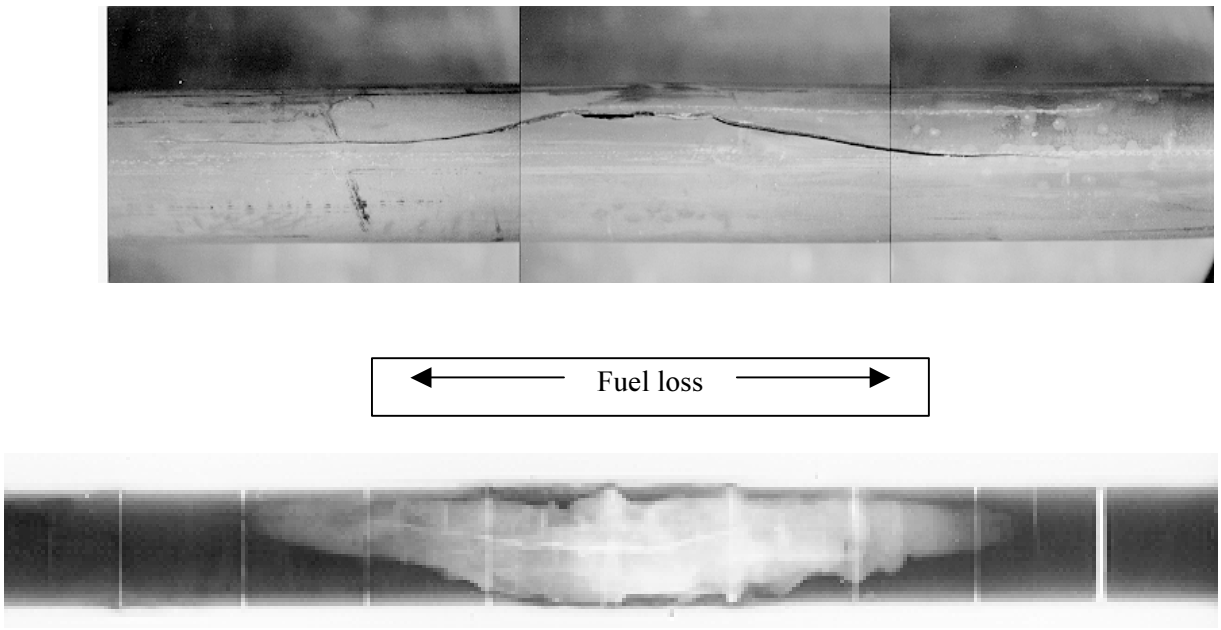

FIG. 1. Visual appearance and neutron radiography of the same clad split.

The sketch below shows how the striations look and how they are related to the starting crack. Often the striations form a feather or fish bone pattern close to the outside of the cladding. This is indicated to the right in Fig. 2.

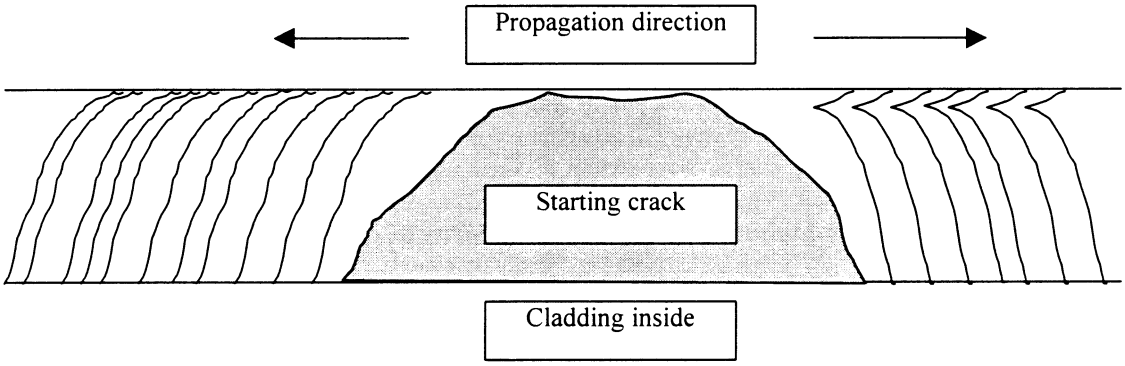

FIG. 2. Macroscopic striations on the fracture surface in relation to the starting crack.

A real example of a starting crack (PCI in this case) and the continued propagation part is shown in the low magnification SEM image in Fig. 3.

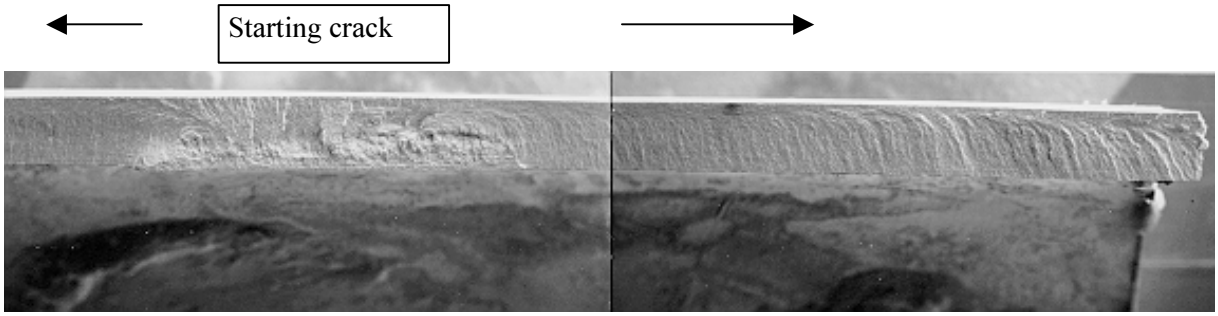

FIG. 3. A PCI starting crack and the propagation in both directions from it.

The splits seem to propagate in straight lines over long distances only deviating when they have to propagate through hydride blisters where the stress pattern is disturbed [2]. A hydride blister with many criss-crossing cracks in the path of a propagating crack has even been seen to act as an obstacle to further propagation. The local hydrogen content of the cladding through which long apparently brittle splits have propagated has been measured to be as low as 150 ppm.

4. MICROSCOPIC FEATURES OF CRACKS

Microscopic observations of clad splits have been performed both on metallographic sections through cracks and on fracture surface specimens in a Scanning Electron Microscope (SEM) and in optical microscope.

Two differently oriented types of metallographic sections were used to characterise the axial splits.

Ordinary tangential/radial cross sections showed that the propagation parts of the axial splits have purely radially oriented fracture surfaces. Often a small plastic deformation can be observed close to the cladding inside making it impossible to perfectly mate the two opposing fracture surfaces. There are indications that in spite of the brittle appearance of the axial splits the wall thinning can be several per cent. Tangential strain is observed at the cladding inside close to the axial split. This is the reason why the two opposing fracture surfaces do not match in macro scale. When etched to see the hydrides it is commonly observed that there is a zone of *tangentially* oriented hydrides close to the fracture surface, see Fig 4.

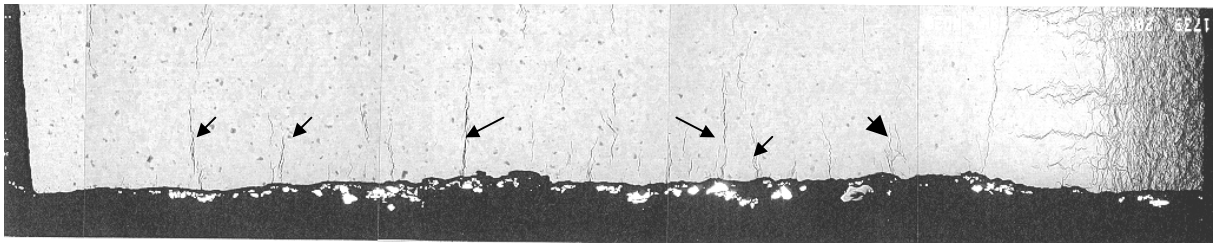

Inside Outside

FIG. 4. Cross section showing one side of a fracture, notice the tangential hydrides (arrowed), 200X.

Tangential/axial sections close to the cladding outside at the axial ends of splits in several cases showed that hydrides had preferentially precipitated just in front of the crack tip, see Fig 5 from [1]. Similar precipitation was shown in a tangential/axial section in [2] and in a tangential/radial section in [4]. The latter case indicates that the amount of precipitated hydride decreases towards the cladding inside. A sketch summarising these findings schematically from the PIE of crack tips are shown in Fig 6.

Fracture surfaces examined in SEM showed that the macroscopic striations are long "hills" and "valleys" 10 to 100 μm wide with steep sides, continuous over a large part of the cladding thickness, see the SEM image in Fig 7 and the sketch in Fig 8.

Fracture surfaces taken at the end of clad splits and examined in SEM revealed that the crack front had propagated furthest close to the cladding outside also giving an insight into how the macroscopic striations are formed. Evidently, the striations follow the local propagation direction of the crack front and thus are at right angles to the crack front at any given time as shown in Fig 9.

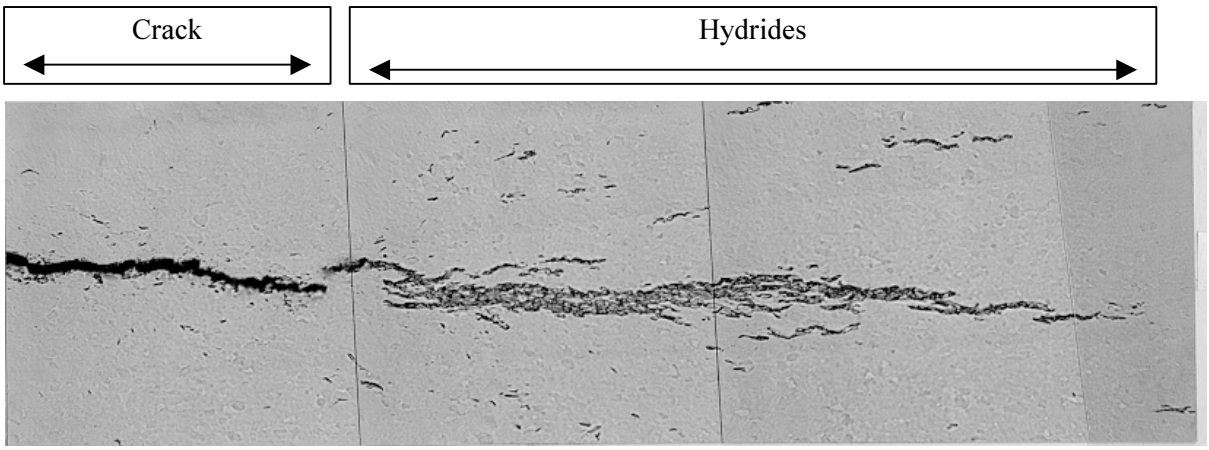

FIG. 5. Hydrides precipitated in front of a crack tip, 300X.

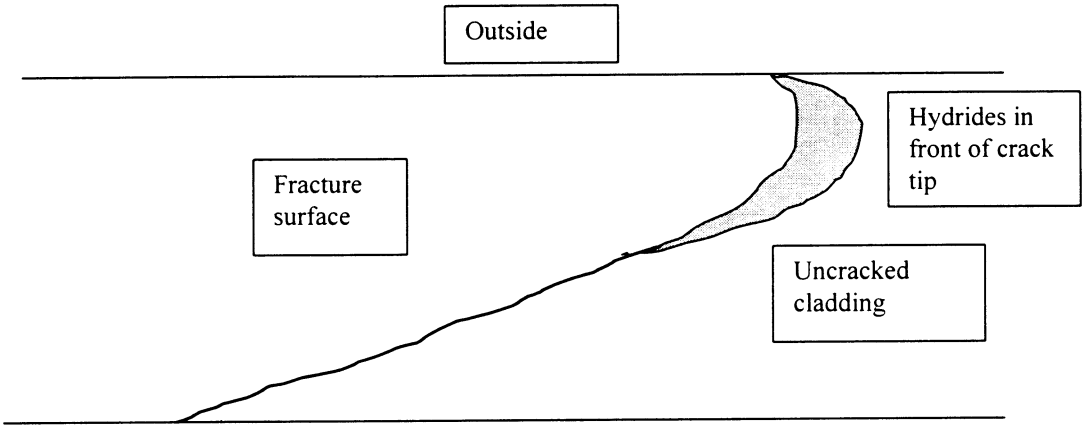

FIG. 6. Sketch of hydride precipitation found in metallography at crack tips.

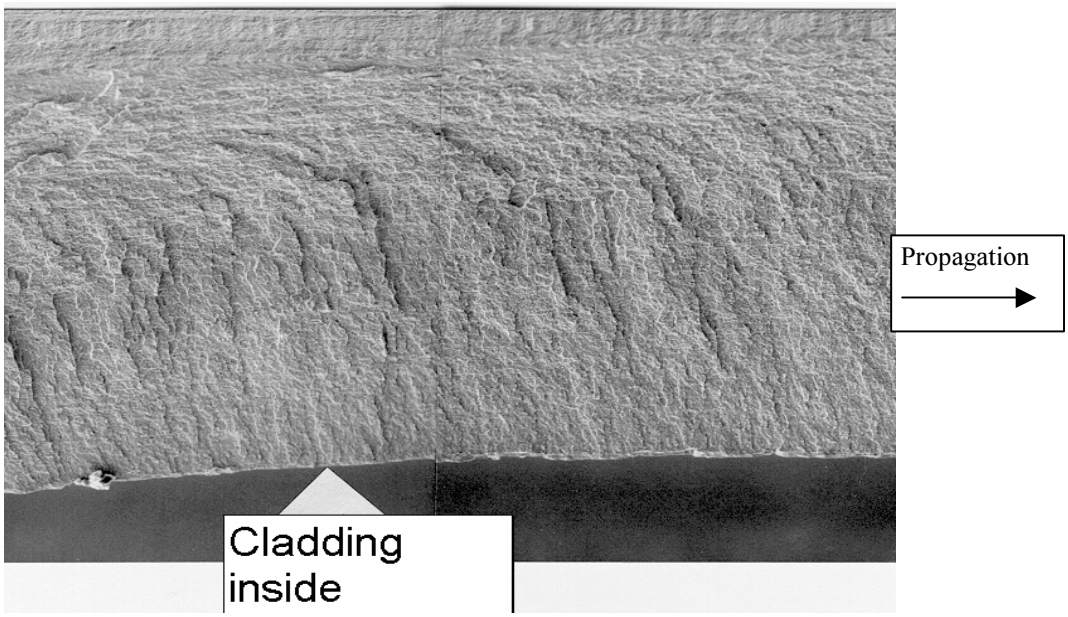

FIG. 7. SEM image showing striations of "hills" and "valleys", 100X.

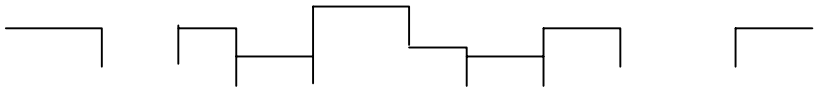

FIG. 8. Sketch of a tangential/axial section through hills and valleys on a fracture surface.

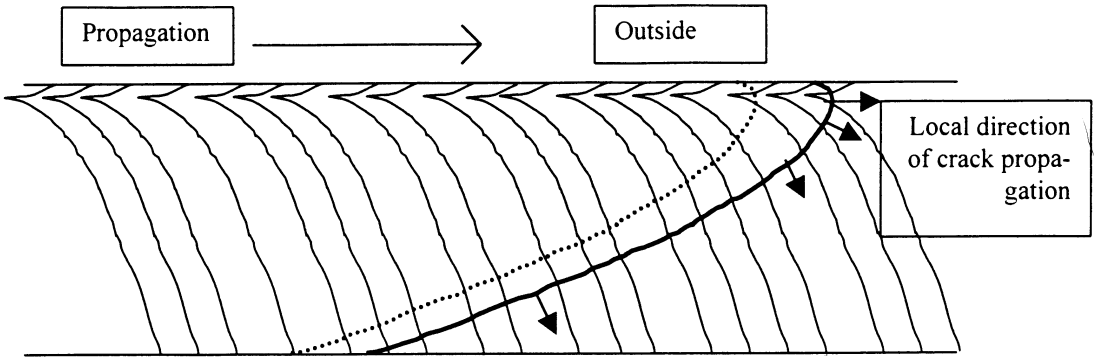

FIG. 9. Reconstruction of a crack front at right angles to the striations.

When viewing the cladding inside bordering to the fracture surface in SEM it was observed that the inside oxide layer contained a number of cracks in the axial direction, see Fig 10. The area with cracked inside oxide extended about 200 μm in the tangential direction from the fracture surface. The oxide acts as a crackle lacquer during plastic deformation of the inner part of the cladding when the crack front approaches the cladding inside during propagation of the axial split. This observation agrees quite well with the zone of plastic deformation close to the cladding inside, which was seen in the cross section of Fig. 4.

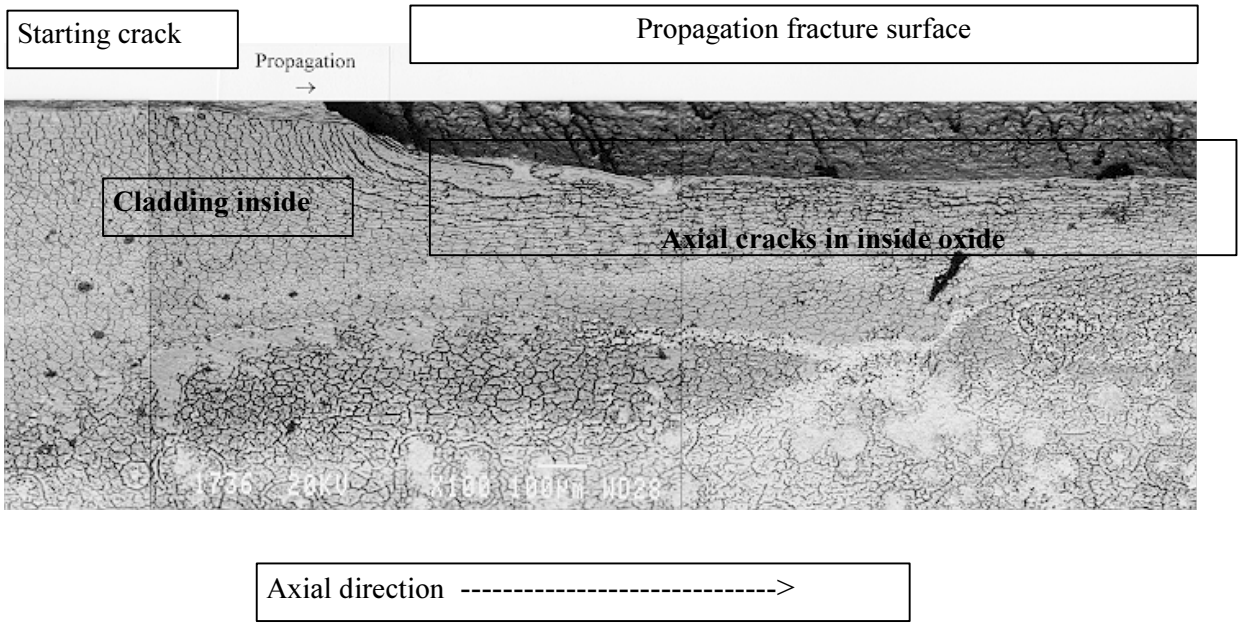

FIG. 10. Cracks in the inside oxide layer parallel to the fracture surface, 90 X.

The microscopic character of the fracture surface is often obscured by the oxidation caused by the continued operation of the reactor before the failed rod can be taken out. Only if the reactor is stopped immediately after an axial split failure or if the split is produced in a test reactor, can the unaltered fracture surfaces be studied. Such an example is shown in Fig. 11.

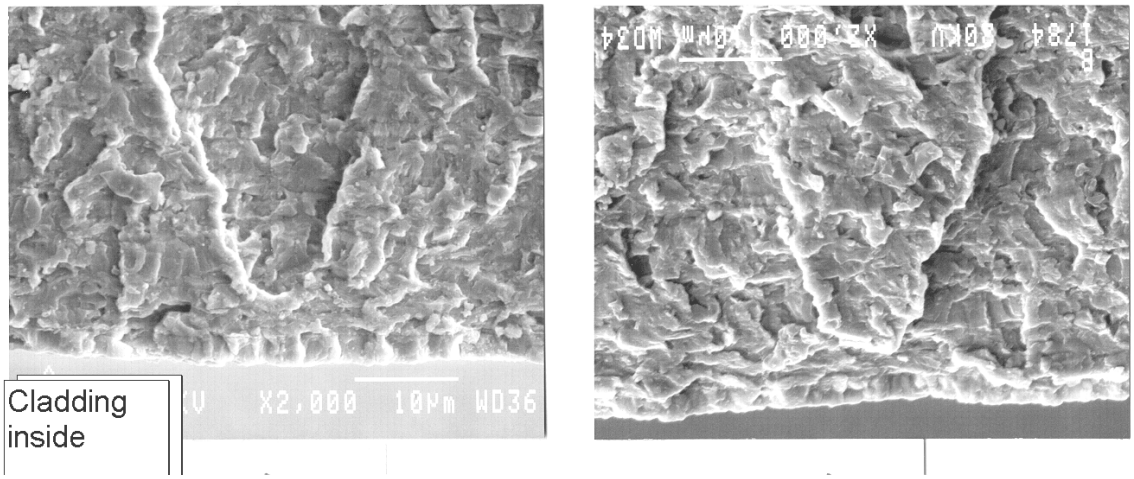

FIG. 11. SEM images of two mating fracture surfaces close to the cladding inside,1300X.

The surface is characterised by quasi cleavage surfaces parallel to the macro plane of the whole crack. By comparing the two opposing fracture surfaces, it is evident that on a microscopic level there is an almost perfect fit between the two sides of the crack. Thus, a "hill" on one fracture surface always corresponds to a "valley" on the mating fracture surface. The only ductile features seen on the surfaces are shear patterns on the steep sides connecting "valleys" with "hills". This shear occurs when the two fracture surfaces separate during the crack opening process.

5. DRIVING FORCES

The basic driving force, which keeps a crack propagating, is the hoop stress in the cladding. This hoop stress is in turn caused by the pellets expanded by thermal expansion at high linear heat ratings. Since rods with long axial splits are open to the coolant the pellets will also be oxidised by steam lowering their thermal conductivity thus increasing the temperature and the thermal expansion above that normal for a given linear heat rating. Lowering the linear heat rating is thus an effective means to eliminate the propagation process. As evidence for this statement, it can be noted that no axial splits have been observed in 9X9 or 10X10 rods in Swedish reactors. The earlier use of pure Zr-liner in some rods made the stress level even higher due to the rapid oxidation of the liner if such a rod failed. The addition of alloying elements to the liner to increase its corrosion resistance should make such liner rods more similar to non liner rods in case of a primary failure.

6. SUMMARY

The following statements can be made regarding axial splits based on the present knowledge.

Apparently brittle cracks can propagate in cladding with hydrogen content as low as 150 ppm.

Both PCI cracks and secondary hydride blisters can act as starting cracks.

Striations on fracture surfaces are parallel to the direction of local crack propagation and thus perpendicular to consecutive crack fronts.

Axial clad splits exhibit local plastic deformation of the cladding, observed as wall thinning of several per cent.

Cross sections through axial clad splits show tangentially oriented hydrides.

Sections at the tip of axial clad splits show precipitation of hydride in front of the crack tip.

The fracture surfaces are brittle in appearance and in microscopic scale show a perfect fit of the two opposing surfaces.

REFERENCES

[1] JONSSON, Å., HALLSTADIUS, L., GRAPENGIESSER, B., LYSELL, G., Failure of a barrier rod in Oskarshamn 3. ANS/ENS Topical Meeting on LWR Fuel Performance Avignon, France 1991.

[2] SCHRIRE, D., GRAPENGIESSER, B., HALLSTADIUS, L., LUNDHOLM, L., RÖNNBERG, G., LYSELL, G., JONSSON, Å., FRENNING, G., Secondary defect behaviour in ABB BWR fuel. Light Water Reactor Fuel Performance: International Topical Meeting, American Nuclear Society, West Palm Beach, Florida 1994.

[3] EDSINGER, K., DAVIES, J.H., ADAMSON, R.B., Degraded Fuel Cladding Fractography and Fracture Behaviour. ASTM meeting on Zirconium in the Nuclear Industry, Toronto, Canada 1998.

[4] KIN-FU LIN, CHUNG-SHING CHUNG, J. JUNG YEH, JEN-HONG CHEN, SHUI-SHU CHU, LI-FU LIN, Investigation on the post-defect deterioation of nonbarrier BWR fuel rods. Light Water Reactor Fuel Performance: International Topical Meeting, American Nuclear Society, West Palm Beach, Florida 1994.

LIST OF PARTICIPANTS

ARGENTINA

A. Denis
Nuclear Fuels Department, CNEA-CAC,
Av. del Libertador 8250, 1429 Buenos Aires
Fax: 005411 4754 7434
E-Mail: denis@cnea.edu.ar

A.C. Marino
Advanced Design and Econ. Assessment Department, CNEA-CAB,
Av. Bustillo, Ruta 9, km 500, 8400 San Carlos de Bariloche,
Pcia. Río Negro,
Tel.: 0054 2944 445178
Fax: 0054 2944 445100
E-Mail: marino@cab.cnea.gov.ar

BELGIUM

D. Boulanger
Belgonucléaire, Avenue Ariane 4, BE-1200 Brussels,
Fax: 32 2 774 0547

CANADA

M. Tayal
AECL — CANDU, 2251 Speakman Drive, SP2F4,
Mississauga, Ontario, L5K IB2,
Fax: 001905 822 0567
E-Mail: tayalm@aecl.ca

CHINA

M. Ran
Institute of Atomic Energy, P.O. Box 375-57,
Beijing 102413,
Fax: 86 10 685 13717
E-Mail: yanjy@ihw.com.cn

CZECH REPUBLIC

J. Zymak
Nuclear Research Institute Rez plc,
CH-250 68 Rez
Fax: 420 2 209 409 60
E-Mail: zym@nri.cz

FINLAND

K. Sarparanta
Teollisuuden Voima Oy, Olkiluoto NPP,
FIN-27160 Olkiluoto,
Fax: 358 2 8381 5209
E-Mail: kathe.sarparanta@tvo.tvo.elisa.fi

J.O. Stengard
VTT Energy, Nuclear Energy, P.O. Box 1604, FIN-02044 VTT,
Fax: 358 9 456 5000
E-Mail: jan-olof.stengard@vtt.fi

K. Valtonen
Radiation and Nuclear Safety Authority, P.O.Box 14, FIN-00881 Helsinki,
Fax: 358 9 759 883 820
E-Mail: keijo.valtonen@stuk.fi

FRANCE

P. Blanpain
FRAMATOME, 10 rue Juliette Récamier,
F-69456 Lyon Cedex 06,
Fax: 33 4 72 74 88 33
E-Mail: pblanpain@framatome.fr

S. Bourreau
CEA/DMT/SEMI/LEMO, FR-91191 Gif sur Yvette,
Fax: 33 1 69 08 93 24
E-Mail: bourreau@cea.fr

P. Garcia
CEA/DEC/SDC, CEA Centre de Cadarache,
FR-13108 St. Paul lez Durances Cedex,
Fax: 33 4 42 25 29 49
E-Mail: Garcia@come.cad.cea.fr

M.C. Granjean
EDF/SEPTEN, 12-14 Avenue Dutrievoz,
FR-69628 Villeurbanne Cedex,
Fax: 33 4 72 82 77 13
E-Mail: Marie-claire.Granjean/septen/de/edfgdf/fr@ed

S. Lansiart
CEA/DMT/SEMI/LEMO, FR-91191 Gif sur Yvette,
Fax: 33 1 69 08 26 81
E-Mail: sylvie.lansiart@cea.fr

C. Maury
EDF/SEPTEN, 12-14 Ave. Dutrievoz,
FR-69628 Villeurbanne Cedex
Fax: 33 4 72 82 77 11
E-Mail: claire.maury@edfgdf.fr

R. Salot
CEA/DEC/SECC, CEA centre de Grenoble,
17 rue des Martyrs, FR-38054 Grenoble Cedex,
Fax: 33 4 76 88 51 51
E-Mail: salot@dtp.cea.fr

GERMANY

S. Langenbuch
GRS Forschungsgelände, DE-85748 Garching,
Fax: 49 89 32004 599
E-Mail: lab@grs.de

F. Sontheimer
Siemens AG, KWU NBTM, P.O. Box 32 20,
DE-91050 Erlangen,
Fax: 49 9131 18 4799
E-Mail: Fritz.Sontheimer@erl19.siemens.de

HUNGARY

D. Sarkadi
Hungarian Atomic Energy Authority,
Margit krt. 85, HU-1024 Budapest,
Fax: 36 75 311 471

HUNGARY (cont.)

J. Zsoldos
Hungarian Atomic Energy Authority,
HEA NSD, Il. Margit krt. 85, HU-1359 Budapest 114,
Fax: 36 75 311 471
E-Mail: h13478zso@ella.hu

INDIA

M.P. Antony
IGCAR, Indira Gandhi Centre for Atomic Research,
Kalpakkam, Tamil Nadu,
Fax: 91 411 440 360

B.K. Dutta
Bhabha Atomic Research Centre,
Reactor Safety Division, Hall-7,
Trombay, Mumbai 400085,
Fax: 91 22 550 5151 / 91 22 551 9613
E-Mail: bkdutta@magnum.barc.ernet.in

JAPAN

H. Hayashi
NUPEC — Nuclear Fuel Department,
Fujita Kankou Toranomon Bldg, 3-17-1,
Toranomon, Minato-ku, Tokyo 105,
Fax: 81 3 5470 5544
E-Mail: h-hayashi@nupec.or.jp

M. Ichikawa
The Japan Atomic Power Company,
Ohtemachi Bldg. 6-1 Chome, Ohtemachi,
Chiyoda-Ku, Tokyo 100-0004,
Fax: 0081 3 3213 5990
E-Mail: michio-ichikawa@japc.co.jp

N. Ikatsu
Nuclear Fuel Industries, Ltd,
3135-41 Muramatsu, Tokai-mura Naka-gun, Ibaraki
Fax: 81 029 287 8222
E-Mail: ikatsu@nfi.co.jp

NORWAY

T. Tverberg
OECD Halden Reactor Project,
Institutt for Energiteknikk, P.O.Box 173,
NO-1751 Halden,
Fax: 47 69 21 22 01
E-Mail: terjet@hrp.no

SPAIN

M.T. del Barrio
CIEMAT / OECD Reactor Proj., Os Alle 13,
NO-1777 Halden,
Fax: 47 69 21 22 01 / 34 91 346 6233
E-Mail: maria.barrio@hrp.no

J.C. Garcia-Cuesta
CIEMAT, Avda. Complutense 22, ES-28040 Madrid,
Fax: 34 91 346 6233
E-Mail: jc.garcia@ciemat.es

SPAIN (cont.)

M. Quecedo
Uranio S.A., (ENUSA), Empresa Nacional de,
ES-28040 Madrid,
Fax: 0034 91 34 74 215
E-Mail: mqg@enusa.es

M. Recio Santamaria
Consejo de Seguridad Nuclear,
Area de Ingenieria Nuclear, Justo Dorado, 11,
ES-28040 Madrid
Fax: 34 91 346 0588
E-Mail: mrs@csn.es

SWEDEN

P. Abry
ABB Atom AB, Finnslätten,
SE-721 63 Västeras,
Fax: 46 21 34 72 51
E-Mail: philippe.abry@seato.mail.abb.com

S. Borell
ABB Atom AB, SE-721 63 Västeras,
Fax: 46 21 34 77 33
E-Mail: sten.borell@seato.mail.abb.com

S. Djurle
Studsvik Nuclear AB, Svanvägen 20,
SE-611 62 Nyköping,

S.K. Eriksson
ABB Atom AB, S-721 63 VÄSTERÅS,
Fax: 0046 21 34 77 33
E-Mail: sven.eriksson@seato.mail.abb.com

B. Grapengieser
ABB Atom AB, S-721 63 VÄSTERÅS,
Fax: 0046 21 34 77 33
E-Mail: bjorn.grapengiesser@seato.mail.abb.com

V. Grigoriev
Studsvik Material AB, SE-611 82 Nyköping,
Fax: 46 155 26 31 50
E-Mail: vgrigoriev@nuclear.studsvik.se

J. In de Betou
Swedish Nuclear Power Inspectorate, SE-106 58 Stockholm,
Fax: 46 8 661 90 86
E-Mail: jan@ski.se

T. Jonsson
Studsvik Nuclear AB, SE-611 82 Nyköping,
Fax: 0046 155 26 31 56
E-Mail: tord.jonsson@nuclear.studsvik.se

SWEDEN (cont.)

G. Lysell
Studsvik Nuclear AB, SE-611 82 Nyköping,
Fax: 46 155 26 31 56
E-Mail: gunnar.lysell@nuclear.studsvik.se

K. Malén
Studsvik Nuclear AB, SE-611 82 Nyköping,
Fax: 46 155 26 31 56
E-Mail: karl.malen@nuclear.studsvik.se

P. Rudling
Vattenfall Fuel AB, SE-162 87 Stockholm,
Fax: 46 8 17 86 40
E-Mail: peru@fuel.vattenfall.se

D. Schrire
Studsvik Nuclear AB, SE-611 82 Nyköping,
Fax: 46 155 26 31 56
E-Mail: david.schrire@nuclear.studsvik.se

UNITED KINGDOM

A. Clarke
British Energy, Nuclear Techn. Group,
Nuclear Techn. Branch, Barnett Way,
Barnwood, Gloucester GL43RS,
Fax: 44 1452 652 206
E-Mail: A.Clarke26@ne.british-energy.com

P. Cook
BNFL THORP, Sellafield, Seascale, Cumbria UK CA20 IPG,
Fax: 44 1946 785389

T. Shaw
AEA Technology, Building B7, Windscale,
Seascale, Cumbria CA20 IPF
Fax: 44 19467 72606
E-Mail: tim.shaw@AEAT.co.uk

UNITED STATES OF AMERICA

J. Davies
GE Materials Technology, Vallecitos Nuclear Center,
6705 Vallecitos Road, Sunol, CA 94586
Fax: 1 925 862 4515
E-Mail: John.Davies@gene.GE.com

IAEA

P. Menut
Nuclear Fuel Cycle and Materials Section,
Division of Nuclear Fuel Cycle and Waste Technology,
Wagramer Strasse 5, P.O. Box 100, A-1400 Vienna, Austria
E-Mail: P.Menut@iaea.org